HYDRAULIC CONVEYING OF METALLIC PLATELETS

by

Anastassios Tatsis, B.Sc (Eng)

A thesis submitted for the degree

of Doctor of Philosophy of the University

of London and for the Diploma of

Membership of the Imperial College

Chemical Engineering

and

Chemical Technology

January, 1987.

I dedicate this work

to my wife MARIA-ALCINA and

our children JOANNA and GEORGE

ABSTRACT

Hydraulic conveying offers some important advantages in the handling of freshly comminuted radioactive Magnox waste. Work has been performed with suspensions of regular shaped metallic platelets in an attempt to simulate actual Magnox swarf. A series of experiments was performed using aluminium platelets 9-12 mm long and about 2 mm thick. Values of terminal velocities and drag coefficients were obtained and found to be in excellent agreement with theoretical predictions based on appropriate "shape factors".

A pipe rig with 2" and 4" pipe diameters, was employed to pump a pre-classified, closely graded sample of Dexion stampings up to concentrations of about 10% by volume (approximately 23% by weight). In each case, pressure drop data for a range of slurry flows were correlated in the horizontal and vertical pipe sections.

Existing empirical correlations, such as the Durand and Condolios equation, were found to fit the data requiring only small modifications to the constants involved. The results were interpreted by postulating that each platelet behaves as if it were an "aerofoil" in a fully developed pipe flow. The effect of particle shape on pumping power has been evaluated.

The significance of this work is discussed and potential directions for further research are indicated.

ACKNOWLEDGEMENTS

LIST OF CONTENTS

- 7 -

Enclosure of Publication:

LIST OF FIGURES

LIST OF TABLES

LIST OF PLATES

LIST OF SYMBOLS

UNITS

A   constant: property of slurry in the pseudo-

homogeneous flow regime, $\dfrac{K\,g\,D\,V_t}{V_m^3}$ -

a   Richardson and Zaki exponent   -

A_p particle projected area viewed perpendicular to the

plane of maximum stability,

$\dfrac{\pi\,d_v^2}{4}$ for a volume equivalent sphere L^2

A_v surface area of volume - equivalent sphere L^2

A_x cross-sectional area of pipeline L^2

B   constant, property of slurry in the fully stratified

flow regime, $33f_w'$ -

b   breadth of particle   L

C_D drag coefficient,

$\dfrac{4\,(S-1)\,d\,g}{3\,V_t^2}$ for a free settling sphere   -

$\dfrac{2\,(S-1)\,g\,t}{V_t^2}$ for a free settling platelet   -

$1.328/Re^{0.5}$ for a flat shearing surface; laminar

flow   -

$0.072/Re^{0.2}$ for a flat shearing surface; turbulent

flow   -

C_v delivered volumetric solids concentration   -

C_w delivered solids concentration by weight   -

D   internal diameter of pipe   L

d   particle diameter   L

da	elemental area	L^2
d_a	diameter of sphere with same projected area as particle	L
dh	elemental height	L
d_v	diameter of volume equivalent sphere	L
$d_{1,2}$	particle diameters measured at right angles to each other	L
d_{50}	mean particle diameter	L
$d\theta$	elemental angle	-
e_1	flatness ratio, $\dfrac{b}{t}$	-
e_2	elongation ratio, $\dfrac{l}{b}$	-
E_s	specific energy consumption	$L^2 T^{-2}$
f	denotes mathematical function	-
F	Magnus force, $\rho_w\, d\, \Gamma\, \Delta u$	$M\,L\,T^{-2}$
F_D	drag resistance force	$M\,L\,T^{-2}$
F_f	integral force acting on leading face of platelet	$M\,L\,T^{-2}$
F_L	lift force	$M\,L\,T^{-2}$
f_m	mean Darcy-Weisbach friction factor for slurry, $\dfrac{8\,\tau_o}{\rho_m\, V_m^2} = \dfrac{2\,i\,g\,D}{V_m^2}$	-
f_w	single-phase Fanning friction factor, $\dfrac{2\,\tau_o}{\rho_w\, V_m^2} = \dfrac{i_w\,g\,D}{2\,V_m^2}$	-
f_w'	single-phase Darcy-Weisbach friction factor, $\dfrac{8\,\tau_o}{\rho_w\, V_m^2} = \dfrac{2\,i_w\,g\,D}{V_m^2}$	-
Fr	Froude number, $\dfrac{V_m}{\sqrt{gD}}$	-
Fr'	Froude number corrected for the relative weight of solids in H_2O, $\dfrac{V_m}{\sqrt{g\,D\,(S-1)}}$	-

F_s total shear force acting on the two elevated sides of

the platelet $M\ L\ T^{-2}$

F_t total shear force acting on the top surface of the

platelet $M\ L\ T^{-2}$

g acceleration due to gravity $L\ T^{-2}$

Ga Galileo number, $d^3\ (S - 1)\ g\ [\dfrac{\rho_w}{\mu_w}]^2$ -

h_f frictional head loss L

h platelet height measured from pipe wall L

h^+ $\dfrac{V_\tau\ h}{\nu_w}$ -

i total hydraulic gradient, (m water/m pipeline)   -

$I.D.$ denotes internal pipeline diameter   -

i_h friction gradient due to solids in the heterogeneous

flow regime, (m water/m pipeline)   -

i_s friction gradient due to solids in the stratified

flow regime, (m water/m pipeline)   -

i_w hydraulic gradient attributed to water-wall friction,

(m water/m pipeline)   -

k pipe roughness L

K constant, shape factor   -

coefficient in drag resistance term (see Appendix A;

units vary)

K_A the ratio of terminal velocity of particle to the

terminal velocity of sphere with the same projected

area   -

Ke volume coefficient of equi-dimensional particle,

$\dfrac{\text{volume of equi-dimensional particle}}{d^3}$ -

K_V the ratio of terminal velocity of particle to the

terminal velocity of sphere with the same volume   -

K_1 volume coefficient of an irregular particle,

$$\frac{\text{volume of particle}}{d_a{}^3}$$ -

K_2 shape coefficient of a non-isometric particle,

$$\frac{Ke}{e_1 \sqrt{e_2}} = \frac{Ke\ t}{\sqrt{1\ b}}$$ -

K_{2A} K_A based on K_2

K_2' Same as K_2 but based on the actual projected area

of the particle A_p, $\dfrac{Ke\ t}{\sqrt{A_p}}$ -

K_{2A}' K_A based on K_2' -

K_3 shape factor based on the ratio of equivalent

diameters for the particle, $(d_a/d_v)\ \dfrac{t\ d_a}{\sqrt{1\ b}\ d_v}$ -

l length of particle   L

L length of pipe   L

m constant, property of slurry   -

n Durand index   -

M mass of particle   M

M' mass of displaced fluid   M

M_s solids throughput $M\ T^{-1}$

Mtpa   denotes Mega tonnes per annum   -

N_d dimensionless particle diameter group,

$$\frac{4\ g\ (S-1)\ d^3}{3\ v_w^2}$$ -

P_h total stagnation pressure $M\ L^{-1}\ T^{-2}$

P_s static pressure $M\ L^{-1}\ T^{-2}$

Q volumetric flow rate $L^3\ T^{-1}$

R stratification ratio, $\left[\dfrac{V_{th}}{V_m}\right]^m$; $(V_m \geq V_{th})$ -

Re_o shear velocity particle Reynolds number, $\dfrac{d\ \sqrt{\tau_o\ \rho_w}}{\mu_w}$ -

Reynolds number based on particle length, $\dfrac{V_h\, x}{\nu_w}$ -

Re_D Reynolds number based on pipe diameter, $\dfrac{\rho_w\, V_m\, D}{\mu_w}$ -

Re_d Reynolds number based on particle diameter, $\dfrac{\rho_w\, V_m\, d}{\mu_w}$ -

S relative density of solids, $\dfrac{\rho_s}{\rho_w}$ -

s distance moved by particle   L

S_m mean realative density of slurry, $\dfrac{\rho_m}{\rho_w}$ -

t platelet thickness   L

   time of motion   T

V velocity of particle at time t after the onset of

   motion $L\,T^{-1}$

   volume of volume equivalent sphere, $\dfrac{\pi\, d_v^3}{6}$ L^3

Ve effective vertical velocity fluctuation $L\,T^{-1}$

V_{cr} critical slurry velocity for incipient suspension $L\,T^{-1}$

V'_{cr} ratio of critical to terminal velocity, $\dfrac{V_{cr}}{V_t}$ -

V_h fluid velocity at height h $L\,T^{-1}$

V_m mean slurry velocity $L\,T^{-1}$

V_p particle volume, $\dfrac{\pi\, d^3}{6}$ for a spherical particle L^3

   gross volume of sample L^3

V_t terminal settling velocity of a single particle in an

   infinite water medium $L\,T^{-1}$

V'_t hindered settling velocity for a given volumetric

   concentration of particles C_v, $V_t\,(1 - C_v)^a$ $L\,T^{-1}$

V_{th} value of V_m at threshold of turbulent suspension $L\,T^{-1}$

V_{ts} terminal settling velocity of a spherical particle

   in an infinite water medium $L\,T^{-1}$

V_w	local velocity of water in pipe flow	$L\ T^{-1}$
V_τ	shear velocity, $\sqrt{\dfrac{\overline{\tau_o}}{\rho_w}}$	$L\ T^{-1}$
W	gross weight of sample, mean particle weight	$M\ L\ T^{-2}$
W_{ap}	apparent weight of platelet under water	$M\ L\ T^{-2}$
x	length of particle in x-direction	L
y	length of particle in y-direction	L
z	length of particle in z-direction	L
α	acceleration of particle	$L\ T^{-2}$
Γ	circulation around an object	$L^2\ T^{-1}$
ΔP	frictional pressure drop in pipe	$M\ L^{-1}\ T^{-2}$
Δu	difference between the velocity of the particle and that of a similarly placed fluid a considerable distance away, $= V_t$ for vertically rising flow	$L\ T^{-1}$
θ	angle subtended by contact load	-
λ	ratio $= 1 - 1/S$	-
μ_w	dynamic viscosity of water	$M\ L^{-1}\ T^{-1}$
ν_w	kinematic viscosity of water	$L^2\ T^{-1}$
ξ	sphericity, $\dfrac{A_v}{A_p}$	-
Λ	macro scale of turbulence	L
ρ_m	mean slurry density	$M\ L^{-3}$
ρ_s	density of solids	$M\ L^{-3}$
ρ_w	density of water	$M\ L^{-3}$
σ	denotes standard deviation of the mean	-
τ_o	shear stress at the wall for a pipe containing water alone	$M\ L^{-1}\ T^{-2}$

ϕ normalised difference between slurry and clear water

hydraulic gradients, $\dfrac{i - i_w}{C_v i_w}$ -

angle of sliding friction, angle of repose (wet or

dry)   -

ψ weighted densimetric Froude number (after Durand),

$$\dfrac{g\ D\ (S - 1)}{V_m^2\ \sqrt{C_D}}$$ -

ψ' weighted densimetric inverted Froude number (after

Newitt), $\dfrac{V_m^3}{g\ D\ V_t\ (S - 1)}$ -

Ω angle subtended by elliptical profile   -

1. INTRODUCTION

The use of hydraulic transport in the nuclear industry is not only a novel application but it also provides great potential where remote handling and full automation are required. The present work was undertaken with particular reference to the conveying of the active Magnox resulting from the de-cladding of spent fuel from nuclear power stations. Although the size to which the Magnox swarf should be reduced by comminution has not yet been decided, it is almost certain to result in effectively two-dimensional particles (i.e. length $>>$ thickness). Despite a wealth of literature concerned with slurry pipelining and the hydrodynamic parameters associated with each material to be pumped, very little relates to the unusual platelet shape obtained after comminution.

Magnox is an alloy comprising 99.3% magnesium, the remaining 0.7% being mainly aluminium. When spent fuel is decanned the resulting swarf is stored in silos which act as cooling ponds. Under water, magnesium oxidises according to:

$$Mg + 2H_2O \rightarrow Mg(OH)_2 + H_2 + Heat \qquad \qquad .... (1.1)$$

The heat liberated by this reaction is entrapped by the magnesium hydroxide which unfortunately acts as a convection barrier. In addition, the H_2 produced constitutes an explosion hazard if allowed to exceed a concentration of 4% in the surrounding air. Therefore, it becomes clear that magnesium swarf cannot be used directly as a test material. However, it has been determined that aluminium provides a good material with which to model the comminution and hydraulic conveying of Magnox pieces and swarf. Aluminium exhibits less tendency than

Magnox to react with air and water over a period of time. Both materials are comparatively light metals; commercial aluminium has a density of about 2629.1 kg m^{-3} as compared with 1738 kg m^{-3} for pure magnesium. In addition, aluminium can be readily obtained in large quantities.

In order to investigate any original effects which might arise from the hydraulic conveying of a two-dimensional material the situation was idealised by using aluminium platelets in the size range 9-12 mm long and about 2 mm thick. Tests have been performed on individual regularly shaped platelets to deduce values for the hydrodynamic parameters required for the predictive equations associated with the hydraulic transport of comminuted Magnox. Of particular importance are the shape factor, terminal velocity and drag coefficients of the platelets. The ultimate objective of the work is to correlate pressure drop as a function of platelet size, speed of flow and delivered concentration. A closed hydraulic conveying loop together with a substantial amount of aluminium platelets (about 0.5 Te) were required and a 100 mm I.D. pipe rig was made available at U.K.A.E.A. Winfrith by B.N.F.L.. Aluminium platelets were obtained by sorting regular Dexion stampings collected off the production line and provided by the Dexion Company.

The experimental results were used to test existing correlations. Moreover they provided the basis for the modelling of a new mechanistic approach for the conveying of platelets in dilute suspensions. This approach is consistent with standard practice used in the study of flow past an "aerofoil".

Finally, the energy requirements have been assessed in terms of shape and concentration.

2. LITERATURE SURVEY

2.1 Introduction

The use of pipelines for transporting fluids has been established for many centuries and fluid flow in pipes is now well understood. However, it is only recently that the hydraulic conveying of two phase mixtures came into practice. For this reason, the main aspects of slurry pipelining have been surveyed, with the aim of identifying the current limits of knowledge and understanding. Much of the past review work has mixed discussion of theory and application. Stern (1), for instance, considered slurry transport technology in relation to South Africa while Rigby (2) took a wide historical view referring to its early development during the American gold rush in the mid-nineteenth century. Between 1914 and 1924 a 600 m pipeline was employed to pump coal from Thames barges to Hammersmith Power Station. Since then, several modern pipelines have been used for hydraulic conveying in excess of 100 km, e.g.

(i) The Ohio Cadiz coal line, built in 1957 pioneered the large scale (147 km x 254 mm I.D.) hydrotransport of material at high throughputs (1.5 MTe yr^{-1}). It was shut down in 1963 for economical reasons.

(ii) The Black Mesa pipeline, 493 km x 457 mm x 5 MTe yr^{-1} which supplies coal to the Mohave Power Station in Southern Nevada.

(iii) The Brazilian Samarco line 400 km x 7 MTe yr^{-1} used for the transport of iron ore concentrate.

Other materials transported hydraulically include limestone (U.K.), gold slime (Australia, South Africa), phosphate (Canada, South Africa), copper concentrate (Papua-New Guinea), copper tailings (Chile), etc..

Up to the present date the transport of solids by pipelines has mainly been restricted to finely divided materials such as mineral concentrates, crushed coal and china clay, the reason being that fine solids can be readily kept in suspension at low fluid velocities, thus ensuring that pressure gradients, energy consumption and wear can be kept to a minimum. Recent interest, though, has swung towards using pipelines for pumping coarse particles up to 50 mm in size. In an overview of slurry transport technology, Lee (3), looked at various means of transporting coal, ranging from very fine concentrated mixtures for direct combustion, to dilute transport of run-of-mine coal. Run-of-mine coal usually reaches a maximum size of 50 mm, and two alternative approaches to its transportation have been proposed. One is to pump it at low concentration using jet pumps, e.g. for ship loading where there is an abundance of water and the pumping distances are short. However, when water is in short supply it is preferable to use high concentration coarse coal suspensions which have been previously stabilised by the addition of fines. The difficulty here would be to find a high pressure pump capable of handling coarse solids.

Some reviews have focussed specifically upon the theory. Shook (4) compared capsule and slurry transport, noting that capsule transport is technically more advanced despite being a later development. Lazarus (5) presented a break-even curve for the two systems. For a 300 m sand-

pipeline, capsules were favoured when throughputs exceeded 300 kg s^{-1}. Capsules had the advantage that they could be made neutrally buoyant by not filling them completely, whilst slurries were independent of a prefabricated vehicle. Kazanskij (6) presented an especially comprehensive review, listing 37 different empirical correlations obtained between the years 1954-1976 for pressure drop in heterogeneous flow. He concluded that a scale-up criterion based on theory alone would be unreliable through lack of fundamental knowledge about the physics of suspension. Some of the obscurity has been removed by new theoretical developments. These, however, tend to be complex and invariably require the support of a powerful computer, perhaps inaccessible to the pipeline - system design team. Duckworth (7) who reviewed the field at the same time, noted a large number of empirical correlations in more common use than any based purely on theory.

Although the ultimate test of any theory is in its agreement with reliable experimental results, prior theoretical understanding is also necessary. Even in a practical topic like slurry pipelining good theoretical understanding could have favourable economic consequences particularly where long distances are involved.

2.2 Theoretical Aspects of Settling Slurry Systems

2.2.1 Settling suspensions

The main characteristic of the flow of settling slurries is the fact that the solid and liquid phases remain identifiable; there is not, for instance, any increase in the viscosity of the liquid phase on account of its association with the solid particles. The primary objec-

tive is the prediction of head loss as a function of independent design variables. Amongst the important independent parameters for settling slurry systems are pipeline diameter D, operating velocity V_m, mean particle size d, particle size distribution and the properties of the carrier fluid. Kazanskij (6) has provided a guide to the predominant flow regimes, expressed in terms of the particle size alone:

(a) **Homogeneous (d < 40 μm):** the mixture behaves as a single-phase liquid, Newtonian at low solids concentrations and non-Newtonian at higher concentrations. Gravitational forces can be neglected.

(b) **Pseudo-homogeneous (40 μm < d < 150 μm):** under turbulent conditions, the slurry can be transported with a uniform solids concentration across the pipeline, rather like a homogeneous mixture. When allowed to rest, however, it will settle under gravity.

(c) **Heterogeneous (0.15 mm < d < 1.5 mm):** within the range of typical hydrotransport velocities, a solids concentration gradient exists over a cross section of the pipe. Some particles may be sliding along the bed.

(d) **Fully stratified (d > 1.5 mm):** the pipeline contents can be divided into an upper layer of fluid and a lower layer of sliding bed, or "contact layer". Heterogeneous flow is attainable at high velocities only.

Therefore, in determining the flow regime, the velocity of liquid is of great importance. These effects are illustrated in Fig. 2.1a. At

low velocities, no transport occurs and the solids lie in a stationary bed at the pipeline invert, apart from the very fine particles which might be suspended. As the fluid velocity is increased, solids are lifted up in "dunes" and transported from dune to dune in a fashion usually referred to as "saltation". It is not a particularly efficient mode of transport, and there is always the possibility that a dune might block the entire pipeline. Further increasing the fluid velocity initially brings about the heterogeneous regime, in which concentration and size distribution gradients exist over the pipe-depth. Subsequently, in the pseudo-homogeneous regime a strong dependence of head loss on velocity is shown in Fig. 2.1b. Although the minimum point shown may represent a technical optimum, it is usually advisable to run the pipeline at slightly higher velocities. This is to avoid any instabilities which may arise with the system characteristics curve parallel to the pump curve (see Fig. 6.2). Correlations for slurry head loss where the transporting medium is water are often given in the form:

$$i - i_w = f\ (Fr')\ i_w\ C_v \qquad\qquad \dots. (2.1)$$

where

$$Fr' = \frac{V_m}{\sqrt{g}\ D\ (S - 1)} \qquad\qquad \dots. (2.2)$$

C_v = delivered volumetric concentration

S = relative density of solids.

The basis of equation 2.1 is to account for the frictional head loss due to the fluid and that due to the solids. The Froude Fr' number corrected for the relative mass of solids in water, relates the competing effects of inertia and gravity. Fig. 2.1b indicates that head loss

due to particle friction is negligible in the heterogeneous flow regime suggesting that suspended transport is more efficient than sliding transport provided fluid friction f_w can be kept within acceptable limits. For smooth pipes,

$$f_w = \frac{0.316}{Re_D^{0.25}} \quad \text{if } 3000 < Re_D < 100000 \qquad \qquad \text{.... (2.3)}$$

'Blasius equation', or

$$\sqrt{f_w} = 2 \log (Re_D \sqrt{f_w}) - 0.501 \quad \text{if } Re_D > 30000 \qquad \qquad \text{.... (2.4)}$$

'Karman-Nikuradse equation'.

For a given scale of roughness k, f_w can be estimated using the following expression:

$$f_w = 0.25 \, [\log (0.27 \, \tfrac{k}{D} + 5.74 \, (Re_D)^{-0.9})]^{-2} \qquad \qquad \text{.... (2.5)}$$

'Miller (8)'.

Equation 2.5 is only valid for relatively rough pipes as it does not tend to either of the smooth pipe formulae in the limit of zero roughness.

Fig. 2.1c shows that the velocity required to maintain homogeneous flow increases with increasing particle size. The possibility of a stationary bed arises as particle size increases. If the particles are too samll to form stable dunes, then direct transition takes place between a stationary bed and heterogeneous flow. For larger particles,

the transition from stationary to a moving bed takes place at a velocity which is virtually independent of particle size. The transport mechanism in this case is particle "saltation", a phenomenon describing alternate suspension and deposition. The transport of coarse particles has strong economic advantages, especially for coal, and in some cases a moving bed may be the most economic mode. In order to offset the hydraulic restrictions, fines can be added to the solid-liquid mixture to aid the support of the coarse material. The concentration of fines is a direct function of coarse particle concentration and when properly adjusted will produce a stable slurry capable of being pumped in laminar flow. The fines may themselves be transported for an end use or re-routed to the source.

2.2.2 Principles of particle transport

2.2.2.1 Introduction

An understanding of fluid flow in pipelines, though helpful, must be coupled with particle dynamics if settling slurries are to be considered for solids transportation. Principles of classical mechanics, such as dry solid friction, are coupled with three-dimensional "hydrodynamics", so that particles can be considered as suspended objects, subject to drag and lift from the surrounding fluid. The correlations presented in this section provide an insight to these concepts but have limited practical significance.

Regardless of the slurry concentration, mean particle size and distribution, the settling behaviour of a slurry is ultimately governed by the dynamics of each individual particle with respect to its

neighbours, the carrying fluid and the pipe wall. Fig. 2.2 shows the dynamic disposition of a particle situated on the pipe wall and subjected to a pressure gradient enforced by the surrounding medium. Its motion may take the form of either rolling or sliding. If rounded and free of contact with other particles it will tend to roll, otherwise it will be forced to slide along the pipe wall. In the heterogeneous flow regime, the particle population at the wall will certainly be low enough to promote rolling. Rolling promotes lift (Magnus effect) and suspension is aided further. Therefore, it would appear that spherical particles exhibit a sharper transition between sliding and heterogeneous regimes. When a particle is near the pipe invert it experiences a rotation due to the shear of the surrounding boundary layer. The resulting combination of circulation around and relative flow past the particle brings about a lift force F, commonly referred to as the Magnus force which is given by,

$$F = \rho_W \, d \, \Gamma \, \Delta u$$

where ρ_W is the density of carrying fluid, d the particle diameter, Γ is the circulation around the particle and Δu the relative velocity. The circulation around a small particle of arbitrary cross-section is equal to the product of the cross-sectional area and the local fluid velocity gradient in the absence of the particle. For a spherical particle of diameter d in a velocity gradient dV_W/dy therefore

$$F = \rho_W \, \frac{\pi \, d^3}{4} \, \frac{dV_W}{dy} \, \Delta u \qquad \qquad \dots \, (2.7)$$

The strong dependence upon particle size means that for vertical hoisting large objects will tend to migrate towards the pipe axis. For

horizontal conveying it means that the lift to weight ratio is in-dependent of particle size. This can be seen as a possible reason why incipient motion of large particles is independent of their size and explains the transition from a stationary to a moving bed for high particle concentrations in terms of moving dunes of stable form. The Magnus effect may explain the phenomenon of saltation at low concentra-tions. When suspended, fluid drag accelerates the particle to the speed of fluid flow. At this limiting point, relative motion ceases, the Magnus force is eliminated and the particle settles. Conditions for the Magnus effect are restored once again and the whole process may repeat itself. Despite saltation, particles are mostly in contact with the pipe wall and contribute to the total pressure gradient via a solids frictional component.

The Magnus force alone is not capable of sustaining particles in suspension and an alternative lifting mechanism is necessary. This is normally provided by fluid turbulence. Turbulence provides a fluctuat-ing velocity component in the radial direction and can maintain a particle in suspension provided it is substantially greater than the particle's own settling velocity.

The drag force F_D exerted by a fluid on a particle is given by

$$F_D = C_D \frac{1}{2} \rho_W \Delta u^2 A_p \qquad \text{.... (2.8)}$$

where ρ_W is the density of water, Δu is the velocity of the particle relative to that of the fluid, A_p is the area of particle projected on a plane normal to the direction of Δu and C_D is the drag coefficient depending upon the particle Reynolds number, i.e.

$$C_D = C_D \ (Re_d) \qquad\qquad \dots \ (2.9)$$

$$\text{where } Re_d = \frac{\rho_w \ \Delta u \ d}{\mu_w} \qquad\qquad \dots \ (2.10)$$

The drag coefficient C_D which <u>applies</u> when the particle is settling at its terminal velocity V_t in the fluid at rest, has been proposed by Durand and Condolios (24) for correlating results of frictional pressure drop in fluids conveying solids material. It is easily shown that for a sphere of diameter d_v settling at velocity V_t

$$C_D = \frac{4 \ d_v \ g \ (S - 1)}{3 \ V_t^2} \qquad\qquad \dots \ (2.11)$$

For a platelet of cross-sectional area A_p and thickness t settling with its plane normal to the direction of motion (i.e. $\sqrt{A_p} \gg t$), it can be shown that

$$C_D = \frac{2 \ g \ (S - 1) \ t}{V_t^2} \qquad\qquad \dots \ (2.12)$$

The fact that only the thickness of the platelet t appears in equation 2.12 stems from the assumption that the platelet itself is settling with its plane perpendicular to V_t.

Fig. 2.3 illustrates the variation of drag coefficient with particle Reynolds number for the case of smooth spheres and discs.

2.2.2.2 Shape factors

To account for the effect of particle shape is complex beacuse of inadequate methods of defining shape. In the turbulent drag region Worster (9) states that a non-spherical particle orientates itself into the position of greatest drag, (this provides the greatest possible stability), and then follows a sinuous path. An arbitrary definition for an equivalent diameter is required and there are several alternatives.

Godard and Richardson (10) have defined a Galileo number as follows:

$$Ga = \frac{d_a^3 \, \rho_w^2 \, (S - 1) \, g}{\mu_w^2} \qquad \qquad \ldots (2.13)$$

The free falling velocity of an equivalent spherical particle is then calculated from the particle Reynolds number, where

$$Ga = 18 \, Re_{d_a} \quad (if \; Ga < 3.6) \qquad \qquad \ldots (2.14)$$

$$Ga = 18 \, Re_{d_a} + 2.7 \, Re_{d_a}^{1.687} \; (if \; 3.6 < Ga < 10^5) \qquad \ldots (2.15)$$

$$Ga = \frac{Re_{d_a}^2}{3} \; (if \; Ga > 10^5) \qquad \qquad \ldots (2.16)$$

$$and \quad V_{ts} = \frac{Re_{d_a} \, \mu_w}{\rho_w \, d_a} \qquad \qquad \ldots (2.17)$$

This represents the terminal settling velocity of an equivalent sphere which has the same projected area A_p as the particle when viewed

in a direction perpendicular to the plane of greatest stability. The actual settling velocity V_t of a regularly shaped (non-spherical) particle is given by

$$V_t = K\ V_{ts} \qquad\qquad \ldots (2.18)$$

where K is the appropriate velocity correction factor, commonly referred to as the "shape factor". Heywood (11) proposed an empirical parameter based on the projected profile of the particle; the "volumetric shape factor" defined as:

$$K_1 = \frac{V_p}{d_a^3} \qquad\qquad \ldots (2.19)$$

where d_a is the equivalent diameter of a sphere with the same projected area as the particle.

Alternatively, Heywood (12) suggested that an appropriate formula for regular but non-isometric particles is given by

$$K_2 = \frac{Ke}{e_1\ \sqrt{e_2}} \qquad\qquad \ldots (2.20)$$

Ke being the corresponding value of K_1 for an isometric (i.e. equi-dimensional) particle of similar form. The parameters e_1 and e_2 are based on the following particle dimensions:

(i)   The thickness, t, defined as the minimum distance between two parallel planes which are tangential to opposite surfaces of the particle.

(ii) The breadth, b, defined as the minimum distance between two parallel planes which are perpendicular to the planes defining the thickness and tangential to opposite surfaces.

(iii) The length, l, projected on the plane normal to the planes defining t and b, see Fig. 2.4.

The "flatness ratio" is then $e_1 = \frac{b}{t}$ and

The "elongation ratio" is $e_2 = \frac{1}{b}$.

Thus, equation 2.20 becomes

$$K_2 = \frac{Ke\ t}{\sqrt{1\ b}} \qquad\qquad ... (2.21)$$

Tottenham (13) suggested that K_2 should include the actual projected area A_p, i.e.

$$K_2 = \frac{Ke\ t}{\sqrt{A_p}} \qquad\qquad ... (2.22)$$

This is a useful modification for particles whose projected area does not resemble a parallelogram.

Alger and Simon (14), amongst others, have defined a shape factor as

$$K_3 = \frac{t\ d_a}{d_v\ \sqrt{1\ b}} \qquad\qquad ... (2.23)$$

where d_v is the diameter of a sphere having the same volume as the particle.

Heywood (11 and 15) has given values for volumetric shape factors Ke of regular shapes (i.e. sphere, cube, cylinder, tetrahedron, etc.) and approximate values for isometric irregular shapes (i.e. rounded, subangular, and angular). He has also included selected natural particles. Clift, Grace and Weber (16) reviewed Heywood's work and give an empirically correlated velocity factor K_A, for $0.1 < K < 0.4$, fitted at specific values of $N_{d_a}^{1/3}$ as shown in Fig. 2.5a. Since K_A is relatively insensitive to $N_{d_a}^{1/3}$ interpolation for K_A at other values of $N_{d_a}^{1/3}$ is straightforward. The value of K_A is then used in the place of K in equation 2.18.

Wadell (17 and 18) proposed that the sphericity ξ defined as the ratio of the surface area of a volume - equivalent sphere A_v to the actual surface area of the particle A_p could be used to correlate drag on irregular particles. The appropriate dimension for the definition of Ga and Re (equations 2.13 and 2.17) is then d_v. Fig. 2.5b shows velocity correlation factors K_v calculated on this basis (19). This approach has found widespread acceptance although there is experimental evidence that terminal velocity does not correlate well with sphericity (20 and 21). It is more appropriate to use Heywood's approach since many natural particles have an oblate shape with one dimension much smaller than the other two and it is certainly well suited for flat objects such as platelets.

2.2.2.3 Interparticle effects

Interparticle effects will influence the effective drag coefficient. Some particles can experience enhanced drag if they become entrained in the wake of large leading particles. When many particles are falling at different rates they can interfere with one another, leading to a phenomenon known as hindered settling. Normally the rate of settling decreases with concentration, and according to Richardson and Zaki (22) the hindered settling velocity V_t' is given by:

$$V_t' = V_t (1 - C_v)^a \qquad \qquad \dots (2.24)$$

where a is a function of particle Reynolds number Re_d, i.e.

$Re_d = \dfrac{\rho_w V_t d}{\mu_w}$	a
Re < 0.2	4.6
0.2 < Re 1	4.4 $(Re)^{-0.03}$
1 < Re < 500	4.4 $(Re)^{-0.1}$
Re > 500	2.4

C.T. Yang (23) has correlated the critical velocity for incipient suspension to the particle settling velocity by assuming that the logarithmic law for velocity distribution can be applied. The results are shown in Fig. 2.6 and indicate that the critical velocity must be many times the settling velocity for small particles in smooth pipes. When the shear velocity Reynolds number is smaller than 70, the data follow the hyperbola,

$$\frac{V_{cr}}{V_t} = \frac{2.5}{\log \left[\frac{V_\tau \, d}{\nu_W} - 0.06\right] + 0.66} \qquad \ldots (2.25)$$

but it is worth noting that the critical to settling velocity ratio remains constant at 2.05 for fully rough flow of large particles.

2.3   Horizontal Slurry Pipelines

The primary objective is to minimise the power requirements for transporting solids of a given concentration over unit distance. Thus, it is important to be able to correlate the pressure gradient with the independent hydrodynamic parameters.   Durand and Condolios (24) proposed an empirical correlation of the form:

$$\phi = K \, \psi^n \qquad \ldots (2.26)$$

where K and n are constants.   For the experimental conditions in their work, they obtained $K = 150$ and $n = 1.5$.

$$\phi = \frac{i - i_W}{C_V \, i_W} \qquad \ldots (2.27)$$

with   i = hydraulic gradient of slurry

i_W = hydraulic gradient for water alone at the same nominal velocity

$$= \frac{f'_W \, V_m^2}{2 \, g \, D}$$

C_V = delivered volumetric concentration of solids

and $\quad \psi = \dfrac{g\ D\ (S - 1)}{V_m^2\ \sqrt{C_D}}$ $\qquad$ ... (2.28)

Therefore, ϕ represents the normalised difference between slurry and clear liquid hydraulic gradient, whereas ψ is the square of a densimetric Froude number corrected for particle shape by the drag coefficient term. Substituting into equation 2.26 and solving for i we obtain:

$$i = \dfrac{f'_w\ V_m^2}{2\ g\ D} + \dfrac{75\ f'_w\ \sqrt{g\ D}\ (S - 1)^{1.5}\ C_v}{V_m\ C_D^{0.75}} \qquad ... (2.29)$$

The second term which represents the solids frictional effect is inversely proportional to the mean slurry velocity V_m reflecting the fact that suspension flow is more economical than sliding bed.

The slurry velocity which corresponds to a value of minimum hydraulic gradient may be obtained by differentiation of equation (2.29). As a first approximation we may assume that the friction factor f'_w is practically independent of velocity. This leads to:

$$V_{cr} = \dfrac{5.3\ \sqrt{g\ D\ (S - 1)}\ C_v^{0.33}}{C_D^{0.25}} \qquad ... (2.30)$$

Below the critical velocity, in the sliding bed regime, equation 2.29 no longer applies. Fig. 2.7 provided by Durand and Condolios (24) shows the effect of particle size upon the deposition velocity, for solids concentration between 2 and 15 v/o. The decrease in V_{cr} with particle size which is observed between about 0.5 and 1.2 mm at high C_v could be the result of an increase in freedom of movement as the number of particles is reduced.

Newitt, Richardson et al (25) have developed their own correlation for horizontal pipe flow. With the assumption of no slip between the solid particles and water in the direction of flow, Newitt theoretically derived the following equation:

$$\frac{i_h - i_w}{i_w \, C_v} = \frac{K \, g \, D \, V_t \, (S - 1)}{V_m^3} \qquad \ldots (2.31)$$

By correlating the accumulatd data from tests on fine coal, perspex and sands flowing down a 25.4 mm I.D. pipe in water suspension, they obtained a value of $K = 1100$.

Newitt's equation applies for closely-graded particles in heterogeneous suspension, though it may be applied to the transport of mixtures of widely differing sizes with some loss of accuracy. Equation 2.31 has been found to be compatible in reliability with that of Durand and Condolios.

Over the years, many researchers have proposed modifications to the empirical constants in equations 2.26 and 2.31 so that the correlations will fit their own experimental data. Zandi and Govatos (26) collated over 2500 points from various sources and compared three existing heterogeneous correlations with the data. They claim that the Durand equation was by far the best but they have suggested three mutually exclusive correlations of their own:

Homogeneous flow regime

$$\phi = 81 \, \psi^{1.5} \quad ; \quad \psi^{-1} < 40 \, C_v \qquad \ldots (2.32)$$

Heterogeneous flow regime,

$$\phi = 280 \, \psi^{1.93} \quad ; \quad 40 \, C_v < \psi^{-1} < 10 \qquad \qquad \ldots (2.33)$$

$$\phi = 6.3 \, \psi^{-0.354} \quad ; \quad \psi^{-1} > 10 \qquad \qquad \ldots (2.34)$$

Thus, at high velocities, (i.e. equation 2.34), it would appear that collisions between the particles might contribute to an increasing turbulence leading to higher friction gradients ϕ than would be normally expected. In addition, equation 2.34 provides a better transition from pseudo-homogeneous into the homogeneous flow regime than equation 2.32, which neglects the contribution of solids to the effective slurry density.

For large particles the sliding bed regime may be the only economic mode of operation. Newitt et al (25) offered a separate expression for the case of bed deposit flow:

$$\frac{i_s - i_w}{i_w \, C_v} = \frac{66 \, (S - 1) \, g \, D}{V_m^2} \qquad \qquad \ldots (2.35)$$

Owing to the large size of particles, fully rough, turbulent flow, may be assumed for which the Darcy friction factor f'_w based on the slurry velocity is virtually constant. Therefore, equation 2.35 may be re-written as:

$$i_s - i_w = 33 \, f'_w \, C_v \, (S - 1) \qquad \qquad \ldots (2.36)$$

which indicates that the head loss due to solids is independent of either pipe diameter, or slurry velocity or particle drag coefficient.

Under these conditions it is best to replace the fluid friction factor f'_W in equation 2.36 with a coefficient of solid friction, since the particles are merely dragged along the bottom of the pipe. Wilson et al (27) have done so by replacing "33 f'_W" in equation 2.36 with

$$"2 \ f_S \ [\frac{\sin (\theta) - \theta \cos (\theta)}{\pi}]"$$

where f_S is the friction coefficient between the particles and the pipe wall and θ is the angle of deposit (see Fig. 6.9). They used the bed slip model approach which is based on an analysis of hydrostatic type forces acting on a bed of particles within a conduit. Babcock (28) in an independent investigation of a sliding bed, has concluded that the incremental head loss is proportional to the volumetric concentration only in the fully developed sliding bed flow regime. This was later confirmed by Chhabra and Richardson (29). Babcock and Richardson used sand slurries of up to 40% by volume; they found a good fit between equation 2.36 and their experimental results when insignificantly small adjustments were made on the coefficient.

Apart from the empirical correlations discussed earlier, a theoretical approach initiated by Wilson and Watt (30) have produced a number of mathematical relationships based on fundamental principles. Firstly, they pointed out that the influence of turbulence in the suspension of solids ought to be taken into account in scaling up pilot - plant data as its effect is a function of pipe size. Using a Prandtl mixing length for the definition of the scale of turbulence, they suggest that comparatively large particles will dampen the effective vertical velocity fluctuation Ve, whereas small particles will not. Since the pipe diameter is the upper limit of mixing length the ratio

d/D must be a significant factor in Ve. The final result (equation 2.37) shows the effect of d/D on the threshold velocity for the initiation of turbulent suspension V_{th} in terms of particle settling velocity V_t:

$$\frac{V_{th}}{V_t} = 0.6 \sqrt{\frac{8}{f'_w}} \exp\left[\frac{45\ d}{D}\right] \qquad \qquad \ldots (2.37)$$

where the empirical constants have been fitted mainly on the data provided by Babcock (28). Wilson (31 and 32) developed this concept further into a unified analysis for pipeline flow by considering separately the effects due to suspended and contact load respectively. Although to date it has not received sufficient attention, possibly due to difficulty of interpretation, it remains a powerful design tool capable of handling a wide particle size distribution. Clift et al (33) have used this method for scaling mixed regime slurries in the pseudo-homogeneous and bed load regimes. They distinguished between the head loss gradient for the pseudo-homogeneous component i_h and the contact load component i_s with a fraction R of solids conveyed as a stratified load, i.e.

$$i = R\ i_s + (1 - R)\ i_h \qquad \qquad \ldots (2.38)$$

equation 2.38 after substituting i_h from equation 2.31 with $A = \dfrac{K\ g\ D\ V_t}{V_m^3}$ and i_s from equation 2.36 with $B = 33\ f'_w$, may be written as

$$\frac{i - i_w}{C_v\ (S - 1)} \equiv \frac{i - i_w}{S_m - 1} = B\ R + A\ i_w\ (1 - R) \qquad \qquad \ldots (2.39)$$

where S_m is the ratio of the mean slurry density to that of the liquid. B and A are properties of the slurry in fully stratified and pseudo-homogeneous flow respectively. The parameters A, B and K have to be determined, where

$$R = [\frac{V_{th}}{V_m}]^m = K \, V_m^{-m} \qquad \ldots \ (2.40)$$

and V_{th} is defined by equation 2.37. For hetero-dispersed materials, m should be treated as a property of the slurry to be determined by tests; typical test results giving a value of m close to 1.7. Substituting equation 2.40 in equation 2.39 gives:

$$\frac{i - i_w}{S_m - 1} = K \, B \, (V_m)^{-m} + A \, i_w \, (1 - K \, V_m^{-m}) \qquad \ldots \ (2.41)$$

Alternatively using Fanning's equation together with equation 2.40 in equation 2.39 we obtain:

$$\frac{f_m - f_w}{S_m - 1} = A \, f_w + \frac{K}{2} \, B \, D \, g \, V_m^{-(m + 2)} - K \, A \, f_w \, V_m^{-m} \qquad \ldots \ (2.42)$$

A may be obtained from Fig. 2.8a.

B may be obtained from Fig. 2.8b.

The value of $\frac{i - i_w}{S_m - 1}$ may be found from equation 2.41 for $V_m > V_{th}$, otherwise it is taken as equal to B. Clift's method has been tested for two types of sand (foundry d_{50} = 290 mm, masonry d_{50} = 420 mm) as well as for crushed granite (d_{50} = 680 mm) in two pipe sizes (viz. 440 mm I.D. and 203 mm I.D.). However, the approach remains mechanistic.

From all the correlations considered in this section, Durand's formulation (equation 2.26) is perhaps the most commonly used. It seems to fit the widest range of data, it is attractively simple and can be adjusted in ways which make physical sense.

2.4   Vertical Slurry Pipelines

Vertical pipeline flow of slurries is reasonably well understood and simpler to correlate. Worster and Denny (34) suggested that the pressure gradient in excess of the static lift resulting from vertically rising flow is the sum of two effects: the friction pressure gradient and the pressure gradient due to the weight of solids being hoisted. For a unit length of pipe the former is given by i_w whilst the latter (effectively a static head) equals C_v (S - 1), i.e.

$$i = i_w + C_v \ (S - 1) \qquad \qquad \ldots \ (2.43)$$

As a result of free settling, particles conveyed upwards in a vertical pipe, (see Fig. 2.9 pipe section I), move with an average velocity $V_{wu} - V'_{tu}$. This leads directly to an increase in the local concentration of solids. Furthermore, the fluid velocity V_{wu} is expected to exceed the mean slurry velocity V_m so that momentum is conserved.

In contrast, particles travelling downwards with a vertical fluid stream (Fig. 2.9 pipe section III) will exceed the fluid velocity V_{wd} by their slip velocity V'_{td} making the net downward translation particle velocity $V_{wd} + V'_{td}$. Since the hindered settling velocity $V'_{t(u,d)}$ is particle concentration dependent, the values of V'_{tu} and V'_{td} will differ in magnitude.

Worster (35) has derived an expression to deduce approximately the in situ concentration C_{vu} in a vertically rising flow from the delivered concentration C_v:

$$C_{vu}^2 + C_{vu} \left[\frac{V_m}{V_t} - 1\right] - C_v \frac{V_m}{V_t} = 0 \qquad \ldots (2.44)$$

If the particle settling velocity is small compared to the mean slurry velocity, C_{vu} approximates to the value of the delivered solids concentration.

Bain and Bonnington (36) have altered equation 2.43 slightly to account for the fact that the water velocity V_{wu} is greater than the mean slurry velocity V_m, i.e.

$$i = i_w \left[\frac{V_{wu}}{V_m}\right]^2 + C_v (S - 1) \qquad \ldots (2.45)$$

Newitt et al (37) pioneered the correlation of pressure drop for vertical solids transport and developed the following correlation from tests with sand, sircon, manganese dioxide and perspex particles in 13 m x 25 mm and 8 m x 50 mm columns:

$$\frac{i - i_w}{i_w C_v} = 0.0037 \sqrt{\frac{g\,D}{V_m^2}} \left[\frac{D}{d}\right] S^2 \qquad \ldots (2.46)$$

To enable comparison with correlations for horizontal pipes (see equation 2.26), equation 2.46 has been written as follows:

$$\phi = 0.0037 \, Fr^{-1} \left[\frac{D}{d}\right] S^2 \qquad \ldots (2.47)$$

where

$$Fr = \frac{V_m}{\sqrt{g\ D}} \qquad \qquad \dots (2.48)$$

It is interesting to note the strong dependence upon relative density, the inclusion of the pipe to particle diameter ratio and the absence of particle drag coefficient. Increasing the specific gravity S would lead implicitly to an increase of the in situ solids concentration, thus providing a reason for the high power. Unlike equation 2.26, the head loss due to vertical transport is a decreasing function of particle diameter, suggesting that coarse particles contribute less friction. This could be explained in terms of the Magnus force which would move large particles away from the pipe wall. Such particle migration would produce a high concentration in the pipe core thus reducing particle - wall collisions. Newitt et al (37) used materials in the size range 0.1-3.0 mm and observed that the fine particles were transported in a homogeneous manner whilst coarse particles formed an axial core surrounded by a clear water annulus. The head loss in this case was very close to that produced by the carrier fluid alone.

Wilson et al (38) in a study of friction mechanisms at high volumetric concentrations (about 50%) carried out experiments with 0.3-1.7 mm sand in a 25 mm I.D. pipe rig. They confirmed earlier observations by Newitt and showed that at high solids concentrations interparticle collisions were greatly restricted, thus contributing little to the overall head loss. In a comparison of specific energy consumption in dilute (up to 25 v/o) and dense phase (up to 50 v/o) conveying of solid - water mixtures, Streat (39) recommended dense phase vertical transport of coarse particles. He considered two pipeline diameters, (76 mm and 305 mm) and suggested the use of indirect means for pumping (i.e. lock hopper or tube feeders).

In an earlier investigation, Streat et al (40) provided a separate equation to predict the hydraulic gradient in a vertical pipe in dense flow, i.e.

$$i = (C_v (S - 1) + 1) (1 + i_w) \qquad \qquad \dots (2.49)$$

In essence, equation 2.49 states that total hydraulic gradient is the sum of gravitational and frictional components based on the slurry density.

2.5 Pipeline Inclination and Blockage

While vertical pipelines for solids transport are of direct interest in the mining and dredging industries, long distance transport depends mostly on sloping lines to negotiate rugged terrain. The degree of inclination employed will normally determine the likelihood of blockage during shut-down. In order to re-establish the slurry flow after shut-down, Wood (41) found that pressure gradients twice as high as those at the deposit velocity are often required. In addition, if the heterogeneous regime cannot be restored at once, saltation may lead to the formation of dunes and to more serious blockages. In the event of plug formation considerable pressure gradients are required to overcome the static friction.

Okada et al (42) have considered plugs forming at the bottom of a sloping pipeline and have shown that higher pressures are required to dislodge them when the flow is downwards rather than upwards. This apparent paradox can be explained in terms of the relative position of fines and coarse particles after shut-down. At the point of shut-down,

large particles settle out first and are overlaid by the fines. This situation would afford a more effective plug to downward flows. Clearly then, any pipeline inclined beyond the solids sliding angle is liable to such a blockage. Unfortunately, solids momentum effects reduce the value of the 'dynamic' sliding angle for downward flows below the 'static' sliding angle which is about 30 . Therefore, a further limitation is imposed having a notable impact on the construction costs. In practice, operating slopes of up to 10-15% are thought to be safe.

In an experimental investigation of natural materials, transported in sloping pipelines, Kao and Hwang (43) found that for upward slopes the pressure gradient first increased with slope, reached a maximum and then fell away near the vertical position. Increasing the pipeline slope enhances the degree of particle slip resulting in a higher in situ concentration. Near the vertical, however, solids tend to form a centre core and losses are considerably reduced through lack of particle-wall interaction. Therefore, a combination of horizontal and vertical sections could offer a good steady state with better restart characteristics than an equivalent sloping line. The entire contents of a sloping line are likely to slump into an extensive plug at the bottom, whereas the smaller volume within the equivalent vertical leg ought to be less serious.

Worster and Denny (34) have shown that the increase or decrease of pressure gradient in an inclined pipe due to the presence of solids is the vectorial sum or difference of the excess gradients due to the solids in the corresponding horizontal and vertical pipes joining the same end points. This is to say that the increase or decrease in the pressure drop in the inclined pipe due to the solids is equal to the

algebraic sum of the pressure drop increase due to solids in the corre-
sponding horizontal and vertical legs of pipe as shown in Fig. 2.10.

Stationary Bed (A)

Moving Bed (B)

Heterogeneous Flow (C)

Homogeneous Flow (D)
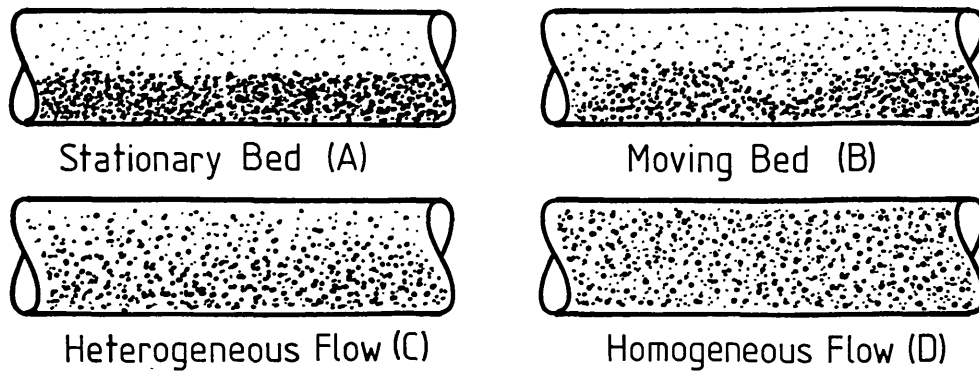
(a) Flow patterns
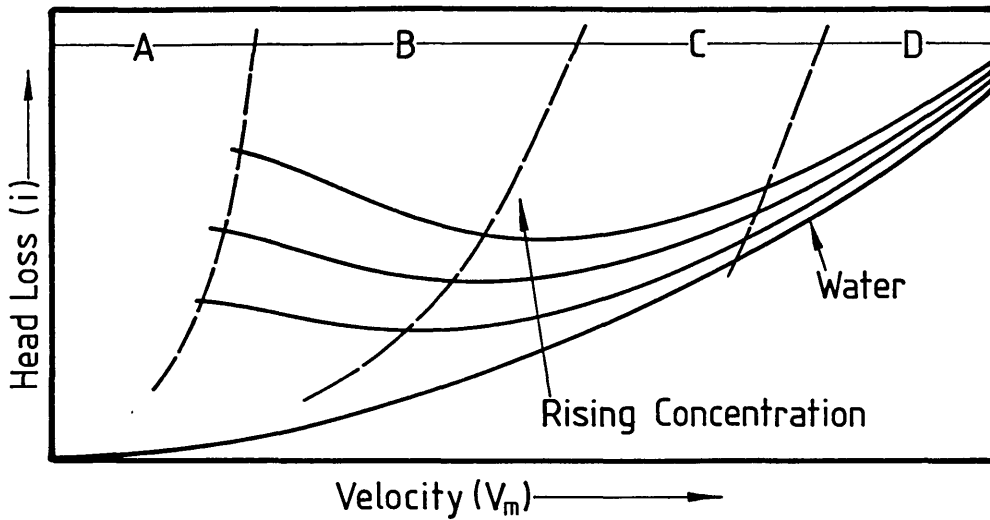
(b) Effect of solids concentration
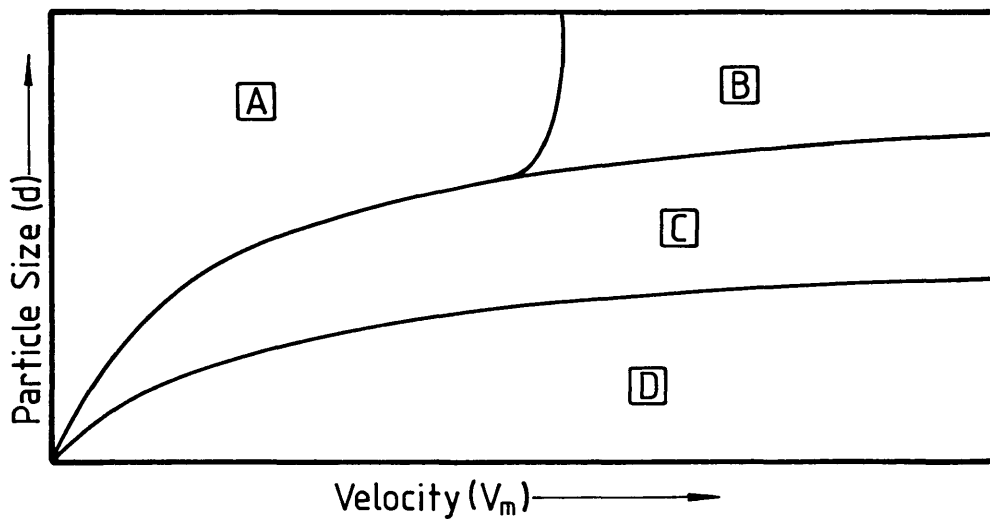
(c) Effect of particle size

Fig. 2·1

Flow regimes for pipe flow of settling slurries
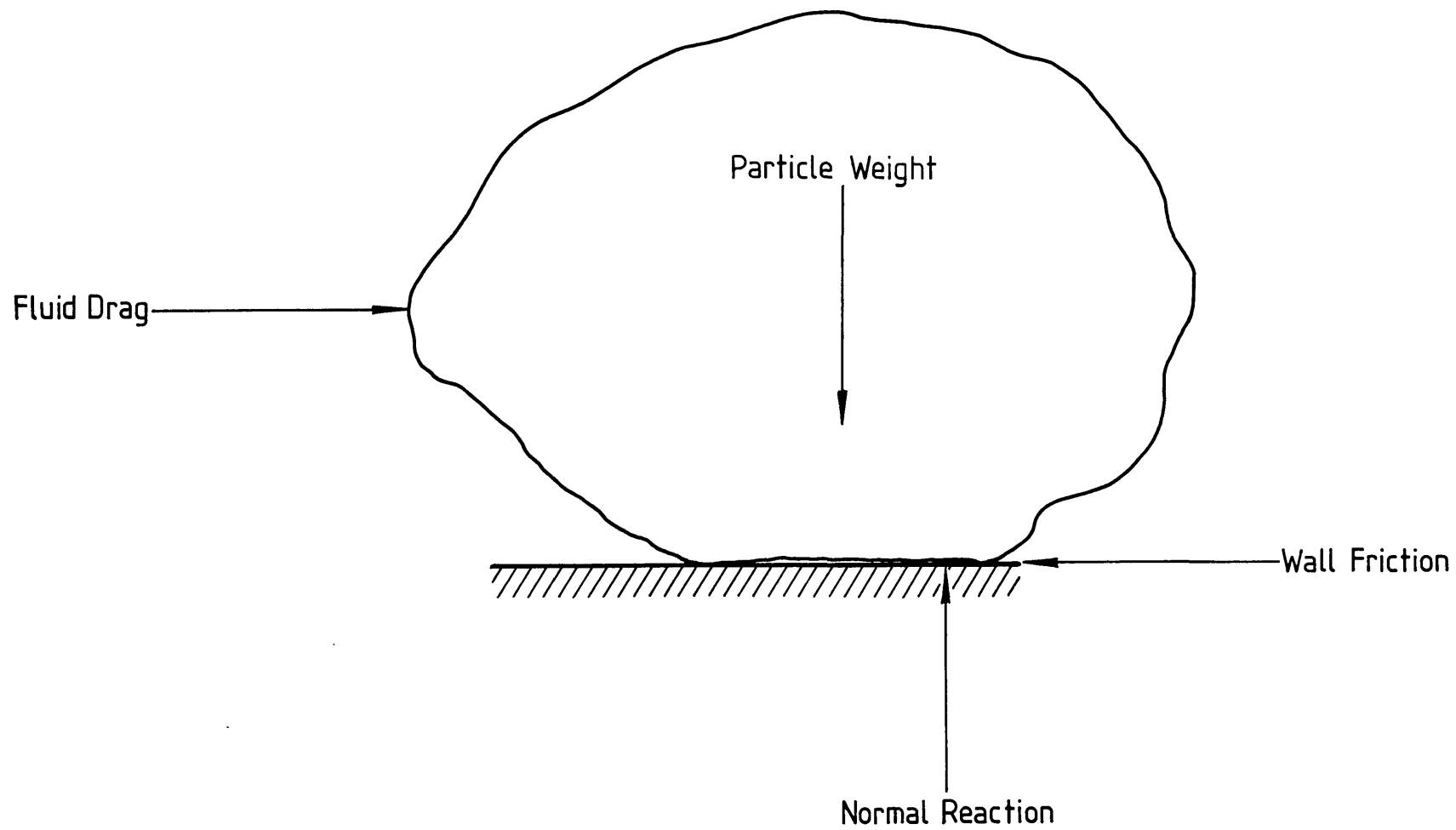
Fig. 2·2   Forces acting on a settled solid particle
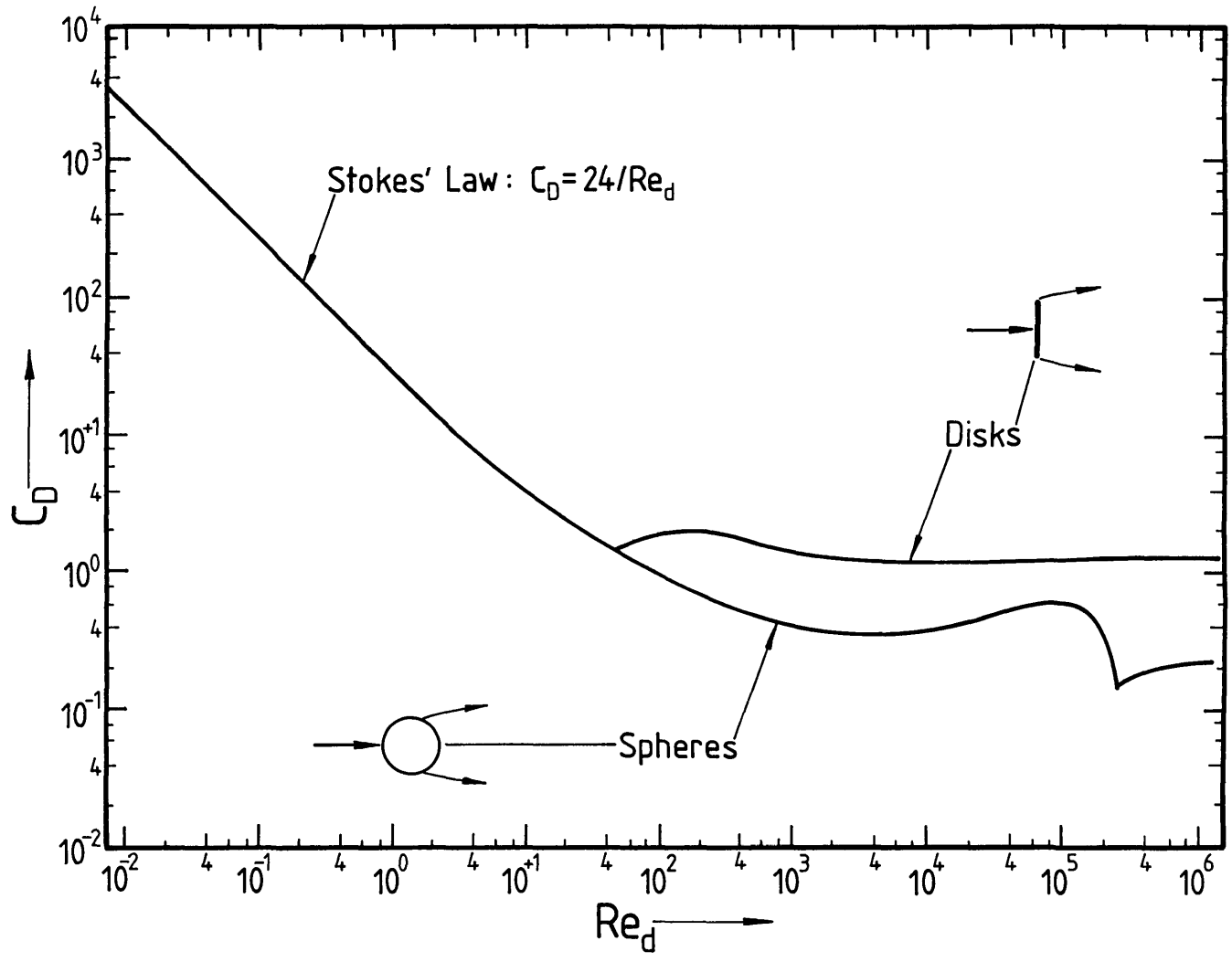
Fig. 2·3

Drag coefficients for various particle Reynolds numbers
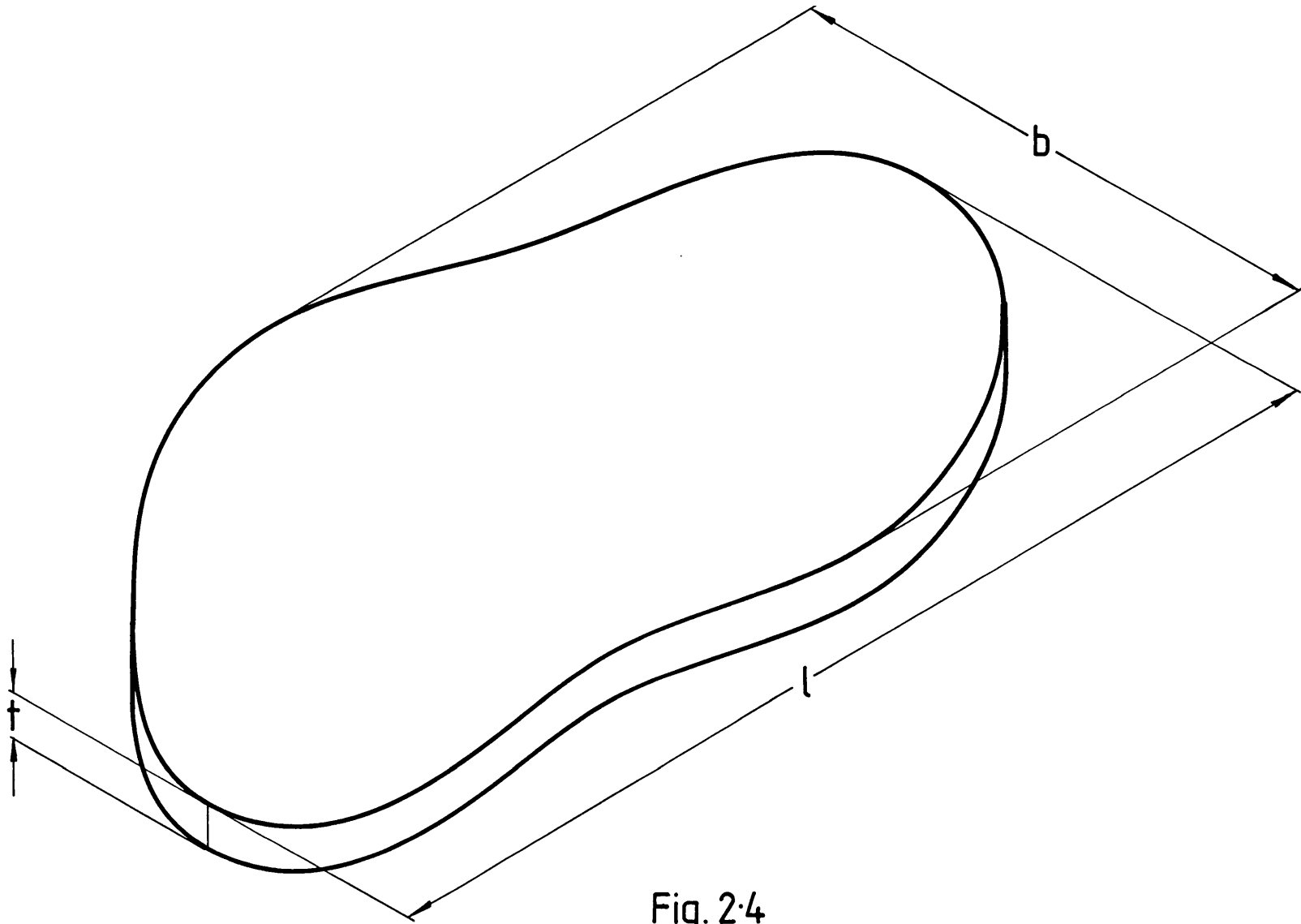
Fig. 2·4

Length, Breadth and Thickness definitions for a platelet

$N_d^{1/3}$	K_A (0·1 < K < 0·4)
1	$0·1040 + 1·538K$
$10^{1/2}$	$0·1270 + 1·526K - 0·10K^2$
10	$0·1975 + 1·575K - 0·45K^2$
$10^{3/2}$	$0·1660 + 1·496K - 0·30K^2$
100	$0·0665 + 1·907K - 1·05K^2$

Table of correlations for K_A
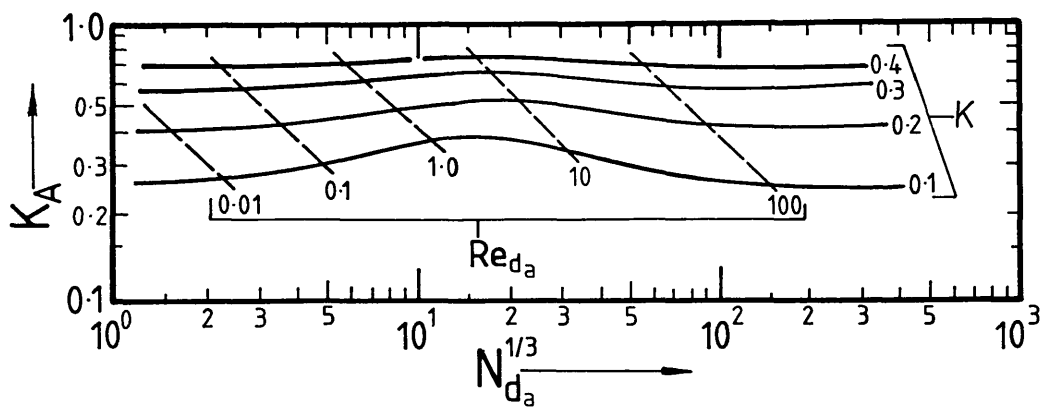
(a) Sphere area equals particle area (projected)
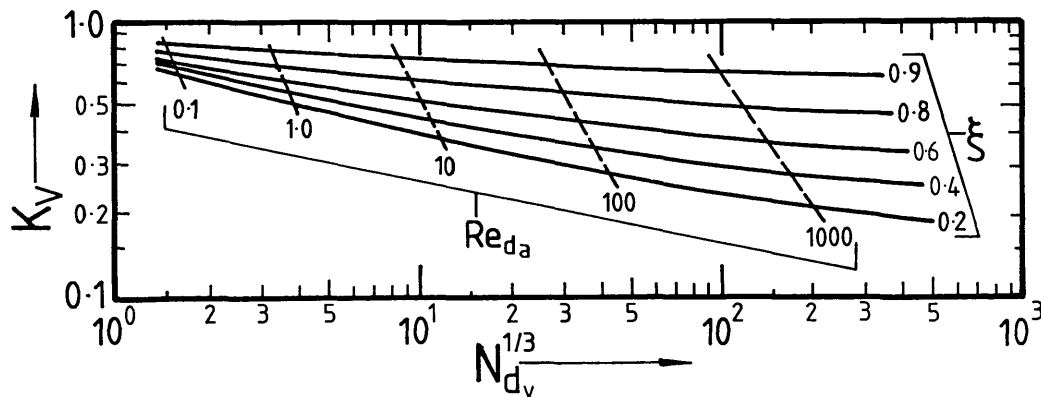
(b) Sphere volume equals particle volume

Fig. 2·5

Graphical presentation of velocity correction factors K_A and K_V

$$V'_{cr} = V_{cr}/V_t$$

$$Re_0 = \frac{d}{\mu_w}\sqrt{T_0\rho_w}$$
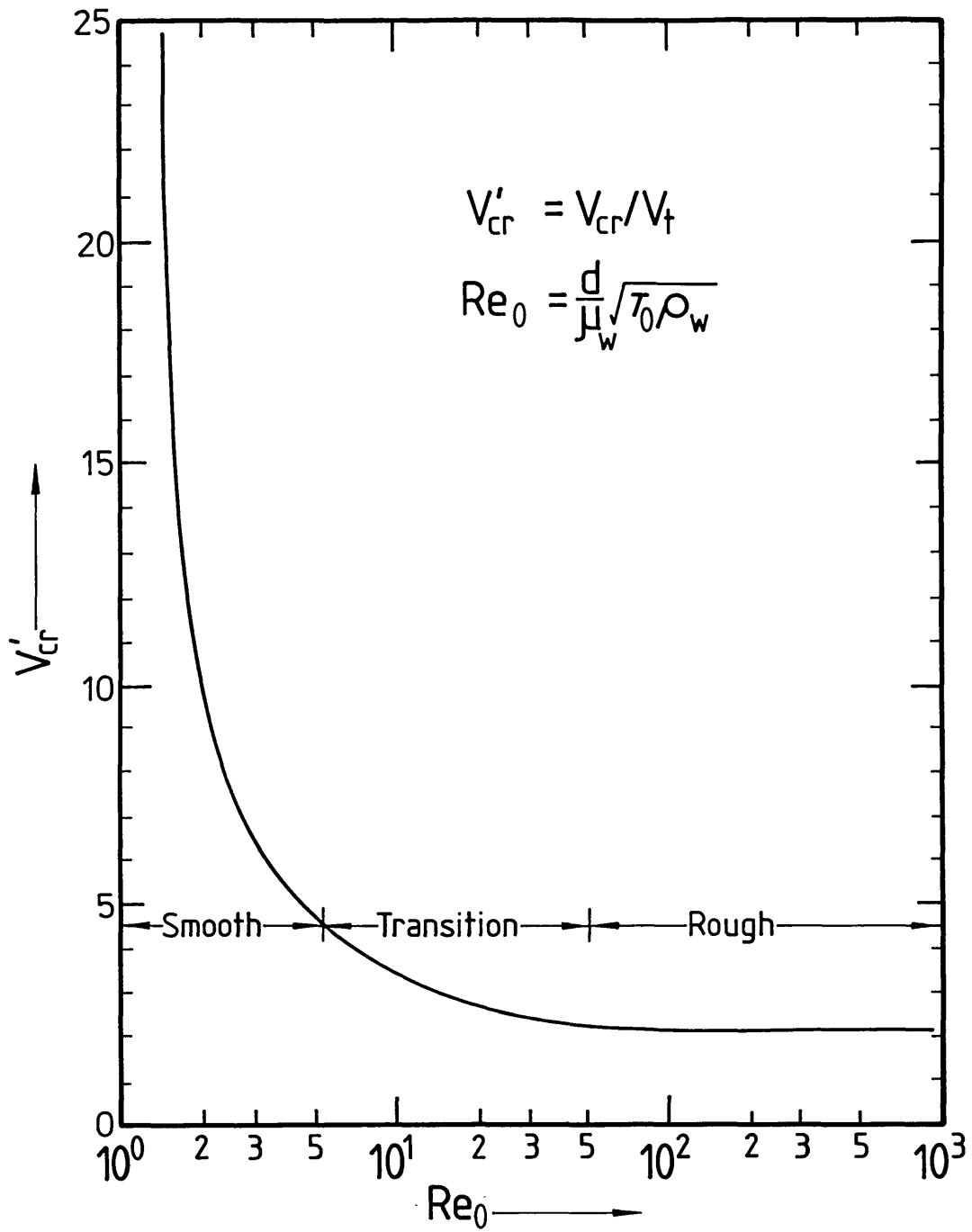
Fig.2·6

Critical velocity versus shear particle Reynolds number
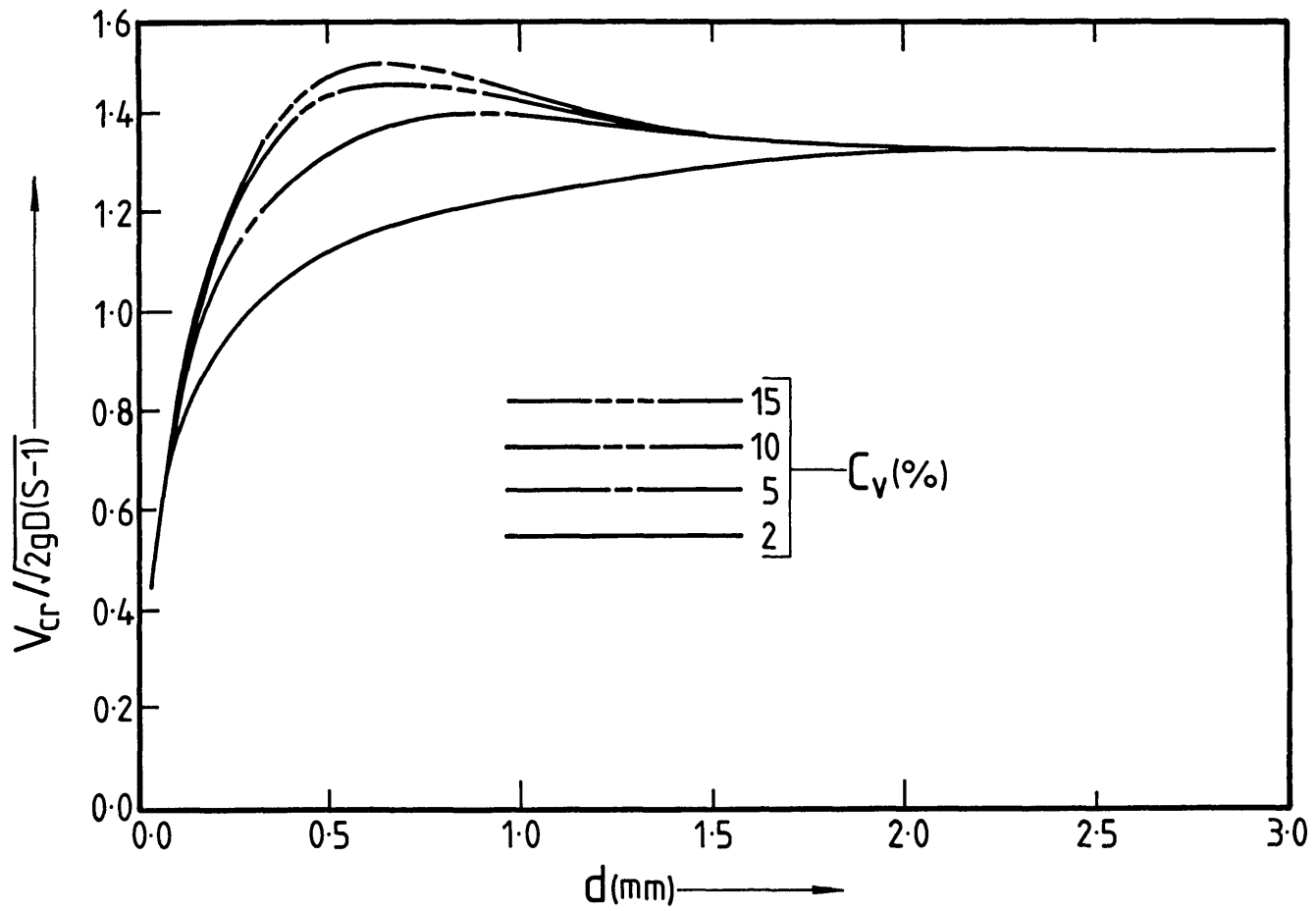
Fig. 2·7

Critical Froude number versus particle size and concentration by volume
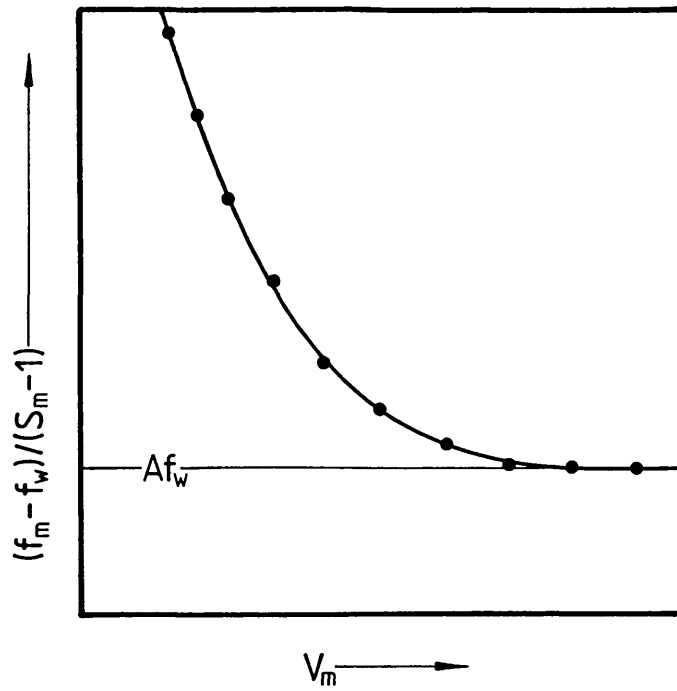
(a) Fully suspended flow
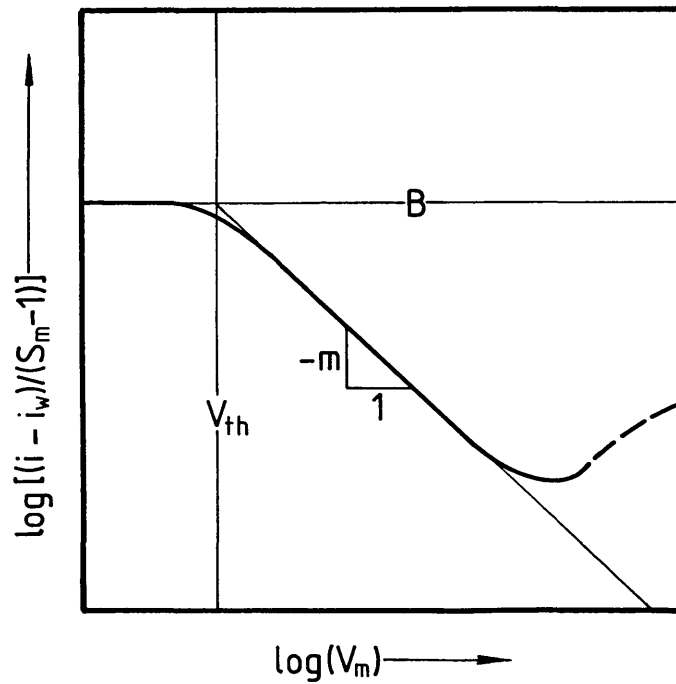
(b) Heterogeneous flow

Fig. 2·8

Graphical determination of solids effect constants A and B
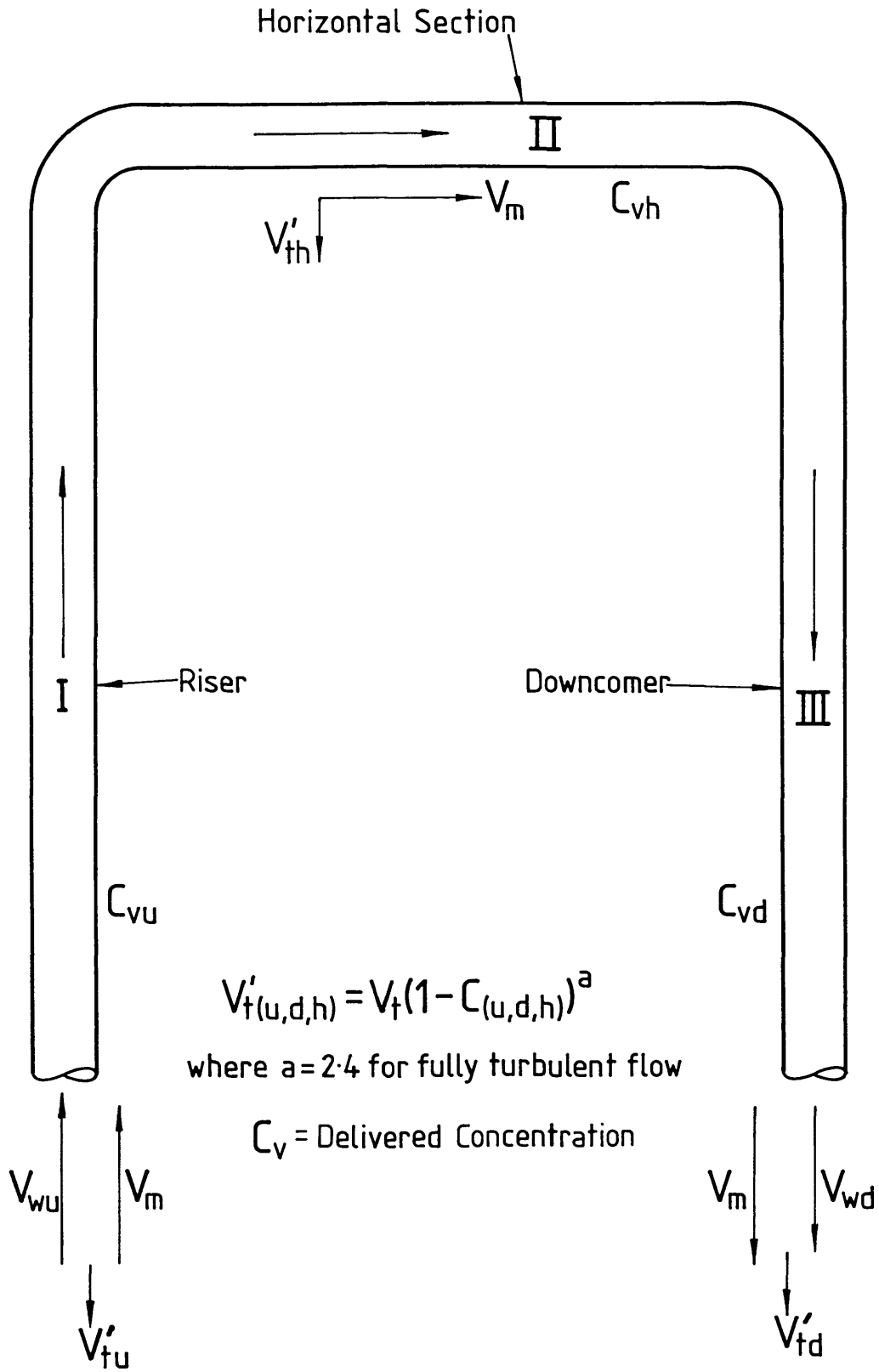
Fig. 2·9

Effect of flow direction on in situ suspended solids concentration
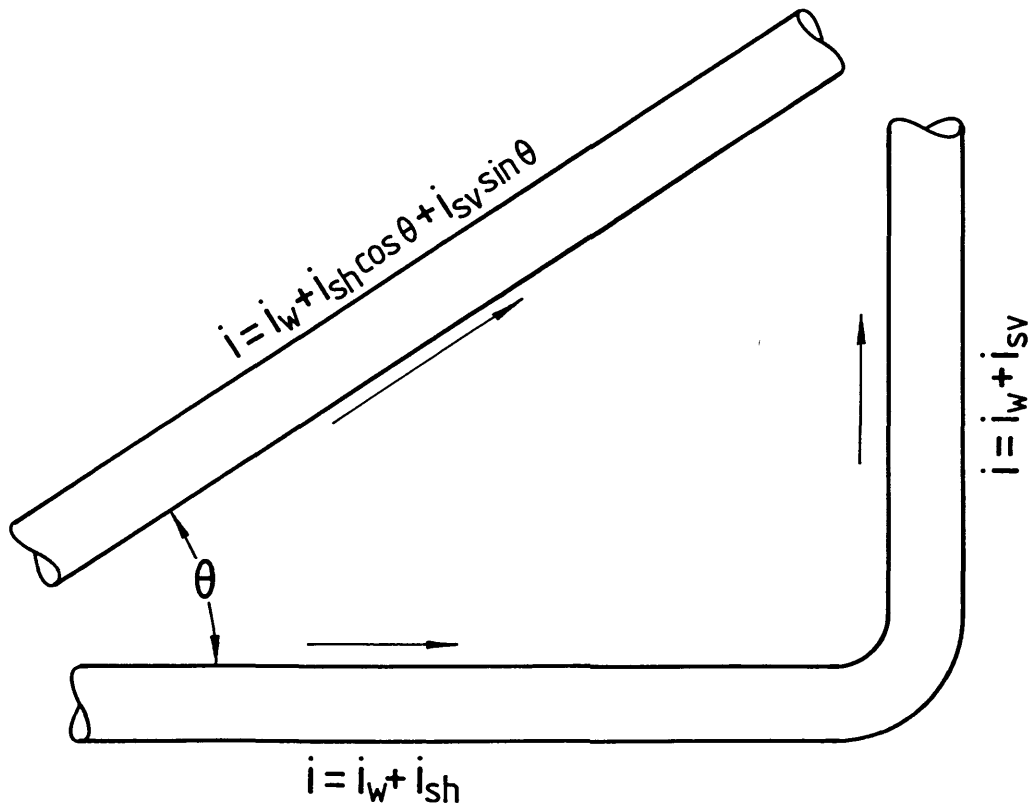
Fig. 2·10

Flow in inclined pipes

3. EXPERIMENTAL

3.1 Description of Apparatus for the Characterisation of Aluminium Platelets

A 3 m glass column with internal diameter 4" (=101.6 mm) was used to determine the terminal velocities of individual aluminium platelets, clusters of sand and other objects. The column was erected vertically and a 4" to $1\frac{1}{8}$" (=28.8 mm) reducing section was connected to the lower end, see Fig. 3.1. A $1\frac{1}{8}$" Quickfit glass tap was bolted to the bottom of the reducing section. This enabled water to be drained from the system and thus made it possible to retrieve the particles.

Accurate determination of the free fall velocity of small - particles required the design and installation of an electrical timing mechanism. Two photodiode arrays mounted on to the column wall 2 m apart and each located directly opposite a point source of ordinary light acted as sensors. More than three column diameters (= 304.8 mm) separated the water surface from the upper array. This distance, calculated in Appendix A, is intended to allow particles released from rest to accelerate to terminal settling velocity before timing commences. If a descending particle crosses the light sensitive areas (sensors 1 and 2) an electronic timer is operated for that period. The time taken by the particle to travel between the two trigger levels is then displayed to the nearest millisecond. For maximum trigger sensitivity the timing device is best operated in a dark room. Sensitivity is a function of the quality of shadow projected by the descending particle on to the photodiodes.

In addition to the timing mechanism, a magazine was designed and fitted directly above the mouth of the column to control the release of particles (see Fig. 3.2 and Plate 3.1). This consists of two aluminium discs (8" = 203.2 mm DIA each) mounted centrally on to a vertical shaft which is directly driven by a small electric motor and gearbox. The upper disc (loading disc) is $\frac{1}{4}$" (= 6.35 mm) thick and contains 15 holes, 1" (= 25.4 mm) DIA which are evenly distributed along a peripheral annulus. This disc is made to rotate against a $\frac{1}{8}$" (= 3.175 mm) thick disc which is fixed and carries only one identical hole at the same radial distance. The magazine is coupled to the glass column so that the column axis is parallel to the driving shaft, and the hole in the lower disc is concentric with the top of the column. A gap of only a few centimetres separated the magazine from the water surface. Therefore, if actuated, the magazine will cause particles to be released at the axis of the pipe.

A third aluminium disc ($\frac{1}{8}$" thick x 2" DIA), the guide disc, which is mounted in the middle section of the driving shaft is used to control the magazine advance. Fifteen 2 mm DIA holes spaced equally around the perimeter make the guide disc a replica of the loading disc. The peripheral annulus containing the holes is then made to rotate through an infra-red beam set up by a photocell which is fixed on to the superstructure. When the beam is broken the motor remains activated and turns the shaft until the next hole is encountered. The beam is then made, the motor-circuit breaks and the cartridge stops. The system may be reset from ground level by pressing the 'call for next particle' button. The guide and loading discs are offset so that each pass clears the dispensing hole. With the aid of a variac control, the speed of rotation was kept to a minimum (i.e. loading-disc just turning), thus making it possible to approximate a 'release from rest situation'.

Finally, the column was fitted with a water mains supply in order to top-up after each particle retrieval.

3.2   Description of the 4" I.D. Hydraulic Conveying Rig at Winfrith

A flow diagram of the rig at Winfrith on which horizontal and vertical pressure measurements were made is shown in Fig. 3.3. An isometric view of the rig is presented in Plate 3.2. All the metal pipework was made of commercial grade mild steel (B.S. 3601-410) with an average internal diameter of 4.07" (= 103.5 mm) and 5.4 mm wall thickness. Flexible plastic tubing, (or bellows), of the same I.D. was used at four points in the circuit to provide smooth bend connections for the steel piping. Pressure tapping points were provided at various intervals along the metal pipework as shown in Fig. 3.3.

The feed tank was partitioned in the middle by a steel mesh which passed water but retained solids, i.e. aluminium platelets. Thus, solids were kept in one half while the other fed clear water directly into the conveying loop. A steel gate located at the base of the solids-containing section enabled control of the rate at which aluminium was added to the circuit. The gate aperture could be adjusted by means of a screw-thread operating wheel as shown in Plate 3.2. It should be noted, however, that even with the gate-wheel in the fully shut position, there was always a nominal gap of about 15 mm.

A Wemco torque flow pump model F4 was used to pump the slurry mixture. This pump had a top rotational speed of 1,500 r.p.m., was capable of 10 hp and operated on a three-phase supply (i.e. 415 V at 50 Hz). By varying the pulley size on either pump or motor shaft it is

possible to preset the pump rotational speed, thus setting the maximum available manometric head. This facility can be very useful when a speed-variac control is not installed and flow regulation is operated by means of a by-pass valve.

During the course of this work three different motor/pump pulley combinations were tried:

MOTOR PULLEY DIAMETER / (mm)	PUMP PULLEY DIAMETER / (mm)	PUMP ROTATIONAL SPEED / (r.p.m.)
1. 140	160	1260
2. 200	315	915
3. 160	315	732

While provision was also available to change the pump impeller only one size 280 mm DIA was used throughout these experiments. There are several advantages in using a torque-flow pump with platelet type material. Fig. 3.4 shows how the recessed design of the shaft and impeller ensure that long or tangled items can be transferred without risk of fouling the rotating parts. The continuous open flow passage ensures that degradation and wear on both pump and particles are kept to a minimum. This greatly increases pump lifetime without loss of performance.

Two Tee-Angle-Bends were used as means of branching-off the short section leaving the pump. These provided three possible outlets shown as points A, B and C in Fig. 3.3 and each was fitted with the 4" lever

operated plug valve at the downstream end. The solid/liquid mixture passed through the main valve A which formed the base of the vertically rising section. Although this valve could be used as a coarse control of flow rate its main function was to shut-down the circuit so that the pump was never started under full load conditions. In addition, a bypass valve B was located immediately downstream of the pump. When this valve was opened, the loop was short-circuited and up to one half of the total flow could be bypassed directly into the feed tank. Valve C was normally kept shut but could be used as a second bypass. In practice, this route offered the path of least resistance to the flow. Under normal operating conditions this was quite undesirable; nevertheless, it proved very useful for clearing away blockages forming between A and B. The total length of pipeline was about 35 m. Slurry returned to the tank through a flexible pipe and down a chute. When required the bellows could be removed from the chute and the slurry allowed to fill a 250 l plastic sampling vessel. In this way, the mean slurry rate as well as the delivered solids concentration could be measured; the sample was subsequently returned to the main tank.

The rig included a 4" I.D. Kent magnetic flowmeter and two differential-pressure measuring devices. These instruments are discussed in the following sections.

3.2.1 Measurements

3.2.1.1 Frictional pressure gradient - horizontal leg

Two pressure tappings 11.96 m apart were available on the horizontal test section of the rig. The upstream tapping was positioned

well over ten pipe diameters (= 1.04 m) away from the bend immediately preceding the horizontal pipe, so that end effects were negligible. Two Bell & Howell type BHL-4050 strain gauge transducers were used. For maximum possible sensitivity the upstream and downstream units had a useful operational range of only 3 bar (= 44.085 psi = 3×10^5 Nm^{-2}) and 2 bar (= 29.39 psi = 2×10^5 Nm^{-2}) respectively; they were both calibrated in psi. The transducers were very sensitive to pressure surges caused by the sudden closure of an on-line valve. During the course of the experiments one such incident damaged the upstream transducer which was replaced by a 5 bar unit. Each transducer arrived on site already calibrated together with a digital display unit incorporating the signal amplifier and the Wheatstone-Bridge balance circuit. Voltage signals produced in each device were displayed both individually and also in a backed-off manner through a channel of a multi-pen chart recorder. Thus a direct indication of the differential pressure drop along the horizontal test section was established. A 0.1 mV strong signal caused a mechanical displacement of 0.1" (= 2.54 mm) on the recording pen. This was equivalent to 0.1 psi (= 6.895×10^3 Nm^{-2}).

Steady flow was established in the circuit prior to taking a pressure drop reading. When a sample was about to be taken the chart recorder speed was increased from 0.5 min cm^{-1}, (usual idling speed), to 6 sec cm^{-1}, a pencil mark was made on the chart and a stop watch started. Similarly, the end of each sampling interval was noted and a run number was assigned. Sampling itself was normally carried out by a second operator in charge of the bellows at the end of the piping. The gate was shut to cut-off the solids, while the weight and volume of the sample were being measured, then valve A was closed in a quasistatic manner. Thus, under no flow conditions, the zero differential pressure

error relating to the preceding run could be traced on the charts. The recorder speed was then reset to 0.5 min cm^{-1} and if necessary the backed-off signal was balanced out. Allowing for the possibility of mechanical offsets, this operation would normally make the tip of the recording pen return to its reference position. The maximum zero-error recorded thus had an absolute value of about 0.44 psi (= 3.033 x 10^3 Nm^{-2}) and would have amounted to a discrepancy of 20% if it were not taken into account. This certainly justified the time invested in repeating this lengthy operation at the end of each experimental run. At low superficial velocities, however, the time required for the material to spread evenly throughout the rig was too long to allow for a shut-down thus a different approach had to be taken in checking the zero-error: the transducers were first valved off and then removed from the test section. At this position they were both subjected to atmospheric pressure which made it possible to obtain a trace for the zero-error while the rig was still running. The transducers were subsequently reassembled in a reverse manner of operation.

Using the chart records the appropriate voltages could be confirmed at leisure and converted to pressure drops in SI units. Often, slight fluctuations in the concentration of aluminium in the pipe and the presence of turbulent eddies caused the pen recorder to flicker rapidly by ±1 mV. Thus, the operator needed to average the trace over the sampling time, a task which was simplified considerably by expanding the time-scale, (i.e. increasing the chart recorder speed). Measurements, were usually made with an accuracy greater than 2%. In other words, the scale could be read to the nearest ±0.02 mV and signals normally exceeded 1 mV.

3.2.1.2 Frictional pressure gradient - vertical leg

Three pressure tappings with a spacing of 2.30 m between them were available on the vertical section. Unfortunately, the lowest tapping was just downstream of the Tee-Angle-Bend which made it useless for experimental purposes. Thus the first tapping to be used was positioned at least twenty pipe diameters (> 2.3 m) away from the bend. Since a second set of transducers was not available an inverted U-tube manometer was used (see Plate 3.2) and the pressure drop was measured as a difference in height between columns of water. Plastic tubes filled with water connected the manometer open ends to the relevant points on the rig via small taps. A separate tap located at the tube invert could be used to let in compressed air in order to adjust the initial height of water in the limbs - about half way up under no flow conditions. Owing to the existence of this back-pressure in the event of draining the main loop the manometer was isolated to prevent loss of water through the transmission lines.

It is worth noting the way in which the U-tube was set up: static heads were automatically counter-balanced therefore any manometric height differences were purely due to dynamic conditions developed by slurry-flow in the pipe. Hence, there was no need to account for the height of the water column separating the two tappings. The same would not have been true, however, if diaphragm type transducers had been used.

Although it was expected that the height differences recorded by such a manometer would be too small to measure accurately, on most experimental runs the actual pressure difference across the 2.3 m of

pipe exceeded 100 mm of water. Unfortunately, oscillations associated with the pressure drop reading were severe. Since the height differences were time dependent it was decided to use an average value based on at least ten individual readings taken during the course of each run. The height difference on the manometer would vary typically by about ±15 mm of water.

Generally, this method of measuring pressure differences was much less precise or sensitive when compared to the transducers, and at best probably accurate only to ±10%. Another problem associated with this manometer was the accumulation of aluminium fines in the transmission lines over fairly short time intervals. This not only hindered the natural response of the device but also coloured the visible sections. To overcome this the manometer was regularly flushed with fresh water.

3.2.1.3 Superficial slurry velocity

Superficial slurry velocity is denoted by V_m and may be determined by measuring the amount of slurry collected over a known time, i.e. the volumetric flow rate. The superficial velocity is then calculated as the volumetric flow divided by the cross-sectional area of the pipe. This method of material collection was used in all the experimental runs performed. In order to maximise the time for which the output stream could be sampled, a calibrated 250 l receiving vessel was used. Water levels were measured against marks made at 5 litre intervals on the vessel walls. Volumes were estimated to the nearest litre whilst timings were read with a confidence of ±0.1 sec.

Because the calculation of the delivered solids concentration is based on and is particularly sensitive to the sample volume (see section 3.2.1.4), it is important to ascertain reliable calibration data for the sampling vessel. Such calibration lines are shown in Fig. 3.5. Line 1 is the calibration line obtained at the beginning of the campaign. The shift away from the line of agreement was attributed to a gradual deformation of the base of the vessel subjected to prolonged use. Although this was not immediately obvious to the eye the deformation progressed sufficiently during the work to be later confirmed. Since a replacement tank was not available it was decided to make use of the original but to monitor the rate of its deformation. After 104 runs a second calibration, shown as line 2 revealed that a further shift had taken place. At the end of the campaign (i.e. after 130 runs), a third calibration produced data points which virtually coincided with line 2. This meant that no further deformation had taken place - probably a reflection of the fact that fairly low concentrations had been used between runs 104 and 130. Assuming a linear rate of deformation with respect to time a mean slope was estimated (see Appendix B) resulting in the following equation:

$$\frac{\text{TRUE VOLUME}}{(1)} \simeq 1.036 \frac{(\text{INDICATED VOLUME})}{(1)} \qquad \qquad \dots. (3.1)$$

Equation 3.1 formed an overall mean and was applied as a correction factor to all volume data.

A magnetic flowmeter was also built into the hydraulic circuit as shown in Fig. 3.3 The dynamic response of this instrument provided a useful back-up measurement of the flow rate. In principle, the meter registered flow in terms of the solution conductivity between two elec-

trodes. It performed quite adequately for water alone but in the presence of aluminium platelets tended to give spurious and wildly flickering readings - often as much as ±100 g.p.m.. This was almost certainly due to aluminium particles successively "shorting" and "earthing" the meter's electrodes. Clearly then the magnetic flowmeter was not well suited to measureing the flow of water/metal slurries, nevertheless, it proved extremely useful in the overall control and operation of the rig. The output signal from this meter was relayed simultaneously on to an analog device calibrated in gallons/minute, as well as into a separate channel of the multi-pen chart-recorder. It should be noted that owing to the location of the device in the circuit when valve C was opened the flow rate indicated by the meter was irrelevant to the actual flow through the main loop.

3.2.1.4 Delivered solids concentration

The delivered volumetric solids concentration C_v can be easily calculated using the sample collected for volume flow rate measurement. From a knowledge of the total mass W and volume V_p of the sample, C_v can be evaluated using

$$C_v = \frac{(W/V_p - \rho_w)}{(\rho_s - \rho_w)} \qquad \dots \text{(3.2)}$$

At low solids concentrations the ratio W/V_p tends to unity making C_v infinitesimally small and very sensitive to values in V_p. Although measurements in V_p were normally made with a confidence better than ±1.0% the error involved was often sufficient to give negative values of C_v. Clearly then there was a tendency towards over-estimating V_p and a different approach had to be taken with lean samples. First the

aluminium and water mixture was weighed, then the water was carefully decanted from the slurry and the residual aluminium platelets left for a short time to dry. Upon reweighing, the concentration of the aluminium platelets can easily be calculated as a weight per cent C_w. Knowing the densities of aluminium and water allows the corresponding volume per cent concentration to be estimated from:

$$C_v = \frac{\rho_w \, C_w}{S - (S - 1) \, C_w} \qquad \qquad \ldots \ (3.3)$$

Equation 3.3 is plotted in Fig. 3.6 showing the relationship between weight per cent and volume per cent aluminium in water.

3.3 In Situ Solids Concentration - Horizontal and Vertical Test Sections

Load cells can be used to measure the in situ solids concentration in a freely suspended horizontal length of pipe - a change in concentration would be reflected by an alteration in the weight recorded by a cell supporting the pipe. Alternatively the in situ solids concentration in the horizontal and vertical test sections can be measured by a gamma-ray attenuation device. Unfortunately, neither of these options were installed on the Winfrith pipeline and hence it was not possible to measure the in-situ solids concentration directly. It was therefore decided to use values of the delivered solids concentration in the appropriate hydrodynamic equations.

3.4 Overall Experimental Technique in Operating the Hydraulic Conveying Rig

The sequence of principal operations used when starting up and shutting down the rig for a series of experimental runs are given below.

Assuming that the circuit is initially full of water, all the electrical instruments are switched on and allowed to stabilise. After zeroing these devices a slow trickle of water had to be fed to the torque-flow pump gland to ensure a good seal. Next the pump itself can be switched on. The main valve A was then gradually opened to establish water flow in the pipe circuit. This made it safe for the taps connecting to the U-manometer to be turned on. To add solids to the flow the gate was raised until the required aperture was obtained. At this stage, the bypass valve B can also be opened to set the final trim on the flow rate.

The procedure was reversed when shutting the rig down; closing the bypass valve ensured the maximum flow rate of the slurry was through the main loop and so reduces the probability of pipe blockage. Next the solids feeding gate was closed so that water only was passing through the pump, and all the residual aluminium was gradually purged from the system. When tests showed that only water was being returned to the feed tank, valve A can be closed followed by the pump itself.

During some experimental runs where the slurry was pumped at low superficial velocities the pipe work tended to block with aluminium. The sequence of events leading to blockage were thought to be as follows: reducing the main flow rate below the threshold of incipient

fluidisation meant that platelets started to settle out at the bottom of the vertical section. Thus a closed vortex was formed and any forthcoming platelets piled-up behind this plug. The short pipe section connected to the pump rapidly filled stopping the pump. If the pump was allowed to stall then it was necessary to drain the main tank, remove the inlet and outlet pipe sections and hand-remove the solid to free the impeller. Once the pump restarted, water flow alone could be used gradually to move the solids-plug through valves B and C keeping valve A shut. Upon successfully clearing the lower pipe section, the flow was then re-directed into the main loop.

Associated also with low flow rates was the deposition of solids on to the pipe invert along the horizontal sections. The actual process of material stratification was both lengthy and involved a substantial proportion of the total aluminium inventory. To minimise the time intervals between runs, settled solids were allowd to remain in bed formation during shut down. After shuting the gate, this was achieved by allowing the vertical section to clear first before closing valve A. Plate 6.1 shows the relative height to which the platelets have settled following a run at a mean flow rate of approximately 0.6 m/s. The piece of pipe shown to contain this stationary bed formation is that from the middle of the horizontal test section.

A small degree of formation around the edges of the aluminium stampings became apparent after about 125 hours of operation. Although little abrasion or wear was obvious to the naked eye, some degradation had almost certainly taken place, since a small quantity of aluminium fines was noticed in solution. The extent of deformation and wear sustained by individual stampings has been quantified during the classi-

fication of the material and is dealt with in chapter 4. The presence of fines had the effect of colouring the carrier fluid over and above the levels of dissolved rust, thus discouraging the use of a visible section in the circuit. Despite this, high speed photographs taken of the slurry at the point of exit from the pipework were remarkably successful. Plates 3.3, 3.4 and 3.5 are instant captures of the mixture at different superficial velocities and concentrations. These are useful for visualising the actual slurry flow within the pipe.

In operating the rig it was generally noticed that for a given setting of the solids feeding gate the pipeline concentration was a rising function of the mean flow rate. Besides gravity, the only mechanism responsible for the continuous transfer of platelets across the gate gap was that of pump suction. At low flow rates, however, the contribution from the pump was negligible and platelets tended to form a bridge across a gap up to 50 mm wide. Although the solids retaining walls were inclined beyond the angle of repose for this material (i.e. more than 30°), bridging could not be offset by gravity alone. Thus, it would appear the "bridging" is a property characteristic of two dimensional material and some agitation is necessary to ensure a steady feed. The idea was in fact put to practice on the 2" (= 50.8 mm) pipeline assembly which is described in the following section.

The nominal water temperature was 17° C. After an experimental session of about 3 hours, the water temperature in the rig rose by about 1.5° C. This was not enough to alter any of the physcial properties of water significantly.

A Texas Instruments 58 C programmable calculator was used to process the raw data at the end of each run. Thus, a plot of the manometric pressure drop i versus the mean slurry velocity V_m was kept up to date so that new experimental conditions could be simulated in a systematic manner.

3.5 Description of the 2" I.D. Hydraulic Conveying Rig at Winfrith

Using the 4" hydraulic rig as a basis, 2" pipe lengths were fitted to provide new test sections. These were made of the same mild steel grade (B.S. 3601-410) for the vertical leg but stainless steel (E N 58 J Type 316) was used in the horizontal section. The final assembly shown in Fig. 3.7 differs little from the original 4" circuit. The main features of the modified rig are a 4" to 2" reducer located immediately after the bypass between a Kent flowmeter on the downstream side and a 4" plug valve on the upstream side. A meantime frequency device was used to smooth the flowmeter's signal thereby considerably improving confidence in these measurements. This device was also capable of scaling the output signal to suit the receiving unit. A new 250 1 sampling vessel was obtained and calibrated (see Fig. 3.8). To avoid the risk of deformation the vessel was placed on to the scale tray via a steel plate which provided uniform support to the entire base.

Initially, the modified rig was fitted with two 2" plug valves at the positions marked E and E', (see Fig. 3.7), whilst the pump was coupled to a 7.5 kW motor which was driven by a variac speed controller. The first few trial runs resulted in some form of serious blockage. In order to restore the system, whole pipe sections had to be removed to clear the solids. This problem was interpreted as in-

sufficient head and an early decision was taken to change over to an 18 kW motor. As with the 4" assembly, this had to be driven directly, since the variac control unit was not able to support a current demand in excess of 14A. Although this arrangement provided ample hydraulic head major blockages still occurred and attention was then focussed on the main valves.

A close look at the 2" plug valves showed that there was a significiant restriction at the orifice. The valve-port was rectangular and reduced the pipe-bore to half the nominal size. Under flow conditions this changed the flow pattern and induced the formation of aluminium bridges across each valve. These valves were obviously not well suited for platelet material and were thus replaced; first by 2" gate valves and later by 2" ball valves.

Although the rig performance improved significantly when these repetitive blockages were eliminated, neither type of valve functioned satisfactorily at shut down. This is because the valves were too weak to shear platelets caught in their ports. As a result, the flow could not be completely shut off for zero error measurement. Finally, it was decided to eliminate these valves altogether. A geared 4" plug valve was installed just before the reducer. When fully opened, this valve provided a net passage of the same cross sectional area as the main pipeline whilst at shut down it gave a complete seal.

A further difficulty was encountered in controlling the rate at which particulate material was fed to the circuit; bridging was inevitable regardless of the gate positon. Even at high flow rates with the gates fully open, the flow of material was very irregular. This was

attributed to "choking" at the gate clearance caused by the sluggish flow of solids. The problem was obviated by attaching a compressed-air vibrator to the lower part of the feeding tank. Thus mechanically induced vibrations were used to persuade the metal pieces past the gate gap. The vibrator ensured respectable solids concentrations even with the gate fully shut, whereas concentrations of up to 20 v/o were achieved at other gate positions and velocities. Unfortunately, the vibrations were transmitted to the entire rig and had the adverse effect of disabling the flowmeter.

The following pump/motor pulley combinations were used during the course of 70 or so experimental runs:

	MOTOR PULLEY DIAMETER / (mm)	PUMP PULLEY DIAMETER / (mm)	PUMP ROTATIONAL SPEED / (r.p.m.)
1.	140	315	640
2.	160	315	732
3.	140	250	807
4.	200	250	1153

Each combination of settings provided a range of results, whereby the mean flow rate could be adjusted according to the level of solids in the circuit. As the pump rotated faster more material was gradually added into the tank to meet the demand for higher concentrations. Eventually, the total amount of aluminium platelets loaded into the feed tank was estimated at 100 kg.

The system was fitted with two 5 bar transducers in the horizontal section. These were 12.876 m apart and more than 19 pipe diameters (= 1.01 m) separated the high pressure tapping from the upstream bend. The same water manometer used for the vertical leg was connected across a 3.2 m long test section. Here the upstream tapping was more than 39 pipe diameters (= 2.0 m) away from the upstream bend. An Apple IIe computer was used to process the raw data between runs.

Overall the 2" pipe rig proved a lot more difficult to operate. Despite the large number of modifications, it still tended to block but it was relatively easy to restore steady flow. A final inspection of the material showed that no further deformation had taken place. An explanation for this is provided in section 4.2.2.
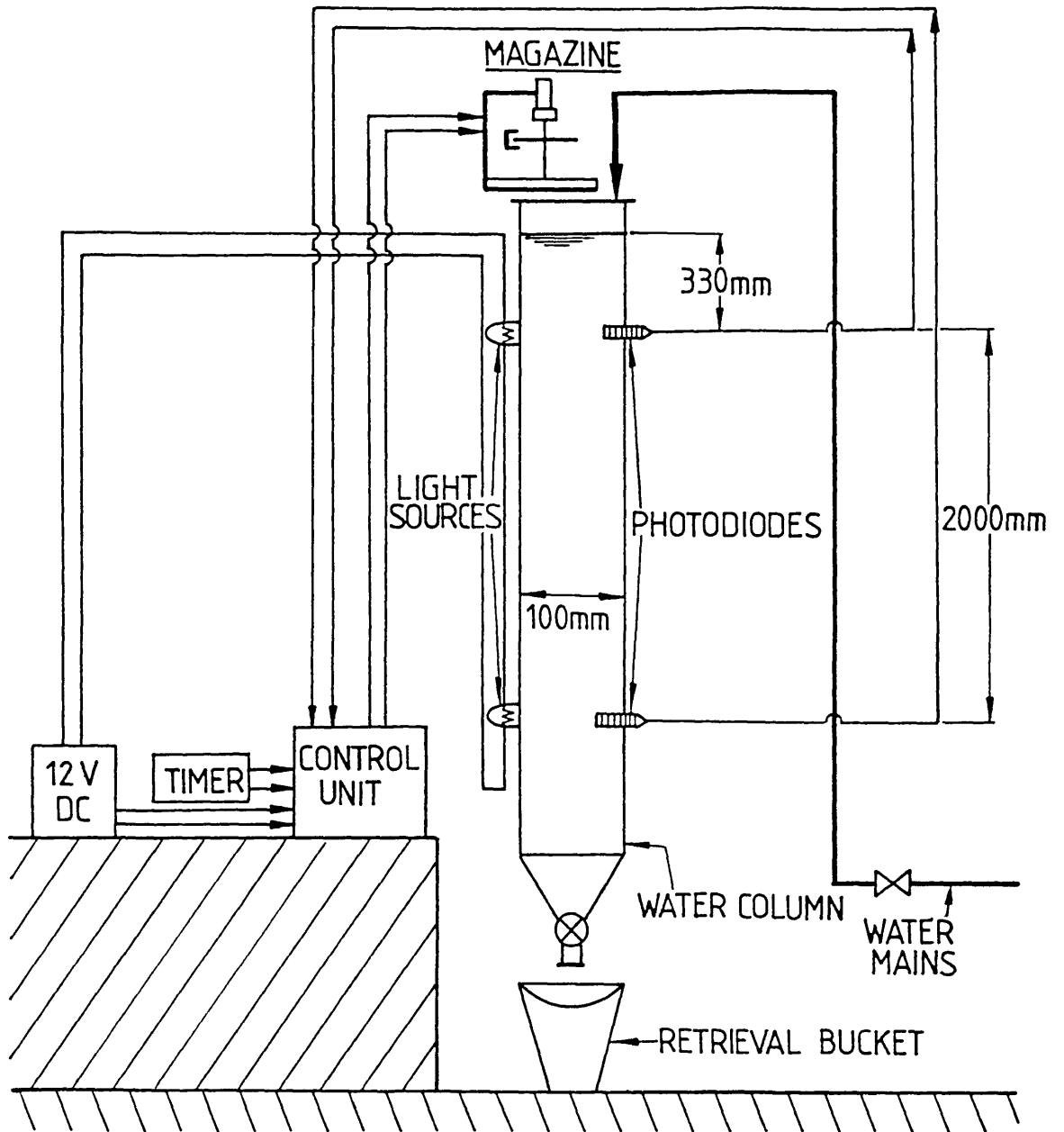
Fig. 3·1

A schematic presentation of the platelet characterisation apparatus.

Motor

Gearbox

Flexible Coupling

Guide

Dispenser

Particle

Bearing Housing

Water Column

Dispenser Disc

24°

3"

15 Holes (1")

4"

Photocell

Guide Disc
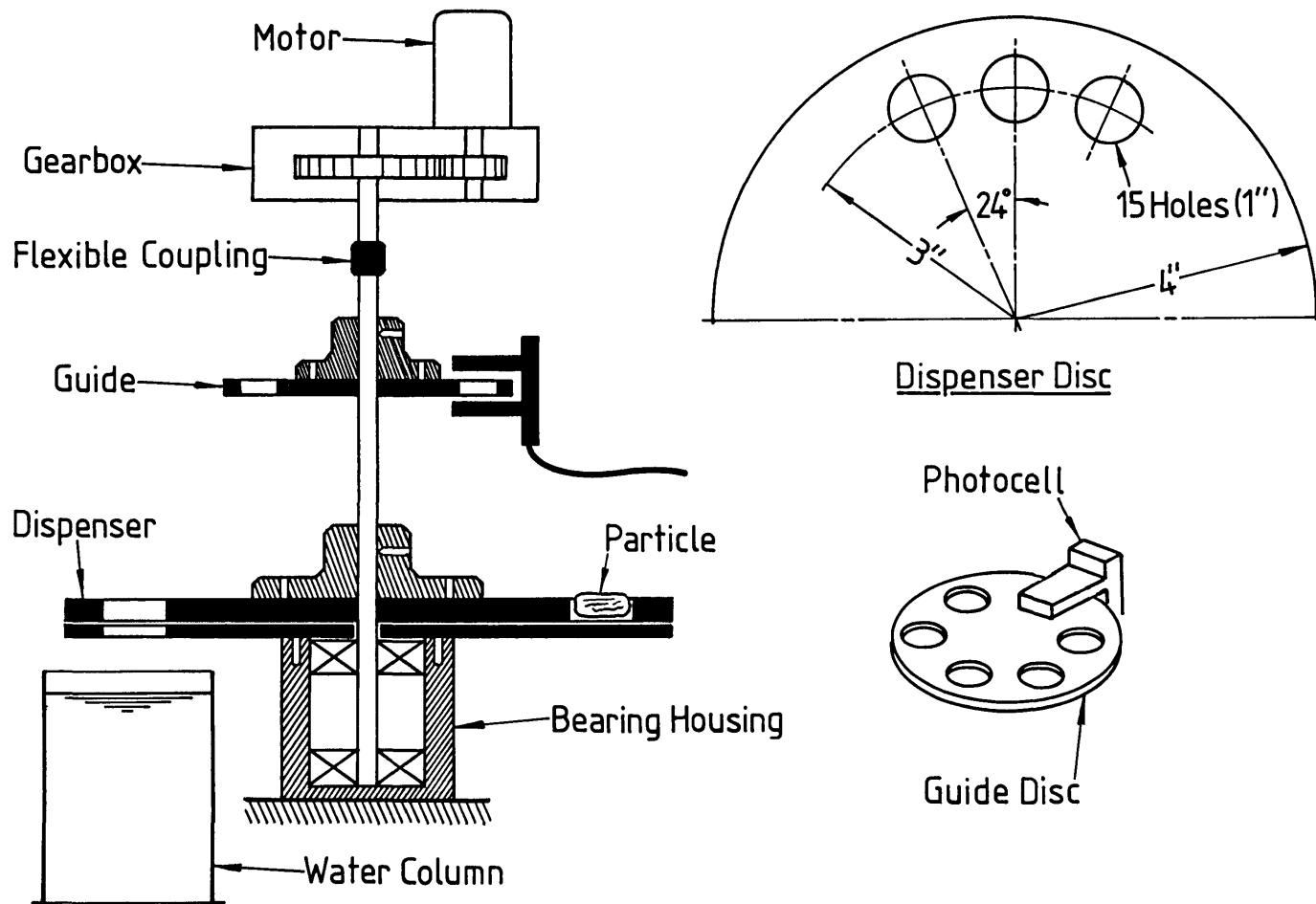
Fig. 3·2

Design of magazine used for the remote release of platelets
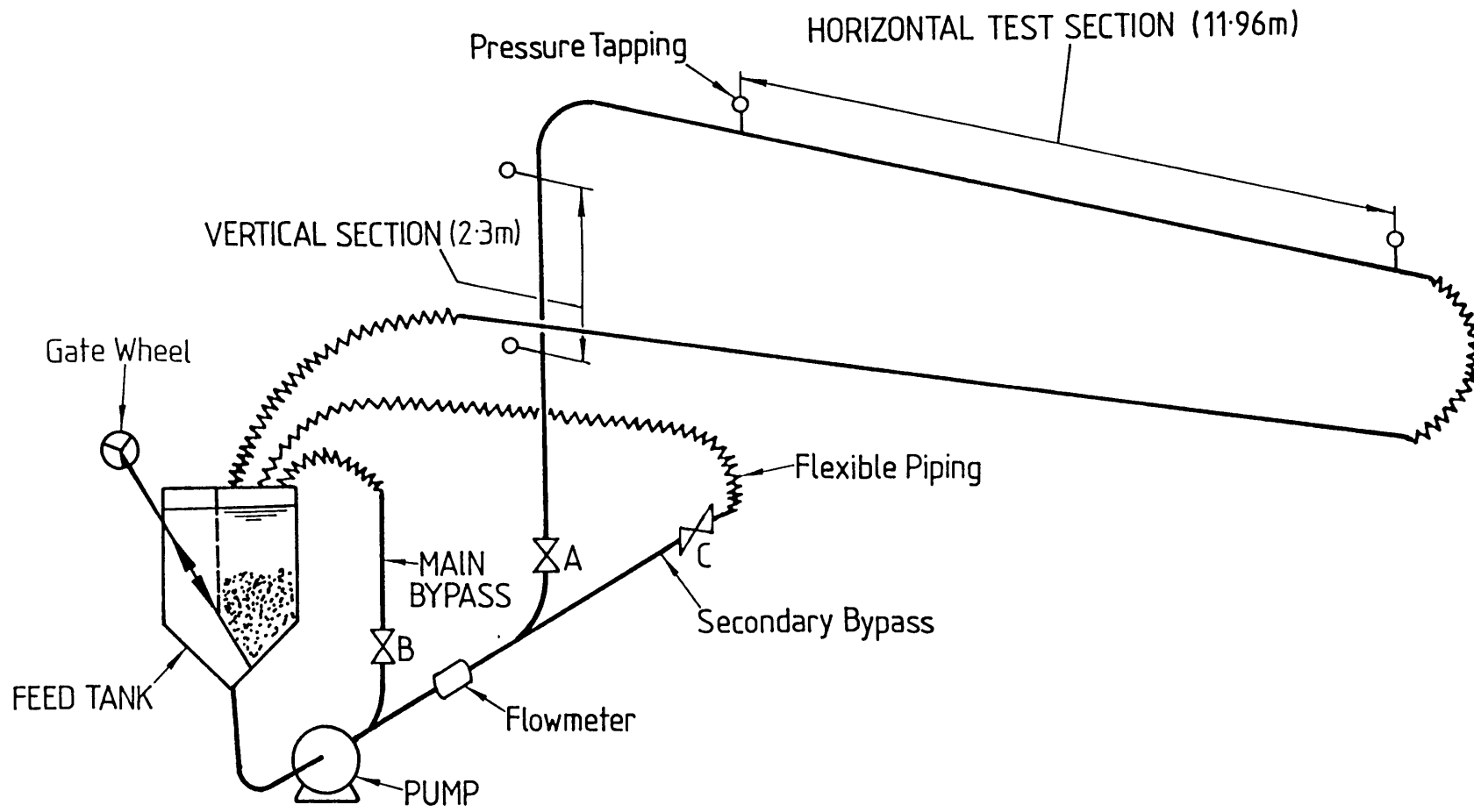
Fig. 3·3   Schematic presentation of 4" hydraulic conveying rig.
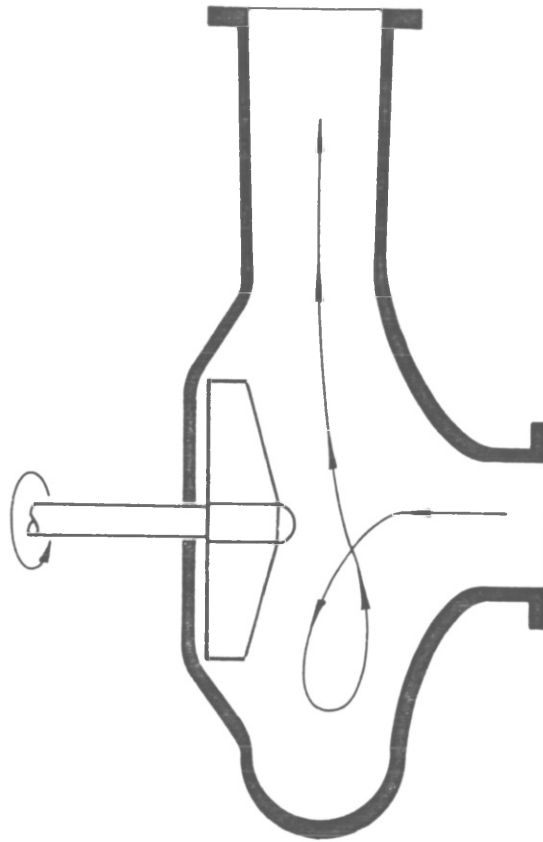
(a) Schematic cross section
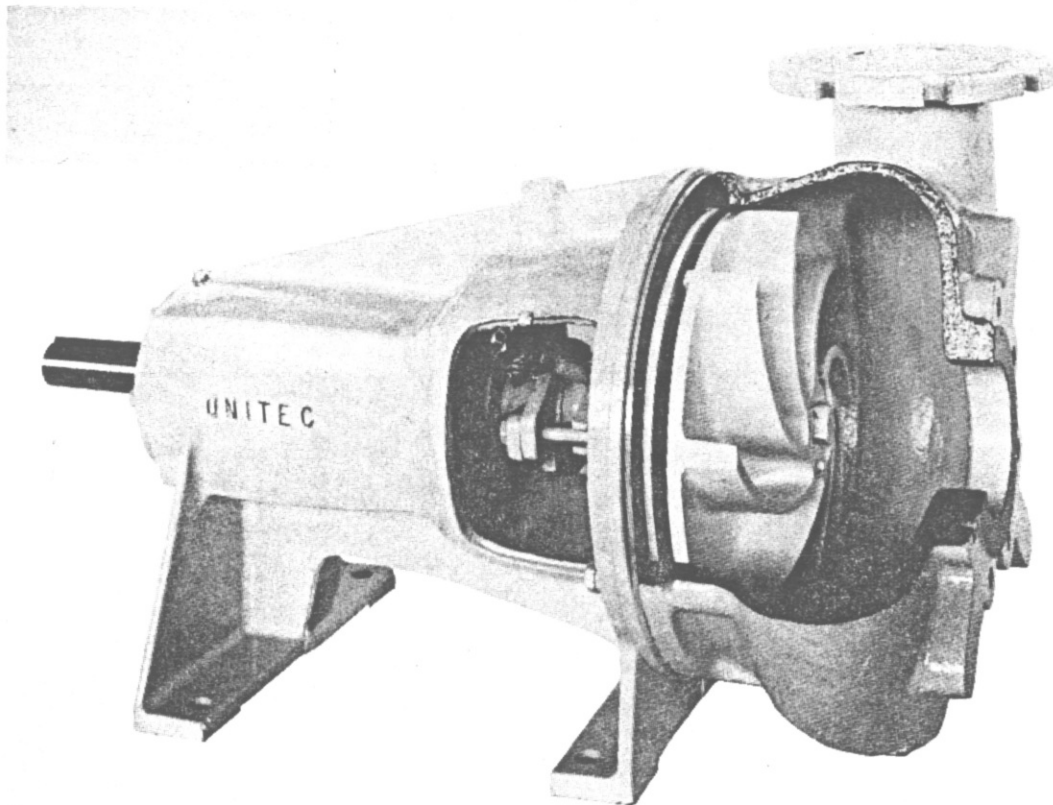
(b) Cut away view

Fig. 3·4 Torque Flow Pump
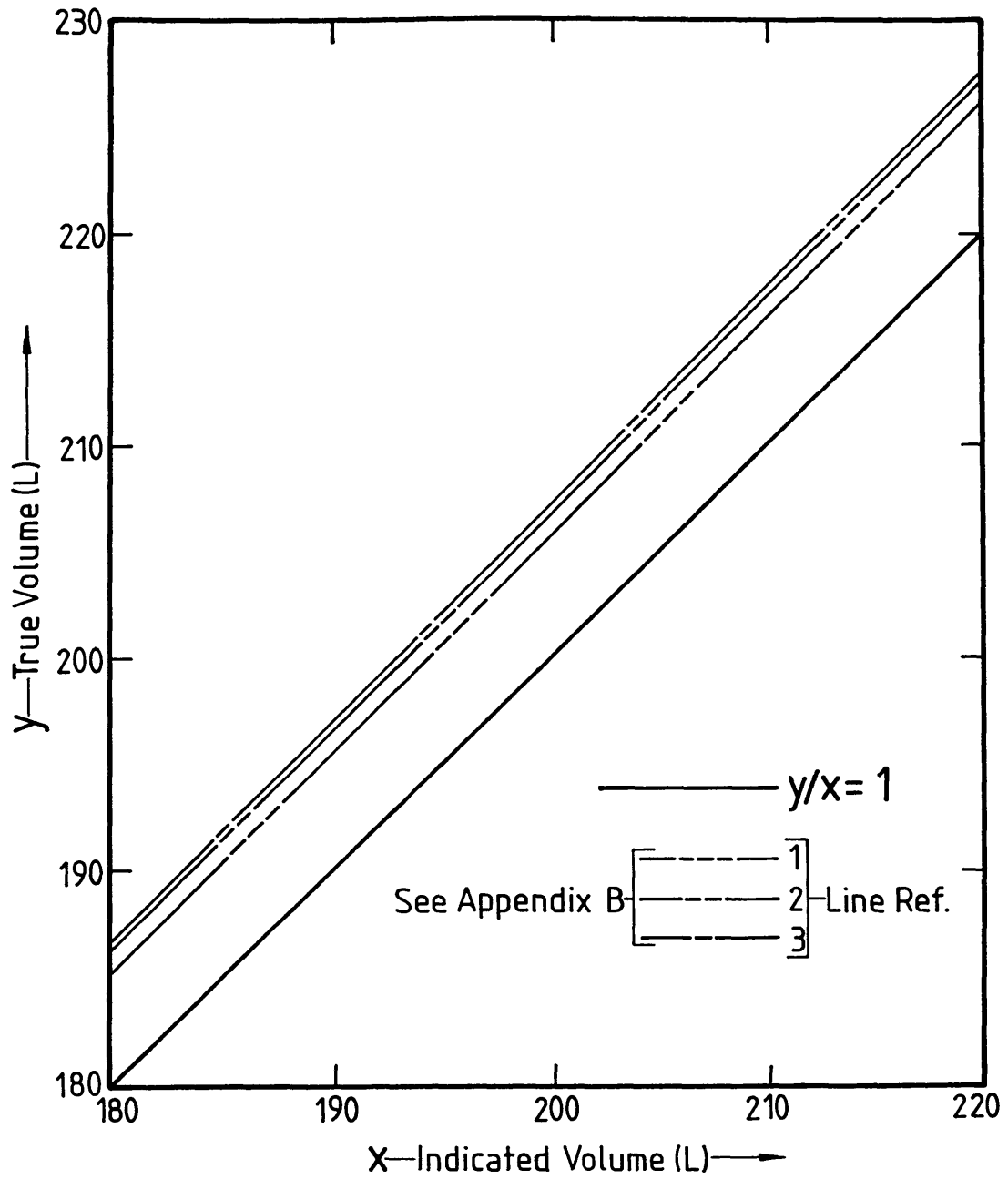
Fig. 3·5

Calibration lines for sampling vessel used in 4-inch pipe tests

$$C_w = SC_v(1+(S-1)C_v)^{-1}$$

$S = S_{Al}$

$S = 1$

$C_w (\%)$

$C_v (\%)$
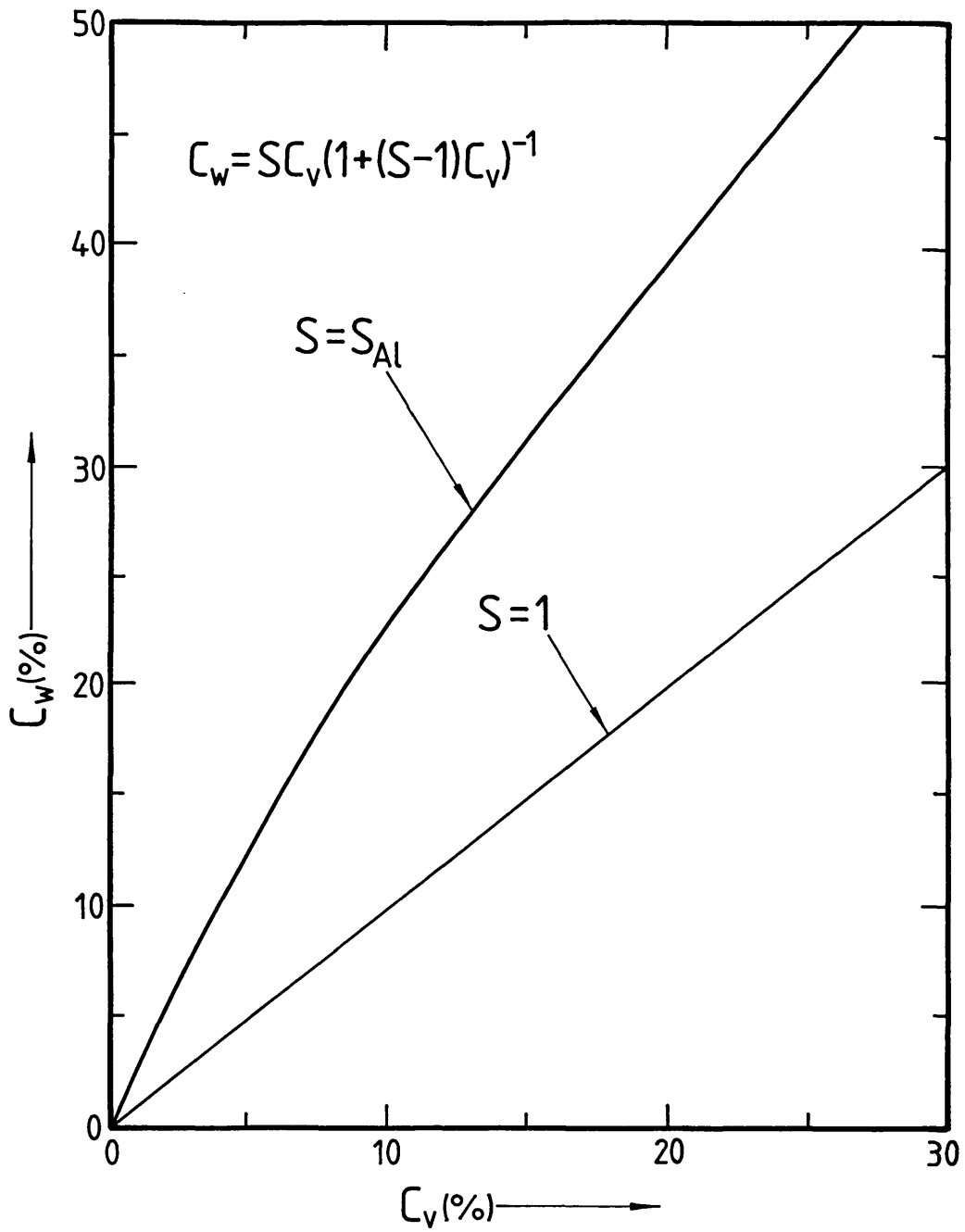
Fig. 3·6

Conversion between W/o and V/o Al in H_2O
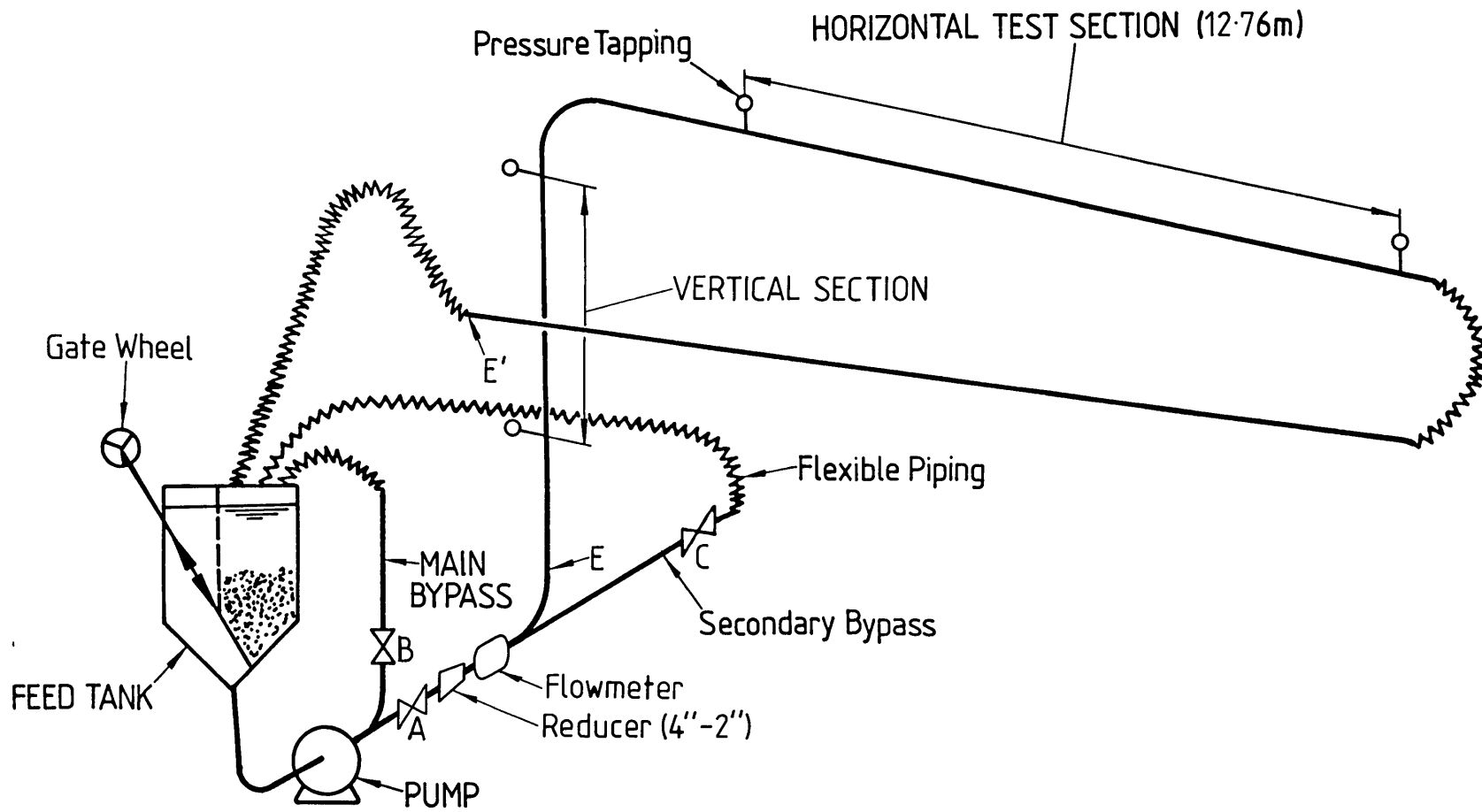
Fig. 3·7   Schematic presentation of 2" hydraulic conveying rig.
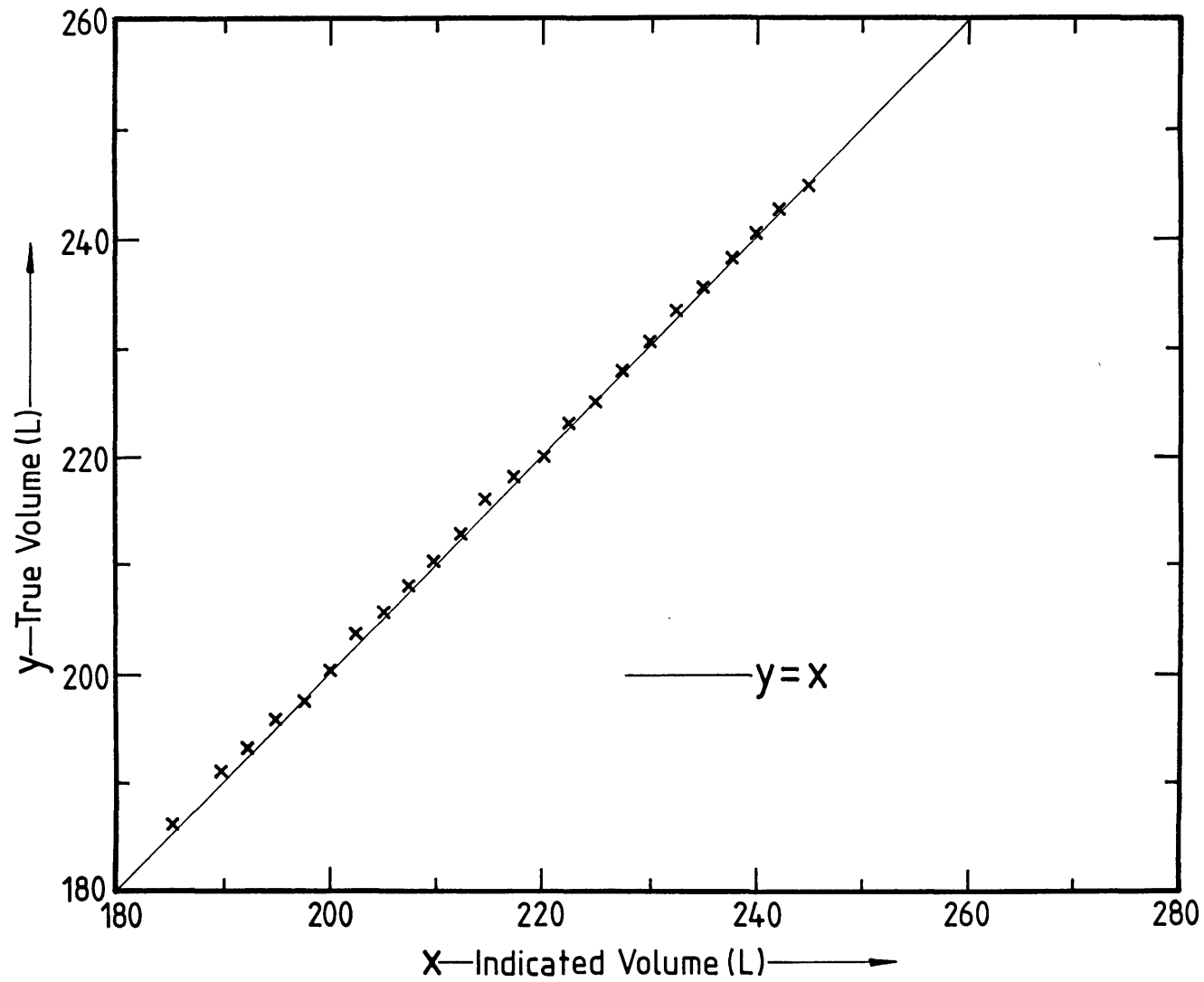
Fig. 3·8

Calibration line for the sampling vessel used in 2-inch pipe tests
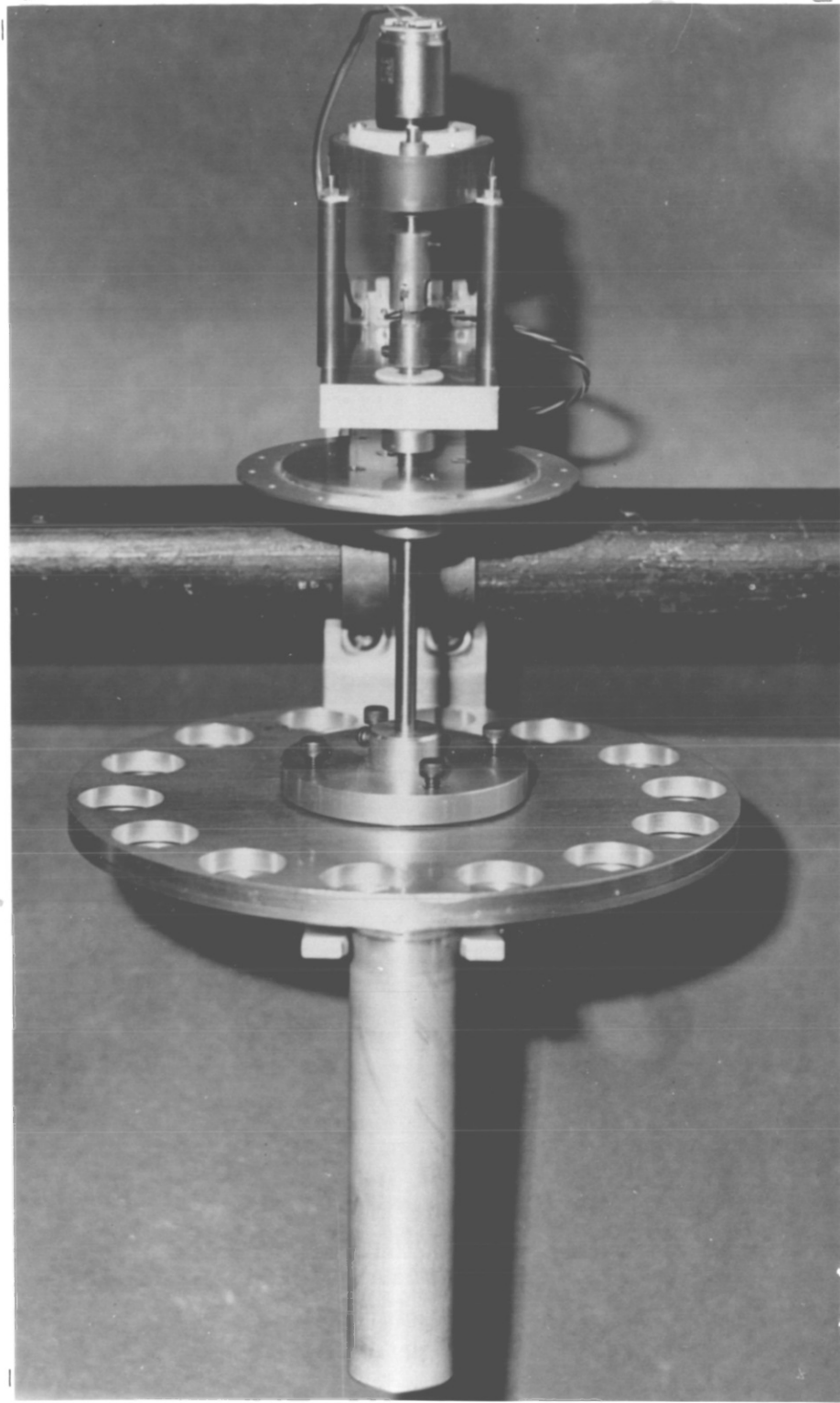
Plate 3.1 : An elevated view of the magazine including a guide tube

(overall height approximately 300 mm)

Plate 3.2

Hydraulic transport and component testing rig

Horizontal flow test section

Experimental concentration meter

Weigh tank

Vertical flow test section

By pass line

Second by pass line

Glass window

Flow meter

Concentration control gate
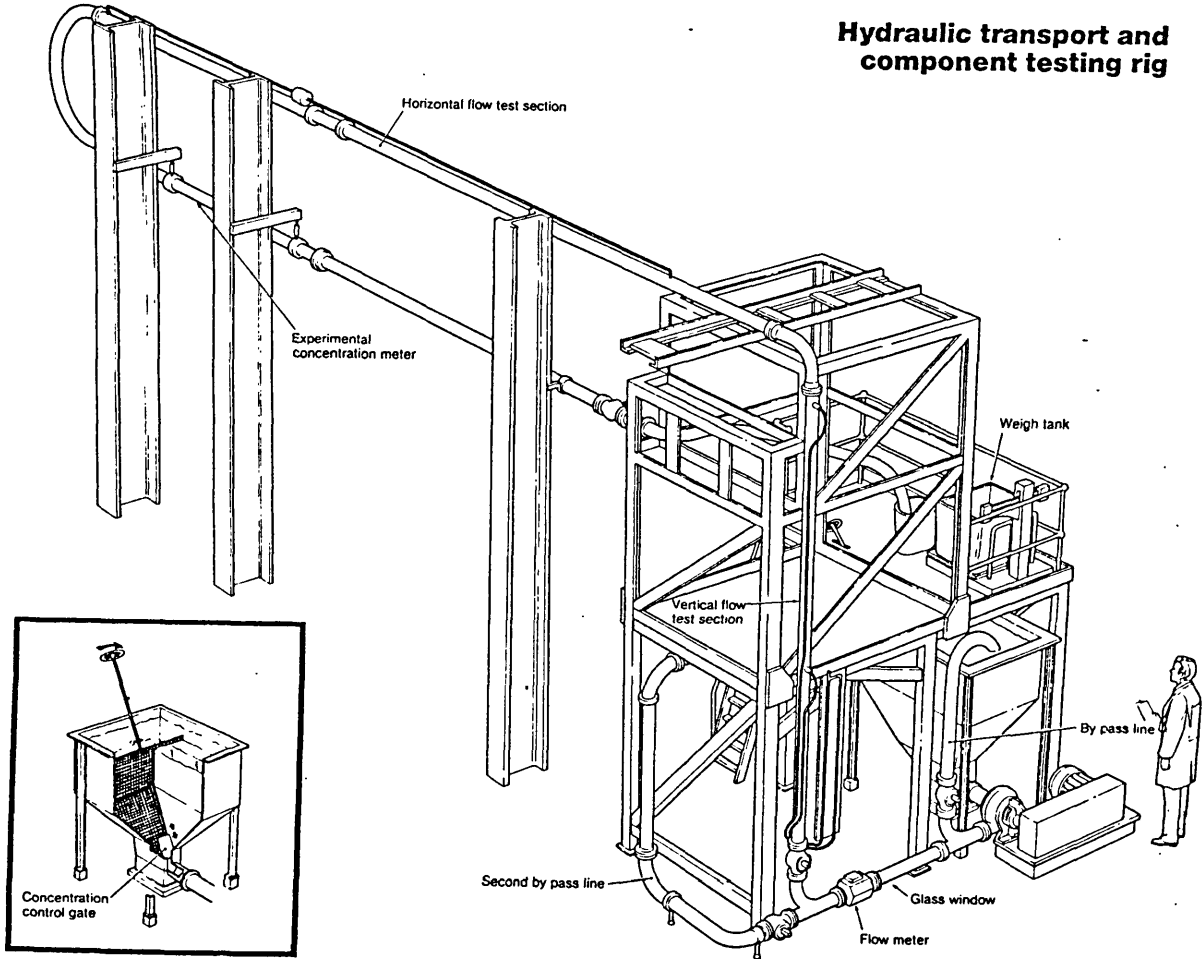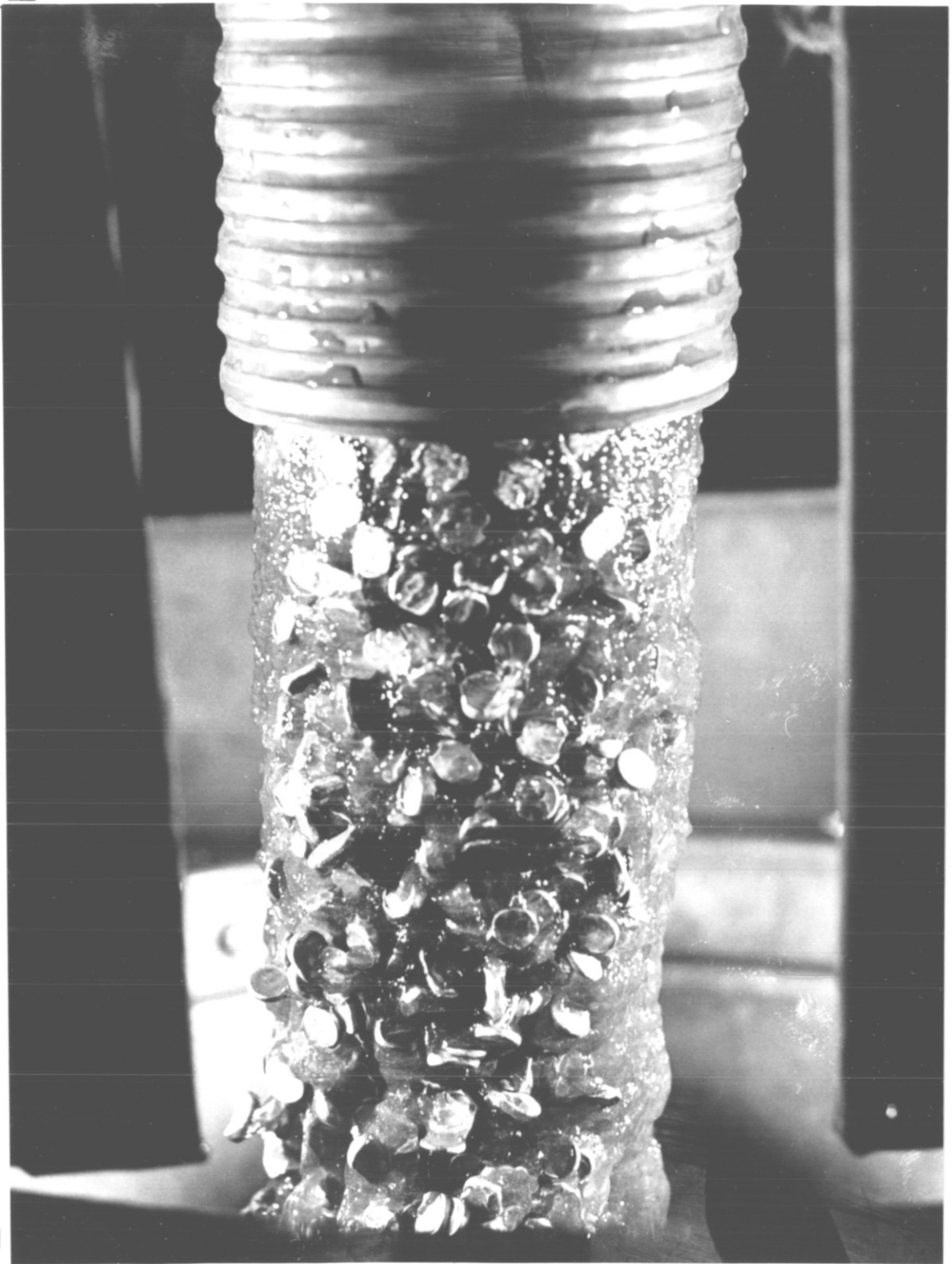
Plate 3.3 : Aluminium slurry being discharged at the end

of the 4" pipeline

$V_m = 3.7 \text{ m s}^{-1}$

$C_v = 4.4 \text{ v/o}$

Plate 3.4 : Aluminium slurry being discharged at the end
of the 4" pipeline

$V_m = 2.8 \text{ m s}^{-1}$

$C_v = 4.1 \text{ v/o}$
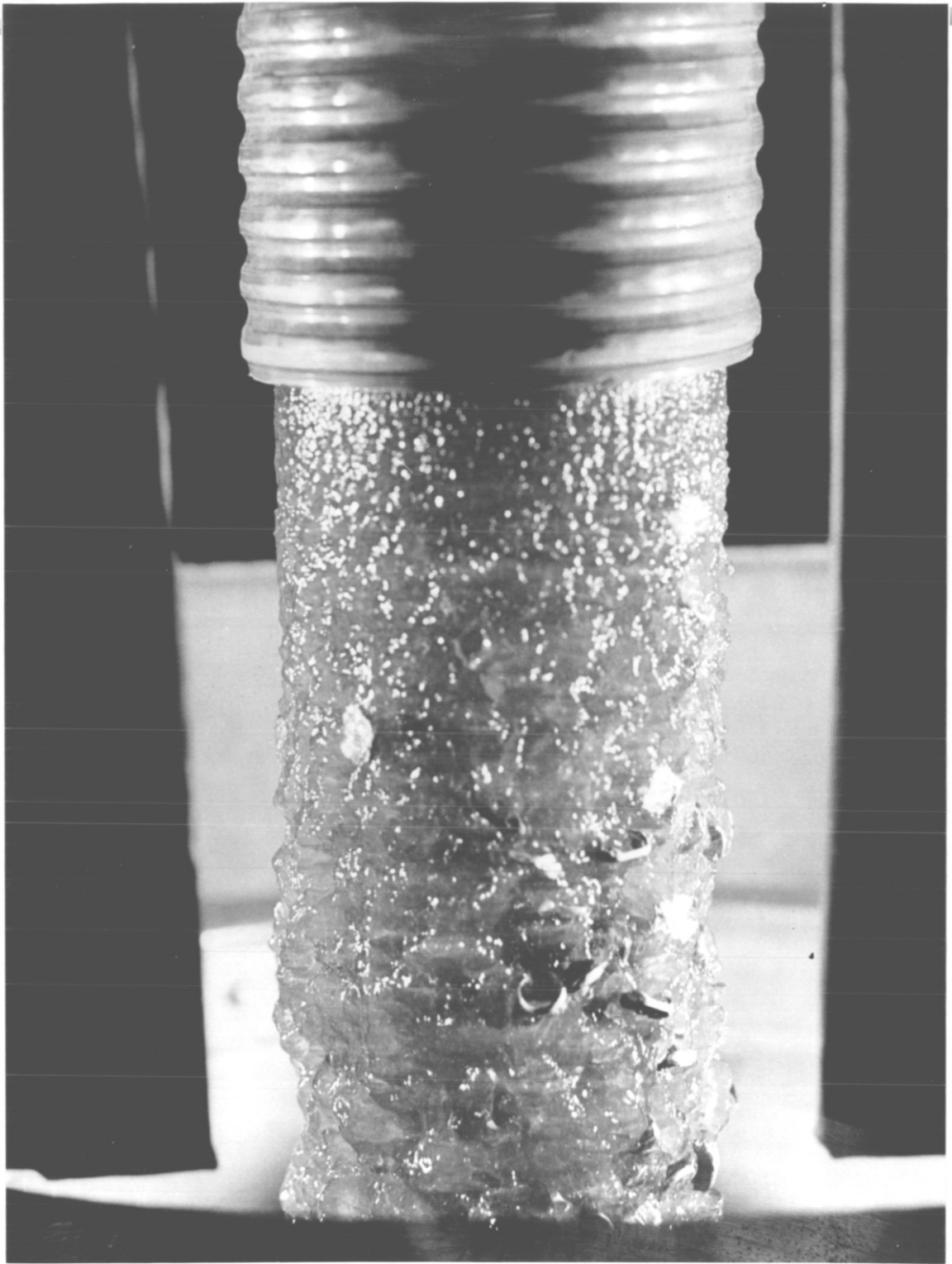
Plate 3.5 : Aluminium slurry being discharged at the end

of the 4" pipeline

$V_m = 0.7 \text{ m s}^{-1}$

$C_v = 1.3 \text{ v/o}$

4.   EXPERIMENTAL MATERIAL USED IN THE HYDRAULIC PIPE RIG

4.1   System Requirements

Light metal 'platelet material' was sought for use in pressure drop measurement experiments. Individual particles were required with simple geometrical shapes and length to thickness ratio greater than 10. The maximum particle dimension should be approximately 1/10th of the pipe diameter. After considering the various possibilities, it was concluded that commercial aluminium offered a good alternative with which to model Magnox.

Aluminium is about 1.5 times heavier than pure Magnesium, reacts only superficially with air and water and it is readily available, (i.e. Al sheeting with nominal thickness around 2 mm). Using the 4", 37 m long pipeline at Winfrith, it was estimated that a minimum of 0.1 m^3 (i.e. 270 kg) of Al platelets were needed to ensure concentrations of up to 30% by volume. Unfortunately, however, the cost analysis for a custom made sample made it prohibitively expensive, (nearly 2,000 pounds sterling in August, 1983). To avoid the manufacturing cost, it was decided to explore the possibility of obtaining similar material from the waste products of a standard operation. Stampings produced in the making of Dexion angle appeared to be suitable. The type of material used has a mean density of 2,629.1 kg m^{-3}. In addition, shapes and sizes of the resulting stampings were found to agree remarkably well with the prescribed standards. Dexion Company supplied 410 kg of mixed Dexion stampings (type D-225).

4.2 Dimensional Classification of Dexion Stampings

Fig. 4.1a shows an isometric view of a Dexion angle piece comprising one cycle of 'oval-like' perforations. The pattern consists of nine holes, (or stampings), which come in four different sizes A, B, C and D. Individual items are metal strips of uniform thickness t and rounded ends. Using the notation of Fig. 4.1b, a length to breadth ratio may be defined as x/y. This varies from unity in the case of platelets D (i.e. perfect discs) to about 5.7 for items A and can be used as a crude criterion of size. For the calculation of appropriate shape factors, however, the exact dimensions of each platelet had to be established with micrometric accuracy.

4.2.1 Classification of fresh material

Platelets which have not yet been pumped through the rig (i.e. fresh stampings) have regular geometrical shapes with readily definable dimensions. The convention used in Fig. 4.1b is in accordance with dimension specification rules given by Clift, Grace and Weber (16), whereby mutually perpendicular pairs of parallel planes tangential to opposite surfaces are considered to define "length" terms. With the exception of item D, each stamping is made up of three sections; two semi-circles separated by a rectangular piece in the middle. Therefore, a simple expression can be used to evaluate the projected area A_p for each platelet, i.e.

$$A_{p\,(A,\ B,\ C)} = \frac{\pi\,y^2}{4} + y\,(x - y) \qquad\qquad \dots\ (4.1)$$

in the case of discs D, equation 4.1 reduces to:

$$A_{p \ (D)} = \frac{\pi \ y^2}{4} \qquad \qquad \dots \ (4.2)$$

Individual measurements on platelet types B, C and D are shown in Appendix C. These are accurate to ± 0.0005 mm and were made by means of a 'Leitz UML - digital - S type' travelling microscope. After the first few measurements, it became apparent that regardless of the type of group there was a finite tolerance of ≤ 0.02553 mm (= 0.001") on each dimension. This was particularly evident with the thickness t so that visual separation was made possible. Since t is the only parameter to appear in the calculation of the platelet drag C_D, (see equation 2.12 in section 2.2.2.1), it was decided to subdivide each group into slim S and thick T items. The dimensions of length x and breadth y, however, varied randomly within a subgroup. Since the contribution of x,y in equation 2.12 is via the terminal settling velocity V_t where $V_t = f(A_p)$ and $A_p = f \ (x,y)$, it was decided to treat these parameters as a compound quantity.

In order to establish the constituent concentrations of each group and subgroup in the overall mixture, a large sample of fresh material was analysed. For this purpose, 2,163 platelets were hand sorted. The results are shown in Table 4.1. Alternatively, an estimate for the concentration can be obtained using the material cycle. It is gratifying to note that concentrations obtained by sorting are in close agreement with predictions from the material cycle. Both items B and C show a consistent subgroup concentration of about 70%/30% slim to thick platelets. The small discrepancy of item D is probably not significant, but an average D subgroup concentration of 75%/25% will be used.

A number of preliminary tests using the 4" pipeline, loaded with about 80 kg of material, revealed that platelets A were not really suitable for use in this system. Besides promoting the formation of solid bridges at sensitive locations, (such as valve ports), these extra long items were severely deformed by the pump impeller. This greatly increased the "tangle-ability" of the material which lead to further bridging and blocking. Plate 4.1 shows the extent of deformation sustained by a sample of particles during the first few runs.

Thus, it was decided to discard group A and re-assess the remaining material. In doing so, however, it was feared that the original sample would be severely attenuated. Although item A represents only 11.11% of the Dexion stampings, the weight proportion is significantly greater. Since the weight of individual platelets is directly proportional to their cross-sectional area, the fractional weight loss can be estimated from:

$$\frac{W_A}{W} = \frac{\frac{1}{9} A_p(A)}{\frac{1}{9} A_p(A) + \frac{4}{9} A_p(B) + \frac{2}{9} A_p(C) + \frac{2}{9} A_p(D)} \qquad \qquad \dots \dots (4.3)$$

Using equations 4.1 and 4.2 with mean x,y values from Appendix C, expression 4.3 yields $\frac{W_A}{W} = 0.352$. Hence, after removing platelets A, the useful material reduces to just

410 (1 - 0.352) = 265 kg

A 10 mm square sieve was used to separate the long items in a relatively short time. Table 4.2 contains the new concentrations of the

remaining items in the useful sample. By weighing each subgroup separately, it was possible to establish the mean platelet weight which is characteristic of the group. Hence, the weight per cent concentration of each group was also established. The left column in Table 4.3 provides a quick reference to overall dimensions of fresh platelets including intermediate results.

4.2.2 Classification of pumped platelets

During about 110 experimental runs using the 4" pipe rig, the platelets were periodically examined to check for any obvious deformation. Plate 4.1 shows a comparative view between fresh and used items of all groups. Although group D (i.e. disc-shaped platelets), remained virtually unaltered, items B and C showed a progressive curling of the edges. This was thought to be the result of compressive forces acting along the x-axis. Effectively this made the shape of a typical platelet look very similar to the cross section of an I-Beam when viewed through a third angle projection (i.e. x,z plane). This regular change in shape was believed to be responsible for strengthening the stampings thereby reducing the risk of further deformation. In order to quantify the physical changes observed, it was decided to analyse a small sample of used platelets.

At the end of the 4" pumping tests, 150 platelets were selected, 50 D's' and 100 B's' and C's' mixed. At this stage, it was virtually impossible to distinguish between the two latter groups. The platelets were numbered and weighed individually to the nearest 0.1 mg. Using the same optical device, x,y,z dimensions were also measured. In particular, the thickness t of items B and C were recorded at the middle

and also at each curled end. Using a "bubble" sorting routine the data were sorted in order of particle weight and are tabulated in Appendix D. Hence, step changes in particle weight could be used as guide lines in identifying the platelet group (see Fig. 4.2). This shows some merging of platelet weights in the B/(S) and C/(T) subgroups for a total of 47 particles. The distinction, however, was simplified by using the abundance ratio of C/(T)/B/(S) = 7.03%/37.6%, i.e. 9/38 platelets respectively.

Plates 4.2 and 4.3 are close-up photographs of platelets (numbers 20,90 and 45,91 respectively), showing clearly the curling of the material at the edges. Using data from Appendix D, new, average dimensions were calculated for the used particles. For direct comparison these are tabulated alongside the original values and are shown in the second column of Table 4.3.

It is appropriate to estimate the mean platelet thickness in a way which takes into account the curling of the edges. Although individual measurements in thickness are useful in assessing the extent of deformation at specific locations, the task of deducing an overall mean equivalent thickness is by no means a simple one. Alternatively, the mean platelet thickness can be estimated from the combined knowledge of volume and cross sectional area. Platelet volumes can be found accurately from

$$V_p = \frac{\text{Mean Platelet Weight (see Table 4.2)}}{\text{Material Density}} \qquad \dots (4.4)$$

The results are summarised at the end of Table 4.3.

4.3 Dimensions of an Equivalent Platelet or Sphere

The Dexion stampings were fully classified before and after their use in pressure drop tests. Table 4.4 provides characteristics dimensions of a typical platelet, as well as diameters for a 'volume equivalent sphere' and 'a sphere of the same cross-sectional area'. The table is sub-divided into two parts:

(i) Part A shows mean (platelet and sphere) dimensions which are relevant to the 4" pipe tests. During these tests, a linear rate of deformation has been assumed for simplicity.

(ii) Part B provides mean values which refer to the state of the material immediately after the 4" tests. Although 'used platelets' were employed for the 2" pipe tests, no further deformation took place.

The results shown in Table 4.4 will be used in the following chapter to determine appropriate shape factors which are necessary for the hydraulic description of the material.
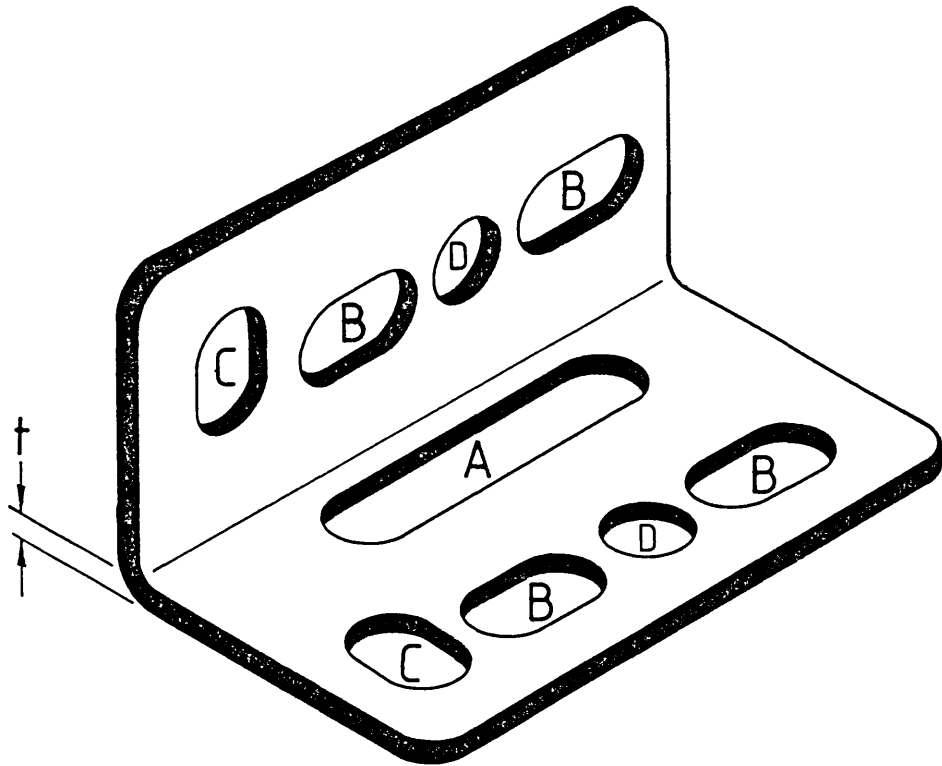
(a) Isometric view of Dexion Angle (one cycle)
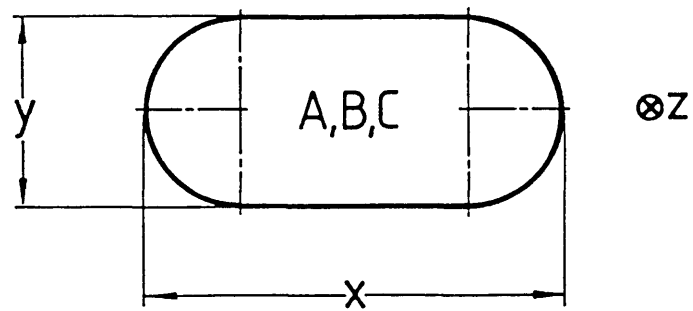
(b) Plan view of typical Dexion Stamping

Fig. 4·1
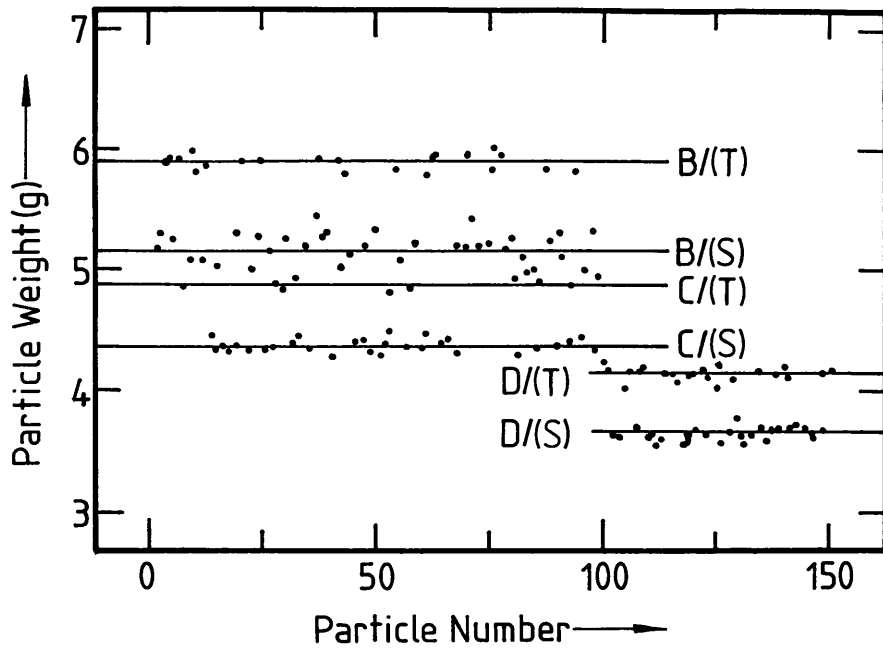
Fig. 4·2

Group identification of used platelets

Table 4.1 : Group and subgroup % concentration of items

A, B, C and D in the overall sample of

Dexion stampings

ITEM REFERENCE	No. of PLATELETS (Hand Sorted)	% CONCENTRATION OF PLATELETS IN		
		SUBGROUP	OVERALL SAMPLE	MATERIAL CYCLE (See Fig. 4.1)
A/(S)* A/(T)* $\bar{A}$	 141		 6.5	 11.11
B/(S) B/(T) $\bar{B}$	760 326 1086	69.98 30.02 	 50.21	 44.44
C/(S) C/(T) $\bar{C}$	330 144 474	69.62 30.02 	 21.91	 22.22
D/(S) D/(T) $\bar{D}$	347 115 462	75.11 24.89 	 21.36	 22.22
TOTAL =	2163 platelets			

(*) : S and T denote "SLIM" and "THICK" platelets respectively

Table 4.2 : Classification of Dexion Stampings used in pipe tests

ITEM	No. of ITEMS Hand-Sorted	MEAN PLATELET WEIGHT		WEIGHT LOSS	CONCENTRATION	
		<NEW> (g)	<USED> (g)	(%)	(No/o)	(w/o)*
B/(S)	760	0.5347	0.5174	-3.235	37.60	
B/(T)	326	0.6043	0.5883	-2.648	16.11	
B	1086	0.5556	0.5387	-3.042	53.71	60.16
C/(S)	330	0.4476	0.4366	-2.458	16.41	
C/(T)	144	0.5040	0.4869	-3.393	7.03	
C	474	0.4645	0.4517	-2.758	23.44	21.95
D/(S)	347	0.3754	0.3634	-3.197	17.14	
D/(T)	115	0.4182	0.4136	-1.100	5.71	
D	462	0.3882	0.3785	-2.499	22.85	17.88
TOTAL	2022 platelets					
OVERALL AVERAGE		0.4960	0.4817	-2.883		

(*) : The (w/o) concentration is based on the mean weight of new platelets.

Table 4.3 : A comparison between the dimensions of <u>new</u> and
<u>used</u> platelets

ITEM	<NEW> x̄ - DIM (mm)	<USED> x̄ - DIM (mm)	AVERAGE % DEFORMATION IN X - DIMENSION
B/(S)	14.9289	12.2364	
B/(T)	14.7703	11.7247	
B	14.8813	12.0829	-18.805
C/(S)	12.8778	11.5981	
C/(T)	12.7057	11.3409	
C	12.8262	11.5209	-10.177
D/(S)	10.4775	10.3670	
D/(T)	10.3188	10.1826	
D	10.4378	10.3209	-1.120
OVERALL AVERAGE	<u>13.3842</u>	<u>11.5486</u>	<u>-13.715</u>

	ȳ - DIM (mm)	ȳ - DIM (mm)	AVERAGE % DEFORMATION IN X - DIMENSION
B/(S)	9.4627	9.3699	
B/(T)	9.2708	9.2548	
B	9.4051	9.3354	-0.741
C/(S)	9.5130	9.3699	
C/(T)	9.2879	9.1874	
C	9.4455	9.3784	-0.710
D/(S)	10.4888	10.3804	
D/(T)	10.3283	10.2493	
D	10.4487	10.3476	-0.968
OVERALL AVERAGE	9.6530	9.5768	-0.789

Table 4.3 continued

	XS-AREA (mm)^2	XS-AREA (mm)^2	AVERAGE % DEFORMATION OF XS-AREA
B/(S)	122.0510	95.8332	
B/(T)	118.4861	90.1269	
B	120.9815	94.1213	-22.202
C/(S)	103.0854	90.5157	
C/(T)	99.5010	86.1044	
C	102.0101	89.1923	-12.565
D/(S)	86.3124	84.5323	
D/(T)	83.7091	81.9757	
D	85.6616	83.8932	-2.064
OVERALL AVERAGE	108.4640	90.6288	-16.443

(*)	MEAN-HEIGHT (mm)	MEAN-HEIGHT (mm)	AVERAGE % DEFORMATION OF MEAN HEIGHT
B/(S)	1.7487	2.0535	
B/(T)	2.0065	2.4828	
B	1.8260	2.1823	+19.513
C/(S)	1.7511	1.8346	
C(T)	2.0093	2.1508	
C	1.8286	1.9295	+5.518
D/(S)	1.7468	1.6351	
D/(T)	2.0256	1.9191	
D	1.8165	1.7061	-6.078
OVERALL AVERAGE	1.8244	2.0142	+10.403

(*) : Mean-height values for "used" platelets have been deduced from mean-platelet volumes

Table 4.4 : Principal particle dimensions

(A) : DIMENSIONS OF A TYPICAL PLATELET USED IN THE 4"-PIPE TESTS
Mean Length : $\bar{x}$ = 12.4664 mm Mean Breadth : $\bar{y}$ = 9.6149 mm Mean XS-Area : $\overline{A_p}$ = 99.5464 mm^2 Mean Height : $\bar{t}$ = 1.9193 mm Mean Volume : $\bar{V}$ = 191.0594 mm^3 Mean Weight : $\bar{W}$ = 0.5023 g Diameter of volume equivalent sphere : d_v = 7.1459 mm Diameter of xs-area equivalent sphere : d_a = 11.2580 mm
(B) : DIMENSIONS OF A TYPICAL PLATELET USED IN THE 2"-PIPE TESTS
Mean Length : $\bar{x}$ = 11.5486 mm Mean Breadth : $\bar{y}$ = 9.5768 mm Mean XS-Area : $\overline{A_p}$ = 90.6288 mm^2 Mean Height : $\bar{t}$ = 2.0142 mm Mean Volume : $\bar{V}$ = 182.5445 mm^3 Mean Weight : $\bar{W}$ = 0.4799 g Diameter of volume equivalent sphere : d_v = 7.0381 mm Diameter of xs-area equivalent sphere : d_a = 10.7420 mm

Plate 4.1 : A comparative view between new and used platelets

A, B, C and D denote new platelets

A', B', C', and D' denote used platelets
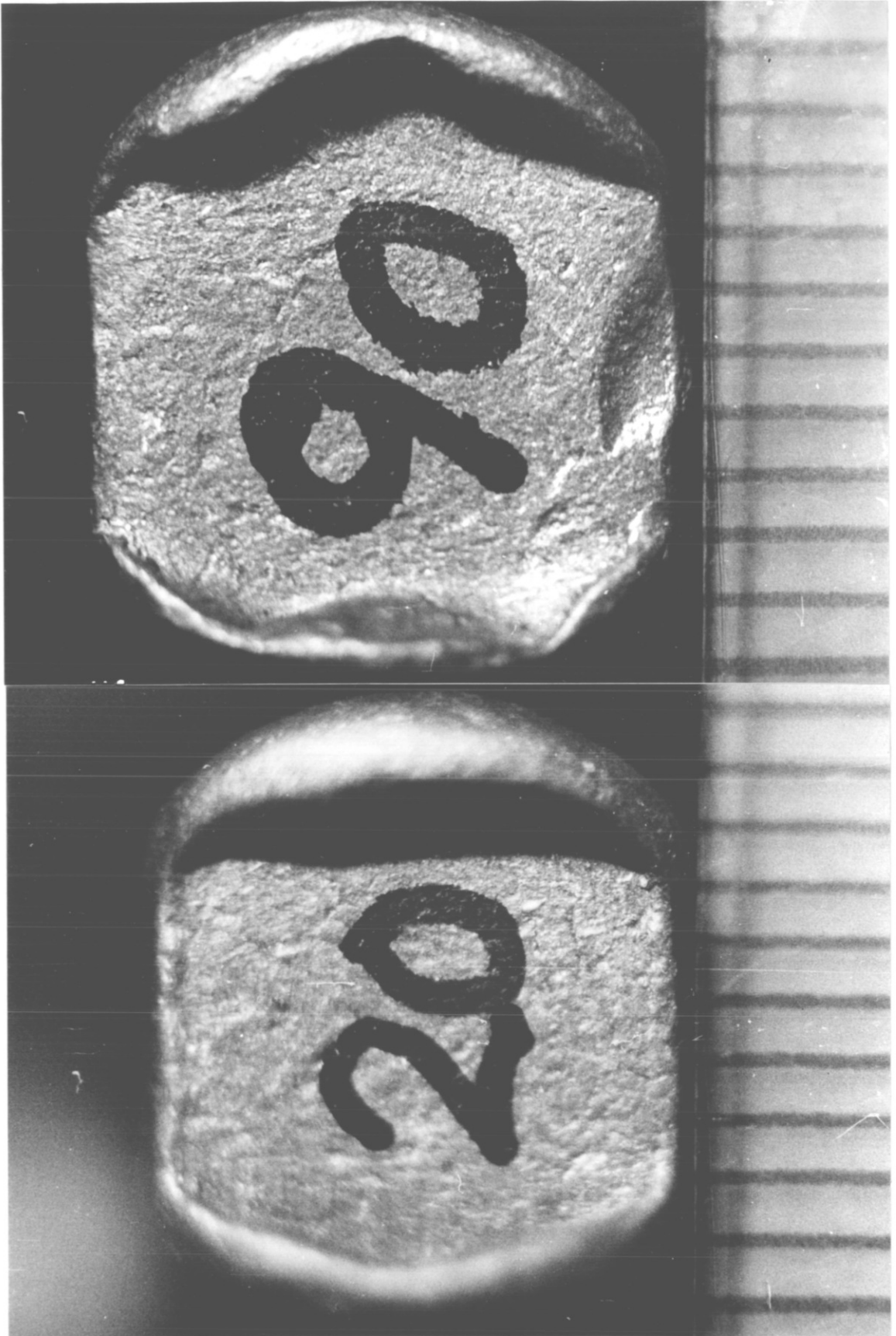
Plate 4.2 : A close-up view of used items 20 and 90 (group B) showing

the curling at the edges
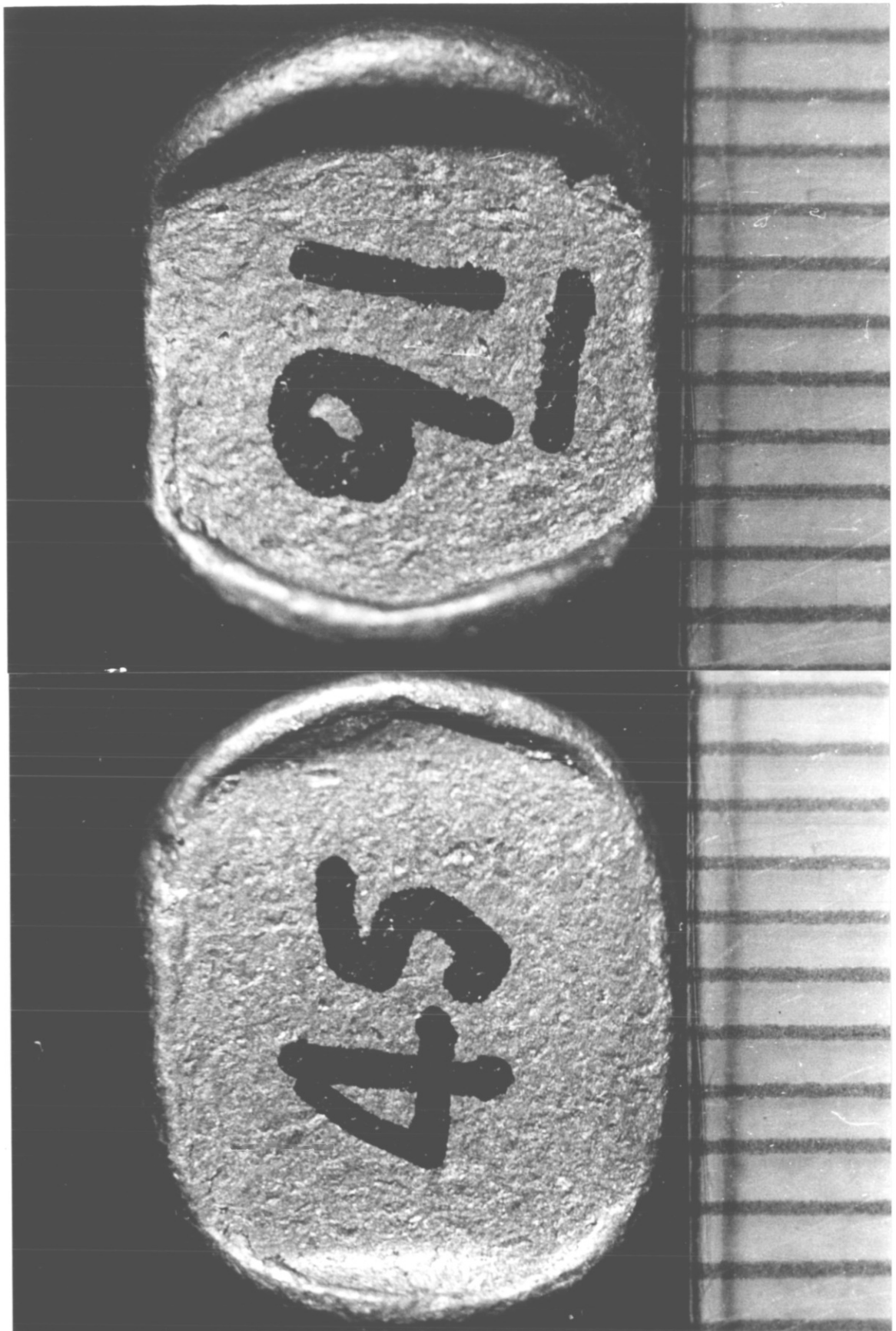
Scale : (mm)

Plate 4.3 : A close-up view of used items 45 and 91 (group C) showing
the curling at the edges

Scale : (mm)

5. HYDRODYNAMIC PROPERTIES OF DEXION STAMPINGS

5.1 Introduction

The prediction of terminal settling velocity for a non-spherical particle falling freely through water requires the knowledge of a suitable "shape factor". In the case of Dexion stampings, appropriate shape factors were found using the method outlined in section 2.2.2.2. Alternatively, the terminal settling velocity was determined experimentally by means of the 4" water column (see section 3.1). The results were compared and the definition of shape factor was physically modified to yield a compatible answer. For a meaningful comparison, however, it was essential to establish the influence of the pipe wall on the descent of individual platelets.

5.2 Pipe Wall Effects

In order to establish the effect of the pipe wall on particles descending axially in the 4" water column, it was decided to perform tests using spheres with a mean density similar to that of the test material. Although aluminium spheres are not commercially available, glass ballotini provides an excellent substitute. These glass balls are reasonably spherical and have a density only marginally less than aluminium; 2560 kg m^{-3} compared with 2629.1 kg m^{-3} for Dexion stampings. Hence, a sample of glass spheres with a suitable range of diameters was selected and the items were classified into six different groups according to size (see Appendix E - Part A).

First, each particle was checked for sphericity by taking two independent measurements of the particle diameter at right angles. If the fractional error based on the mean diameter was greater than 5%, the item was rejected. Then, using the Students' t-test, it was statistically established that items of the same group were identical within 3.1% when working at the 95% confidence level. For the case of glass spheres in group 1, these operations are illustrated more clearly in Part B of Appendix E. Using mean group diameters in the algorithm of section 2.2.2, it was possible to predict the free terminal settling velocity for each size. The results are shown in Table 5.1.

In order to proceed with the experimental determination of the terminal settling velocities, the glass spheres were dropped individually, from rest, down the 4" water column. All the data and results from these tests are included in Appendix F. The number of drops performed with each group of particles was sufficiently high to ensure a low probable error in timing, usually <2%. Occasionally, a sphere would descend adjacent to the column wall and/or collide with it - timings obtained thus were rejected. Runs where air bubbles adhered to a particle were also discarded. Fig. 5.1 shows the final agreement between the predicted and measured velocities. Apart from spheres with d = 3.637 mm, the results correlate remarkably well within a 5% error band. This provides strong evidence that for particles up to about 12 mm in diameter, the effects due to the pipe wall are negligible and can be safely ignored.

5.3   Experimental Determination of Terminal Settling Velocity for the

Test Material

5.3.1 Terminal settling velocity of fresh stampings

It is pertinent first to describe the method of fall of individual particles. All particles were released from rest by means of the magazine installed at the top of the water column. In general, they descended with their edges facing the column walls and their maximum projected area parallel with the water surface. Various effects were noted during the descent, and size as well as shape tended to dictate how pronounced each effect was.

5.3.1.1   The descent of discs

These disc-shaped particles, descended "flat" with a slow "spin" around a vertical axis. The overall path of the fall differed only slightly from a vertical line. During the descent, small eddies tended to affect the particle edges causing them successively to rise and fall. This phenomenon was named "tilting" and meant that the particle did not always present its greatest surface area facing vertically downwards. Tilting was never observed to be sufficiently pronounced to overturn a particle.

5.3.1.2   The descent of oval shapes

Unlike the discs, the trajectory described by "oval"-shaped stampings usually deviated substantially from the vertical. The large length to breadth ratios caused the particles to describe quite well defined

wide arcs while moving down the column; even more so for B particles. In spite of this, the stampings did not use the full width of the column and only rarely collided with the glass walls. For these items, "tilting" was sufficiently pronounced to flip a particle right over. One final effect, termed "slipping", is worth recording: the particle would swing from side to side and tilt while descending, then suddenly, usually just after it had reached maximum lateral displacement from the centre of the column, it would slip smoothly through the water. The slip would usually last for 200-300 mm of rapid descent before tilting recommenced. During this time, the particle would also undergo some horizontal displacement. Fortunately, this unpredictable pheonomenon occurred but rarely.

Fig. 5.2 shows a diagramatic representation of the mode of descent for the different types of platelets following from direct observations. An attempt has been made to break the pattern into a number of constituent secondary motions. Each particle had its terminal velocity measured on at least 56 independent runs. The data collected thus, are shown in Appendix G and the derived results are presented in the first column of Table 5.2.

5.3.2 Terminal settling velocity of used platelets

After about 110 runs of pressure drop tests using the 4" pipe rig, the terminal settling velocity of used stampings was reassessed by means of the 4" water column. Although physical changes had been small and were not expected to significantly affect either pattern of fall or velocity itself, individual tests revealed otherwise.

The descent of items D appeared only slightly more turbulent in terms of "tilting" and "swinging". In contrast, items C and B fell considerably more smoothly: "slipping" disappeared altogether while the effects of "tilting" and "swinging" were substantially reduced. This remarkable phenomenon was attributed to the presence of the metal curls at those edges of the stamping which were furthest apart. In fact, it was thought that these localised swellings of material acted as counter weights with a stabilising effect on tilting. In contrast to fresh stampings, "swinging" now took place in the y-z plane (not the x-z plane), which is normal to the direction of "tilting" (y-axis). The overall path of items B and C approximated a vertical line. This was reflected in settling velocities higher than those of fresh stampings. The relevant data are included in Appendix H and a summary of the results is presented in Table 5.2.

5.4 Theoretical Determination of the Terminal Settling Velocity for the Test Material

Despite "tilting" and the various other oscillations which occurred during descent, it was felt that the maximum projected area could be used as a valid parameter in terminal velocity calculations. Even during the most turbulent descents, each particle did present its maximum surface area towards the base of the column at frequent intervals. To try and modify the terminal velocity calculations to take into account the many disruptive effects would have been unnecessarily complex.

The method used to determine the terminal settling velocity of a two dimensional shape in water is outlined in section 2.2.2.2. This

calculation can be extended to a wide range of particle shapes, but so far it has been applied only to granular material and approximately spherical objects. Dexion stampings are unusual specimens and provide an interesting test of the theory. The steps required by this routine are shown explicitly in Table 5.3. The cases of 4" and 2" pipe tests have been considered using platelets of equivalent dimensions, (refer also to Tables 4.3 and 4.4). Following the evaluation of the terminal settling velocity for a sphere with an area based equivalent diameter d_a, it is necessary to obtain a value for the volumetric coefficient

$$K_1 = \frac{V_p}{d_a^3} \equiv Ke$$

As a first approximation, it has been assumed that each stamping derives its shape from an equi-dimensional cylinder of length d, i.e.

$$Ke = \frac{\pi\, d^2\, d}{4\, d_a^3} \qquad \qquad \cdots \cdot (5.1)$$

For a cylinder which is descending along its main axis $d = d_a$ and equation 5.1 reduces to

$$Ke = \frac{\pi}{4} = 0.785 \qquad \qquad \cdots \cdot (5.2)$$

Using either

$$K_2 = \frac{Ke\ t}{\sqrt{l\ b}} \quad \text{or} \quad K_2' = \frac{Ke\ t}{\sqrt{A_p}}$$

the terminal settling velocity was predicted for each case of pipe diameter. The calculated velocity was higher than the measured one (c.f. Table 5.2) - typically by about 17%. Obviously, this method of

accounting for the effect of shape was unsatisfactory. The next stage was to repeat the relevant part of the routine using a different value of Ke. Assuming the isometric shape was that of a cube (Ke = 0.696), the correlation overpredicted the velocity by an average of approximately 10%. Finally, employing an approximate volumetric factor Ke = 0.560 which is proposed by Heywood (11) for rounded isometric irregular shapes, the velocities calculated via K_2' agreed within approximately 1.5% of the experimental results.

This shows remarkable agreement and provides strong evidence that the use of a "rounded isometric irregular particle" with Ke = 0.560, accurately models the derivative shape of a typical Dexion stamping. Further, it confirms the earlier hypothesis that a single platelet of equivalent dimensions could be assigned to represent the entire material. Although the results differ only slightly, values of measured rather than predicted velocities will be used in further calculations.

5.5   The Effect of Platelet Thickness in Terminal Velocity Tests

No attempt was made to distinguish between drops of "slim" and "thick" items when carrying out terminal velocity tests using the 4" water column. In fact, the effect of thickness variation on the settling velocity is quite insignificant when compared to the uncertainties introduced by the disruptive phenomena of "tilting", "swinging", "slipping" etc.. To appreciate the relative magnitude of these effects, let us consider the following case.

Take for instance, group C of used platelets. According to Table 4.3, the average thicknesses of "slim" and "thick" items are 1.8346 mm

and 2.1508 mm respectively. Using the routine of Table 5.3, the corresponding terminal settling velocities are estimated at 208 mm/s and 228 mm/s. Experimentally, however, the minimum and maximum timings obtained for a mixed sample of items C are 8.103 s and 9.924 s with respective velocities of 244 mm/s and 200 mm/s. The experimental results encompass the upper and lower values of predicted velocities suggesting that the special effects associated with the descent of individual stampings outweigh thickness differences in the resulting value of settling velocity.

Clearly then, under these circumstances, the resolution of the timing mechanism is impaired and such fine differences in platelet thickness cannot be detected with confidence.

.
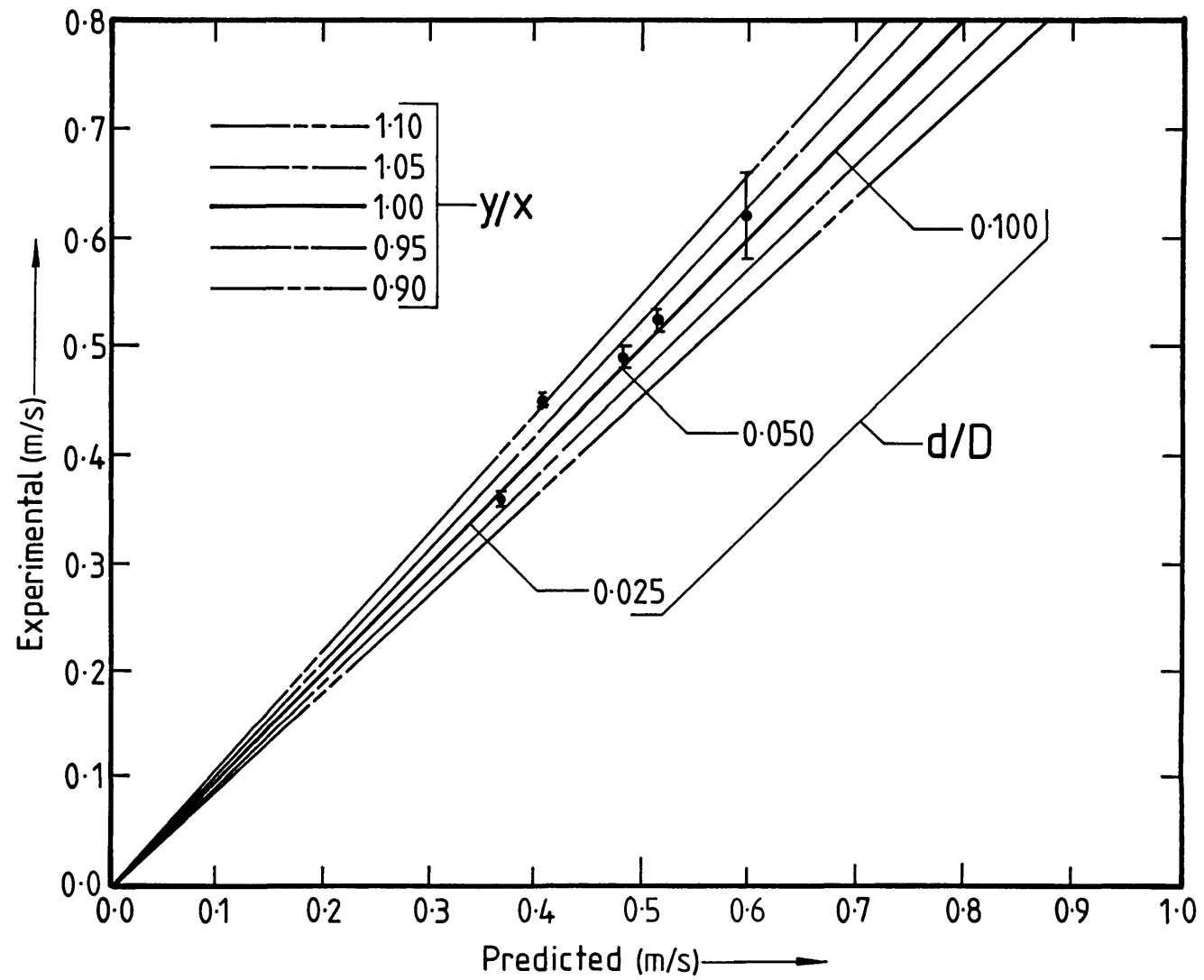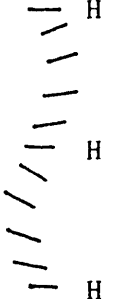
Fig. 5·1

Terminal settling velocities for glass spheres

Fig. 5.2 : Diagramatic representation of the mode of descent
for aluminium platelets

PLATELET TYPE d_a/ mm	Re_{d_a} of DESCENT	TYPES OF SECONDARY MOTION				
		VERTICAL	SPIN	TILTING	SMALL SWING	SLIPPING
THE TRUE MOTION IS OBTAINED BY SUPERIMPOSING THE APPROPRIATE CONSTITUENT SECONDARY MOTIONS				H ... H ... H		
NEW D d_a = 10.444	2086	**	*	*	*	
C = 11.397	2287	**	*	*	**	*
B = 12.411	2464		*	**	***	**
USED D d_a = 10.355	2176	*	*	**	**	
C = 10.657	2249	*	*	*	*	
B = 10.947	2478	**	*	*	*	
c.f. GLASS SPHERE d_a = 11.827	8435	***				

(*) : Number of * denotes the relative intensity of each effect (qualitative)

(H) : denotes horizontal position.

Table 5.1 : Predicted terminal settling velocity for glass spheres

GROUP No #	MEAN DIAMETER d (mm)	Ga_d -	Re_d -	V_{ts} $(mm\ s^{-1})$
1	2.934	384591	1074	368
2	3.637	732570	1482	410
3	5.115	2037774	2472	486
4	5.821	3003392	3001	518
5	7.814	7265064	4668	600
6	11.828	25190861	8693	739

The values of the physical parameters used in the calculation of the above results are given below:

$$\rho_s = 2560\ \text{kg m}^{-3}$$

$$\rho_w 20^\circ\ C = 997.2\ \text{kg m}^{-3}$$

$$\mu_w = 1002\ \times\ 10^{-6}\ \text{kg m}^{-1}\ \text{s}^{-1}$$

$$g = 9.81\ \text{m s}^{-2}$$

Table 5.2 : Comparison between experimental and predicted
terminal settling velocity (T.S.V.) for aluminium platelets

	EXPERIMENTAL				PREDICTED			
GROUP	NEW PLATELETS V_t (mm s^{-1})	USED PLATELETS V_t (mm s^{-1})	CHANGE ON V_t %	MEAN (T.S.V.) $\overline{V_t}$ (mm s^{-1})	PLATELETS USED IN 4" PIPE TESTS		PLATELETS USED IN 2" PIPE TESTS	
					Ke = 0.560			
					$K_2...$	$K'_2...$	$K_2...$	$K'_2...$
D	201 ± 8	212 ± 6	+5	206 ± 7				
C	202 ± 5	212 ± 6	+5	207 ± 6	(see Table 5.3)			
B	199 ± 6	227 ± 11	+14	213 ± 9				
OVERALL MEAN (T.S.V.)	220 ± 9			210 ± 8	203	213	207	219

1.4% OVERESTIMATED

0.5% UNDERESTIMATED

Table 5.3 : Stepwise calculation of the terminal settling velocity for pumped platelets using three alternative values of (Ke)

PLATELET PARAMETERS	4" PIPE TESTS			2" PIPE TESTS		
1 (mm)	12.466			11.5486		
b (mm)	9.615			9.577		
t (mm)	1.919			2.014		
d_a (mm)	11.258			10.742		
Ga_{d_a} (-)	2.269×10^7			1.971×10^7		
Re_{d_a} (-)	8250.06			7689.41		
V_{ts} (mm s^{-1})	736			719		
ISOMETRIC SHAPE	CYLINDRICAL	CUBIC	ROUNDED	CYLINDRICAL	CUBIC	ROUNDED
Ke	0.785	0.696	0.560	0.785	0.696	0.560
$K_2 = \dfrac{Ke\ t}{\sqrt{l\ b}}$	0.1376	0.1220	0.0982	0.1503	0.1333	0.1072
$N_{d_a}^{1/3}$	3.121			2.979		
K_{2A} (see Fig. 2.5)	0.3347	0.3113	0.2755	0.3525	0.3279	0.2877
$V_{t1} = V_{ts}\ K_{2A}$	246	229	202	253	235	206
$A_p = \dfrac{\pi\ d_a^2}{4}$	99.543			90.629		
$K_2' = \dfrac{Ke\ t}{\sqrt{A_p}}$	0.1509	0.1338	0.1076	0.1661	0.1473	0.1185
K_{2A}' (see Fig. 2.5)	0.3546	0.3290	0.2896	0.3762	0.3480	0.3047
$V_{t2} = V_{ts}\ K_{2A}'$	261	242	213	270	250	219

6.   RESULTS AND DISCUSSION

6.1   Introduction

Measurements of pressure drop for the flow of water carrying aluminium platelets 9-12 mm long x 2 mm thick in 2" and 4" I.D. pipelines were carried out. The water velocities ranged from 0.4 to 4.2 m/s and the concentration of platelets from 0 to 10% by volume of mixture.

In this chapter, the results for flow in horizontal pipelines are presented and discussed. The data is fitted with existing correlations and platelet transportation is explained in terms of an 'aerofoil' mechanism.

The measurements of pressure drop for flow in the vertical pipelines were subject to large experimental error. In some cases, the errors were thought to be of the same order as the excess pressure drop caused by the presence of the platelets. Therefore, it was felt that no reliable correlation could be produced with the available data. For this reason the vertical results have been relegated to Appendix J where due consideration is given to their accuracy before plotting them in a comparative manner to show the general trend.

6.2   Pressure Drop Correlation for Water Only

Water tests were performed using 4" and 2" pipe diameters to establish the head loss due to the liquid phase alone. The Fanning equation for the frictional pressure drop over a length L of pipe is given by

$$\Delta P = 4 \ f_w \ \frac{L}{D} \ \frac{1}{2} \ \rho_w \ V_m^2 \qquad\qquad \dots\dots (6.1)$$

or, in terms of the hydraulic gradient i_w which is the frictional head loss h_f divided by the pipe length L:

$$i_w \equiv \frac{h_f}{L} = 4 \ f_w \ \frac{1}{D} \ \frac{V_m^2}{2 \ g} \qquad\qquad \dots\dots (6.2)$$

The Fanning friction factor f_w depends upon the nature of flow (i.e. whether laminar or turbulent) inside the pipe as well as upon the internal surface of the pipe (i.e. whether rough or smooth). For the range of Reynolds numbers obtained in this work, the flow was always turbulent and therefore a Blasius type equation was used, i.e. $f_w = K/Re^n$ where K and n are constants. The data in Figs. J.1 and J.2 for the two horizontal pipelines of diameter 4" and 2" respectively, yielded slightly different values of K and n which are listed in Table 6.1. The difference arises purely from the fact that the 4" pipe was made of mild steel and was rougher than the 2" stainless steel pipe. The amount of scatter in the results for the 4" pipeline was comparatively greater than that for the 2" line. The maximum pressure drop in the 4" pipeline was about 2.0 psi, the accuracy of the measurement being ±0.01 psi and this resulted in large scatter particularly at the lower end of the flow rates investigated. In the 2" pipeline the pressure drop over the same length of pipe and at the same flow rate is approximately 2^5 times greater, (i.e. $\Delta P \propto \frac{1}{D^5}$), so that the frictional error is considerably smaller. A full analysis of the experimental errors is included in Appendix J.

Working equations for the hydraulic gradient i_w were obtained by substituting the appropriate expression for f_w into equation 6.2. The resulting expressions are also shown in Table 6.1. These equations were used in calculating the value of i_w required to evaluate the parameter ϕ for a given velocity V_m.

6.3 Pressure Drop Correlation for Water and Aluminium Platelets

6.3.1 Correlation of the results using the Durand and Condolios parameters

One hundred and twelve useful data points were obtained in the horizontal test section of the 4" pipe rig. When the results were correlated using the dimensionless groups proposed by Durand and Condolios, the following expression was obtained (see also Fig. 6.1a and Table 6.2), i.e.

$$\phi = 265 \ \psi^{1.38} \qquad\qquad \dots (6.3)$$

where $\phi \equiv \dfrac{i - i_w}{i_w \ C_v}$ and $\psi \equiv \dfrac{g \ D \ (S - 1)}{V_m^2 \ \sqrt{C_D}}$

For each data point, experimental values of i, V_m and C_v were used as input parameters; C_D was calculated from equation 2.12 and i_w was calculated using the appropriate equation given in Table 6.1.

Fig. 6.1a shows some experimental scatter at extreme values of the velocity range. At low flow rates, the scatter can be easily explained by operating instabilities. In order to obtain a low flow rate the bypass valve had to be opened, and the resulting change in effective

pump characteristic is shown in Fig. 6.2. Thus, when the bypass valve is fully open, there may be three separate operating co-ordinates. This will cause instability in both the flow rate and the horizontal pressure drop. In practice, this gave a bad trace on the chart recorder and reduced confidence in those particular results. Furthermore, it was at these low flow rates that the system was highly prone to blockage. It is possible that in switching from one stable position to another, the velocity will drop below that required for the onset of critical deposition.

Deviations from the straight line at high mean velocities are more difficult to explain. Newitt et al (25) have also observed this effect in their results and have explained the deviations in terms of experimental error. At high mean velocities the hydraulic gradients i and i_w become large and of similar magnitude. Consequently the dimensionless group $i - i_w/i_w$ C_v becomes inaccurate since it is calculated by taking the small difference between two large values, i.e. $i - i_w \rightarrow 0$. The Durand and Condolios correlation evaluated with their own coefficients has also been included for comparison.

When tests were performed using the 2" pipe rig, only 55 useful points were obtained in the available time. This was due to extensive modifications of the pipe rig, whereby several intermediate results (about 20 points) were performed under unfavourable conditions and were thus excluded. The final results, shown in Fig. 6.1b, can be correlated by the equation

$$\phi = 188 \ \psi^{1.44} \qquad\qquad \dots\dots (6.4)$$

the experimental scatter being similar to that found with the 4" pipe-
line.

The differences in the values of the exponents in equations 6.3
and 6.4 from the value of 1.5 proposed by Durand are not considered to
be significant and are well within the scatter of the experimental
results. The differences in the constants, however, are significant and
suggest that the inclusion of the drag coefficient to account for the
effect of particle shape is not entirely satisfactory and that there
must be a fundamental difference in the conveying of platelets as
opposed to rounded particles.

In order to establish the validity of the Durand and Condolios
approach for scale-up calculations, the results for each pipe diameter
were plotted collectively in Fig. 6.3, giving the following equation

$$\phi = 238 \ \psi^{1.41} \qquad \qquad \dots. \ (6.5)$$

Fig. 6.3 and Table 6.2 provide evidence that results obtained from
2" and 4" pipe diameters may be grouped together without significant
loss of accuracy and justify the use of this empirical correlation for
modest scale-up. A comparison between equations 6.3 and 6.4 suggests,
however, that the scale-up correlation is affected by the pipe dia-
meter. Specifically, it might be expected that the ratio of pipe dia-
meter to mean particle size D/d would affect the ϕ - ψ correlation, and
additional experimental work is needed with metallic platelets of
various sizes in several pipe diameters to establish this effect.

6.4 Interpretation of the Results

It is perhaps surprising that the results should be so well corre-
lated using the empirical Durand and Condolios expression. This implies
that the platelets are suspended over a substantial part of the velocity
range. In the absence of independent experimental evidence, the
validity of such an hypothesis will have to be investigated by adopting
a purely theoretical approach.

According to Clift et al (33) a plot of $f_m - f_w/S_m - 1$ as a func-
tion of V_m may be used to show whether values of V_m are sufficiently
high to sustain complete suspension of the solids. Such plots are shown
in Figs. 6.4a and 6.4b for the case of the 2" and 4" pipelines respec-
tively. These plots show that fully suspended flow, (this is represent-
ed by the asymptotic part of the curves), was actually achieved at
velocities of about 1.7 and 2 m/s respectively, in the two cases.
Thence, using equation 2.42 in its asymptotic form at high velocities,
i.e.

$$\frac{f_m - f_w}{(S_m - 1)} = A \, f_w \qquad \qquad \ldots\ldots \, (6.6)$$

the constant A was determined to be 8.6 and 2.4 for the 2" and 4" pipe-
lines respectively. If $A = 1$ then equation 6.6 implies that, in fully
suspended flow the slurry behaves as the "equivalent fluid" with the
viscosity of the carrier fluid and the density of the delivered
slurry. The fact that in the present study A is much larger, suggests
that platelets have an effect in addition to that of merely increasing
the effective density of the slurry. It appears that this arises from
the finite relative motion between the platelets and the fluid which

results in the generation of eddies. The latter are associated with increased frictional dissipation which results in additional pressure drop. This conclusion is corroborated by the results of Pouska and Link (44) who made measurements of the frictional pressure drop in the pumping of dilute suspensions of oil-shale in water. They used three broad particle size ranges (top sizes, 4.7, 13 and 25 mm) with volumetric concentrations ranging from 5% to 25% in pipelines of diameter 150 mm and 200 mm, the slurry velocity ranging from 1 to 5 m/s. Oil shale is a naturally occurring friable rock which, after crushing, assumes a relatively flat profile. While these authors do not explicitly quote the values of the constant A, as defined here, their results enable its value to be determined. Thus, for example, at a volumetric concentration of 6.5% of 25 mm solids and a velocity of 5 m/s in the 150 mm pipe, (this is high enough to ensure fully suspended flow), A was estimated to be 3.7 whereas at a concentration of 25% with 4.7 mm solids at the same velocity its value was about 5.7.

An independent estimate of the threshold velocity for turbulent uplift can be obtained using equation 2.37. This predicts the minimum velocities required for turbulent suspension as 7.4 and 4.6 m/s respectively. These values are considerably greater than those deduced from Fig. 6.4. There may be a number of reasons why equation 2.37 is not suitable for use with platelet material. Two possible reasons are discussed below:

(i)   Although the value of V_t employed in equation 2.37 is experimentally determined, it is still necessary to estimate an appropriate value for d; of the various alternatives, a sphere settling at the same terminal velocity was selected. The diameter of a

sphere settling at the same terminal velocity as the mean particle size of the platelet material used was estimated to be 1.5 mm. Using this equivalent sphere diameter makes equation 2.37 self consistent, but unfortunately, it does not simulate an aluminium platelet in physical terms.

(ii) Secondly, Wilson pointed out that the turbulent velocity correlation factor (exp K d/D) is highly dependent on the ratio d/D, K being a constant. In determining this constant, he correlated a large amount of data for which d $\ll$ D. In the present case, however, d is of the same order as D. As the particle diameter becomes a significant fraction of the macro-scale of turbulence, Λ, the predetermined value of K (=45) cannot be expected to apply rigorously.

Alternatively, an attempt was made to interpret this phenomenon in terms of the onset of platelet deposition in the pipe. Zandi (45) lists a number of empirical correlations to estimate the critical velocity V_{cr} below which solids begin to settle on the bottom of the pipe, thus forming a moving bed. Although the use of such correlations has gradually fallen out of favour, they are still useful in providing an approximate answer. One of the correlations cited by Zandi is that of Durand and Condolios who expressed the Froude number at the critical deposit velocity as a function of the particle size and concentration (see Fig. 2.7). Using an overall mean concentration of say 3% for both pipes, this correlation predicts that the critical deposit velocity of a Dexion stamping should be about 1.7 m/s and 2.5 m/s for the 2" and 4" pipes respectively. For the case considered the results are reasonably satisfactory, but there are a number of reasons why in general this correlation may be invalid for platelets.

Firstly, Durand and Condolios developed this correlation for spherical particles. Secondly, their original work was performed with sand and gravel up to 3 mm in size; extension of their results to aluminium platelets with maximum dimension about 10 mm has here been made on the basis that the Froude number remains constant. Thirdly and most important, there is no experimental evidence that platelets travel as a sliding bed.

In conclusion, it appears that both the Wilson and Durand approaches are inadequate for the treatment of flat objects. Therefore, it is felt that a fresh physically based approach should be considered which takes into account the actual shape of a platelet.

6.5   The Aerofoil Approach

Consider a single aluminium platelet resting on the inner wall of a horizontal pipe under no flow conditions. The vertical component of the reaction at the interface counterbalances the apparent weight of the submerged particle $W_{ap} = A_p \, t \, (\rho_s - \rho_w) \, g$, i.e. the platelet remains stationary. In order to set the platelet into sliding motion a force is required to overcome the horizontal component of the reaction at the wall. This has a magnitude of $W_{ap} \tan \phi$, where ϕ is the angle of solid friction. This force is normally provided by axial fluid flow in the containing pipeline. Fig. 6.5c shows the various sub-forces acting at a given height in fully developed flow. These are mainly due to the dynamic pressure exerted on the leading face and shear stresses associated with the free sides which are parallel with the direction of flow. In order to establish the state of equilibrium at a given flow rate, it is necessary to estimate the magnitude of each force. To facilitate this task, a number of simplifying assumptions are made:

(A) **Assumptions related to the geometry of the pipe/platelet system**

(i) The radius of curvature of the containing pipe is large so that the platelet lies flat and no fluid flow occurs at the interface.

(ii) The x-y dimensions of each platelet are approximately equal so that it is reasonable to assume geometric symmetry. This makes the maximum total force independent of the platelet orientation with respect to the direction of flow.

Furthermore, an order of magnitude analysis shows that the force exerted on the leading face is by far the greatest. Thus, the profile of the leading edge is an important factor in calculating the relevant force. The least favourable situation in terms of the effective dynamic pressure arises when a heavy platelet, (type B), is positioned so that the leading face is defined in the y-z plane. In this case, a refinement is introduced, i.e. the leading face is curved in both y and z directions, the radii of curvature being $\frac{y}{2}$ and $[\frac{t}{2} \cos \theta; \frac{t}{2}]$ respectively. The latter describes an elliptical profile and varies between a semi-circle at $\theta = 0^{\circ}$ and a straight line at $\theta = 90^{\circ}$ (see Fig. 6.6).

(iii) Finally, it is assumed that for reasons of maximum stability, (i.e. even pressure distribution on the projected area), the platelet orientates itself so that the direction of flow is parallel with one of the base defining axes.

(B)   Assumptions related to fluid flow around the platelet

(i)   It is assumed that there is no flow separation at the leading edge
of the platelet despite the fact that the flow becomes fully
turbulent above the buffer zone, (this extends to a height of
approximately 0.2 mm), and the platelet profile poses a step
change to on-coming streamlines. This implies that the fluid
comes to isentropic rest against the leading face and new
turbulent boundary layers develop along the shearing faces. There
is, however, no flow around the trailing edge. These assumptions
are illustrated schematically in Figs. 6.5a and 6.5b.

The geometry of a typical platelet is shown in Fig. 6.6.
Consider an elemental area da. This is defined by the inter-
section of a horizontal strip dh, a distance h from the pipe wall
and a solid section $d\theta$ describing an angle θ with the direction of
flow. As the flow is frictionless, the Bernoulli equation applies
and the total stagnation pressure acting normally on the projec-
tion of da in the direction of flow is given by

$$P_h = P_s + \frac{1}{2} \rho_w V_h^2 + \rho_w g h \qquad \qquad \dots \dots (6.6)$$

where P_s = static pressure

$\frac{1}{2} \rho_w V_h^2$ = dynamic pressure

V_h = fluid velocity at height h

$\rho_w g h$ = hydrostatic pressure

Similarly, an expression may be written for the total pressure
acting on the corresponding elemental area located on the trailing

face. Hence, the net pressure in the x-direction equals P_h (leading) - P_h (trailing). Since there is no flow around the trailing face the dynamic component is zero. In addition, the hydrostatic components will cancel as they are equal in magnitude and act in opposite directions.

(ii) Assuming that the platelet length is infinitesimally small compared to the rate of frictional pressure drop along the pipe, then the components of static pressure also cancel.

Thus, the integral force acting on the whole of the leading face for a flat profile is given by

$$F_f = \frac{1}{2} \left[\int_0^t \rho_w V_h^2 \, y \, dh \right] \qquad \qquad \dots \text{(6.7)}$$

or for a curved profile

$$F_f = 2 \left[\frac{1}{2} \int_0^{(\pi/2)} \int_0^t \rho_w V_h^2 \frac{y}{2} \cos \theta \cos \Omega \, dh \, d\theta \right] \qquad \dots \text{(6.8)}$$

where the local velocity V_h may be estimated using the Von-Karman (46) equation for a logarithmic velocity profile, i.e.

$$V_h = V_\tau \, h^+ \qquad \qquad \dots \text{(6.9)}$$

if $h^+ < 5$

$$V_h = V_\tau \, (11.51 \log h^+ - 3.05) \qquad \qquad \dots \text{(6.10)}$$

if $5 < h^+ < 30$

$$V_h = V_\tau \ (5.67 \ \log \ h^+ + 5.46) \qquad \qquad \ldots (6.11)$$

if $h^+ > 30$

where $V_\tau = \sqrt{\tau_o/\rho_w}$ and $h^+ = (V_\tau \ h/\nu_w)$

τ_o may be found from the single phase pressure drop tests, i.e.

$$\tau_o = \frac{\Delta P \ D}{4 \ L} \qquad \qquad \ldots (6.12)$$

where $\Delta P = i_w \ L$ and $i_w = \frac{2 \ f_w \ V_m^2}{g \ D}$

Apart from the force acting on the leading face, shearing forces develop on the surface areas of the surrounding sides due to the shear stresses. Depending on the flow regime a drag coefficient may be found as follows,

$$C_D = 1.328/\sqrt{Re} \qquad \qquad \ldots (6.13)$$

if $h^+ < 30$ or,

$$C_D = 0.072/Re^{0.2} \qquad \qquad \ldots (6.14)$$

if $h^+ > 30$

where $Re = \dfrac{V_h \ x}{\nu_w} \qquad \qquad \ldots (6.15)$

The total shear force acting on the two elevated sides of a flat profile may be found from,

$$F_s = 2 \left[\frac{1}{2} \int_o^t \rho_w V_m^2 C_D x \, dh \right] \qquad \ldots (6.16)$$

or of a curved profile

$$F_s = 2 \left[\frac{1}{2} \int_o^t \rho_w V_m^2 C_D (x-y) \, dh \right] \qquad \ldots (6.17)$$

Finally, the shear force acting on the top surface of a flat profile is calculated by

$$F_t = \frac{1}{2} \rho_w V_t^2 C_D x y \qquad \ldots (6.18)$$

or of a curved profile

$$F_t = \frac{1}{2} \rho_w V_t^2 C_D (x-y + \frac{\pi y^2}{4}) \qquad \ldots (6.19)$$

Thus, by using an estimated initial value for the mean slurry velocity, the sum of all the hydrodynamic forces may be calculated by integrating over the active area of the platelet. The result is compared with the horizontal component of the reaction at the wall and the velocity is then adjusted accordingly until

$$F_f + F_s + F_T = W_{ap} \tan \phi \qquad \ldots (6.20)$$

i.e. the instant the platelet begins to slide.

The sliding angle ϕ was determined experimentally by placing a number of platelets onto a fully submerged steel platform. By gradually raising one edge of the platform, the angle of inclination at which the platelets began to slide down the plane was recorded. This was found to be approximately 22° compared with about 25° under dry conditions.

The system of forces acting upon the platelet are responsible for setting up competing moments about the bottom edge of the trailing face. The weight of the platelet provides an anti-clockwise moment which acts to sustain contact with the pipe wall. In contrast, clockwise moments produced by the hydrodynamic forces tend to up-turn the platelet. Expressions for the equivalent moments can be easily derived from equations which define elemental forces. Each turning moment is obtained by multiplying the local force by the distance between its line of application and the pivoting edge, e.g. F_s h = side elemental moment in Fig. 6.6. In this way, it is possible to obtain the threshold slurry velocity required for equilibrium of the turning moments. At this velocity, the platelet becomes buoyant and inclines to the horizontal by levering against the pivoting edge (see Fig. 6.7). Once inclined, a lift force F_L will be generated due to differential pressure created by fluid flowing faster over the upper than lower surface. At this point, the platelet behaves like an aerofoil and it will lift and become "fluid-born". Thereafter, it is expected to follow a trajectory similar to that shown in Fig. 6.7; i.e. the platelet is carried into the main stream of flow and accelerates to the local velocity of the fluid by projecting the maximum cross sectional area to the direction of flow. This is the most stable position, since the driving force is provided by the greatest possible dynamic pressure. As the relative velocity is reduced the platelet will re-orientate horizontally, settle and the

process will repeat. The reason for settling is due to "stalling" caused by a sudden drop in the driving force as the platelet switches orientation. If the mean slurry velocity is increased well beyond the threshold for up-lift, then excess lift will be available even at small differential velocities so that relatively long periods of suspension may be sustained.

Critical velocities were calculated for the onset of sliding for the case of a platelet with a curved profile. Values of 0.53 m/s and 0.61 m/s were obtained for 2" and 4" pipe diameters respectively. These results are in good agreement with the lowest possible velocities for on-set of motion recorded during slurry tests (c.f. Figs. 6.4a and 6.4b). Similarly, the minimum velocities required for platelet up-lift were estimated at 1.74 m/s and 2.14 m/s in each case. These predictions are in excellent agreement with the velocities at which asymptotic values are reached in Figs. 6.4a and 6.4b.

Although these results were obtained for single particles, it is expected that groups of platelets within dilute mixtures will behave similarly. Some dumping is, however, likely to occur due to inter-particle collisions. Overall, the results provide strong evidence to suggest that platelets suspend more readily than granular material. This confirms the assumption of partially suspended flow which is further supported by the following:

(i)   When the data were plotted according to Fig. 2.8b, no linear part could be identified.

(ii) Figs. 6.8a and 6.8b give the results fitted by equation 2.31 which was proposed by Newitt (25) for heterogeneous suspensions. Once again the degree of correlation is excellent and since platelets assume relatively high drag coefficients, the present work favours Newitt's assumption of no slip between solid particles and water.

6.6 A Comparison of the Results using the "Bed-Slip" Model

Having established that suspended flow is the prevailing mode of transport above mean velocities of about 2 m/s, it is important to explain the conveying mechanisms which take place in the velocity range 0.6 to 2 m/s. Since a sliding-bed type of flow is to be expected in this range, the "Bed-Slip" model first proposed by Wilson (31) has been employed to analyse the problem. According to Streat (27), the total pressure drop in a sliding bed is given by,

$$i = 2 f_s (S - 1) C_b [\frac{\sin \theta - \theta \cos \theta}{\pi}]$$

$$+ 2 f_d \frac{\rho_{mb}}{\rho_w} \frac{\theta}{\pi} \frac{V_b^2}{D g}$$

$$+ 2 f_t \frac{\rho_{mt}}{\rho_w} \frac{(\pi - \theta)}{\pi} \frac{V_t^2}{D g}$$

$$+ \frac{2 f_s f_b}{\tan \phi} \frac{\theta}{\pi} \frac{(V_t - V_b)^2}{D g} \qquad \ldots (6.21)$$

where the symbols are as defined in the Ref. 27 and θ is shown clearly in Fig. 6.9. The significance of the terms on the right hand side of the equation are as follows:

1st - contribution due to sliding friction between solids and the pipe wall

2nd - contribution due to fluid flow through the bed section

3rd - contribution due to fluid flow in the free pipe section

4th - contribution due to shear stress at the upper surface of the moving bed.

Equation 6.21 is not simple to use for the general case which it describes. Many of the quantities required for the calculation of the hydraulic gradient are presently unknown, e.g. individual velocities and local concentrations. However, the task can be simplified by making a number of reasonable assumptions, i.e.

$$V_b \sim V_t \sim V_m$$

$$f_t \sim f_b$$

$$\rho_{mt} \sim \rho_w$$

$$f_t \sim f_d \frac{\rho_{mb}}{\rho_w} \sim f_s$$

For a given value of the in situ volumetric concentration, the deposit angle θ can be estimated from the geometry of the system and i may then be predicted using velocity as the input parameter. Figs. 6.10a and 6.10b compare experimental data with predictions and show that equation 6.21 over-predicts the experimental results above about 2 m/s. This is to be expected since the critical suspension velocity for platelets is approximately 2 m/s and suspensions compare favourably

against sliding loads in terms of head loss. Below the critical velocity of deposition, however, the results are underpredicted by a factor of about 3. This is very surprising since it appears to negate the "bed-slip" model.

The calculation of i requires the angle of deposit θ. In this work θ was based on values of delivered rather than in situ solids concentration. Whilst $C_v \simeq C_{vh}$ for fully suspended flow, the formation of a sliding bed at sub-critical velocities leads to a differential increase of the in situ solids concentration. If a stationary bed exists, then relatively few particles are transported by saltation over the surface of the bed resulting in $C_v \ll C_{vh}$. In either case, the solids concentration measured by sampling at the pipe exit does not relate to the actual in situ concentration and is likely to be much smaller than the latter.

Consider, for instance, the case where $C_v \simeq 2\%$ at a mean velocity of about 0.6 m/s. At this in situ solids concentration the estimated angle of deposit is about 35°, whereas an angle of about 75° is required in equation 6.21 to match the results. The latter implies an in situ volumetric concentration of 15%. There is some experimental evidence to suggest that this is possible. During some tests with the 4" pipe rig at low velocities (~ 0.6 m/s), the flow was gradually reduced to zero whilst a constant feed of solids was maintained. Hence, despite a risk of serious blockage the solids were allowed to retain their position within the pipeline during a complete shut down. Following one such run, the water was carefully drained and a short pipe section was removed from the horizontal leg. This was found to be almost half full of solids (see Plate 6.1), although the pipe itself was delivering at a concentration of about 1.8% by volume.

In conclusion, low velocities may lead to the formation of either a sliding bed regime or even stationary deposits with saltation of aluminium platelets. The application of the "Bed-Slip" model is of limited value unless the in situ concentration is determined directly.

6.7 Head Loss Associated with the Hydraulic Conveying of Metallic Platelets

6.7.1 The effect of shape on head loss

Consider a hydraulic system conveying granular material. Suppose that the system parameters, that is, the properties of the carrier fluid, pipe diameter, mean velocity, mean particle volume (not shape), volumetric concentration, relative density of solids etc. are fixed. Assume that only particle shape is allowed to vary. What is the effect of shape on head loss? Let us analyse the two case studies for 'spherical' particles and platelets.

The effect of particle shape on head loss can be predicted using the Durand equation with drag coefficients of 1.360 for platelets and 0.444 for volume equivalent spheres. In this case, the calculated ratio ϕ for spheres and platelets is independent of velocity at a value of 2.31.

Fig. 6.11 shows the actual head loss for platelets obtained experimentally and given by equation 6.5 compared with the predicted head loss for volume equivalent spheres using the Durand equation. In this case, the ratio of ϕ for spheres and platelets is a function of mean velocity and can be expressed as follows:

$$\frac{\phi_{spheres}}{\phi_{platelets}} = \frac{150 \ \psi_{spheres}^{1.5}}{238 \ \psi_{platelets}^{1.41}} = \frac{150}{238} \ [\frac{g \ D \ (S-1)}{V_m^2}]^{0.09} \ [\sqrt{\frac{C_{D \ platelets}}{C_{D \ spheres}}}]^{0.09}$$

$$\ldots \ (6.22)$$

For the system parameters used in this study equation 6.22 simplifies to:

$$\frac{\phi_{spheres}}{\phi_{platelets}} = \frac{1.505}{V_m^{0.18}} \qquad \ldots \ (6.23)$$

where $2 < V_m < 4$ m/s (i.e. fully suspended flow) and D = 4".

Fig. 6.11 predicts that the head loss in conveying metallic plate-lets is less than for volume equivalent spheres though the ratio $\phi_{spheres}/\phi_{platelets}$ falls from 1.34 at 2m/s to 1.17 at 4 m/s.

At low velocities, (i.e. less than about 2 m/s), transport takes place in a sliding bed regime and wall friction accounts for most of the pressure drop regardless of particle shape. Conversly, particle suspension dominates at higher velocities and the pressure drop therefore becomes dependent on particle drag which arises from the relative velocity of fluid. The inclusion of platelet drag in equation 6.5, however, was made on the assumption that platelets travel with their plane perpendicular to the direction of flow. Clearly, in practice, this does not apply and their plane is thought to alternate between the maximum and minimum projections to the direction of flow as postulated in Fig. 6.7. Thus, the effective drag coefficient is substantially smaller than 1.360 resulting in a higher head loss than that predicted by the Durand equation. These physical effects are born out in the

relatively high values of the asymptotes obtained in Figs. 6.4a and 6.4b. Equation 6.23 predicts, however, that at relatively high velocities, (i.e. greater than about 10 m/s), the frictional head loss is virtually independent of particle shape. At velocities in excess of 10 m/s there is little or no slip between the particles and the fluid so that particle drag has no effect on the head loss and the mixture behaves as a heavier fluid with mean density ρ_m. At intermediate velocities, however, the effect of drag due to particle shape is important. Fig. 6.11 shows that the conveying of metallic platelets at a velocity of say about 3 m/s incurs nearly 25% less head loss than the pumping of volume equivalent spheres.

In general, it can be concluded that particle shape is important, though further experimentation is required to rigorously quantify the effect.

6.7.2 The effect of concentration on the consumption of energy

Figs. 6.12a and 6.12b show the specific energy consumption for metallic platelets transported in horizontal pipes. The specific energy consumption per unit of solids throughput is compared at four levels of concentration using lean mixtures. The power consumption is based on the frictional energy loss for slurry flow whilst the throughput is related to the mean slurry velocity, pipe diameter and solids concentration.

The specific energy consumption E_s is derived from the energy required to transport a unit mass of solids over a unit distance.

$$\Delta P = i \; \rho_w \; g \; (N \; m^{-3}) \qquad \qquad \text{... (6.24)}$$

The volumetric flow rate at a mean velocity V_m is

$$Q = \frac{\pi}{4} D^2 V_m \; (m^3 \; s^{-1}) \qquad \qquad \text{... (6.25)}$$

power consumption per meter of pipe

$$= \Delta P \; Q \; (W \; m^{-1}) \qquad \qquad \text{... (6.26)}$$

solids throughput

$$M_s = Q \; C_v \; \rho_s$$

$$= \frac{\pi}{4} D^2 V_m C_v \rho_s \; (kg \; s^{-1}) \qquad \qquad \text{... (6.27)}$$

Hence, $E_s = \dfrac{\Delta P \; Q}{M_s} = \dfrac{i \; g}{S \; C_v} \; (J \; kg^{-1} \; m^{-1}) \qquad \qquad \text{... (6.28)}$

in more useful units

$$E_s = 0.2778 \; \frac{i \; g}{S \; C_v} \; (kWh \; Te^{-1} \; km^{-1}) \qquad \qquad \text{... (6.29)}$$

$$M_s = 2.477 \times 10^{-2} \; (D^2 \; V_m \; \rho_s \; C_v) \; (MTe \; yr^{-1}) \qquad \qquad \text{... (6.30)}$$

For a particular value of C_v the specific energy consumption is dependent only on the value of i which can be predicted using equation 6.5. Thus, E_s is a function of pipe diameter, mean velocity, particle size and provides a convenient parameter for comparing the effectiveness of pumping platelet slurries.

Figs. 6.12a and 6.12b show a strong dependence of the specific energy consumption on solids throughput especially at low concentrations. A concentration of 1 v/o causes a sharp rise in the specific energy consumption producing a "run-away" situation at very small throughputs. E_S is calculated by substituting equations 6.3 and 6.4 into equation 6.29, i.e.

$$E_S = K \left[\frac{g \ d \ (S - 1)}{V_m^2 \ \sqrt{C_D}} \right]^\alpha \frac{i_w \ g}{S} + \frac{i_w \ g}{S \ C_v} \qquad \ldots (6.31)$$

where $i_w \propto V_m^\beta$

assuming for simplicity that $\alpha = 3/2$ and $\beta = 2$, it is easily seen that the first term on the right of equation 6.31 becomes very small at large values of V_m, so that

$$E_S \simeq \frac{i_w \ g}{S \ C_v} \rightarrow \infty \qquad \ldots (6.32)$$

Since E_S varies according to V_m^2 each curve is expected to pass through a minimum shown clearly in Fig. 6.12b. However, as the concentration increases the specific energy becomes less sensitive to the velocity. At 8 v/o a wide plateau is formed showing little variation of E_S with M_s.

These figures show quite convincingly that there is a strong incentive to use moderately high concentrations, especially for large pipe diameters.
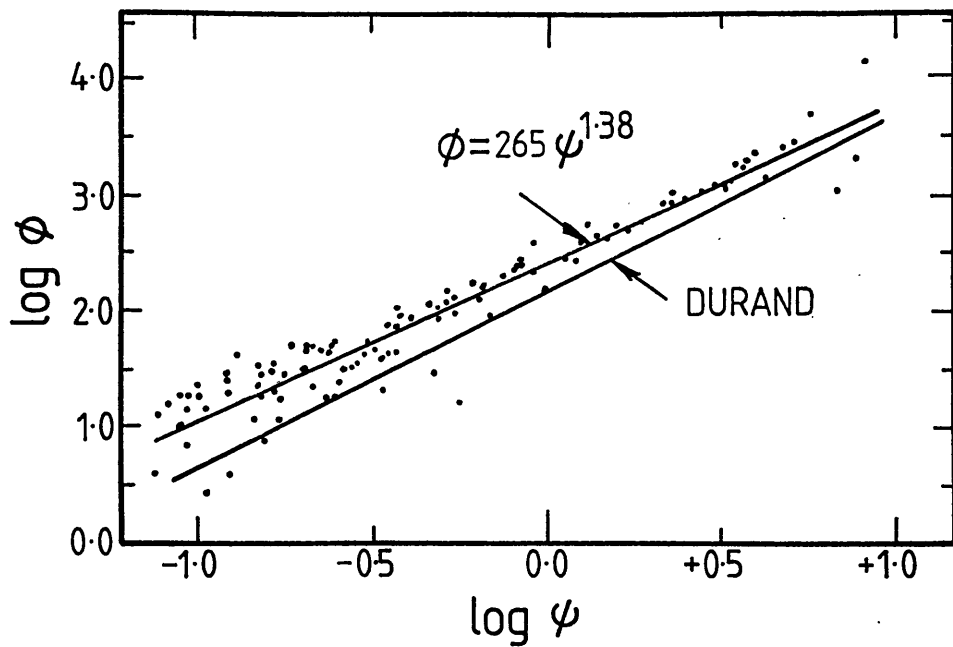
(a) 4" ID Test Section
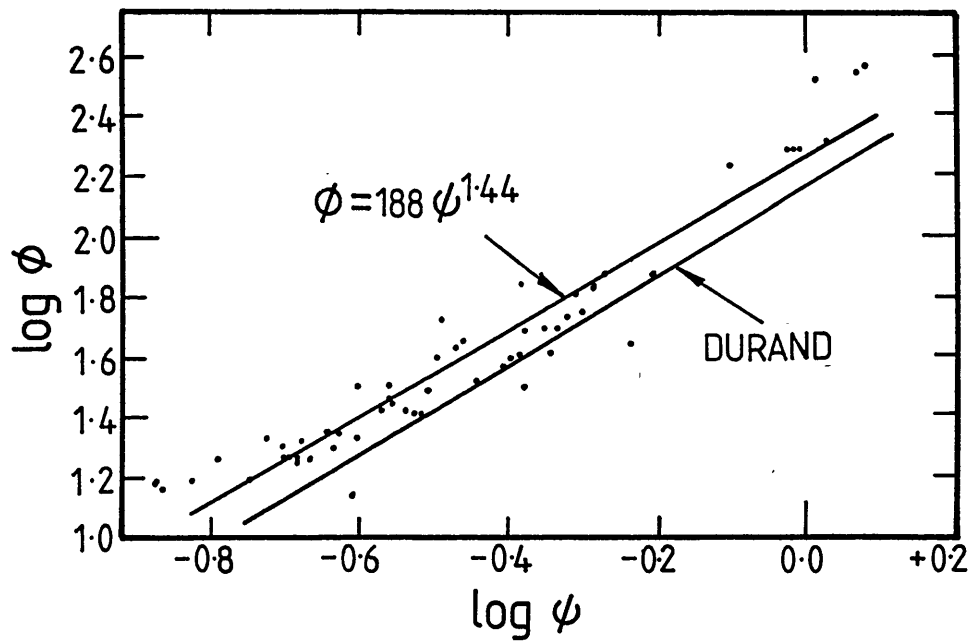
(b) 2" ID Test Section

Fig. 6·1

Log ϕ vs log ψ data for individual horizontal sections
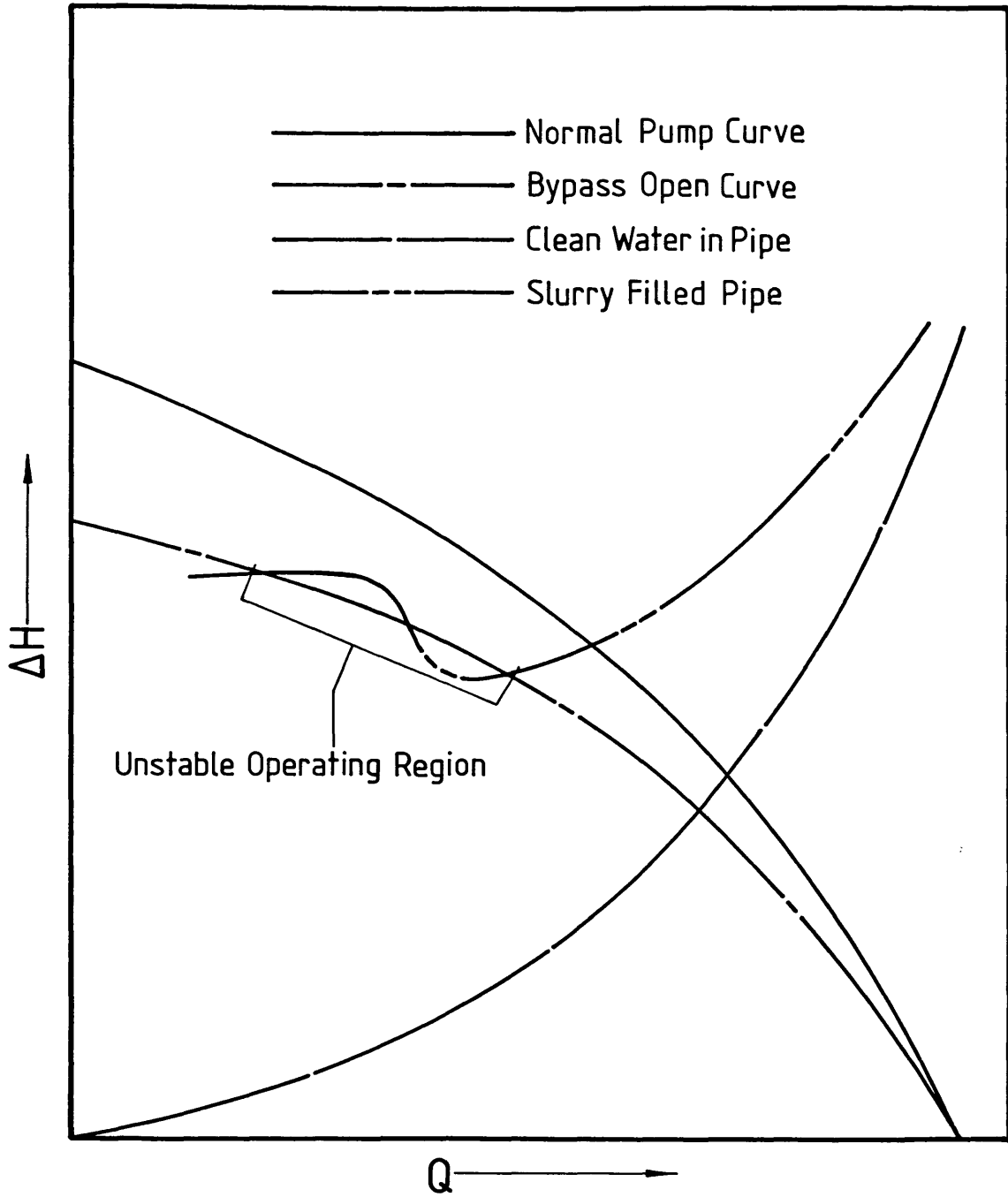
Fig. 6·2

Illustration of instability caused by use of a bypass
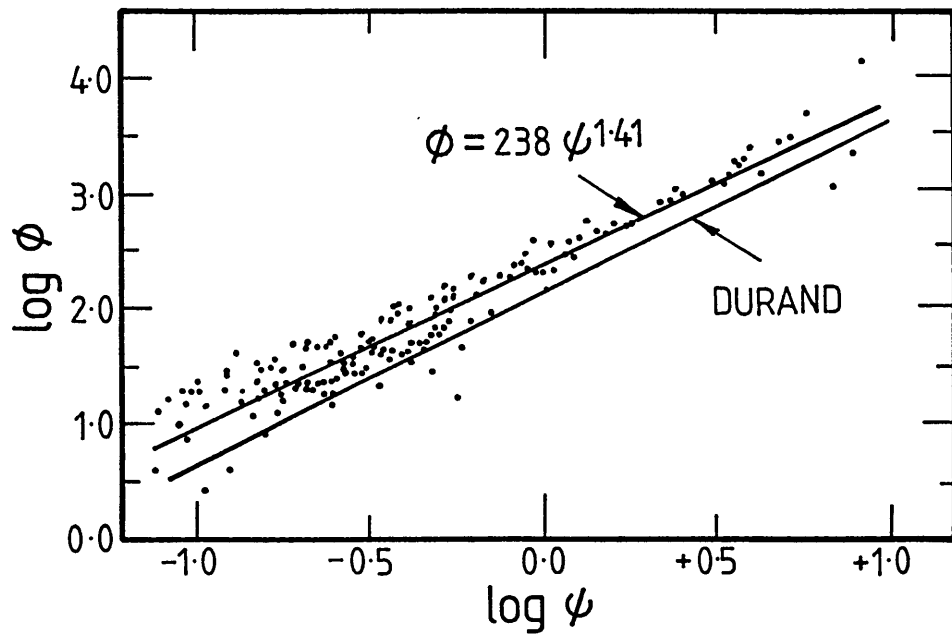
$$\phi = 238 \, \psi^{1\cdot41}$$

DURAND

Fig. 6·3

Log ϕ vs log ψ data collected for 2″and 4″horizontal sections
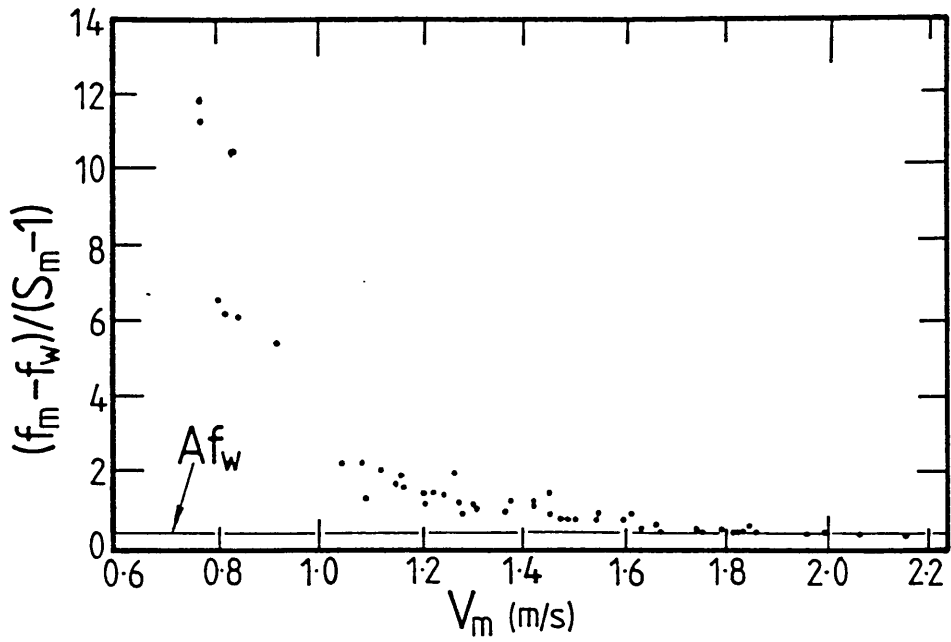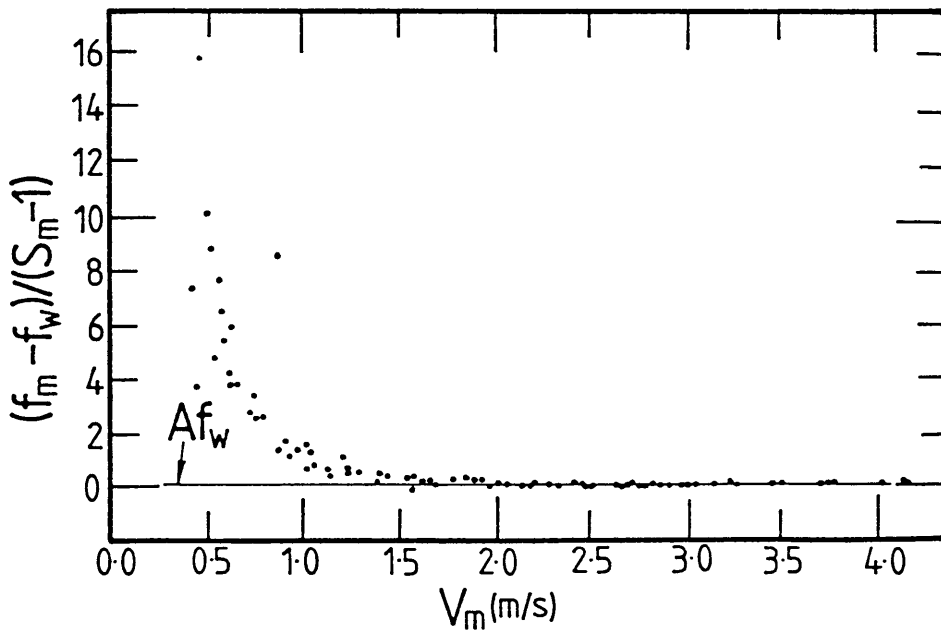
(a) 2" ID Test Section

(b) 4" ID Test Section

Fig.6·4 $(f_m - f_w)/(S_m - 1)$ vs V_m data-horizontal
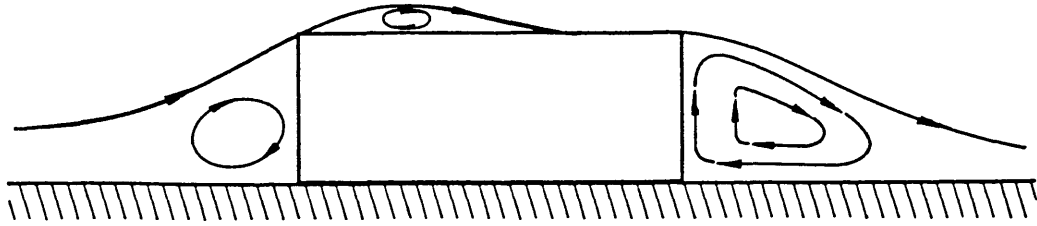
(a) Qualitative streamline pattern
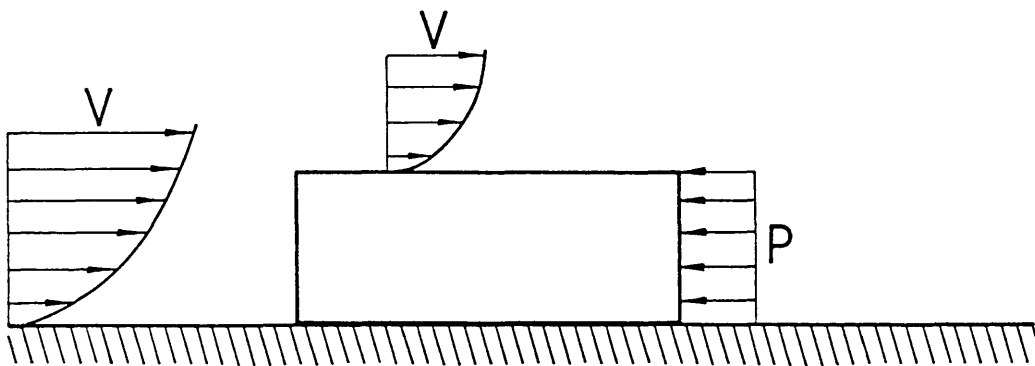
(b) Assumed velocity and pressure profiles
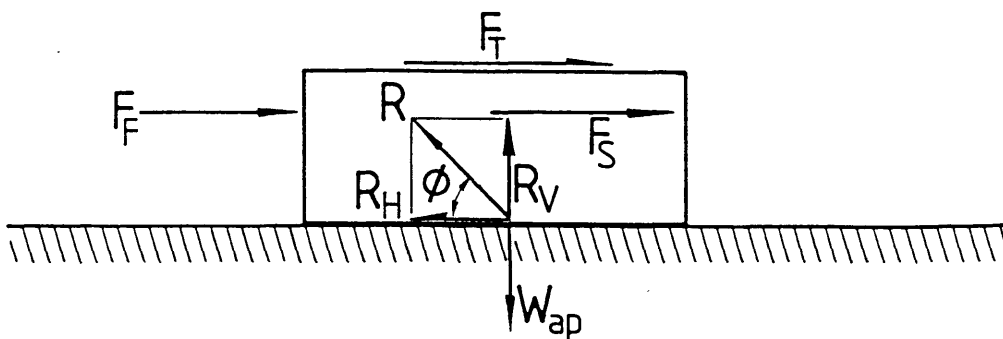
(c) Main forces acting on the platelet

Fig. 6·5

$$\Omega = \tan^{-1}\left|\frac{2h-t}{2x'}\right|$$

$$\left[\frac{2x'}{t\cos\theta}\right]^2 + \left[\frac{2h-t}{t}\right]^2 = 1$$
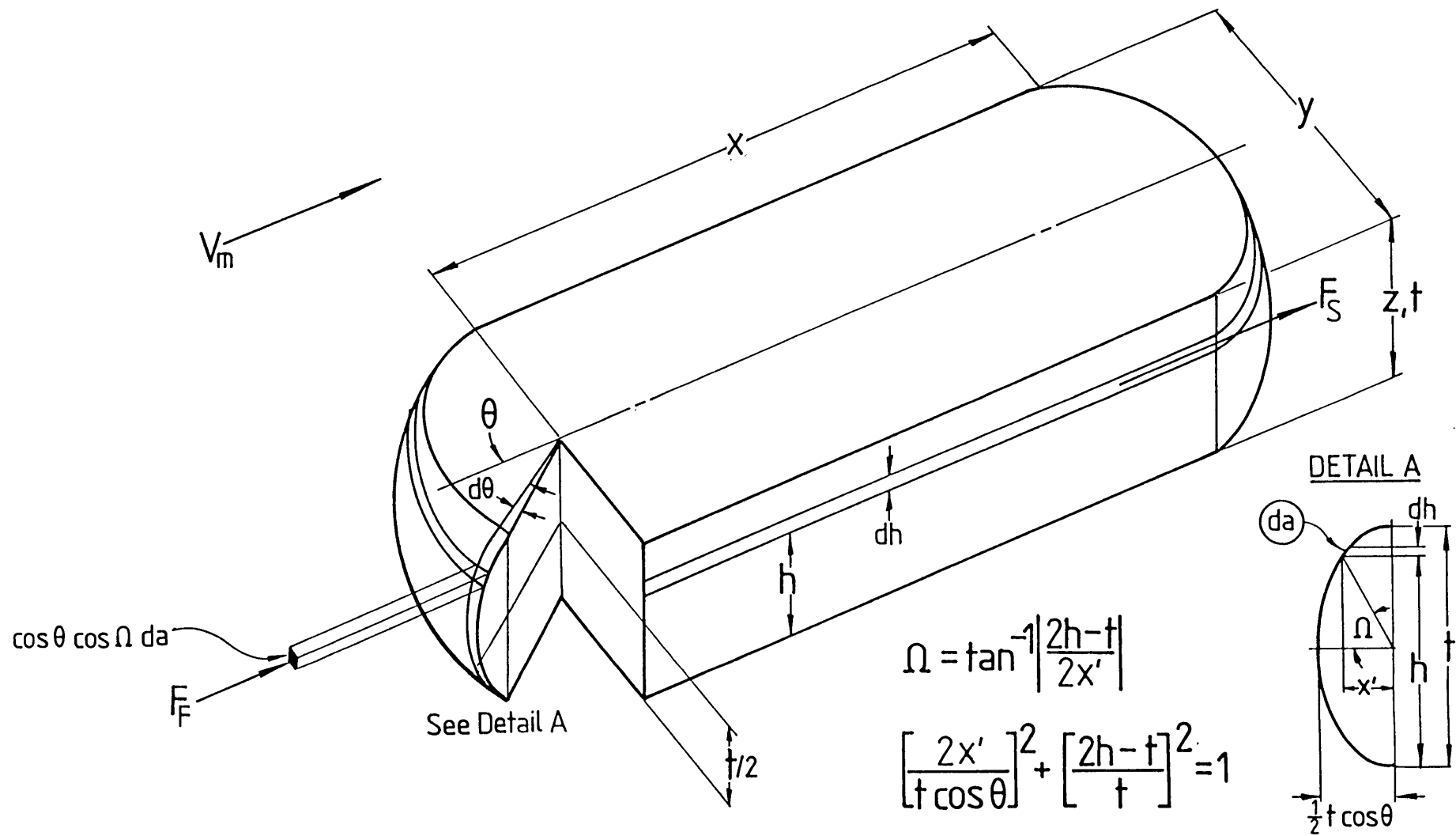
Fig. 6·6

Definition of a typical platelet profile
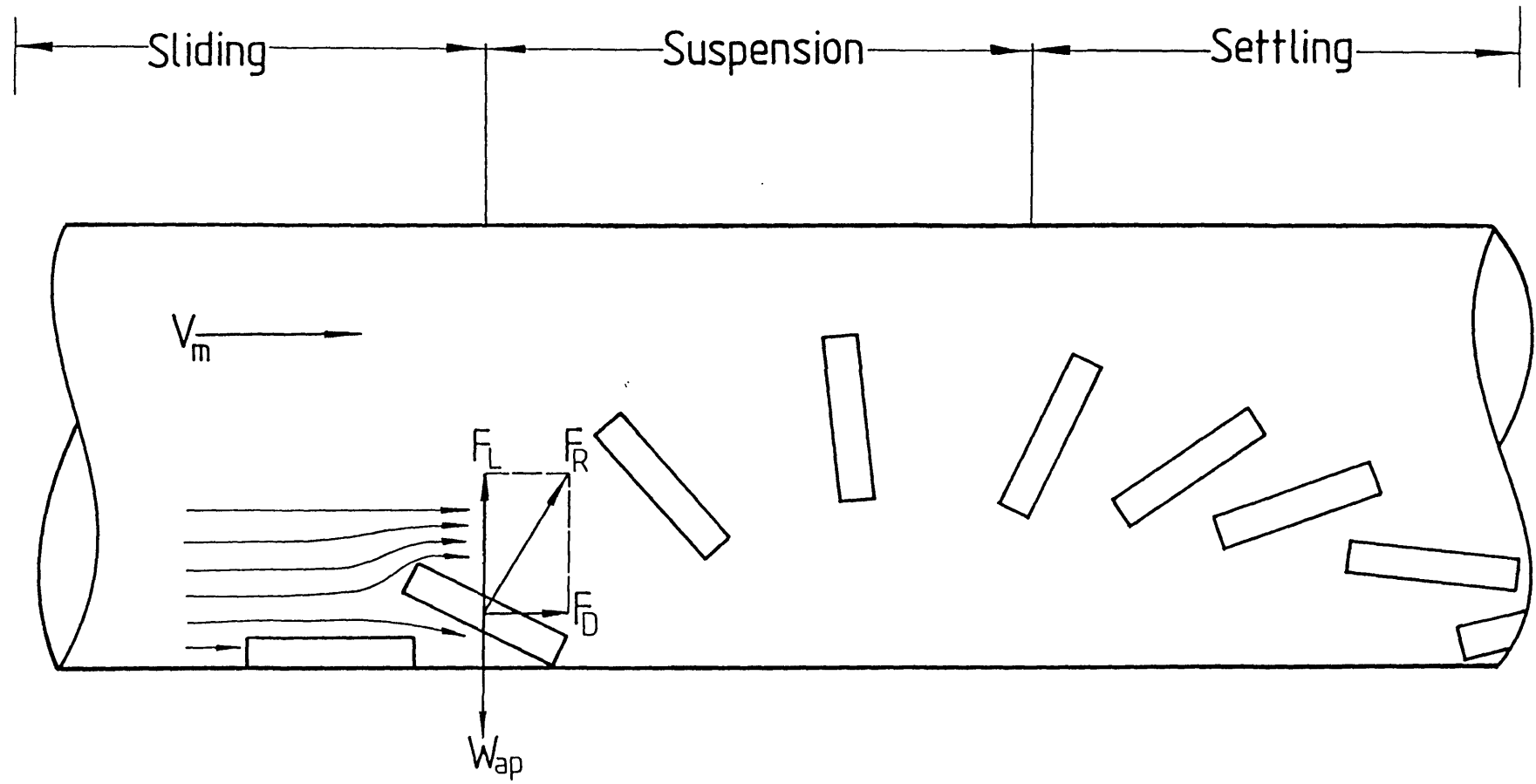
Fig. 67

Likely trajectory of individual platelet in fully developed pipe flow
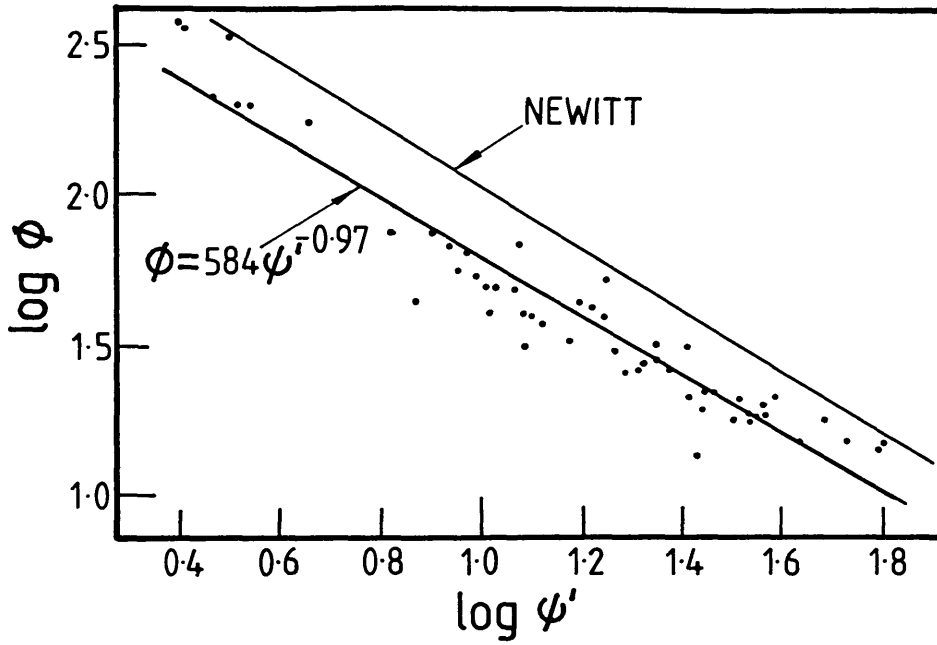
(a) 2″ ID Test Section
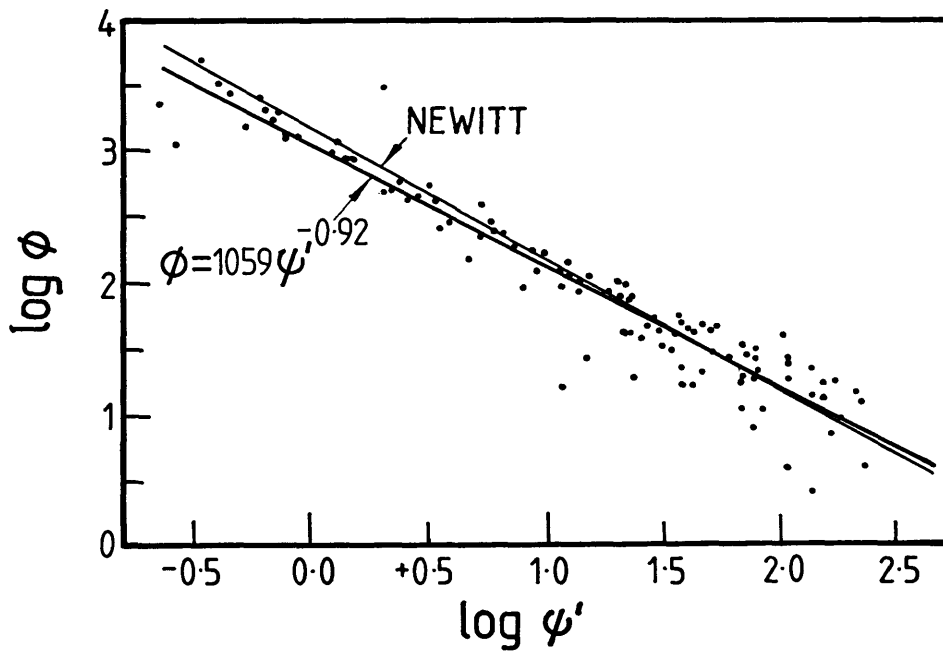
(b) 4″ ID Test Section

Fig. 6·8

Log ϕ vs log ψ' data for individual horizontal sections
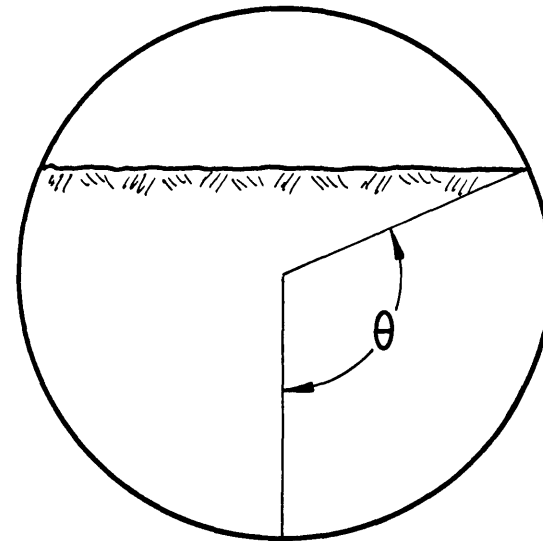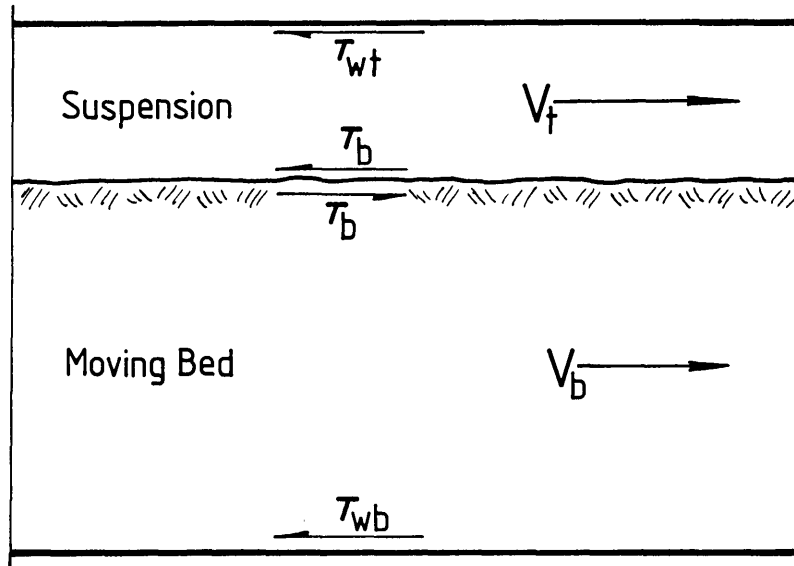
Fig. 6·9

Definition sketch for Bed Slip Model

X • • • • • Results using Table 6·2 equations

x————— Bed Slip model predictions

0———— Clean Water Line
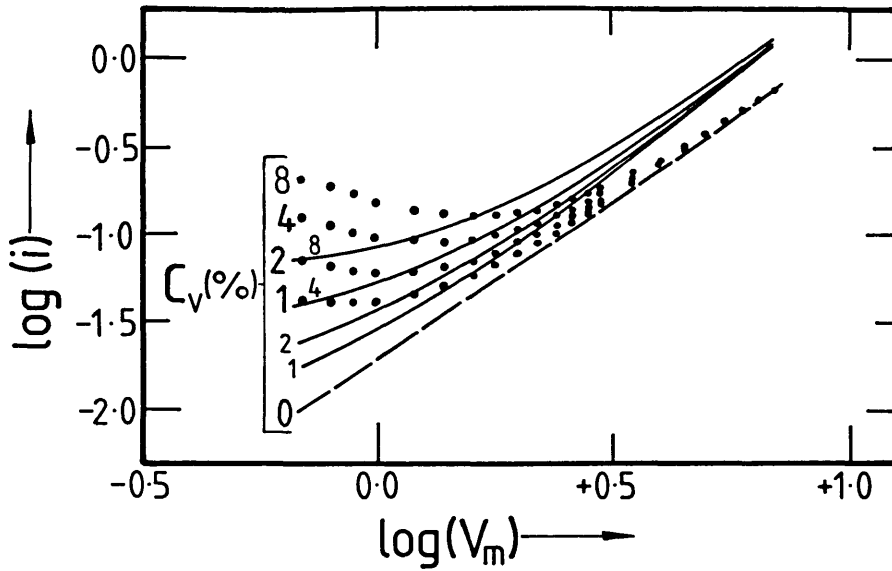
(a) 2″ ID Test Section
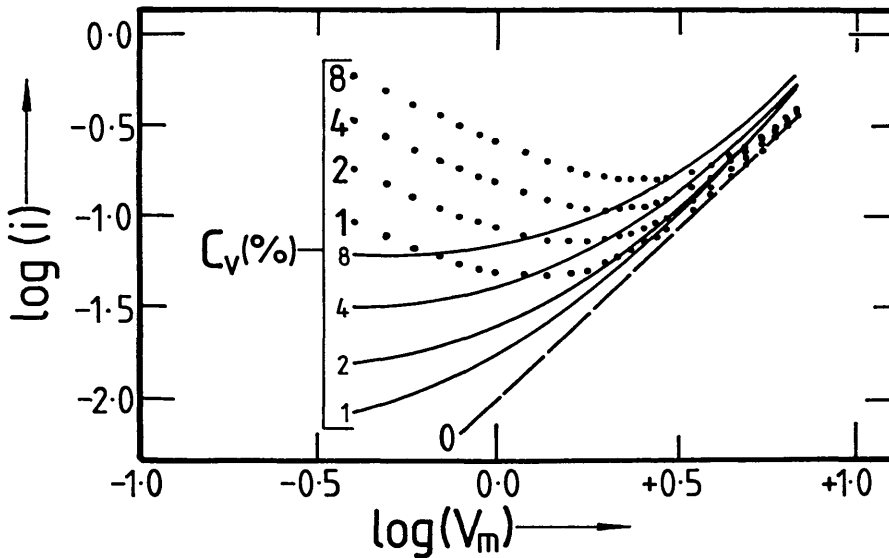
(b) 4″ ID Test Section

Fig. 6·10

Comparison of horizontal pipe section results with Bed Slip model
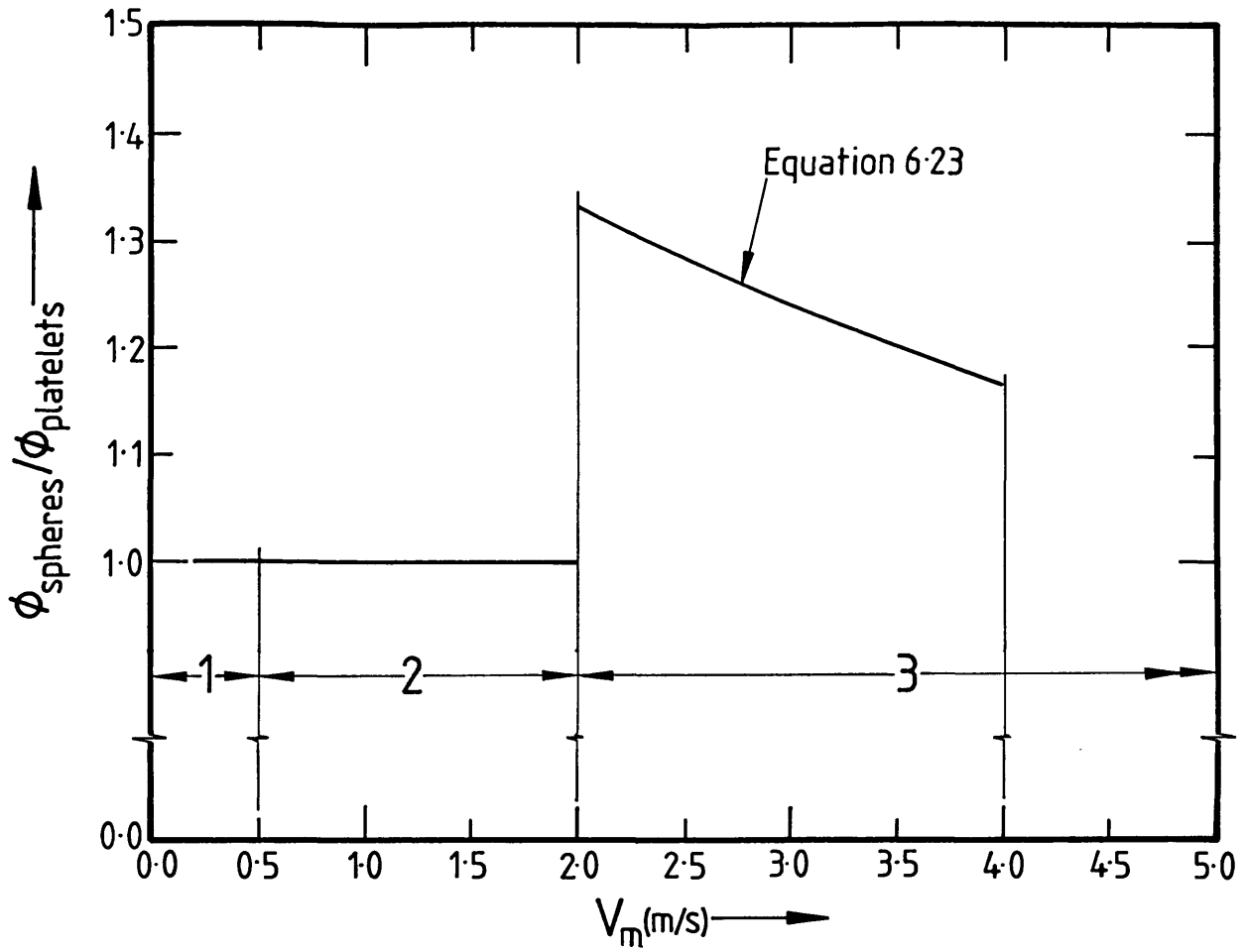
Fig. 6·11

The influence of particle shape on head loss

FLOW REGIMES

1.Stationary Deposit
2.Sliding Bed Flow
3.Full Suspension
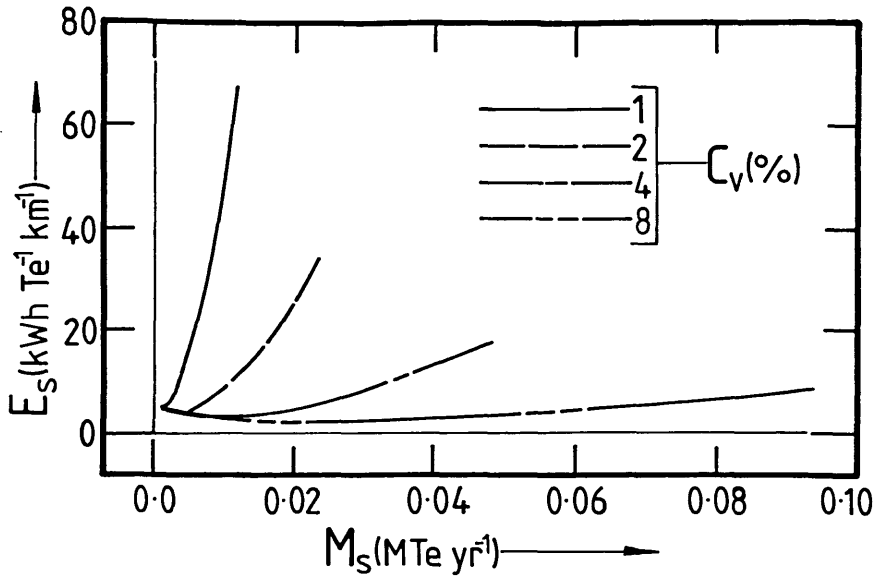
(a) 2" ID Test Section
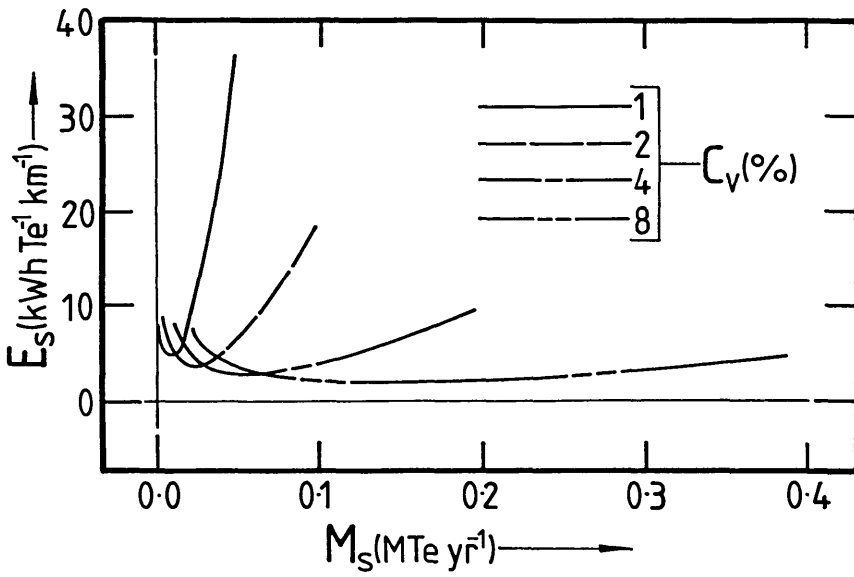
(b) 4" ID Test Section

Fig. 6·12

Specific energy consumption for horizontal platelet transport

Table 6.1 : Correlation of pressure drop data in the

horizontal pipes

(WATER FLOW)

Pipeline	$i_w = i_w (V_m)$	Coefficient of Correlation	Standard Error of Estimate	$f_w = f_w (Re)$
2" (stainless steel)	$1.945 \times 10^{-2} V_m^{1.799}$	0.9947	0.0393	$\dfrac{0.0428}{Re^{0.201}}$
4" (mild steel)	$9.451 \times 10^{-3} V_m^{1.842}$	0.9923	0.0554	$\dfrac{0.006}{Re^{0.16}}$

Table 6.2 : Correlation of pressure drop data in the horizontal

pipes (TWO-PHASE FLOW)

Pipeline	$\phi = K \psi^n$	Coefficient of correlation	Standard error of estimate
2" (stainless steel)	$\phi = 188 \, \psi^{1.44}$ (Durand and Condolios)	0.9551	0.1097
	$\phi = 584 \, \psi^{-0.97}$ (Newitt)	0.9564	0.1082
4" (mild steel)	$\phi = 265 \, \psi^{1.38}$ (Durand and Condolios)	0.9558	0.2263
	$\phi = 1059 \, \psi^{-0.917}$ (Newitt)	0.9556	0.2194
Collective data 4" and 2"	$\phi = 238 \, \psi^{1.41}$ (Durand and Condolios)	0.9510	0.2119

Plate 6.1 : A cross-sectional view of a horizontal pipe length
depicting closely the actual in situ conditions at
low flow rates

Data:

I.D. = 4"

$V_m = 0.6 \text{ m s}^{-1}$

$C_v \approx 1.8 \text{ v/o}$

Height of solids deposit ≈ 0.42 D, (equivalent to $C_{vh} = 15$ v/o)

i = 0.1 m H_2O / m pipe

7. CONCLUSIONS

7.1 Material Classification and Hydrodynamic Parameters

A large sample of Dexion stampings have been classified before and after use in hydraulic conveying tests. The stampings are aluminium platelets, approximately 9-12 mm long and about 2 mm thick and are segregated into three distinct subgroups B, C and D according to size and shape (see Table 4.2).

A 4" diameter water column fitted with a high resolution timing device was used to determine the terminal settling velocity of each shape with an accuracy better than 5%, i.e.

PLATELET TYPE	B (mm/s)	C (mm/s)	D (mm/s)
FRESH STAMPINGS	200 ± 6	202 ± 5	201 ± 8
USED STAMPINGS	227 ± 11	212 ± 6	212 ± 6

A modified shape factor based on the particle thickness and projected area was established and used to predict settling velocities to within 1.4%. This shape factor may also be useful in predictions for other sizes of aluminium platelets.

The drag coefficient C_D for a platelet, (thickness, t,) can be expressed as:

$$C_D = \frac{2 \, g \, (S - 1) \, t}{V_t^2} \qquad\qquad (7.1)$$

Christiansen and Barker (47) suggested that there is no change in the drag coefficient for a particle above a threshold size of 1.5 mm. However, this work indicates that the drag coefficient does not become independent of particle size.

Normally, the drag force on a falling platelet depends on particle shape, orientation and fluid turbulence. Earlier work by the author (48) using aluminium discs, rectangles and triangles in the same size range revealed that the drag force increases appreciably with size because of platelet instabilities. Such instabilities cause substantial deviation from a vertical trajectory (see Fig. 5.2), thus altering the drag forces and increasing the wall effect by shifting the platelet closer to the interface. In contrast, curling at the edges of used platelets was seen to produce a stabilising effect.

7.2   Pressure Drop Prediction

A pipe rig fitted with 2" and 4" diameter pipes was used to pump dilute suspension of metallic platelets at flow rates ranging from 0.5 to 4 m/s and concentrations up to about 10% by volume. The results were found to correlate well using the Durand type equations, and the following expressions were obtained:

$$\phi = 188 \, \psi^{1.44} \qquad\qquad (7.2)$$

for the 2" pipeline

$$\phi = 265 \ \psi^{1.38} \qquad\qquad\qquad \dots (7.3)$$

for the 4" pipeline

$$\text{or} \quad \phi = 238 \ \psi^{1.41} \qquad\qquad\qquad \dots (7.4)$$

using all the results collectively. The latter provides strong evidence in favour of using the Durand equation for limited scale-up.

The results have been interpreted by analysing the transport mechanisms associated with the hydraulic conveying of platelets. A good understanding of the mechanisms involved is not possible without reliable prediction of the transition velocities. The well accepted method of Wilson (30) used for the evaluation of the threshold velocity V_t for turbulent suspension, i.e. the point at which turbulent support is first initiated, predicts values many times higher than those indicated in Fig. 6.4. Whilst this method appears to give good estimates of V_m for values of d/D about 0.005 its use for ratios of up to 0.2 in this work is certainly not valid.

Similarly, though the semi-empirical approach of Durand and Condolios (24) provides acceptable predictions it lacks mechanistic and physical rigour and is therefore of limited value.

Under these circumstances an alternative analysis was developed by considering the platelet as a thick aerofoil in fully developed pipe flow. Thus, by making a number of assumptions regarding the geometry and fluid flow around the platelet it was possible to estimate mean slurry velocities at which individual platelets either begin to slide or become fully suspended, i.e.

Critical/Threshold Velocity	$V_{SLIDING}$ (m/s)	$V_{SUSPENSION}$ (m/s)
2" Pipe	0.53	1.74
4" Pipe	0.61	2.14

The velocities given in the second column are in excellent agreement with independent predictions shown in Figs. 6.4a and 6.4b. It is on this basis that the aerofoil approach is proposed as a reliable method for the prediction of threshold velocities in the pumping of platelet material at low concentrations. Scale-up is an inherent feature of this method.

The results have also been analysed by the "Bed-Slip" model and adequate interpretation is provided. The conclusions drawn thereby confirm a critical velocity for platelet suspension of about 2 m/s.

7.3 Power Consumption Associated with the Hydraulic Conveying of Platelets

Firstly, the effect of particle shape on head loss has been considered by comparing a notional head loss calculated for volume equivalent spheres with the actual experimental head loss obtained for platelets. For the range of velocities considered in this study, the head loss ratio for the two shapes takes the form

$$\frac{\phi_{spheres}}{\phi_{platelets}} = \frac{1.505}{V_m^{0.18}}$$ (7.5)

$$2 < V_m < 4 \ m/s$$

$$D = 4"$$

Equation 7.5 confirms that the pumping of platelets incurs less head loss and hence requires less power than volume equivalent spheres. Further work is required, however, to establish the extent to which head loss is affected by shape.

An analysis of the specific energy consumption as a function of solids throughput indicates quite clearly that moderately high concentrations in large pipe diameters provide the most economical method for the hydraulic conveying of metallic platelets. For example, approximately 40 kW is required to convey 8 v/o aluminium swarf at 0.25 M Te yr^{-1} over a distance of 500 m at 4.5 m/s in a 4" diameter pipeline. In order to attain the same throughput using Magnox swarf, the slurry velocity must be increased to 6.8 m/s requiring a power supply of 110 kW. The feasibility of such a design is based on a mean slurry velocity which is sufficiently high to ensure heterogeneous suspensions, thereby minimising the risk of blockage particularly when handling radioactive material.

8.   REFERENCES

(1)   Stern, D.J.   Pipeline Transportation of Solids, The
                                     Certificated Engineer, pp.119-140,
                                     (June, 1971).

(2)   Rigby, G.R.   Slurry Pipelines for the
                                     Transportation of Solids. Mechanical
                                     Engineering Transactions (I.E.
                                     August), Paper M1173, pp.181-189,
                                     (1982).

(3)   Lee, H.M.   An Overview of Proposal Coal Slurry
                                     Technologies and Their Cost Saving
                                     Applications. Proc. Seventh
                                     International Technical Conference on
                                     Slurry Transportation, Slurry
                                     Transport Association, Lake Tahoe,
                                     Nevada, (U.S.), pp.217-223, (March,
                                     1982).

(4)   Shook, C.A.   Developments in Hydrotransport. The
                                     Canadian Journal of Chemical
                                     Engineering, Vol. 54, pp.13-25,
                                     (February, 1976).

(5)   Lasarus, J.H.   Comparison of Suspended Sediment Flow
                             and Capsule Tranformation in
                             Pipelines. The South African
                             Mechanical Engineer, Vol. 28, pp.319-
                             326, (August, 1978).

(6)   Kazanskij, I.   Scale-up Effects in Hydraulic
                             Transport Theory and Practice.
                             Hydrotransport 5 (BHRA), Hannover,
                             (F.R.G.), Paper B3, pp.47-80, (May,
                             1978).

(7)   Duckworth, R.A.   The Hydraulic Transport of Materials
                             By Pipeline. The South African
                             Mechanical Engineer, Vol. 28, pp.291-
                             306, (August, 1978).

(8)   Miller, D.S.   Internal Flow Systems. BHRA, The
                             Fluid Engineering Centre Series, Vol.
                             5, pp.290, (1978).

(9)   Worster, R.C.   Experimental Methods of Studying the
                             Flow of Solid/Liquid Systems. Proc.
                             of Coll. on Hyd. Trans. of Coal, Nat.
                             Coal Board, (1952).

(10) Godard, K.,   Chem. Eng. Sci., Vol. 24, p.363,
      Richardson, J.F.   (1969).

(11) Heywood, H.   Uniform and Non-Uniform Motion of

                                    Particles in Fluids. Symp.

                                    Interaction Fluids and Parts, Inst.

                                    Chem. Eng., pp.1-8, London, (1962).

(12) Heywood, H.   Powder Metallurgy, Vol. 7, pp.1-28,

                                    (1961).

(13) Tottenham, A.M.L.   Hydraulic Conveying of Aluminium

                                    Swarf. MSc Report, Imperial College

                                    (Chem. Eng.), London, (1981).

(14) Alger, R.A. and   Fall Velocity of Irregular Shaped

     Simon, D.B.   Particles. (ASCE), HY3, (May, 1968).

(15) Heywood, H.   Proc. Inst. Mech. Eng., Vol. 140,

                                    pp.257-347, (1938).

(16) Clift, R., Grace, J.R.   Bubbles, Drops and Particles.

     and Weber, M.E.   Academic Press, London. (1978).

(17) Wadell, H.J.   Geol., Vol. 41, pp.310-331, (1933).

(18) Wadell, H.J.   Franklin Inst., Vol. 217, pp.459-490,

                                    (1934).

(19) Govier, G.W. and Aziz, K.   The Flow of Complex Mixtures in

                                    Pipes. Van Nostrand Reinhold, New

                                    York (1972).

(20) Briggs, L.I.,   Sediment Petrol, Vol. 32, pp.645-656,
     McCulloch, D.S. and   (1962).
     Moser, F.J.

(21) Stringham, G.E.,   U.S. Geol. Surv., Prof. Pap. 562-C,
     Simons, D.B. and Guy, H.P. (1969).

(22) Richardson, J.F. and   Sedimentation and Fluidisation, Trans.
     Zaki, W.N.   Inst. Chem. Engrs., Vol. 32 (I),
                               pp.35-53, (1954).

(23) Yang, C.T.   Incipient Motion and Sediment
                              Transport. Journal of the Hydraulics
                              Division (ASCE), HY10, pp.1679-1704,
                              (October, 1973).

(24) Durand, R. and   The Hydraulic Transport of Coal and
     Condolios, G.   Solids in Pipes. Colloquium on
                              Hydraulic Transport, National Coal
                              Board, London, (1952).

(25) Newitt, D.M.,   Hydraulic Conveying of Solids in
     Richardson, J.F.,   Horizontal Pipes. Trans. Inst. Chem.
     Abbott, M. and Turtle, R.B. Engrs., Vol. 32 (II), pp.93-113,
                              (1955).

(26) Zandi, I., Govatos, G.   Heterogeneous Flow of Solids in
                                Pipelines. Proc. ASCE, Journal of the
                                Hydraulics Division, Vol. 93, HY3,
                                pp.145-159, (May, 1967).

(27) Wilson, K.C., Streat, M.   Slip-Model Correlation of Dense Two-
     and Bantin, R.A.   Phase Flow. Hydrotransport 2 (BHRA),
                                Warwick, (U.K.), Paper C4, pp.1-10,
                                (September, 1972).

(28) Babcock, H.A.   The Sliding Bed Flow Regime.
                                Hydrotransport 1 (BHRA), Warwick
                                (U.K.), Paper H1, pp.1-16, (September,
                                1970).

(29) Chhabra, R.P.,   Hydraulic Transport of Coarse Gravel
     Richardson, J.F.   Particles in a Smooth Horizontal
                                Pipe. Chem. Eng. Res. Des., Vol. 61,
                                pp.313-317, (September, 1973).

(30) Wilson, K.C. and Watt, W.E. Influence of Particle Diameter on the
                                Turbulent Support of Solids in
                                Pipeline Flow. Hydrotransport 3
                                (BHRA), Colorado (U.S.A.), Paper D1,
                                pp.1-9, (May, 1974).

(31) Wilson, K.C.   A Unified Physically Based Analysis of

                                       Solid-Liquid Pipeline Flow.

                                       Hydrotransport 4 (BHRA), Alberta,

                                       Canada, Paper A1, pp.1-16, (May,

                                       1976).

(32) Wilson, K.C.   Deposition - Limit Nomogram for

                                       Particles of Various Densities in

                                       Pipeline Flow. Hydrotransport 6

                                       (BHRA), Canterbury (U.K.), Paper A1,

                                       pp.1-12, (September, 1979).

(33) Clift, R., Wilson, K.C.   A Mechanistically Based Method for
      Addie, G.R. and   Scaling Pipeline Tests for Settling
      Carstens, M.R.   Slurries. Hydrotransport 8 (BHRA),

                                       Johannesburg (S.A.), Paper B1, pp.91-

                                       101, (August, 1982).

(34) Worster, R.C. and   Hydraulic Transport of Solid Material
      Denny, D.F.   in Pipes. Proc. I. Mech. E., Vol. 169

                                       (32), pp.563-586, (1955).

(35) Worster, R.C.   Experimental Methods of Studying the

                                       Flow of Solid-Liquid Mixtures in

                                       Pipes. Proc. Colloquium on Hydraulic

                                       Transport of Coal, National Coal

                                       Board, Paper III, pp.35-38, London,

                                       (November, 1952).

(36) Bian, A.G. and Bonnington, S.T.

Hydraulic Transport of Solids by Pipelines. Oxford-Pergamon (1970).

(37) Newitt, M.C., Richardson, J.F. and Gliddon, B.J.

Hydraulic Conveying of Solids in Vertical Pipes. Trans. Inst. Chem. Engrs., Vol. 39, pp.93-100, (1961).

(38) Wilson, K.C., Brown, N.P. and Streat, M.

Hydraulic Hoisting at High Concentrations: A New Study of Friction Mechanisms. Hydrotransport 6 (BHRA), Canterbury (U.K.), Paper F2, pp.269-282, (September, 1979).

(39) Streat, M.

A Comparison of Specific Energy Consumption in Dilute and Dense Phase Conveying of Solid-Water Mixtures. Hydrotransport 8 (BHRA), Johannesburg, (S.A.), Paper B32, pp.111-122, (August, 1982).

(40) Cloete, F.L.D., Miller, A.I. and Streat. M.

Dense-Phase Flow of Solid-Water Mixtures Through Vertical Pipes. Trans. Inst., Chem. Engrs., Vol. 45, T392, (1976).

(41) Wood, D.J.

Pressure Gradient Requirements for the Re-Establishments of Slurry Flow. Hydrotransport 6 (BHRA), Canterbury (U.K.), Paper D4, pp.217-228 (September, 1979).

(42) Ocada, T., Hisamitsu, N.   Experiments on Restart of Reservoir
Ise, T. and Takeishi, Y.   Sediment Slurry Pipeline.
Hydrotransport 8 (BHRA), Johannesburg
(S.A.), Paper H3, pp.399-414, (August,
1982).

(43) Kao, D.T.Y. and   Critical Slope for Slurry Pipelines
Hwang, L.Y.   Transporting Coal and other Solid
Particles. Hydrotransport 6 (BHRA),
Canterbury (U.K.), Paper A5, pp.57-74,
(September, 1979).

(44) Pouska, G.A. and   Investigation of head losses in coarse
Link, J.M.   oil shale slurries. Hydrotransport 5,
Paper 42, May, 1978.

(45)   Advances in Solid-Liquid Flow in Pipes
and its Application. Ed by Iraj
Zandi, Pergamon, (1971).

(46) Von Karman, T.   Turbulence, Jl. R. Aeronaut. Soc. 41,
pp.1109-41, (1937).

(47) Christiansen, E.B. and   The Effect of Shape and Density on the
Barker, D.H.   Frere Settling of Particles at High
Reynolds Numbers.

(48) Tatsis, A.   The Drag Coefficient of Platelets Settling at their Terminal Velocity. Interim Report, Dept. of Chem. Eng., Imperial College, 1982.

General:

(49) Perry, R.H. and Chilton, C.H.   Chemical Engineers Handbook, McGraw-Hill Kogakusha, 5th Edition (1973).

APPENDIX A

KINEMATICS OF PARTICLES SETTLING FREELY IN A QUIESCENT FLUID

(A)   If a particle is moving in a fluid at a velocity which is not equal to the terminal velocity, the difference between the effective force causing motion and the drag resistance F_D is available for acceleration of the particle. Thus, if a particle starting from rest is moving downwards under gravitational force but has not yet reached the terminal velocity, the drag will be less than the effective weight of the particle and the difference will produce positive acceleration α

i.e. $(M - M')g - F_D = M \alpha$ .... (A.1)

where M is the mass of the particle and M' the mass of displaced fluid. Rearranging we obtain;

$$\alpha = \lambda \ g - \frac{F_D}{M}$$ .... (A.2)

where

$$\lambda = \frac{\rho_s - \rho_w}{\rho_s} = \frac{M - M'}{M}$$ .... (A.3)

Equation A.1 describes fully the motion of a particle in a given fluid-particle system. According to the flow regime,

$$\frac{F_D}{M} = K \ V \quad \text{where} \quad K = \frac{1.8 \ \mu_w}{\rho_s} d^2 \quad ; \text{ laminar flow}$$

$$= K \ V^2 \qquad = \frac{0.33 \ \rho_w}{\rho_s \ d} \qquad ; \text{ turbulent flow}$$

$$= K \ C_D \ Re^2 \qquad = \frac{0.03 \ \mu_w^2}{4 \ \rho_s \ \rho_w \ d^3} \qquad ; \text{ transitional flow}$$

Ileywood (11) has solved equation A.2 for fully turbulent flow and gives the following parameters:

- Particle terminal settling velocity V_t:

$$V_t = [\frac{g \ d \ (S - 1)}{0.33}]^{0.5} \qquad \qquad \dots \dots (A.4)$$

- Time taken to accelerate from rest up to velocity V:

$$t = \frac{1}{2 \ K \ V_t} \ \ln \frac{V_t + V}{V_t - V} \qquad \qquad \dots \dots (A.5)$$

- Velocity V reached in a given time interval t:

$$V = V_t \ \tanh (K \ V_t \ t) \qquad \qquad \dots \dots (A.6)$$

- Distance s covered whilst accelerating up to velocity V:

$$s = \frac{1}{2 \ K} \ \ln \frac{V_t^2}{V_t^2 - V^2} \qquad \qquad \dots \dots (A.7)$$

(B)   In the case of a large glass spheres (d = 11.827 mm) in fully turbulent flow $Re_d \approx 8,700$ then K = 1.087 mm^{-1} and s = 285.9 mm. Here the value of V = 0.999 V_t has been used. The result suggests that when a large glass sphere is released from rest in infinite water medium, a minimum distance of s_{min} = 285.9 mm is required

before it reaches its terminal velocity of 738.6 mm s^{-1} (see Table 5.1). Since this represents the fastest particle considered in this work, it follows that an "acceleration" distance of 286 mm will be adequate for any other item. The actual distance allowed between the water surface and the point where timing commenced was 330 mm (= 3.25 column diameters).

APPENDIX B

CALIBRATION LINES FOR SAMPLING VESSEL USED IN 4" PIPE TESTS

With reference to Fig. 3.5, line 1 represents the calibration line for the sampling at the beginning of the experimental campaign, i.e.

$$\frac{\text{True Volume}}{(1)} = 1.038 \frac{\text{Indicated Volume}}{(1)} - \frac{1.462}{(1)} \qquad \dots \text{(B.1)}$$

Similarly, line 2 represents an independent calibration following 104 experimental runs. A further calibration taken after a total of 132 experimental runs coincides with line 2. Thus, line 2 represents the upper limit of the vessel deformation and can be expressed as follows:

$$\frac{\text{True Volume}}{(1)} = 1.035 \frac{\text{Indicated Volume}}{(1)} + \frac{0.375}{(1)} \qquad \dots \text{(B.2)}$$

Assuming the rate of deformation with respect to time is linear, a mean calibration line can be estimated. As a first approximation, however, the line bisecting the acute angle formed by lines 1 and 2 is calculated.

Solving B.1 and B.2 simultaneously the point of intersection can be calculated with co-ordinates x = 612.333, y = 634.14.

The slope is given by

$$\frac{1}{2} \tan \left(\text{atan} \ (1.035) + \text{atan} \ (1.038) \right) = 1.036 \qquad \dots \text{(B.3)}$$

and the equation becomes,

$$\frac{\text{True Volume}}{(1)} = 1.036 \; \frac{\text{Indicated Volume}}{(1)} - \frac{0.237}{(1)} \qquad \dots \; (B.4)$$

Finally, the overall mean calibration line can be found by setting the deformation rate equal to zero after the 104th run. This is equivalent to rotating line (B.4) about the point of intersection towards line (B.2). The degree of rotation is determined by weighting factors, used in the calculation of the new slope. These factors represent fractions of the total number of experimental runs, i.e.

$$\tan\left[\; \frac{28}{132} \; \text{atan} \; (1.035) + \frac{104}{132} \; \text{atan} \; (1.036)\;\right] = 1.0358 \qquad \dots \; (B.5)$$

Thus, the final equation takes the form,

$$\frac{\text{True Volume}}{(1)} = 1.0358 \; \frac{(\text{Indicated Volume})}{(1)} - \frac{0.115}{(1)} \qquad \dots \; (B.6)$$

Equation B.6 is represented in line 3 in Fig. 3.5 and is referred to as equation 3.1 in section 3.2.1.3 of chapter 3.

APPENDIX C

DIMENSIONAL CLASSIFICATION OF NEW PLATELETS

(GROUPS B, C AND D)

GROUP/ SUBGROUP	ITEM No	LENGTH (x) (mm)	BREADTH (y) (mm)	THICKNESS (t) (mm)	$\bar{x}$ (mm)	$\bar{y}$ (mm)	$\bar{t}$ (mm)
D/(S)(18)	1	10.4650	10.4650	1.7270			
	2	10.5155	10.5155	1.7525			
	3	10.4900	10.4900	1.7270			
	4	10.4650	10.4650	1.7525			
	5	10.4395	10.4650	1.7270			
	6	10.4395	10.4900	1.7525			
	7	10.4900	10.4650	1.7270			
	8	10.4395	10.4650	1.7270	10.4775	10.4888	1.7468
	9	10.5155	10.5155	1.7270	±	±	±
	10	10.4650	10.4900	1.7525	0.0187	0.1488	0.0151
	11	10.5155	10.5155	1.7270			
	12	10.4650	10.4900	1.7525			
	13	10.4900	10.4650	1.7780			
	14	10.4650	10.4900	1.8035			
	15	10.4900	10.4900	1.7780			
	16	10.5155	10.5410	1.7525			
	17	10.4395	10.4900	1.7270			
	18	10.4900	10.4900	1.7525			
D/(T)(8)	19	10.2615	10.2615	2.0065			
	20	10.2615	10.2870	2.0575			
	21	10.4650	10.4650	2.0575	10.3180	10.3283	2.0256
	22	10.2870	10.2870	2.0065	±	±	±
	23	10.2615	10.2615	2.0320	0.0563	0.0628	0.0152
	24	10.2870	10.2870	2.0065			
	25	10.4395	10.4902	2.0065			
	26	10.2870	10.2870	2.0320			
C/(S)(17)	27	12.9030	9.4740	1.7525			
	28	12.8770	9.5250	1.7525			
	29	12.8780	9.4740	1.7270			
	30	12.9030	9.4995	1.7780			
	31	12.8770	9.4995	1.7270			
	32	12.8780	9.4995	1.7525			
	33	12.8780	9.5505	1.7525			
	34	12.8525	9.5250	1.7525	12.8778	9.5130	1.7511
	35	12.8780	9.5250	1.7525	±	±	±
	36	12.8780	9.4995	1.7020	0.0104	0.0150	0.01863
	37	12.8780	9.5250	1.7525			
	38	12.8525	9.5250	1.7525			
	39	12.8780	9.5250	1.7020			
	40	12.9030	9.5505	1.8035			

APPENDIX C CONTINUED

	41	12.8780	9.4995	1.8035			
	42	12.8780	9.4995	1.7525			
	43	12.8525	9.5250	1.7525			
C/(T)(9)	44	12.6240	9.2455	2.0065			
	45	12.7000	9.2202	2.0065			
	46	12.7255	9.2965	2.0065			
	47	12.6240	9.2455	2.0065	12.7057	9.2879	2.0057
	48	12.7000	9.2202	2.0065	±	±	±
	49	12.8780	9.5250	2.0065	0.0505	9.2879	2.0093
	50	12.6745	9.2455	2.0065			
	51	12.7000	9.2965	2.0320			
	52	12.7255	9.2965	2.0065			
B/(S)(20)	53	14.9100	9.3980	1.7525			
	54	14.9860	9.4740	1.7525			
	55	14.8845	9.4740	1.7525			
	56	14.9350	9.4995	1.7020			
	57	14.8590	9.4995	1.7270			
	58	14.9100	9.4995	1.8035			
	59	14.9350	9.4235	1.7525			
	60	13.9605	9.4490	1.7780			
	61	14.9860	9.4740	1.7270	14.9289	9.4627	1.7487
	62	14.8845	9.4995	1.7270	±	±	±
	63	14.9605	9.4235	1.7270	0.0245	0.0245	0.0169
	64	14.8845	9.4995	1.7525			
	65	14.9100	9.4995	1.8035			
	66	14.9605	9.4740	1.7525			
	67	14.9605	9.4740	1.7270			
	68	14.9100	9.4740	1.7525			
	69	14.9605	9.4490	1.7525			
	70	14.9605	9.4740	1.7525			
	71	14.9100	9.3980	1.7270			
	72	14.9100	9.3980	1.7525			
B/(T)(6)	73	14.7830	9.2200	1.9810			
	74	14.7830	9.4995	2.0065	14.7703	9.2708	2.0065
	75	14.7575	9.2200	2.0065	±	±	±
	76	14.7575	9.2455	2.0065	0.0094	0.0759	0.0109
	77	14.7830	9.2200	2.0320			
	78	14.7575	9.2200	2.0065			
OVERALL AVERAGE VALUES					13.3842	9.6530	1.8244

APPENDIX D

DIMENSIONAL CLASSIFICATION OF USED PLATELETS

GROUP/ SUBGROUP	ITEM No #	WEIGHT ASCENDING ORDER (g)	LENGTH (x) (mm)	BREADTH (y) (mm)	THICKNESS		
					(t_M) (mm)	(t_L) (mm)	(t_R) (mm)
D/(S)(29)							
1	117	0.3540	10.8955	10.4500	1.8380		
2	112	0.3561	10.4205	10.4080	1.7820		
3	127	0.3562	10.3135	10.3120	1.8270		
4	132	0.3567	10.3065	10.2170	1.8330		
5	113	0.3588	10.3530	10.3510	1.8515		
6	136	0.3597	10.3160	10.2495	1.8295		
7	104	0.3600	10.2545	10.4650	1.8255		
8	110	0.3600	10.2440	10.3805	1.7510		
9	147	0.3600	10.6115	10.3220	1.8760		
10	131	0.3610	10.4015	10.2440	1.8700		
11	118	0.3614	10.4355	10.2560	1.7905		
12	111	0.3615	10.3230	10.3440	1.8525		
13	103	0.3621	10.3715	10.3180	1.7900		
14	123	0.3623	10.2910	13.3130	1.8345		
15	102	0.3626	10.3820	10.4050	1.6980		
16	133	0.3629	10.4085	10.3990	1.8195		
17	146	0.3647	10.3255	10.9670	2.0060		
18	121	0.3650	10.3380	10.3255	1.8520		
19	128	0.3654	10.4640	10.4095	1.8270		
20	137	0.3664	9.4115	10.3725	1.8515		
21	149	0.3665	10.4070	10.3075	1.8085		
22	145	0.3667	10.4070	10.4310	1.8290		
23	107	0.3670	10.4120	10.4020	1.8455		
24	139	0.3674	10.4485	10.3785	1.8310		
25	144	0.3680	10.4130	10.4105	1.8240		
26	142	0.3684	10.4100	10.3585	1.8395		
27	135	0.3691	10.4235	10.4085	1.9080		
28	143	0.3704	10.4450	10.4515	1.8750		
29	130	0.3790	10.4110	10.3790	1.9305		
AVERAGE VALUES		0.3634	10.3670 ± 0.2747	10.3804 ± 0.1630	1.8379 ± 0.0368		
D/(T)(21)							
30	125	0.4027	10.1200	10.0530	2.2070		
31	105	0.4040	10.1415	10.1150	2.2085		
32	116	0.4082	10.1635	10.1530	2.1060		
33	124	0.4102	10.1600	10.1700	2.1600		
34	129	0.4107	10.1600	10.1875	2.0780		
35	119	0.4111	10.2030	10.1515	2.1080		
36	141	0.4128	10.1975	10.1995	2.1625		

APPENDIX D CONTINUED

37	148	0.4130	10.1185	10.1570	2.2445		
38	114	0.4135	10.0825	10.4430	2.1185		
39	115	0.4138	10.2165	10.9355	2.1630		
40	134	0.4142	10.1650	10.1205	2.1770		
41	138	0.4143	10.0770	10.2420	2.1065		
42	120	0.4151	10.2590	10.2420	2.1065		
43	122	0.4151	10.2520	10.2490	2.1595		
44	106	0.4170	10.2060	10.2325	2.1820		
45	150	0.4172	10.2740	10.2350	2.1060		
46	108	0.4173	10.2290	10.4165	2.0915		
47	140	0.4174	10.2370	10.2760	2.1715		
48	101	0.4180	10.1360	10.1400	2.1960		
49	109	0.4188	10.2130	10.3260	2.5930		
50	126	0.4210	10.2230	10.2270	2.1560		
AVERAGE VALUES		0.4136	10.1826 ± 0.0371	10.2493 ± 0.1236	2.1734 ± 0.0711		
C/(S)$_{(32)}$							
51	100	0.4255	11.5080	9.4195	1.7685	2.9865	2.8990
52	40	0.4268	11.8745	9.2880	1.9950	2.6315	2.5510
53	81	0.4286	11.5415	9.4540	1.7085	2.8830	2.7195
54	67	0.4291	11.4875	9.4375	1.8430	2.9335	2.7060
55	50	0.4295	10.9685	9.5240	1.8555	3.5700	3.2845
56	48	0.4314	11.3075	9.4110	1.9375	3.0620	2.7820
57	17	0.4332	11.6295	9.4365	1.9065	2.7720	2.7160
58	98	0.4332	11.5345	9.4820	1.7070	2.8365	2.7155
59	14	0.4335	11.4895	9.3675	1.8425	2.7775	2.7135
60	21	0.4337	11.5340	9.4255	1.7920	2.7755	2.7350
61	35	0.4337	11.6155	9.4665	2.0730	2.8835	2.8060
62	25	0.4340	11.7315	9.5190	1.7345	3.0480	2.7460
63	85	0.4343	11.5515	9.4980	1.7655	2.7380	2.7165
64	19	0.4354	11.5550	9.4505	1.7480	2.8620	2.8410
65	27	0.4354	11.8455	9.4770	1.7215	2.9635	2.8860
66	56	0.4364	11.7500	9.4815	1.7265	2.7740	2.7450
67	59	0.4364	11.5500	9.4990	1.7980	2.8710	2.7580
68	16	0.4366	11.6490	9.4910	1.1980	2.7600	2.7450
69	89	0.4370	11.5855	9.4260	1.7145	2.9220	2.8170
70	51	0.4380	11.5275	9.5325	1.7710	2.9115	2.6625
71	31	0.4387	11.3555	9.3055	1.8340	2.8970	2.8585
72	64	0.4391	11.4730	9.4440	1.7670	2.9455	2.8580
73	66	0.4397	11.5225	9.5065	1.6885	2.8635	2.8440
74	65	0.4398	11.6990	9.4515	1.6865	2.7725	2.7015
75	46	0.4414	11.7405	9.4940	2.0275	2.8185	2.7235
76	45	0.4416	11.7505	9.5020	1.7505	2.5890	2.6220
77	92	0.4416	12.2045	9.4770	1.8565	2.2845	2.2590
78	95	0.4424	11.6645	9.4740	1.8220	2.7840	2.6120
79	60	0.4457	11.8040	9.4970	1.7500	2.6925	2.6030
80	33	0.4458	11.6175	9.4970	1.7755	3.0030	2.9375
81	13	0.4460	11.8240	9.5100	1.9340	3.0415	2.8620
82	53	0.4490	11.5335	9.4855	1.9350	3.1540	2.9880

APPENDIX D CONTINUED

AVERAGE VALUES		0.4366	11.5981 ± 0.1362	9.4603 ± 0.0385	1.8296 ± 0.0996	2.8689 ± 0.1392	2.7642 ± 0.1135
C/(T)(9)							
83	52	0.4812	11.5020	9.2125	2.0520	3.0480	2.8620
84	57	0.4817	11.5760	9.1970	2.0460	3.0025	2.8275
85	29	0.4850	11.4850	9.1670	2.1490	2.9445	2.9235
86	7	0.4851	11.3000	8.9915	2.0830	3.0915	3.0330
87	93	0.4874	11.4390	9.2420	2.0585	3.1025	3.0780
88	28	0.4876	9.8265	9.1010	2.3550	4.5350	4.1690
89	86	0.4903	11.5455	9.1975	2.0715	3.1330	3.0510
90	32	0.4914	11.8470	9.3695	2.0340	2.8120	2.7210
91	80	0.4921	11.5470	9.2085	2.2985	3.5050	3.3080
AVERAGE VALUES		0.4869	11.3409 ± 0.3953	9.1874 ± 0.0689	2.1275 ± 0.0800	3.2416 ± 0.3508	3.1336 ± 0.2951
B/(S)(38)							
92	99	0.4933	11.5805	9.1955	1.9610	3.1355	3.1245
93	83	0.4960	11.5425	9.3575	1.8995	3.9795	3.8260
94	84	0.4977	11.5815	9.3920	1.7070	3.4920	3.3985
95	96	0.4981	11.5985	9.2660	2.0320	3.1480	2.9585
96	22	0.5000	11.4070	9.3570	2.0020	4.1935	3.9220
97	42	0.5002	11.5080	9.2895	1.8005	4.1285	4.0565
98	15	0.5025	11.6755	9.2615	2.2105	3.2035	3.1080
99	55	0.5072	11.5485	9.3615	2.2085	4.3270	4.2945
100	11	0.5076	11.4355	9.3320	2.1620	4.2800	4.2260
101	8	0.5079	11.4705	9.3155	1.7810	4.1540	4.1130
102	91	0.5097	11.6425	9.3995	1.7395	4.1980	4.0655
103	82	0.5100	11.4690	9.3790	1.7815	4.2650	4.2200
104	44	0.5134	13.3795	9.3710	1.9385	3.1690	3.1150
105	26	0.5159	12.8455	9.3480	1.8145	3.6940	3.3845
106	1	0.5164	11.4675	9.2740	1.7505	4.4425	4.4380
107	78	0.5166	14.5315	9.4225	1.7530	2.3140	2.2750
108	73	0.5178	11.6310	9.4270	1.7850	4.2355	4.0145
109	72	0.5182	12.4910	9.4255	1.7750	3.8155	3.8140
110	47	0.5190	11.5630	9.4070	1.7335	4.5245	4.2340
111	34	0.5192	11.4930	9.3940	2.0070	4.4690	4.4145
112	69	0.5196	15.3800	9.3530	1.7240	1.7870	1.2235
113	68	0.5200	11.5345	9.3840	1.8355	4.1545	4.0045
114	58	0.5205	12.5105	9.4195	2.1560	3.8550	3.8270
115	74	0.5205	14.5315	9.4225	1.7530	2.3140	2.2750
116	88	0.5226	12.9800	9.4120	1.7605	3.6070	3.3225
117	5	0.5245	11.5815	9.3950	1.7870	4.2585	4.0690
118	38	0.5245	11.6990	9.3405	1.8345	4.4970	4.4895
119	30	0.5247	11.6045	9.4365	1.7380	4.3450	4.2335
120	79	0.5252	13.1305	9.4790	2.0195	2.9725	2.9490
121	23	0.5275	11.4910	9.4185	1.8680	4.3165	4.1870
122	18	0.5283	11.4925	9.3260	2.4770	4.6040	4.2490
123	90	0.5291	11.4655	9.5055	1.9750	4.5105	4.3620
124	2	0.5293	11.8855	9.2005	1.8360	4.1805	4.1525
125	39	0.5296	13.8505	9.4204	2.2665	3.1040	2.8685
126	49	0.5309	12.7135	9.9260	1.8265	4.7405	4.6145

APPENDIX D CONTINUED

127	97	0.5317	13.4635	9.4725	1.7835	3.5065	3.1035
128	71	0.5420	11.5060	9.3955	1.8520	4.7990	4.5295
129	36	0.5450	14.3030	9.4030	2.4175	2.6950	2.3460
AVERAGE VALUES		0.5174	12.2364 ± 0.7360	9.3699 ± 0.0475	1.9145 ± 0.1345	3.8215 ± 0.4945	3.6792 ± 0.5229
$B/(T)_{(21)}$							
130	43	0.5773	11.4675	9.2510	2.0810	4.5250	4.0750
131	61	0.5788	11.5590	9.3195	2.2220	4.5855	4.3495
132	94	0.5796	11.4635	9.1455	2.4940	4.6580	4.5310
133	10	0.5812	11.3050	9.0060	2.0515	4.6170	4.5980
134	54	0.5823	11.6485	9.1505	2.1825	4.5165	4.4080
135	75	0.5826	11.6170	9.4215	1.9165	4.4930	4.1735
136	87	0.5829	11.4795	9.3670	2.3825	4.2555	4.1385
137	12	0.5838	11.4900	9.1725	2.1055	4.7695	4.5505
138	41	0.5898	11.5970	9.3035	3.1045	4.4800	4.4250
139	3	0.5900	11.5545	9.2010	2.0855	4.7980	4.7925
140	20	0.5900	11.4520	9.1775	2.2200	4.8265	4.6705
141	24	0.5900	11.3500	9.2720	2.1045	4.7515	4.2670
142	37	0.5905	11.6665	9.1500	2.2425	4.7020	4.5125
143	6	0.5909	11.2390	9.3305	2.4620	4.9645	4.9410
144	4	0.5912	11.4595	9.2185	2.0275	4.5800	4.6275
145	62	0.5918	11.5705	9.3605	2.0725	4.4050	4.3415
146	77	0.5935	13.3660	9.2190	2.0375	3.2005	3.1870
147	70	0.5940	11.6300	9.3560	2.3070	4.4675	4.1870
148	63	0.5946	11.5935	9.3725	2.1090	4.3670	4.1559
149	9	0.5986	11.4905	9.3000	2.5775	4.6275	4.4835
150	76	0.6000	14.2220	9.2570	2.0210	3.0645	2.9600
AVERAGE VALUES		0.5883	11.7247 ± 0.4788	9.2548 ± 0.0680	2.2289 ± 0.1789	4.4597 ± 0.3185	4.3031 ± 0.3155
OVERALL AVERAGE VALUES		0.4817	11.5486	9.5768	1.9676	3.2414	

APPENDIX E

DIMENSIONAL CLASSIFICATION OF GLASS SPHERES

GROUP #	ITEM #	d_1 at 1 to d_2 (mm)	(mm)	$\dfrac{d_1 + d_2}{2}$ (mm)	$\dfrac{2\,\left| d_1 - d_2 \right|}{d_1 + d_2}$ (%)	$\bar{d} \pm p.\epsilon.^*$ (mm)	ERROR (%)
1	1.1	2.9815	2.8720	2.9267	3.7		
	1.2	2.9762	2.8853	2.9306	3.7		
	1.3	2.9925	2.9100	2.9512	2.8	2.9339	
	1.4	3.0195	2.9120	2.9657	3.6	±	±1.7
	1.5	2.9780	2.8930	2.9355	2.9	0.013	
	1.6	2.8925	2.9160	2.9042	0.3		
	1.7	2.9240	2.9230	2.9235	0.03		
2	2.1	3.5835	3.6380	3.6069	1.5	3.6371	
	2.2	3.6975	3.5995	3.6485	2.7	±	±3.1
	2.3	3.7057	3.6061	3.6560	2.7	0.018	
3	3.1	5.0605	5.1170	5.0862	1.1	5.1154	
	3.2	5.2305	5.0290	5.1298	3.9	±	±2.1
	3.3	5.1030	5.1578	5.1304	1.0	0.017	
4	4.1	5.7460	5.7720	5.7590	0.5	5.8214	-
5	5.1	7.7700	7.7810	7.7790	0.1	7.8141	-
6	6.1	11.7690	11.8255	11.7973	0.5		
	6.2	11.7795	11.8420	11.8108	0.5		
	6.3	11.8860	11.9200	11.9030	0.3		
	6.4	11.8310	11.7970	11.8140	0.3	11.8275	
	6.5	11.8180	11.7620	11.7900	0.5	±	±1.0
	6.6	11.8670	11.8950	11.8810	0.2	0.035	
	6.7	11.8420	11.6860	11.7640	1.3		
	6.8	11.9120	11.8810	11.8970	0.3		
	6.9	11.6640	11.8665	11.7653	1.7		
	6.10	11.7530	11.9525	11.8530	1.7		

(*)   The probable error p.ε. in the mean group diameter is given by
±0.6745 σ where σ is the standard deviation of the mean.

APPENDIX F

EXPERIMENTAL DETERMINATION OF THE TERMINAL SETTLING

VELOCITY FOR GLASS SPHERES

GROUP:	1	2	3	4	5	6
$\bar{d}$ (mm)	2.934	3.637	5.115	5.821	7.821	11.828
	TIME TAKEN TO DESCEND A HEIGHT OF 1980 MM (sec)					
RUN NO. 1	5.788	4.282	3.925	3.758	3.632	2.793
2	5.798	4.443	3.988	3.749	3.127	2.722
3	5.617	4.356	4.017	3.763	3.782	2.800
4	5.450	4.333	4.202	3.754	2.909	2.781
5	5.612	4.312	3.973	3.857	3.498	2.783
6	5.573	4.325	3.915	3.737	3.810	2.790
7	5.388	4.253	3.986	3.842	3.751	2.788
8	5.518	4.359	4.024	3.768	2.872	2.749
9	5.395	4.297	4.150	3.842	3.307	2.811
10	5.472	4.293	3.966	3.770	2.868	2.552
11	5.496	4.221	3.945		3.277	2.789
12	5.762	4.301	3.989		2.985	2.760
13	5.417	4.265	4.176		2.866	2.834
14	5.513	4.347	3.926		3.236	2.705
15	5.589	4.331	4.082		3.700	2.777
16	5.454	4.344	3.953		3.260	2.775
17	5.479	4.240	3.985		3.378	2.708
18	5.504		4.002		3.409	2.762
19	5.448		3.875		2.861	2.897
20	5.439		3.942		2.856	2.722
21	5.605		3.815		2.961	2.765
22	5.395		3.959		3.299	2.709
23	5.425		3.953		2.842	2.725
24	5.485		3.955		2.857	2.781
25	5.512		3.968		2.853	2.785
26	5.483		4.180		2.909	
27	5.434		3.920		3.278	
28	5.405		4.152		3.296	
29	5.438		3.891		2.849	
30	5.527					
31	5.464					
32	5.475					
33	5.449					
34	5.517					
35	5.469					
36	5.458					

$\bar{t} \pm$ p.ϵ. (s)	5.504 $\pm$ 0.073	4.312 $\pm$ 0.035	3.994 $\pm$ 0.065	3.783 $\pm$ 0.030	3.190 $\pm$ 0.221	2.763 $\pm$ 0.041
$\therefore$						
$\bar{V}_{ts} \pm$ p.ϵ.* (mm s^{-1})	360 $\pm$ 5	459 $\pm$ 4	496 $\pm$ 8	523 $\pm$ 4	621 $\pm$ 43	717 $\pm$ 11

(*)   Probable error of a compound quantity.

If a number of measured quantities have means m_1, m_2, ... m_n with probable errors α_1, α_2, ... α_n respectively then the standard error of any function f (m_1, m_2, ... m_n) is α where

$$\alpha^2 = [\frac{\partial f}{\partial m_1}]^2 \ \alpha_1^2 + \ldots + [\frac{\partial f}{\partial m_n}]^2 \ \alpha_n^2 \qquad \ldots . \text{(F.1)}$$

In the case of terminal settling velocity,

$$f = V_{ts} = \frac{\text{distance travelled}}{\text{mean time}} = \frac{s}{m_1} \qquad \ldots . \text{(F.2)}$$

where s = 1980 mm = constant.

$$\text{Thus } \alpha^2 = [\frac{\partial V_{ts}}{\partial m_1}]^2 \ \alpha_1^2 = - [\frac{s}{m_1^2}]^2 \ \alpha_1^2 \qquad \ldots . \text{(F.3)}$$

$$\text{or} \quad \alpha = \pm \frac{\alpha_1 \ m_1}{m_1^2} \qquad \ldots . \text{(F.4)}$$

For spheres in GROUP 1 m_1 = 5.504 s and α_1 = 0.073 s giving $\alpha \simeq \pm 5$.

APPENDIX G

EXPERIMENTAL DETERMINATION OF THE TERMINAL SETTLING VELOCITY

FOR NEW DEXION STAMPINGS

GROUP B				GROUP C		GROUP D	
RUN No #	TIME (sec)	RUN No #	TIME (sec)	TIME (sec)		TIME (sec)	
1	9.027	29	10.571	9.621	9.502	9.977	11.403
2	9.858	30	9.621	9.383	9.501	9.383	9.027
3	9.740	31	10.571	9.620	9.740	9.858	10.334
4	9.977	32	10.452	10.334	10.215	9.621	9.383
5	9.265	33	9.858	9.265	9.858	9.620	9.502
6	10.215	34	10.069	10.215	9.977	10.334	9.502
7	9.621	35	9.894	9.502	9.976	9.977	10.214
8	10.334	36	9.740	9.740	9.978	9.976	9.512
9	10.452	37	10.334	9.734	10.096	11.165	9.987
10	10.334	38	10.215	10.690	10.215	10.037	9.990
11	9.621	39	10.571	9.027	9.501	9.383	10.455
12	9.740	40	9.502	10.452	9.858	9.621	9.621
13	10.096	41	9.502	9.502	9.977	9.967	9.858
14	9.858	42	9.621	9.265	9.265	10.452	9.858
15	10.096	43	9.621	9.502	9.858	10.690	9.621
16	10.452	44	9.265	9.858	9.739	9.501	9.265
17	9.740	45	9.383	9.739	9.858	9.383	10.215
18	10.096	46	9.739	9.858	9.621	11.402	9.502
19	9.977	47	9.502	10.096	9.977	10.215	9.146
20	10.809	48	9.620	9.026	10.452	9.858	9.740
21	9.621	49	9.265	9.977	9.500	9.502	10.670
22	10.334	50	10.333	9.621	9.977	10.927	9.739
23	10.215	51	10.215	9.977	9.977	9.740	9.740
24	9.858	52	9.977	10.689	9.858	8.671	9.265
25	10.215	53	9.624	9.739	9.383	9.265	10.452
26	10.571	54	10.096	9.502	10.334	9.383	10.334
27	9.265	55	9.026	9.500	9.978	9.977	9.383
28	10.452	56	10.097	10.452	9.739	9.495	9.503
$\bar{t} \pm$ p.ε. = 9.925 $\pm$ 0.294 s				9.818 $\pm$ 0.254		9.868 $\pm$ 0.381	
$\therefore$							
$\bar{V}_t \simeq$ 199 $\pm$ 6 mm s^{-1}				202 $\pm$ 5		201 $\pm$ 8	

APPENDIX H

EXPERIMENTAL DETERMINATION OF THE TERMINAL SETTLING VELOCITY FOR

USED DEXION STAMPINGS

GROUP B				GROUP C		GROUP D	
RUN No #	TIME (sec)	RUN No #	TIME (sec)	TIME (sec)		TIME (sec)	
1	8.796	25	8.740	8.812	9.625	9.258	9.764
2	7.698	26	8.005	9.624	9.598	9.699	9.423
3	9.600	27	8.859	9.924	9.697	8.881	9.266
4	8.072	28	9.351	8.944	9.730	9.010	9.302
5	9.245	29	8.726	8.103	9.704	9.426	9.363
6	9.795	30	8.620	9.060	9.736	8.976	9.049
7	8.701	31	7.746	9.445	8.873	9.481	9.070
8	9.374	32	9.290	9.461	9.330	9.089	9.835
9	8.050	33	8.620	8.692	8.659	9.937	9.875
10	8.840	34	9.244	8.995	9.327	9.237	9.054
11	9.508	35	8.148	9.591	8.727	9.904	8.960
12	7.767	36	7.995	9.499	9.779	9.195	9.635
13	9.698	37	7.417	9.615	9.411	10.067	9.077
14	8.695	38	8.843	9.822	8.862	8.990	9.823
15	9.509	39	8.501	9.220	9.514	9.935	9.305
16	8.170	40	8.810	9.417	9.121	9.121	9.838
17	8.567	41	8.636	8.668	9.366	9.359	9.412
18	9.965	42	7.830	9.575	9.693	9.116	9.195
19	8.456	43	8.960	9.562	9.884	9.095	9.223
20	8.200	44	8.856	9.420	8.899	9.892	8.755
21	9.186	45	9.606	9.362	8.852	9.920	8.498
22	8.637	46	7.967	9.470	9.471	9.223	8.634
23	9.617	47	9.585	9.678	9.531	9.767	9.923
24	8.067			9.690		9.510	
$\bar{t} \pm p.\epsilon. = 8.705 \pm 0.430$ s				9.336 ± 0.275		9.360 ± 0.266	
$\therefore$							
$\bar{V}_t \simeq 227 \pm 11$ mm s^{-1}				213 ± 6		212 ± 6	

APPENDIX I

PRESSURE DROP DATA

1. Pressure Drop Data for Clear Water

RUN No #	FLUID VELOCITY ($m \cdot s^{-1}$)	MANOMETRIC GRADIENT (m water / m pipeline)		DELIVERED CONCENTRATION (-) (v/o)
		HORIZONTAL	VERTICAL	
2-INCH PIPELINE				
1	0.526	6.46×10^{-3}	-	-
2	1.148	0.025	0.029	-
3	1.526	0.044	0.043	-
4	1.942	0.071	0.070	-
5	2.206	0.086	0.087	-
4-INCH PIPELINE				
1	0.508	2.05×10^{-3}	-	-
2	0.778	5.86×10^{-3}	-	-
3	0.946	9.96×10^{-3}	-	-
4	1.141	0.012	-	-
5	1.160	0.012	-	-
6	1.364	0.014	-	-
7	1.429	0.021	-	-
8	1.582	0.017	0.029	-
9	1.589	0.025	-	-
10	1.836	0.023	0.036	-
11	2.018	0.035	-	-
12	2.029	0.032	0.044	-
13	2.282	0.044	0.053	-
14	2.386	0.047	0.060	-
15	2.568	0.057	0.067	-
16	2.909	0.064	0.076	-
17	3.024	0.073	0.085	-
18	3.197	0.080	0.097	-
19	3.628	0.114	0.120	-

2. Hydraulic Data for Aluminium Platelets

RUN No #	FLUID VELOCITY (m s^{-1})	MANOMETRIC GRADIENT (m water / m pipeline)		DELIVERED CONCENTRATION (-) (v/o)
		HORIZONTAL	VERTICAL	
2-INCH PIPELINE				
1	0.753	0.084	0.115	1.656
2	0.754	0.102	0.140	2.161
3	0.792	0.068	0.087	2.086
4	0.806	0.130	0.195	4.499
5	0.817	0.070	0.075	1.249
6	0.830	0.098	0.115	3.092
7	0.910	0.106	0.162	3.108
8	1.042	0.051	0.075	1.934
9	1.078	0.109	0.153	5.067
10	1.090	0.033	0.051	1.105
11	1.119	0.084	0.125	3.667
12	1.146	0.065	0.089	2.829
13	1.155	0.080	0.121	3.356
14	1.161	0.076	0.115	3.622
15	1.202	0.061	-	2.481
16	1.204	0.061	0.096	2.947
17	1.223	0.063	0.093	2.481
18	1.236	0.084	0.115	4.011
19	1.257	0.095	0.135	3.218
20	1.269	0.061	0.090	2.565
21	1.280	0.042	0.103	1.262
22	1.299	0.052	0.078	1.692
23	1.304	0.061	0.087	2.529
24	1.359	0.063	0.095	2.549
25	1.371	0.087	0.137	3.409
26	1.414	0.063	0.093	1.681
27	1.420	0.091	0.109	3.743
28	1.447	0.073	0.093	1.772
29	1.450	0.075	0.112	3.170
30	1.467	0.077	0.103	3.799
31	1.488	0.103	0.162	5.636
32	1.498	0.054	0.071	1.307
33	1.504	0.075	0.109	3.179
34	1.538	0.082	0.109	3.288
35	1.541	0.088	0.146	3.313
36	1.596	0.062	0.082	1.406
37	1.631	0.099	0.121	3.584
38	1.630	0.099	0.159	5.532
39	1.659	0.088	0.128	3.563
40	1.659	0.061	0.078	1.182
41	1.660	0.100	0.157	4.730
42	1.668	0.057	0.078	1.230
43	1.732	0.103	0.150	4.533
44	1.751	0.077	0.107	2.452

APPENDIX I CONTINUED

45	1.792	0.081	0.106	2.421
46	1.805	0.076	0.103	1.971
47	1.826	0.074	0.093	1.537
48	1.834	0.086	0.115	2.384
49	1.840	0.111	0.146	4.141
50	1.857	0.762	0.100	1.504
51	1.960	0.076	0.090	1.070
52	1.994	0.116	0.162	3.941
53	2.058	0.116	0.153	3.978
54	2.150	0.130	0.171	4.624
55	2.151	0.142	0.196	5.441

4-INCH PIPELINE

1	0.413	0.055	-	0.200
2	0.425	0.012	0.013	0.255
3	0.452	0.010	0.026	0.336
4	0.491	0.052	0.017	0.410
5	0.515	0.079	-	0.891
6	0.537	0.055	0.015	0.641
7	0.558	0.090	0.017	1.815
8	0.593	0.056	0.025	0.620
9	0.598	0.116	-	1.514
10	0.606	0.108	0.047	1.652
11	0.628	0.056	0.060	0.688
12	0.633	0.105	0.055	2.032
13	0.633	0.097	0.057	1.710
14	0.665	0.092	0.052	1.599
15	0.740	0.056	-	1.023
16	0.759	0.106	0.086	1.573
17	0.779	0.037	0.026	0.633
18	0.796	0.066	0.030	1.155
19	0.877	0.061	-	1.509
20	0.883	0.111	0.077	2.870
21	0.889	0.045	0.019	0.175
22	0.922	0.082	0.045	1.606
23	0.937	0.103	0.060	2.677
24	0.973	0.100	0.056	2.278
25	1.020	0.065	0.060	1.070
26	1.041	0.043	0.044	0.816
27	1.042	0.080	-	2.709
28	1.076	0.088	0.073	2.557
29	1.145	0.060	0.064	2.735
30	1.149	0.186	0.137	6.623
31	1.209	0.093	0.056	1.588
32	1.245	0.093	0.078	2.361
33	1.250	0.120	0.075	3.032
34	0.251	0.057	0.047	1.105
35	1.285	0.079	0.067	1.883
36	1.300	0.141	0.102	4.338
37	1.376	0.053	0.053	2.335
38	1.408	0.110	0.078	2.974
39	1.441	0.063	0.052	1.976
40	1.452	0.127	0.089	3.458
41	1.543	0.105	0.069	3.112

APPENDIX I CONTINUED

42	1.567	0.058	0.055	1.802
43	1.569	0.023	0.043	0.492
44	1.570	0.077	0.068	0.077
45	1.579	0.125	0.096	0.125
46	1.597	0.086	0.071	2.428
47	1.621	0.119	0.103	3.739
48	1.635	0.077	0.070	2.753
49	1.657	0.069	0.063	1.903
50	1.668	0.110	0.080	3.177
51	1.694	0.029	0.043	0.707
52	1.783	0.107	0.091	3.288
53	1.840	0.127	0.052	3.136
54	1.849	0.170	0.132	4.716
55	1.858	0.099	0.095	2.824
56	1.897	0.065	0.072	2.614
57	1.912	0.106	0.093	3.241
58	1.914	0.136	0.115	4.276
59	1.943	0.061	0.068	2.140
60	1.953	0.045	0.054	0.527
61	1.980	0.046	0.073	2.034
62	2.025	0.045	0.065	0.828
63	2.031	0.082	0.085	2.846
64	2.068	0.097	0.101	3.127
65	2.144	0.075	0.084	2.084
66	2.149	0.052	0.073	0.840
67	2.157	0.072	0.095	2.564
68	2.189	0.082	0.093	3.245
69	2.219	0.151	0.132	4.747
70	2.225	0.162	0.146	5.719
71	2.228	0.094	0.101	3.159
72	2.288	0.063	0.082	1.930
73	2.300	0.236	0.208	9.277
74	2.301	0.057	0.071	1.822
75	2.310	0.116	0.120	3.662
76	2.314	0.215	0.183	8.030
77	2.339	0.140	0.135	4.753
78	2.347	0.067	0.082	2.740
79	2.420	0.252	0.205	9.124
80	2.466	0.137	0.132	4.105
81	2.478	0.071	0.113	1.950
82	2.526	0.102	0.110	3.260
83	2.623	0.130	0.134	4.855
84	2.675	0.192	0.178	6.580
85	2.725	0.119	0.130	4.709
86	2.728	0.165	0.167	5.871
87	2.756	0.094	0.113	6.814
88	2.761	0.086	0.108	2.382
89	2.778	0.098	0.113	3.117
90	2.810	0.070	0.091	1.056
91	2.833	0.128	0.143	5.304
92	2.850	0.144	0.173	4.375
93	2.867	0.137	0.152	4.707
94	2.905	0.153	0.136	3.877
95	2.977	0.093	0.121	2.939
96	2.996	0.270	0.251	10.113

APPENDIX I CONTINUED

97	3.060	0.223	0.218	8.142
98	3.145	0.171	0.174	6.138
99	3.230	0.117	0.132	1.044
100	3.253	0.092	0.123	2.715
101	3.267	0.279	0.260	10.444
102	3.452	0.143	0.161	3.878
103	3.468	0.204	0.218	8.538
104	3.479	0.193	0.226	5.747
105	3.505	0.100	0.126	2.216
106	3.512	0.230	0.239	7.752
107	3.716	0.193	0.213	4.605
108	3.767	0.155	0.182	4.497
109	3.788	0.118	0.141	1.111
110	4.026	0.155	0.165	1.695
111	4.131	0.146	0.182	3.412
112	4.142	0.155	0.176	1.618

APPENDIX J

EXPERIMENTAL ACCURACY OF PRESSURE DROP MEASUREMENTS FOR WATER AND

VERTICAL RESULTS FOR PLATELETS

J.1   Frictional Pressure Drop Due to Water Flow (An Error Analysis of the Data)

The friction factor is calculated from equation 6.1 of chapter 6 i.e.

$$f_w = \frac{\Delta P}{\frac{1}{2} \rho_w V_m^2} \frac{D}{4L} \tag{J.1}$$

where

$$V_m = \frac{\dot{Q}}{A} = \frac{4\dot{Q}}{\pi D^2} \tag{J.2}$$

and $\dot{Q} = \dfrac{W}{\rho_w t}$ \hfill (J.3)

Hence, equation J.1 may be reduced to

$$f_w = \text{constant} \, \frac{\Delta P}{L} \, D^5 \, t^2 \, \frac{1}{W^2} \tag{J.4}$$

Taking logarithms of either side and taking the differential of the resulting equation, we obtain

$$\frac{df_w}{f_w} = + \frac{d(\Delta P)}{\Delta P} - \frac{dL}{L} + 5 \frac{dD}{D} + 2 \frac{dt}{t} - 2 \frac{dW}{W} \tag{J.5}$$

The maximum fractional error in the friction factor will occur when the errors compound so that

$$\left| \frac{df_w}{f_w} \right| = \left| \frac{d\ (\Delta P)}{\Delta P} \right| + \left| \frac{dL}{L} \right| + 5 \left| \frac{dD}{D} \right| + 2 \left| \frac{dt}{d} \right| + 2 \left| \frac{dW}{W} \right| \qquad (J.6)$$

With reference to pressure drop measurements in the vertical pipe sections, the height difference recorded by the inverted air-over-water manometer could be read against a scale graduated to the nearest milli-metre. In practice, however, owing to the problem of large oscilla-tions, the accuracy of such measurements was greatly impaired. The most likely cause of these oscillations is thought to be the influence of the relatively large dynamic head compared with the static pressure drop measured across a short pipe section. For example, using a typical roughness value for smooth drawn tubing (such as mild steel pipe) of 1.5 x 10^{-3} mm and assuming a mean water velocity of 2 m/s in the 4" pipeline a friction coefficient of 0.0048 is predicted from the Moody diagram. In this instance equation 6.2 predicts that the static pressure drop across a 2.3 m long pipe section would be approximately 855 N m^{-2}. When this is compared with the equivalent dynamic head of $\frac{1}{2} \rho_w V_m^2 \simeq 2,000$ N m^{-2} it is not surprising that marked oscillations were observed. The large dynamic/static head ratio (= 2.3) implies that minute disturbances of the flow in the vicinity of each pressure tapping results in inaccurate measurement of the static pressure drop. Such disturbances can be identified with the flow instabilities and are commonly produced by secondary flow generated within the upstream bend. Unfortunately, the use of single tapping points in the experimental rig prohibited the verificiation of the existence of secondary flow - if a 'piezometric' ring is used then secondary flow can be confirmed if pressure distribution registered by the piezometer ring

is not axisymmetric. In fact, as pressure drop was measured using single tapping points, the adveristy of the effect of oscillations will have been further increased.

It is estimated that the error in the measurement of height difference resulted in an error of the order of 10% in pressure drop, i.e.

$$\frac{\delta P}{P} = \pm\ 0.1$$

The error margins applied to the other parameters were fixed by the nominal accuracy of those instruments used to measure them (see chapter 3). The resulting fractional errors are estimated to be as follows:

$$\frac{\delta D}{D} = \pm\ 0.001 \qquad\qquad (4" \text{ pipe diameters})$$

$$\pm\ 0.002 \qquad\qquad (2" \text{ pipe diameters})$$

$$\frac{\delta t}{t} = \pm\ 0.005$$

$$\frac{\delta W}{W} = \pm\ 0.001$$

$$\frac{\delta L}{L} \simeq 0$$

Using equation J.6 the maximum possible error in the friction factor for the 4" pipe is given by $\delta f_W = \pm\ 0.117\ f$. Corrections applied accordingly to each value of the friction factor are shown in Figs. J.1 to J.4 as "vertical error bars".

Similarly, the error δRe involved in the calculation of the Reynolds number Re was found from:

$$\frac{\delta Re}{Re} = \frac{\delta W}{W} + \frac{\delta D}{D} + \frac{\delta t}{t} \qquad (J.7)$$

where $\delta Re = \pm 0.007$ Re for the case considered. Thus, the "horizontal error bars" shown in Figs. J.1 to J.4 account for the maximum error involved in the Reynolds number.

The maximum frictional errors associated with each of the pipe sections used are summarised in Table J.1. It is clear that the most influential error occurs in the determination of the pressure drop in the vertical pipe sections. In contrast, the errors associated with measurements of pressure drop in sections of horizontal pipe which were an order of magnitude longer, were proportionally smaller. Another significant source of error, particularly in the calculation of the friction factor f_w, is the mean value of the pipe diameter used. This was obtained by local measurements at the two ends of the removable pieces of pipe comprising the test sections, but no such measurements were possible in the inner parts of those sections. An ordinary seamless mild steel pipe was used which was likely to have small variations in internal diameter created during manufacture as well as localised eccentricities resulting from stresses introduced by the assembled configuration. Now according to equation J.4 the measured friction factor depends on the fifth power of the pipe diameter D. Thus, if the pressure tappings were located at sections where the pipe diameter was significantly different from the measured diameter, the measured pressure drop would be in error. On the other hand, the Reynolds number, Re, varies only inversely with the pipe diameter thus involving only a fifth of the error imposed on f_w see equation J.6.

J.1.1   Horizontal Pipe Sections

Fig. J.1 shows the results obtained from water tests in the 4" horizontal pipe section. Although four of the experimental points lie below the Blasius curve the remaining points have friction factors which are well above those for smooth pipes. It is only the position of the point with the lowest Reynolds number which cannot be explained solely in terms of experimental error. This point will have had its friction factor calculated from a very low reading in pressure drop. In this instance the pressure drop recorded is of the same order as the "zero error" resulting in a highly inaccurate value for the friction factor since the latter is calculated by taking the small difference between two values of similar magnitude. The scatter of the experimental points observed for Reynolds numbers $< 2 \times 10^5$ is probably due to flow instabilities introduced by the use of the bypass.

Fig. J.2 shows the results obtained from water tests in the 2" horizontal pipe sections. There are two main comments on the graph, i.e.

(a)   This pipe section was made of stainless steel tubing as mentioned in chapter 3. It is, therefore, not surprising that within experimental error the results approximate the Blasius curve for smooth pipes.

(b)   A detailed account of the problems encountered during the commissioning of the 2" pipe rig was given in chapter 3. Following each modification further water tests were performed to establish any possible changes in the system's characteristics. These

operations, however, were time consuming and since the overall time available was very limited, the number of data collected in each instance was necessarily small.

J.1.2   Vertical Pipe Sections

Fig. J.3 shows the results obtained from water tests in the 4" vertical pipe section. Although the scatter of the experimental points is well within the large 'vertical error-bars', the data suggest a dependence of f_W on Re which is steeper than that represented by the standard curves of constant relative roughness k/D (i.e. Table J.2 shows f_W vs Re^n functional relationships where n > 0.25). The reason for this is not self evident and an explanation is sought in terms of the following two effects:

(a)   It is likely that a swirl first initiated in the pump may exist throughout the test section. The effect of such a swirl would be to increase the static pressure sensed by the upstream tapping. As the swirl travels through the test section, however, some of the rotational energy is dissipated due to friction at the pipe wall. As a result, the overall pressure drop indicated across the test section is increased. The spiral distance travelled by the peripheral fluid is shorter at higher pipe velocities and hence the overall effect is likely to be more pronounced at the lower range of pipe velocities which probably accounts for the larger deviation shown in Fig. J.3.

(b)   Secondary flow generated within the upstream bend forms an angle with the pipe axis and results in a component of the dynamic head

acting normally to the pipe wall. This component is then rotated by the swirl itself and becomes evenly distributed over the inner surface of the pipe walls leading to a further increase of the static pressure. As the secondary flows die out in the course of flow so is the excess static pressure gradually reduced. The contribution from the dynamic head, however, depends largely on the relative magnitude between static and dynamic heads.

With reference to Fig. J.3 let us assume that the curve based on a relative roughness of $k/D = 0.0005$ may be used to represent the un-affected condition in the vertical test section. If the discrepancy of $\Delta f_W \simeq 0.001$ at $Re \simeq 160,000$ is explained purely in terms of a swirl, the rotational speed required can be estimated using

$$\Delta P = \rho_W \, \omega^2 \, (D/4)^2 \qquad\qquad (J.7)$$

and is found equal to about 12 rad s^{-1} (i.e. about 117 rpm). This is quite possible since it represents only about one tenth of the pump impeller rotational speed. If on the other hand the difference is attributed wholly to secondary flows, an angle of about 4.6° forming between the direction of the dynamic head and the pipe axis is adequate to explain the difference. According to Miller (8) secondary flow with angles up to 45° or more to the mean flow is quite common in the normal engineering range of bend centreline radius to pipe diameter ratios of one to three. In this pipe configuration the ratio is 5 which reduces the turning effect on the flow but the bend itself is quite indifferent to the presence of a swirl, i.e. the bend may create little secondary flow but it cannot break-up an existing swirl travelling through it. In practice, it is more likely that the difference observed is the result of a combination between these two effects.

Fig. J.4 shows the results obtained from water tests in the 2" vertical pipe section. Data where the indicated manometric pressure drop was less than 50 mm were rejected and hence only four points are shown. The comments made about Fig. J.3 apply here also. In this pipeline the ratio of bend centreline radius to pipe diameter equals 4.

J.1.3   Conclusions

The experimental results for water have been validated by comparing the experimental data obtained from tests in 2" and 4" I.D. pipelines with the well accepted Moody charts. Whilst the accuracy of the horizontal pipe results in both pipe sizes has been established beyond any reasonable doubt, the experimental inaccuracies associated with the vertical tests were unacceptably high due to poor instrumentation. In addition, the vertical results show an unusually strong dependence of the friction factor, f_w on the Reynolds number Re. This adverse phenomenon has been attributed to the influence of a strong swirl induced by the pump combined with secondary flows generated within the upstream bend. In view of the uncertainties in the vertical pipe measurements, the results obtained from tests with platelets are of limited value and may only be used to show the general trend.

J.2   Vertical Pressure Drop Correlation with Flow of Platelets

The vertical measured hydraulic gradient from each experimental test was compared with the gradient predicted from equation 2.43, i.e.

$$i = i_w + C_v (S - 1)$$

(J.8)

where i_w was calculated using the appropriate working equation from Table J.2. Figs. J.5a and J.5b show the measured hydraulic gradient plotted against the predicted value for each pipe diameter. Fig. J.6 shows a combined plot using all the available data. The data were correlated using a linear regression technique and the resulting fitted lines as well as the agreement lines (shown as x = y), are included for comparison. The experimental scatter is thought to be mainly due to a 'slug' type flow of platelets which accentuates the fluctuations on the vertical manometer. Figs. J.5a and J.5b show that for either 2" or 4" pipe diameters the results are consistently under-predicted by as much as 20% and 12% respectively.

Considering the first term on the RHS of equation J.8 the discrepancy may be interpreted in terms of the 'turning flow' referred to in section J.3, i.e. the presence of platelets affects the pressure drop by damping both the secondary flow and the axial swirl along the test pipe section itself. The excess pressure drop resulting thus is expected to be more pronounced at the low end of the velocity range which probably accounts for the larger deviation of the results observed with the smaller pipe diameter - the superficial velocities achieved during the tests range from 0 - 2.1 m/s and 0 - 4.1 m/s for the 2" and 4" I.D. pipelines respectively.

Considering the discrepancy with respect to the second term on the RHS of equation J.8 the experimental data collected in the vertical test sections are subject to two adjustments. These corrections are due to density changes which affect the experimental results (refer to chapter 3 for a description of the experimental pipeline). The manometer used across the vertical pipe section contains water-filled sensing lines

which connect the manometer with the tapping points. Thus, the differential manometer used in data collection senses no gravity head for fluid in the vertical pipe section if that fluid has the same density as the water in the manometer sensing lines. Manometer deflections are experienced only when the density of the slurry in the pipeline differs from the sensing liquid or when the slurry in the pipeline differs from the sensing liquid or when there is a friction head due to flow in the test section. If the differential gravity head terms can be calculated and subtracted from the observed manometer reading, the balance is equal to the friction head loss. The first differential gravity head term is a relative density correction due to the temperature difference between water recirculating as the carrier fluid and the stationary water in the manometer sensing lines. Since the platelet/water mixture constitutes a closed recirculating system, the energy imparted to it by the pump is expected to cause a temperature rise during the course of a run. The water manometer sensing lines, however, are likely to acquire and maintain a lower temperature. The resulting differential gravity head can be calculated if the temperatures in both fluids are known. The maximum temperature rise recorded after about a day's continuous running was about 3° C. A sample calculation is included below to show that the effect of temperature differential on the vertical pressure drop was quite insignificant.

Consider a typical run using the 4" pipeline where the delivered solids concentration is 3.0% by volume,

mixture temperature = 20° C

manometer water temperature = 17° C

when the mean slurry velocity is about 2.8 m/s, the experimental head loss is 0.259 m H_2O/2.3 m pipe

at 17° C water density is 998.8 kg/m^3

at 20° C water density is 998.2 kg/m^3

across the 2.3 m vertical test section, the differential gravity head due to water temperature is:

$$\left(\frac{998.8 - 998.2}{998.8}\right) 2.3 = \frac{0.0014 \text{ m } H_2O}{2.3 \text{ m pipe}}$$

$$\% \text{ change} = \frac{0.0014}{0.259} \ 100 = 0.54\% \text{ (negligible)}$$

Still another differential gravity head term is due to the addition of platelets which increase the density of the recirculating slurry. This term can be calculated if the in situ solids concentration is known. The difference between the delivered and in situ concentrations is dictated by the settling velocity of the platelets being hoisted. Since the in situ concentration could not be experimentally determined, this differential gravity term could not be separated from the head loss caused by friction. Using an analytical approach, however, it is possible to obtain an estimate of the in situ concentration from values of the delivered concentration and thereby to approximate the effect of the in situ concentration on the vertical head loss.

As before, consider a test in the 4" vertical pipeline, where,

C_v = 3.0%

V_m = 2.8 m/s

$$t = 1.919 \text{ mm}$$

$$C_D = 1.360$$

and $\quad S = 2.629$

now equation 2.12 may be written as

$$V_t^2 \equiv (V_{wu} - V_s^2) = \frac{2 \text{ g } (S - 1) \text{ t}}{C_D} = 0.045 \qquad \qquad \dots \text{ (J.9)}$$

A volumetric balance for total flow yields the following equation

$$V_m = C_{vu} V_s + (1 - C_{vu}) V_{wu} \qquad \qquad \dots \text{ (J.10)}$$

A similar volumetric balance for solids flow yields the analogous equation

$$C_v V_m = C_{vu} V_s \qquad \qquad \dots \text{ (J.11)}$$

Solving equations J.9, J.10 and J.11 for C_{vu}, V_s and V_{wu}, we find

$$C_{vu} = 3.17\%$$

$$V_{wu} = 2.802 \text{ m/s}$$

$$V_s = 2.735 \text{ m/s}$$

The in situ volumetric concentration is 0.17% higher than the delivered concentration. Although the difference becomes more significant at low velocities it is not sufficiently large to account for the discrepancy in the results.

Clearly the accuracy of the experimental data is too poor to draw any firm conclusions from the vertical pipe results. The above analysis of the errors incurred indicates that the likely presence of secondary flow combined with an axial swirl provide the most influential source of error. Therefore, the vertical correlated results provide only qualitative information and further experimentation is required to establish the application of equation 2.43 in the flow of metallic platelets.
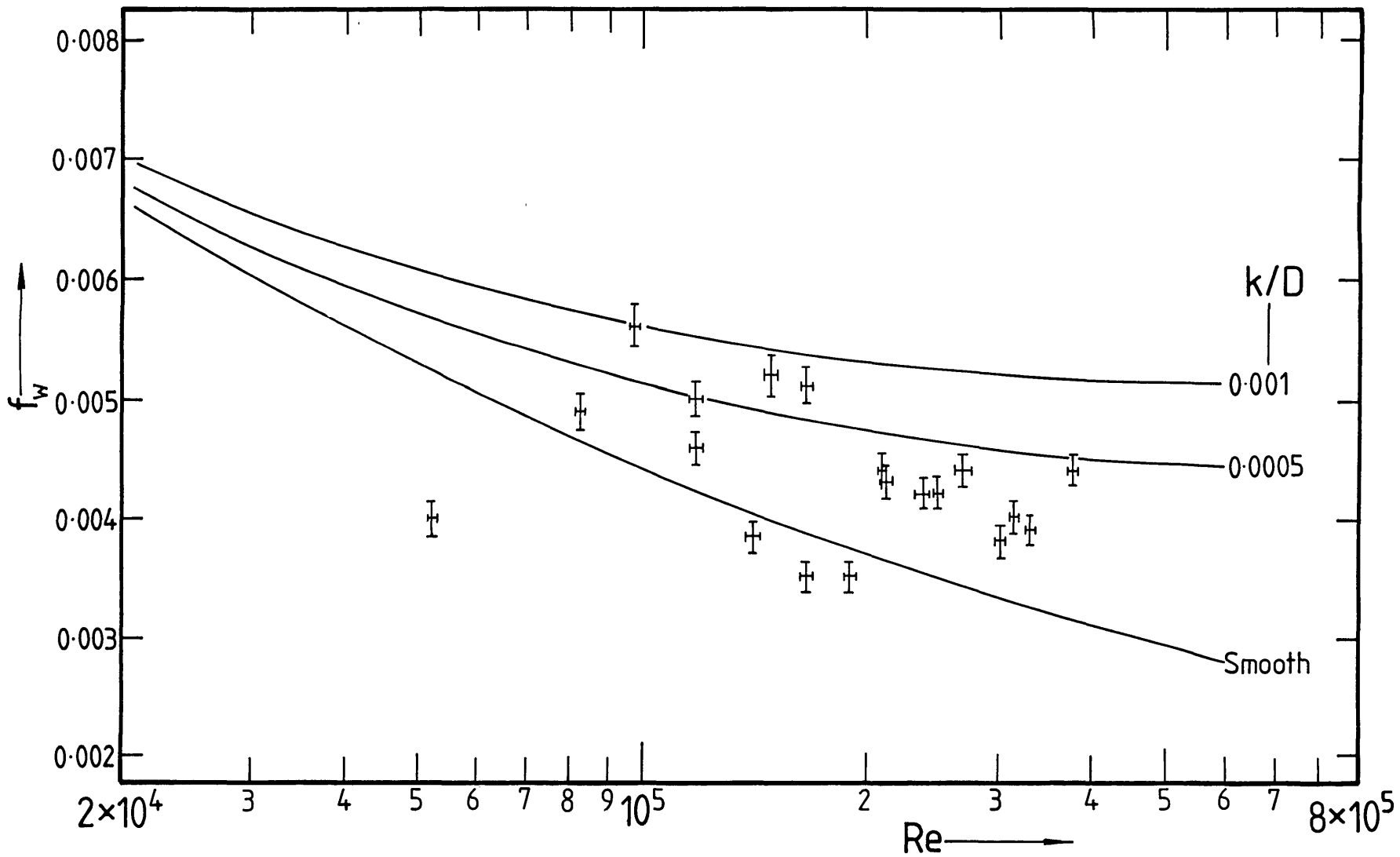
Fig. J·1

Friction factor vs Reynolds number for 4″ horizontal pipe
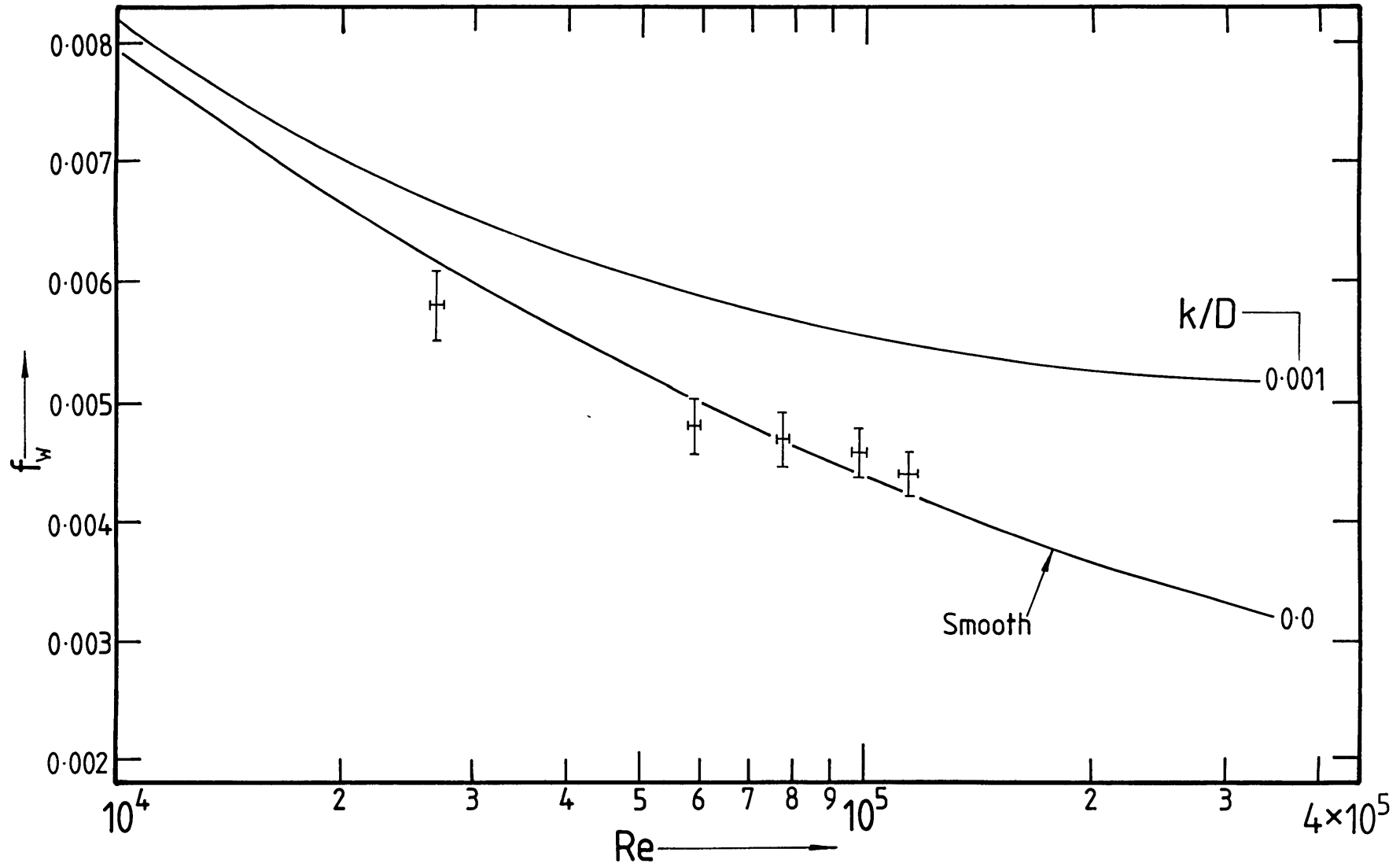
Fig. J·2

Friction factor vs Reynolds number for 2″ horizontal pipe
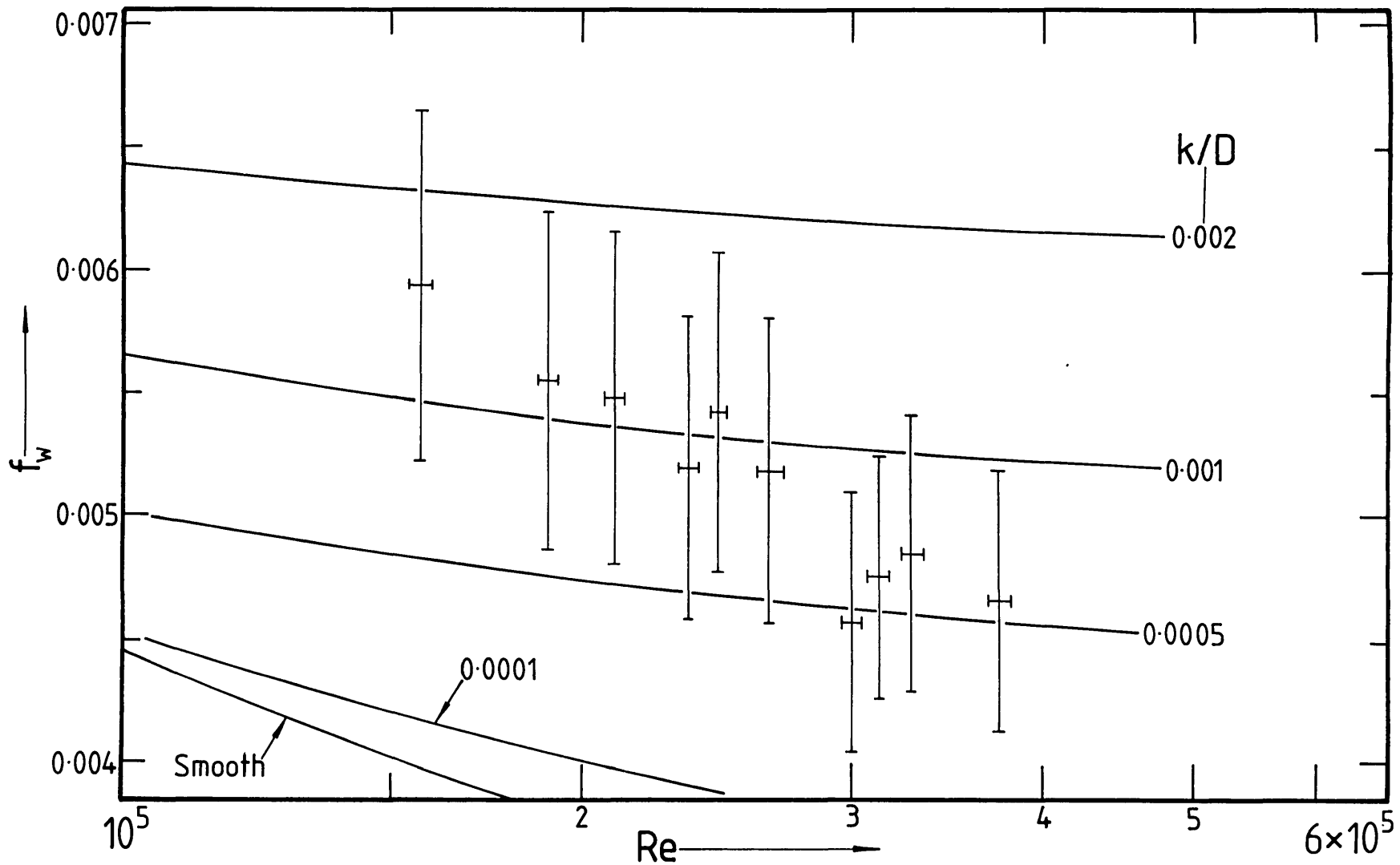
Fig. J·3

Friction factor vs Reynolds number for 4″ vertical pipe
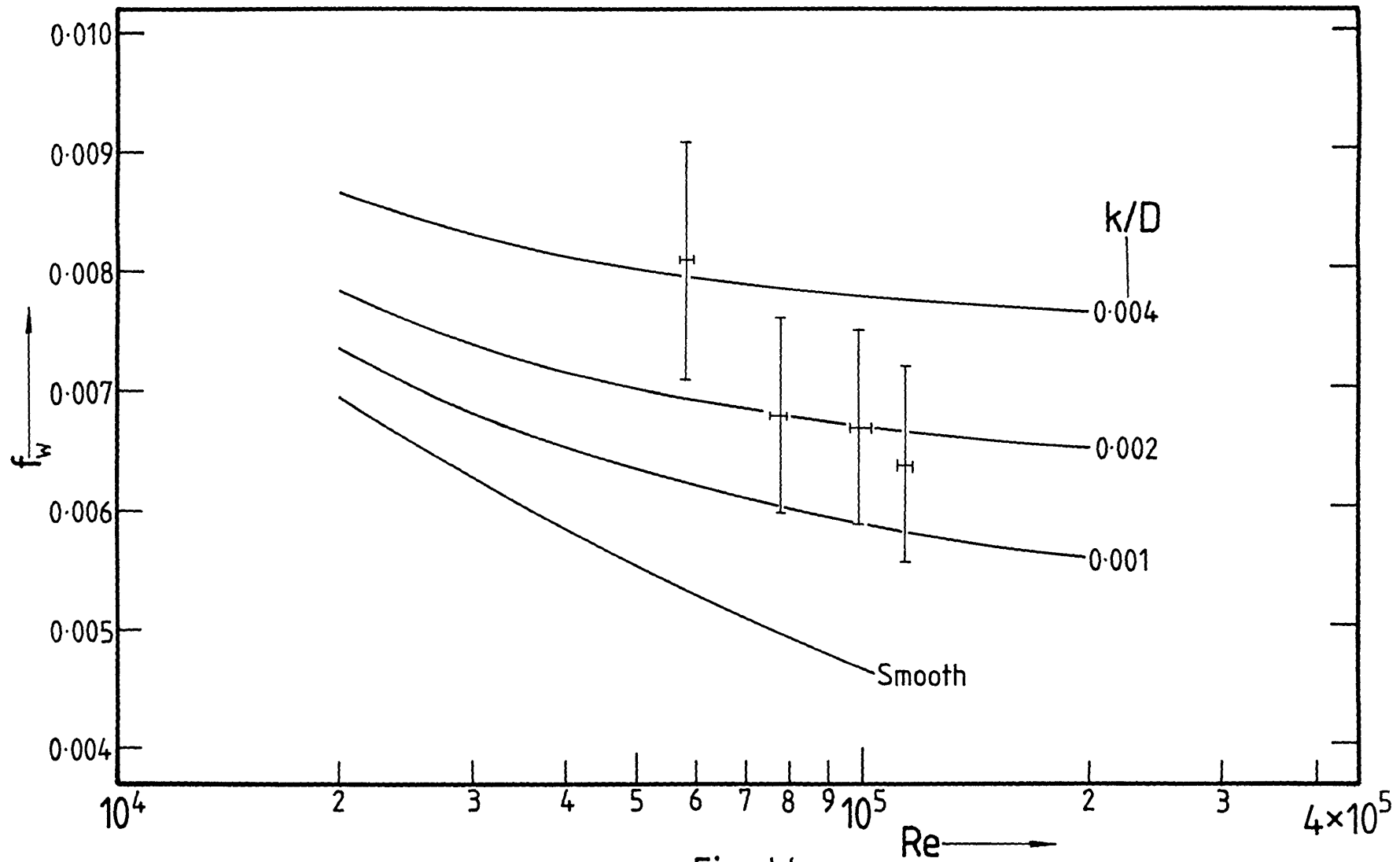
Fig. J·4

Friction factor vs Reynolds number for 2" vertical pipe
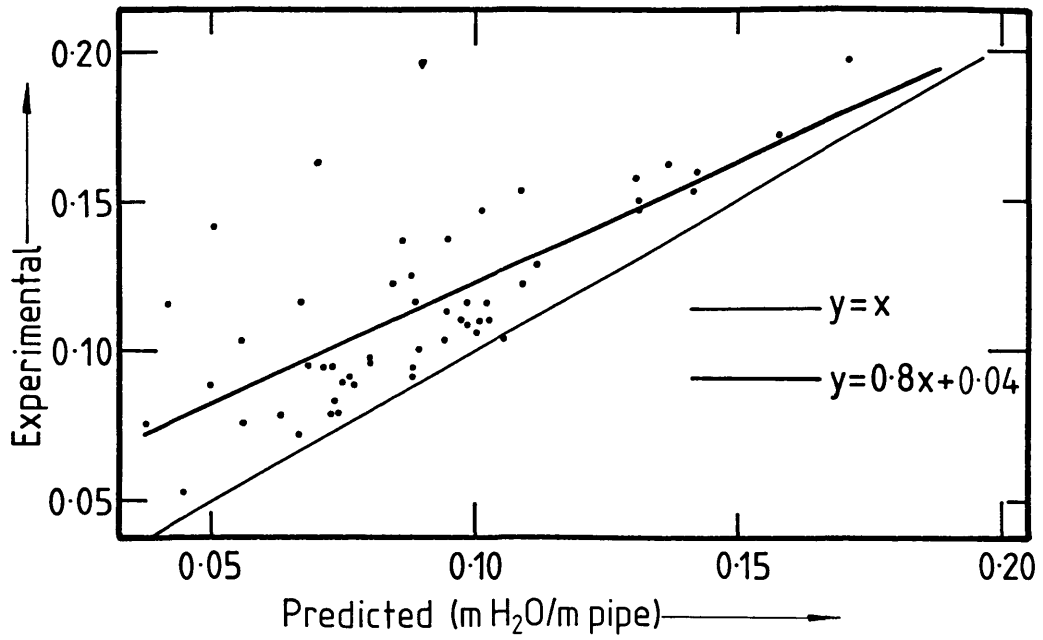
(a) 2" ID Test Section
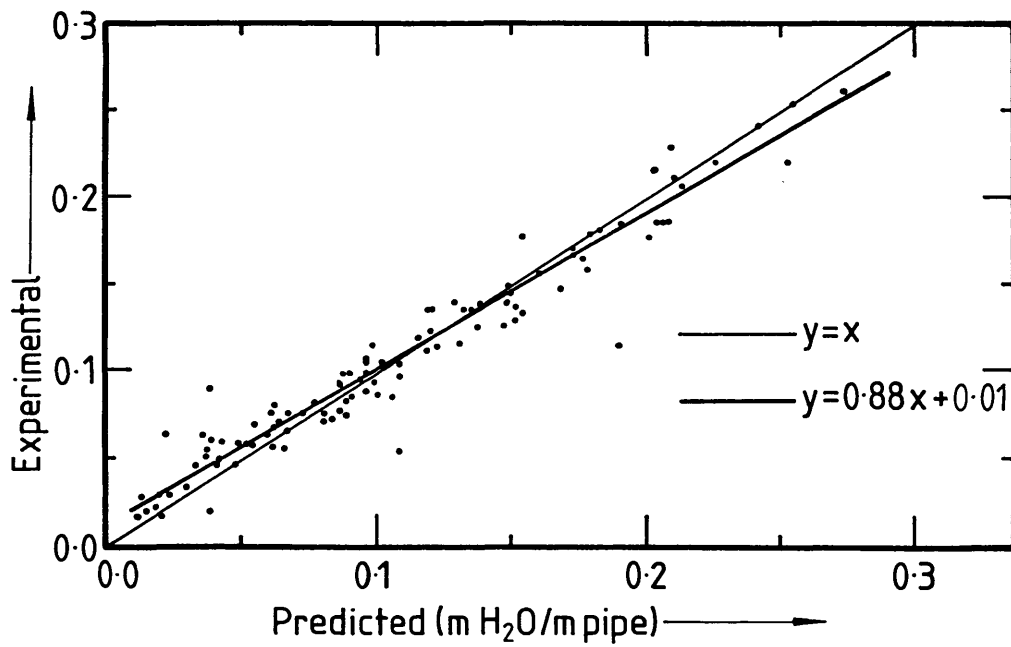
(b) 4" ID Test Section

Fig. J·5

Hydraulic gradients for metallic platelets in vertical flow
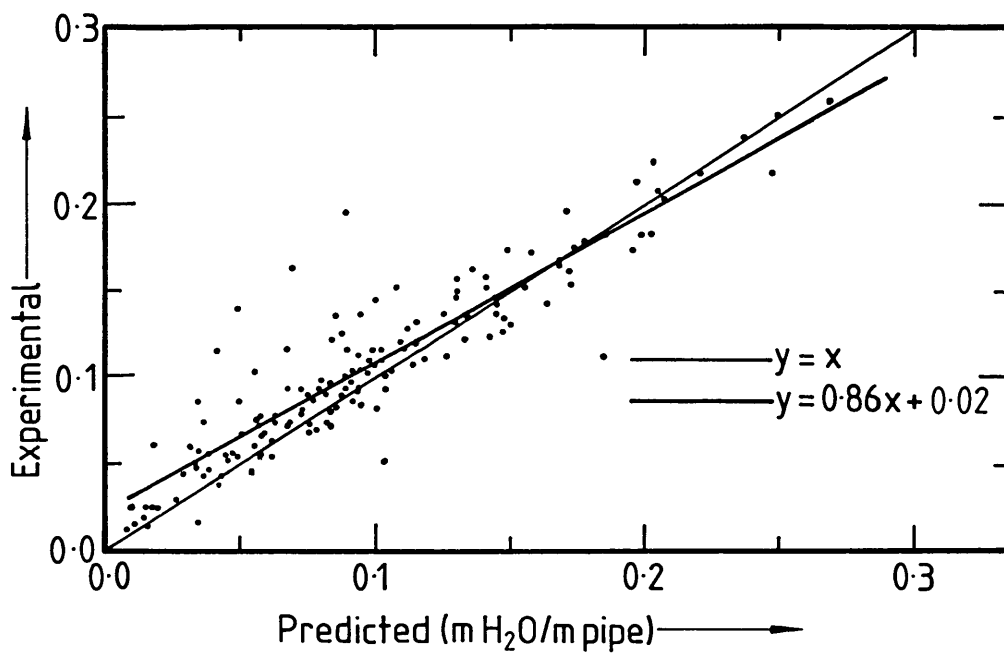
Fig. J·6

Hydraulic gradient in both 2″and 4″ vertical pipe sections

TABLE J.1 : Maximum Fractional Errors Involved in the

Determination of f_w and Re

FRACTIONAL ERROR	2" I.D. PIPELINE		4" I.D. PIPELINE	
	HORIZONTAL SECTION	VERTICAL SECTION	HORIZONTAL SECTION	VERTICAL SECTION
$\dfrac{\delta p}{p}$	± 0.014	± 0.1	± 0.007	± 0.1
$\dfrac{\delta D}{D}$	± 0.002	± 0.002	± 0.001	± 0.001
$\dfrac{\delta t}{t}$	± 0.005	± 0.005	± 0.005	± 0.005
$\dfrac{\delta W}{W}$	± 0.001	± 0.001	± 0.001	± 0.001
$\therefore \ \dfrac{\delta f_{w\ max}}{f} =$ (Equation J.6)	± 0.036	± 0.122	± 0.024	± 0.117
$\therefore \ \dfrac{\delta Re_{max}}{Re} =$ (Equation J.7)	± 0.008	± 0.008	± 0.007	± 0.007

TABLE J.2 : Correlation of Pressure Drop Data in the
Vertical Pipes

PIPELINE	$i_w = i_w (V_m)$	Coefficient of Correlation	Standard Error of Estimate	$f_w = f_w (Re)$
2" (stainless steel)	$2.282 \times 10^{-2} V_m^{1.677}$	0.9966	0.0213	$\dfrac{0.188}{Re^{0.323}}$
4" (mild steel)	$1.342 \times 10^{-2} V_m^{1.689}$	0.9976	0.0142	$\dfrac{0.246}{Re^{0.311}}$

10th International Conference on the
Hydraulic Transport of Solids in Pipes

HYDROTRANSPORT 10

Innsbruck, Austria: 29-31 October, 1986

PAPER F2

"Hydraulic Conveying of Metallic Platelets"

M. STREAT* AND A. TATSIS+

*   Department of Chemical Engineering &
       Chemical Technology,
       Imperial College,
       London.
       SW7 2BY

+   BHRA,
       Cranfield,
       Bedford.
       MK43 0AJ

Summary

One of the options for dealing with radioactive nuclear fuel cladding waste involves comminution as a precursor to further treatment and thus the feasibility of handling such material by hydraulic conveying is of interest.
Experiments have been performed with suspensions of regular shaped metallic platelets to simulate radioactive Magnox swarf. The terminal settling velocity and drag coefficient of aluminium platelets 9-12 mm long and 2 mm thick were measured and found to be in good agreement with theoretical predictions.

A pipe rig with 2" and 4" diameter test sections was used to pump aluminium platelets at volumetric concentrations up to about 10% and flow velocities in the range 0.4-4.2 m/s. Pressure drop data are correlated using established empirical relationships and the mechanism of platelet transportation is explained in terms of an "aerofoil" theory.

SYMBOLS

		Units
A_p	particle projected area	L^2
C_D	particle drag coefficient	–
C_v	volumetric concentration of solids	–
d_s	diameter of volume equivalent sphere	L
D	internal pipe diameter	L
F_F	hydrodynamic force exerted onto the leading face of a platelet	$M\ L\ T^{-2}$
F_L	Froude number at the critical velocity for deposition	–
f_m	fanning friction factor for slurry	–
Fr	Froude number	–
F_S	hydrodynamic force exerted onto the shearing sides of a platelet	$M\ L\ T^{-2}$
F_T	hydrodynamic force exerted onto the upper surface of a platelet	$M\ L\ T^{-2}$
f_w	fanning friction factor for water	–
g	acceleration due to gravity	$L\ T^{-2}$
Ga	Galileo number	–
i	hydraulic gradient due to slurry	–
i_w	hydraulic gradient due to water	–
K	particle shape factor	–
Ke	volume coefficient of equi-dimensional particle	–
Re	Reynolds number	–
S	relative density of solids	–
S_m	mean relative density of slurry	–
t	platelet thickness	L
V_{cr}	critical velocity of solids deposition	$L\ T^{-1}$
V_m	mean slurry velocity	$L\ T^{-1}$
V_t	terminal settling velocity of a single particle	$L\ T^{-1}$
V_t	hindered terminal settling velocity	$L\ T^{-1}$
V_u	critical velocity for turbulent uplift	$L\ T^{-1}$
W_{ap}	apparent weight of a submerged platelet	M
ρ_m	mean slurry density	$M\ L^{-3}$
ρ_w	water density	$M\ L^{-3}$
ϕ	Durand head loss parameter	–
ψ	Durand velocity parameter	–

1.   INTRODUCTION

The majority of thermal nuclear reactors in the United Kingdom use a uranium metal fuel clad in a Magnox can. Magnox is an alloy comprising 99.3% magnesium metal and 0.7% aluminium. When the spent fuel is decanned prior to reprocessing, the resultant swarf is normally stored under water in large concrete silos. Under water, magnesium metal corrodes according to the following reaction:

$$Mg + 2H_2O \longrightarrow Mg(OH)_2 + H_2 + Heat$$
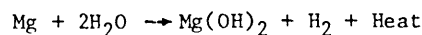
The heat liberated by this reaction is entrapped by the magnesium hydroxide which acts as a convection barrier. In addition, the hydrogen gas produced constitutes an explosion hazard if allowed to exceed a concentration of 4% in the surrounding air. Development work is now in progress to empty the existing storage silos and to evaluate alternative methodology to handle and permanently store future arisings of Magnox waste. One of the process options is to comminute fresh Magnox and then transport to an immobilisation plant. This paper considers the possibility of hydraulic transportation of Magnox swarf in the process cycle. Although the particle size of comminuted Magnox swarf has not yet been decided, it is almost certain to involve "platelets" with a large length to thickness ratio. Despite an abundance of literature concerned with slurry pipelining of naturally occurring materials, very little relates to the unusual shapes anticipated in this work.

To avoid corrosion, aluminium platelets in the size range 9-12 mm long and 2 mm thick were used as the simulant material. Tests were performed at Imperial College with individual platelets to establish their settling characteristics and dilute suspensions of metal platelet/water mixtures were pumped in a custom designed pipe rig which was made available to us by BNFL at the UKAEA-Winfrith Laboratory.

2. THEORETICAL BACKGROUND

2.1 Head Loss in the Pumping of Settling Slurries

The main characteristic of the flow of settling slurries lies in the fact that the solid and liquid phases remain identifiable; there is no increase in the viscosity of the liquid phase due to its association with the solid particles. The primary objectives of this work are firstly to predict and secondly to optimise the head loss as a function of independent design variables. Amongst the important independent parameters for settling slurry systems are pipeline diameter, D, operating velocity V_m, mean particle size d, particle size distribution and the properties of the carrier fluid. Correlations for slurry head loss where the transporting medium is water are often given by the general relationship:

$$\frac{i - i_w}{i_w C_v} = f(Fr) \qquad \ldots (1)$$

$$\text{where } Fr = \frac{V_m}{\sqrt{g\,D\,(S - 1)}}$$

Equation 1 accounts for the frictional head loss due to the fluid and that due to the solids. The Froude number, Fr, corrected for the relative mass of solids in water relates the competing effects of inertia and gravity. Depending on the mean particle size and the superficial velocity of the mixture, transport can take place either as a suspension or in the form of a sliding bed. Where possible, the former is preferred since it offers economical advantages and minimises the probability of blockage.

Durand and Condolios (1) proposed an empirical correlation of the form:

$$\frac{i - i_w}{i_w C_v} = 150 \left[\frac{g\,D\,(S - 1)}{V_m^2 \sqrt{C_D}}\right]^{1.5} \qquad \ldots (2)$$

which for simplicity, is often quoted as $\phi = K\psi^n$.

Newitt, Richardson et al (2) pioneered a theoretical approach to the problem. By assuming no slip between the solid particles and water, they developed the following semi-empirical correlation for the fully suspended flow regime,

$$\frac{i - i_w}{i_w C_v} = 1100 \frac{g\,D\,V_t\,(S - 1)}{V_m^3} \qquad \ldots (3)$$

Over the years, many researchers have proposed modifications to the empirical constants in equations 2 and 3 so that the correlations will fit their own experimental data. For example, Zandi and Govatos (3) collated over 2,500 data points from various sources and compared existing

correlations. They recommended three mutually exclusive correlations of their own which apply over consecutive intervals of the range for ψ.

Newitt et al (2) offered a separate expression for the case of flow with a sliding bed, i.e.

$$\frac{i - i_w}{i_w C_v} = \frac{66\,(S - 1)\,g\,D}{V_m^2} \qquad \ldots (4)$$

Wilson et al (3) used a bed slip model approach which is based on an analysis of the hydrostatic type forces acting on a bed of particles within a conduit. They showed that the total pressure drop with a sliding bed is given by

$$i = 2f_s\,(S - 1)\,C_b\,[\frac{\sin\Theta - \Theta\cos\Theta}{\pi}]$$

$$+ 2f_b\,\frac{\rho_{mb}}{\rho_w}\,\frac{\Theta}{\pi}\,\frac{V_b^2}{Dg} + 2f_t\,\frac{\rho_{mt}}{\rho_w}$$

$$\frac{(\pi - \Theta)}{\pi}\,\frac{V_t^2}{Dg} + \frac{2f_s\,f_b}{\tan\phi}\,\frac{\Theta}{\pi}\,\frac{(V_t - V_b)^2}{Dg} \qquad \ldots (5)$$

where the symbols are defined in the appropriate reference.

Wilson (4) developed this concept further into a unified analysis for pipeline flow by considering separately the effects due to suspended and contact load respectively. Clift et al (5) have used this method for scaling mixed regime slurries in the suspended and bed load regimes. They distinguished between the head loss gradient for the suspended component and the contact load component and showed that the overall head loss is given by

$$\frac{i - i_w}{S_m - 1} = K\,B\,V_m^{-m} + A\,i_w\,(1 - K\,V_m^{-m}) \qquad \ldots (6)$$

where the parameters A, B and m are properties of the fluid and have to be determined experimentally.

2.2 Single Particle Hydrodynamics

Hydraulic conveying may be examined analytically by considering the hydrodynamic forces acting upon the individual particles. Although this approach is simplistic, it is nevertheless useful in providing an insight to the transport mechanisms. At low flow rates, particle transport takes place in a sliding bed. The particles move in "unison" so that particle drag is irrelevant and solid friction at the pipe wall accounts for most of the pressure drop incurred. At higher flow rates, however, the particles travel in suspension and whilst particle drag becomes important, the net result is a reduction in the frictional head loss. The mean slurry velocity which marks the onset of settling in a given pipe, commonly referred to as the "critical velocity of deposition", is often used as a criterion in deciding which mathematical model is most applicable to the type of flow. The type of flow attained in a given pipe diameter is largely determined by the particle size and shape and

hence by the particle drag. The drag coefficient for a sphere falling freely at its terminal velocity through an unbound liquid is given by

$$C_D = \frac{4 \, g \, d \, (S - 1)}{3 \, V_{ts}^2} \qquad \ldots (7)$$

Similarly, for a flat prismatic object of cross-sectional area A_p and thickness t ($\sqrt{A_p} \gg$ t) settling with its plane normal to the direction of motion it can be shown that

$$C_D = \frac{2 \, g \, t \, (S - 1)}{V_{tp}^2} \qquad \ldots (8)$$

The calculation of drag for a non-spherical particle becomes increasingly difficult as the particle shape deviates from spherical. This is partly due to inadequate methods of defining shape but more importantly due to the complex trajectory described by the falling particle. It is generally accepted, however, that when a non-spherical particle is settling in the turbulent flow regime, then it orientates itself into the position of greatest drag (this provides greatest stability) and then follows a sinuous path. The complete analysis of drag variation with particle shape is beyond the scope of this paper and reference is made to the work carried out by Heywood (6). The particle terminal velocity V_t required in equation 7 is derived from the following fluid-particle expression:

$$Ga = 18 \, Re_{ts}$$

$$\text{if } Ga < 3.6 \qquad \ldots (9)$$

or

$$Ga = 18 \, Re_{ts} + 2.7 \, Re_{ts}^{1.687}$$

$$\text{if } 3.6 < Ga < 10^5 \qquad \ldots (10)$$

or

$$Ga = 1/3 \, Re_{ts}^2$$

$$\text{if } Ga > 10^5 \qquad \ldots (11)$$

$$\text{where } Re_{ts} = \frac{V_t \, \rho \, d_s}{\mu} \qquad \ldots (12)$$

For a non spherical particle the settling velocity is adjusted for the effect of shape by multiplying with an appropriate shape factor K, i.e.

$$V_{tp} = K \, V_{ts} \qquad \ldots (13)$$

Heywood (6) has shown that a reliable estimate of K may be obtained using the definition of an equivalent sphere based on the same projected area as the particle, i.e.

$$K = \frac{Ke \, t}{\sqrt{A_p}} \qquad \ldots (14)$$

where

$$Ke = \frac{\text{Volume of particle}}{(\text{equivalent diameter})^3} \qquad \ldots (15)$$

Finally, Heywood (6, 7) gave empirical correlations which may be used to obtain a better estimate of K.

Any additional effects which might arise from hindered settling may be accounted for by using the Richardson and Zaki (8) correlation, i.e.

$$V_t' = V_t \, (1 - C_v)^a \qquad \ldots (16)$$

where a is a function of the particle Reynolds number.

Two of the most commonly used expressions which relate the critical settling velocity of deposition to the terminal settling velocity are given below

$$V_{cr} = F_L \, \sqrt{(2 \, g \, D \, (S - 1))} \qquad \ldots (17)$$

Durand (1) and

$$V_u = 0.6 \, V_t \, \sqrt{2/f_w} \, e^{45 \, d/D} \qquad \ldots (18)$$

Wilson and Watt (9).

3. EXPERIMENTAL

3.1 Experimental Equipment and Procedure

The terminal settling velocity of individual aluminium platelets was determined using a glass column as shown in Fig. 1. A closed loop test rig, shown in Fig. 2, was used to pump dilute suspensions of platelet/water mixtures. Although the rig was built with 4" I.D. piping, provision was made to replace the test sections with different pipe diameters – 2" and 4" configurations were used in this work.

Flow rate was measured by an electromagnetic flowmeter and the mixture density was adjusted by controlling the rate of platelets' entrainment in the suction end of the pump. Both these quantities could be checked by diverting the slurry for a given time into a weigh tank. Slurry velocity was controlled by using either a variable speed drive on the centrifugal solids-handling pump or a bypass.

The frictional pressure drop across the test section of horizontal pipeline was measured using two strain gauge type transducers. The pressure difference was reflected as a voltage signal which was filtered for noise and relayed to a multi-channel UV recorder. Prior to taking a pressure drop reading the flow would be established in the circuit and the rig would be allowed to run for a few minutes to attain a uniform concentration throughout the loop.

A detailed description of the apparatus is given in Ref. 10.

3.2 Experimental Material

It was estimated that about 250 kg of light-metal "platelet material" was required to reach an upper volumetric concentration of 30% using the

Winfrith pipeline. The maximum particle dimensions should be approximately 1/10 of the pipe diameter.

To avoid the manufacturing cost of producing the material out of commercial aluminium sheeting, the possibility of using the waste products of standard operations was explored. Stampings produced in the making of Dexion angle offered an excellent alternative and 410 kg of mixed Dexion stampings were supplied by the Dexion Company.

Fig. 3 shows an isometric view of a Dexion angle length comprising one cycle of perforations. The pattern consists of nine holes (or stampings) which come in four different sizes, "A, B, C" and "D" with maximum particle size ranging from about 58 to 10 mm respectively. Apart from Item D, which has an ordinary disc shape, each stamping is made up of three sections; two semicircles separated by a rectangular piece in the middle. The length to breadth ratio varies from unity for "D" to about 5.7 for "A". The simplicity of geometry facilitates the calculation of the projected area. Following some commissioning tests in the 4" pipeline it became clear that platelets "A" were unsuitable for pumping due to the large d/D ratio (= 0.6).

Platelets "A" were then discarded by sieving and Table 1 shows the size classification of the remaining items (about 260 kg), before and after pumping in the two pipe diameters. The reduction in mean particle size is attributed mainly to wear within the pump volute despite the use of a recessed impeller type pump. Plate 1 is a close-up photograph of two used "B" items confirming that apart from some curling of the material occurring at the distant edges, the overall shape has been retained. Finally Table 2 provides equivalent particle dimensions which are representative of all platelets used in the tests.

3.3 Hydrodynamic Properties of Dexion Stampings

The prediction of terminal settling velocity for a non-spherical particle falling freely through water requires the knowledge of a suitable "shape factor". In the case of Dexion stampings, appropriate shape factors were found using the method outlined under single particle hydrodynamics (see Table 3). Alternatively, the terminal settling velocity of individual platelets was determined experimentally by means of a 4" water column. Initially, ballotini spheres were used in the size range 3-12 mm in order to establish the effect of the column-walls on axially descending particles. The agreement obtained between predicted and experimentally determined values of the terminal settling velocity was to within 5%, suggesting that for particles up to 12 mm in diameter the effects due to the pipe-wall are negligible and can be safely ignored.

When Dexion stampings were tested, their mode of descent was observed carefully and the various effects are summarised in Table 4. It is interesting to note that the small deformation of used platelets resulted generally in a reduction of the number and intensity of secondary motions.

Table 5 shows the experimental results obtained for the various items and draws a comparison with the predicted values of terminal settling velocity. The best agreement, to within

1.5%, was obtained using an approximate volumetric factor Ke = 0.560 which was proposed by Heywood (7) for rounded isometric irregular shapes.

4. RESULTS AND DISCUSSION

4.1 Correlations Using the Durand Parameters

One hundred and twelve useful data points were obtained from pressure drop tests in the 4" pipe diameter. When the results were correlated using the dimensionless groups proposed by Durand and Condolios (1) the following expression was obtained

$$\phi = 265 \, \psi^{1.38} \qquad \ldots (19)$$

where $\phi = \dfrac{i - i_w}{i_w \, C_v}$ and $\psi = \dfrac{g \, D \, (S - 1)}{V_m^2 \, \sqrt{C_D}}$

Each data point was evaluated using i, V_m and C_v as the input parameters whilst C_D was calculated using equation 8 and i_w was obtained from separate water tests. Fig. 4a shows some experimental scatter at extreme values of the ψ parameter. At low flow rates (i.e. large ψ) the scatter can be easily explained in terms of operating instabilities introduced by the use of a bypass. Deviations from the straight line at high mean velocities (i.e. low ψ), were also observed by Newitt et al (2). They pointed out that in this flow regime the quantities i and i_w become large and of similar magnitude. Consequently the dimensionless group ϕ becomes inaccurate since it is calculated by taking the small difference between two large values. The Durand and Condolios correlation evaluated with their own coefficients has also been included for comparison. Fig. 4b shows the results obtained from the 2" diameter tests. The data may be correlated by the equation

$$\phi = 188 \, \psi^{1.44} \qquad \ldots (20)$$

The general comments made on the 4" diameter results apply here also.

The differences in the values of the exponents in equations (19) and (20) from the value of 1.5 proposed by Durand are not considered to be significant and are well within the scatter of the experimental results. The differences in the constants, however, are significant and suggest that the inclusion of the drag coefficient to account for the effect of particle shape is not entirely satisfactory and that there must be a fundamental difference in the conveyance of platelets as opposed to rounded particles.

In order to establish the validity of the Durand and Condolios approach for scale-up calculations the results from each pipe diameter were plotted collectively in Fig. 5, giving the following equation:

$$\phi = 238 \, \psi^{1.41} \qquad \ldots (21)$$

The comparison suggests that the results obtained from the two pipe diameters may be grouped together without significant loss of accuracy – the use of such empirical correlations for modest scale-up is thus justified. A comparison between equations 19 and 20 suggests, however, that the

scale-up correlation is affected by the pipe diameter. Specifically, it might be expected that the ratio of pipe diameter to mean particle size D/d would affect the ϕ - ψ correlation and additional experimental work is needed with metallic platelets of various sizes in several pipe diaemters to establish this effect.

4.2 Interpretation of the Results

The fact that the results correlated well using the Durand and Condolios approach suggests that the platelets were suspended over a substantial part of the velocity range. In the absence of independent experimental evidence, this hypothesis was tested by adopting the Clift et al (5) approach: a plot of $(f_m - f_w)/(S_m - 1)$ as a function of V_m may be used to show whether values of V_m are sufficiently high to sustain the solids in suspension. The asymptotic part of the curves shown in Figs. 6a and 6b confirms that fully suspended flow was actually achieved above mixture velocities of about 1.7 and 2 m/s for the 2" and 4" pipe diameters respectively. Hence, rewriting equation 6 in terms of friction factors, and using it in its asymptotic form at high velocities, i.e.

$$\frac{f_m - f_w}{(S_m - 1)} = A\, f_w \qquad \ldots (22)$$

the constant A was determined to be 8.6 and 2.4 for the 2" and 4" pipelines respectively. If it is assumed that there is no slip between the particles and the liquid, then the solid/liquid suspension behaves as a fluid of a higher density ρ_m with the result that A = 1. The fact that in the present study A is much larger, suggests that platelets have an effect in addition to that of merely increasing the effective density of the slurry. It appears that this arises from the finite relative motion between the platelets and the fluid which results in the generation of eddies. The latter is associated with increased frictional dissipation which results in additional pressure drop. This conclusion is corroborated by the findings of Pouska and Link (11) who made measurements of the frictional pressure drop in the pumping of dilute suspensions of oil-shale in water. Their results yield values of the constant A which are greater than unity and are approximately equal in magnitude to those obtained in the present study.

An independent estimate of the threshold velocity for turbulent uplift can be obtained using equation 18. This predicts the minimum velocities required for turbulent suspension as 7.4 and 4.6 m/s respectively. These values are considerably greater than those deduced from Figs. 6a and 6b. There may be a number of reasons why equation 18 is not suitable for use with platelet material. Two possible reasons are discussed below:

(i)   Although the value of V_t employed in equation 18 is experimentally determined it is still necessary to estimate an appropriate value for d; of the various alternatives, a sphere settling at the same rate as the platelets was selected. The diameter of such a sphere was estimated to be 1.5 mm as opposed to the maximum platelet dimension of about 12 mm. Use of this equivalent sphere diameter makes equation 18

self consistent, but unfortunately, it does not simulate an aluminium platelet in physical terms.

(ii)   Secondly, the predicted velocity is highly sensitive to the value of the constant in the exponential factor. Wilson (9) determined this constant by correlating a large amount of data for which d $\ll$ D. In the present study, however, d is of the same order as D and since the particle size is a significant fraction of the macro-scale of turbulence, the predetermined value of K = 45 cannot be expected to apply rigorously.

Using the Durand and Condolios correlation, given by equation (17), critical settling velocities of 1.7 and 2.5 m/s were predicted for the 2" and 4" pipe diameters respectively. These predictions agree closely with the velocities anticipated from Figs. 6a and 6b but there are several reasons why in general the Durand correlation may be invalid for use with platelets.

Durand and Condolios based their correlation on tests using granular material with a top particle size of about 3 mm; extension of their results to aluminium platelets with maximum dimension about 10 mm has been made on the assumption that the Froude number remains constant. Furthermore, there is no experimental evidence that platelets travel as a sliding bed.

Therefore, in demonstrating that both the Wilson and Durand correlations are inadequate for the case of flat objects, the need for a fresh, physically based approach which takes into account the actual shape of a platelet becomes evident.

4.3 The Aerofoil Approach

Consider a single aluminium platelet resting on the invert of a horizontal pipe. The vertical component of the reaction at the interface counterbalances the apparent weight of the submerged platelet whilst the horizontal component provides a direct measure of the frictional resistance at the solid boundary. Under these conditions the platelet remains stationary and in contact with the pipe wall. Under steady flow conditions, however, a dynamic equilibrium exists due to the hydrodynamic forces which are exerted on the platelet. These forces are generated mainly due to the dynamic pressure acting on the leading face and the shearing stresses associated with fluid drag on the free sides of the platelet, see Fig. 7c. To facilitate an estimate of these forces, a number of simplifying assumptions were made:

(i)   It is assumed that the radius of curvature of the containing pipe is large so that the platelet lies flat and no fluid flow occurs at the interface.

(ii)   The x-y dimensions of the platelets used are approximately equal so that the maximum total force may be assumed independent of particle orientation with respect to the direction of flow. However, an order of magnitude analysis shows that the force exerted on the leading face is by far the greatest which suggests that the magnitude of the force itself will be sensitive to the profile of the leading edge. Fig. 8 shows

the definition of a typical platelet profile (type B) which, if projected to the flow, is expected to develop the lowest head compared with other orientations and platelet shapes. For the preservation of shape continuity between adjoining surfaces a slight refinement has been introduced by using the equation of a semi-variable ellipse to describe the profile of the leading face. The resulting contour varies between a semi-circle at $\Theta = 0°$ and a straight line at $\Theta = 90°$.

(iii) It is further assumed that for reasons of maximum stability the platelet will tend to orientate itself so that the direction of flow is parallel with one of the long axes.

(iv) Figs 7a and 7b illustrate the main simplifications made regarding the flow around each platelet. Basically, it is assumed that the fluid comes to rest isentropically against the leading face, that new turbulent boundary layers develop along the shearing faces and that there is no flow around the trailing edge.

Assumption (iv) implies frictionless flow. Hence, using the Bernoulli equation it can be shown that total force due to the stagnation pressure acting on the leading face is given by

$$F_f = 2 \left[\frac{1}{2} \int_0^{\pi/2} \int_0^t \rho_w V_h^2 \frac{y}{2} \cos \Theta \cos \Omega \, dh \, d\Theta \right] \quad \ldots (23)$$

where the local velocity V_h may be estimated using the appropriate Von-Karman equation for a logarithmic velocity profile. Similarly, it can be shown that the shearing force acting on the elevated sides is given by

$$F_s = 2 \left[\frac{1}{2} \int_0^t \rho_w V_h^2 C_D (x - y) \, dh \right] \quad \ldots (24)$$

where C_D can be expressed as a function of the Reynolds number.

Finally, the shearing force acting on the top surface of the platelet, is given by

$$F_T = \frac{1}{2} \rho_w V_h^2 C_D \left((x - y) + \frac{\pi y^2}{4} \right) \quad \ldots (25)$$

Thus, by using an estimated initial value for the mean slurry velocity, the sum total of all the hydrodynamic forces may be calculated by integrating over the dynamically active area of the platelet. The result is compared with the horizontal component of the reaction at the wall and the value of the mean velocity is iterated until

$$F_F + F_S + F_T = W_{ap} \tan(\phi) \quad \ldots (26)$$

i.e. the instant the platelet begins to slide. The sliding angle (ϕ) was determined experimentally by noting the inclination to horizontal at which several platelets just began

to slide down a submerged steel platform. This was found to be approximately $22°$ compared with about $25°$ under dry conditions.

Besides causing the platelet to slide, the hydrodynamic forces provide up-turning moments about the bottom edge of the trailing face which compete with the stabilising effect of the weight. Thence, it is possible to obtain a new threshold slurry velocity at which the moments balance-out and the platelet becomes "buoyant" by levering against the pivoting edge (Fig. 9). Once the platelet is inclined, a lift force will be generated due to differential pressure created by fluid flowing faster over the upper than lower surfaces respectively. At this instant, the platelet behaves like an aerofoil, it lifts and becomes "fluid borne". Thereafter it is expected to follow a trajectory similar to that shown in Fig. 9; i.e. the platelet accelerates to the local velocity of the fluid by projecting its plane to the direction of flow. At this position the driving force is removed, the platelet "stalls", it then settles under gravity and the process repeats itself. As the pipe velocity is increased, excess lift will be available even at small platelet inclinations so that relatively long periods of suspension may be obtained.

Using the method set out above, critical velocities for the onset of sliding were calculated and were found to be 0.53 and 0.61 m/s for the 2" and 4" pipe diameters respectively. These result are in good agreement with the lowest velocities at which it was possible to pump platelet/water mixtures, see Figs. 6a and 6b. Similarly, the minimum velocities required for platelet uplift were estimated at 1.74 and 2.14 m/s in each case. These predictions are in excellent agreement with the velocities at which asymptotic values are reached in Figs. 6a and 6b.

Although these results were based on the behaviour of a single particle, it is expected that the theory applies to dilute suspensions e.g. less than about 10% by volume. The theory was also tested by plotting the results according to equation 3 proposed by Newitt (2) for heterogeneous suspensions - a reasonable correlation was obtained. The theory was further tested by means of the bed slip model given by equation 5. A comparison of the experimental results with predictions provided by equation 5 confirmed that above a pipe velocity of about 2 m/s, platelet transport takes place in the fully suspended flow regime.

4.4 The Effect of Particle Shape on Head Loss

The effect of particle shape on head loss can be predicted using the Durand equation with drag coefficients of 1.360 for platelets and 0.444 for volume equivalent spheres. In this case, the calculated ratio of ϕ for spheres and platelets is independent of velocity at a value of 2.31.

Fig. 10 shows the actual head loss for platelets obtained experimentally and given by equation 27 compared with the predicted head loss for spheres. In this case, the ratio of ϕ for spheres and platelets is a function of mean velocity:

$$\frac{\phi_{spheres}}{\phi_{platelets}} = \frac{1.505}{V_m^{0.18}} \quad \ldots (27)$$

Fig. 10 predicts that head loss in conveying metallic platelets is less than for volume equivalent spheres. For example, the ratio of

$$(\phi_{spheres}/\phi_{platelets})$$

falls from 1.71 at 0.5 m/s to 1.17 at 4 m/s. In general, it can be concluded that particle shape is important, though further experimentation is required to rigorously quantify the effect.

5. CONCLUSIONS

A large sample of aluminium platelets has been classified before and after use in hydraulic conveying tests. The hydrodynamic properties of individual platelets have been analysed by carrying out a series of terminal settling velocity measurements. A typical aluminium platelet was observed to descend with its plane perpendicular to the direction of motion, the rate of free settling being about 200 mm/s. Using a modified shape factor based on the particle thickness and projected area, i.e.

$$C_D = \frac{2 \, g \, (S - 1) \, t}{V_t^2} \qquad \ldots (28)$$

it was possible to predict the experimental result to within 1.5%.

A pipe-rig fitted with 2" and 4" diameter pipes was used to pump dilute suspensions of metallic platelets at flow rates ranging from 0.5 to 4 m/s and concentrations up to about 10% by volume. The results were found to correlate well using the Durand type equations, and the following expressions were obtained:

$$\phi = 188 \, \psi^{1.44} \qquad \ldots (29)$$

for the 2" pipeline,

$$\phi = 265 \, \psi^{1.38} \qquad \ldots (30)$$

for the 4" pipeline,

$$or \quad \phi = 238 \, \psi^{1.41} \qquad \ldots (31)$$

using all the results collectively. The latter provides evidence in favour of using the Durand equation for limited scale-up. A plot of the non-dimensionless parameter for head loss $(f_m - f_w)/(S_m - 1)$ versus mean slurry velocity was used to assess the transition velocities. The results were interpreted by analysing the transport mechanisms associated with the hydraulic conveying of platelets. The use of existing theoretical or semi-empirical equations for the prediction of the critical velocity of deposition was unreliable due to lack of physical rigour. For this reason an alternative analysis was developed by considering the platelet as a thick aerofoil. Thus, by making a number of assumptions regarding the geometry and fluid flow around the platelet it was possible to estimate mean slurry velocities at which platelets either begin to slide or become fully suspended, i.e.

Pipeline Diameter	$V_{sliding}$ m/s	$V_{suspension}$ m/s
2"	0.53	1.74
4"	0.61	2.14

These velocities are in excellent agreement with the experimental results and it is on this basis that the aerofoil approach is proposed as a reliable method for the prediction of threshold velocities in the handling of platelet material at low concentrations.

Finally, the effect of particle shape on head loss has been considered by comparing a notional head loss calculated for volume equivalent spheres with the actual experimental head loss obtained for platelets. For the range of velocities considered, in this study the head loss ratio for the two shapes takes the form

$$\frac{\phi_{spheres}}{\phi_{platelets}} = \frac{1.505}{V_m^{0.18}} \qquad \ldots (32)$$

$$0.5 < V_m < 4 \text{ m/s}$$

Equation 34 confirms that the pumping of platelets is less energy intensive than volume equivalent spheres, but further work is required to establish the extent to which head loss is affected by shape.

6. ACKNOWLEDGEMENTS

7. REFERENCES

1. Durand, R. and Condolios, G.
   The Hydraulic Transport of Coal and Solids in Pipes, Colloquium on Hydraulic Transport, National Coal Board, London, 1952.

2. Newitt, D.M., Richardson, J.F., Abbott, M. and Turtle, R.B.
   Hydraulic Conveying of Solids in Horizontal Pipes, Trans. Inst. Chem. Engrs., Vol. 32 (II), pp.93-113, 1955.

3. Wilson, K.C. Streat, M. and Bantin, R.A.
   Slip-Model Correlation of Dense Two-Phase Flow. Hydrotransport 2 (BHRA), Warwick (U.K.), Paper C4, pp.1-10, Spetember, 1972.

4. Wilson, K.C.
   A Unified Physically Based Analysis of Solid-Liquid Pipeline Flow, Hydrotransport 4 (BHRA), Alberta, Canada, Paper A1, pp.1-16, May, 1976.

5. Clift, R., Wilson, K.C., Addie, G.R. and Carstens, M.R.
   A Mechanistically Based Method for Scaling Pipeline Tests for Settling Slurries. Hydrotransport 8 (BHRA), Johannesburg (S.A.), Paper B1, pp.91-101, August, 1982.

6. Heywood, H.
   Symp. Interaction Fluids and Parts. Inst.
   Chem. Eng., pp.1-8, London, 1962.

7. Heywood, H.
   Powder Metallurgy, Vol. 7, pp.1-28, 1961.

8. Richardson, J.F. and Zaki, W.N.
   Sedimentation and Fluidisation. Trans. Inst.
   Chem. Engrs., Vol. 32 (I), pp. 35-53, 1954.

9. Wilson, K.C. and Watt, W.E.
   Influence of Particle Diameter on the

   Turbulent Support of Solids in Pipeline
   Flow. Hydrotranpsort 3 (BHRA) Colorado
   (U.S.A.), Paper D1, pp.1-9, May, 1974.

10. Tatsis, A.
    Hydraulic Conveying of Metallic Platelets.
    PhD Thesis, London University, 1985.

11. Pouska, G.A. and Link, J.M.
    Investigation of head Loss in Coarse Oil Shale
    Slurries. Hydrotransport 5, Paper H2, May,
    1978.

TABLE 1 : GROUP % CONCENTRATION OF ITEMS A, B, C AND D IN THE OVERALL SAMPLE OF DEXION STAMPINGS

ITEM	No. OF PLATELETS	% CONCENTRATION OF PLATELETS IN	
REFERENCE	HAND SORTED	OVERALL SAMPLE	MATERIAL CYCLE
A	141	6.5	11.11
B	1,086	50.21	44.44
C	474	21.91	22.22
D	462	21.36	22.22
Total = 2,163 platelets			

TABLE 2 : PRINCIPAL PARTICLE DIMENSIONS

A : DIMENSIONS OF A TYPICAL PLATELET USED IN THE 4" PIPE TESTS

Mean Length	$\bar{x} = 12.4664$ mm
Mean Breadth	$\bar{y} = 9.6149$ mm
Mean XS-Area	$\bar{A}_p = 99.5464$ mm^2
Mean Height	$\bar{t} = 1.9193$ mm
Mean Volume	$\bar{V} = 191.0594$ mm
Mean Weight	$\bar{W} = 0.5023$ g

Diameter of volume equivalent sphere: $d_v = 7.1459$ mm

Diameter of XS-Area equivalent sphere: $d_a = 11.2580$ mm

B : DIMENSIONS OF A TYPICAL PLATELET USED IN THE 2" PIPE TESTS

Mean Length	$\bar{x} = 11.5486$ mm
Mean Breadth	$\bar{y} = 9.5768$ mm
Mean XS-Area	$\bar{A}_p = 90.6288$ mm^2
Mean Height	$\bar{t} = 2.0142$ mm
Mean Volume	$\bar{V} = 182.5445$ mm^3
Mean Weight	$\bar{W} = 0.4799$ g

Diameter of volume equivalent sphere: $d_v = 7.0381$ mm

Diameter of XS-Area equivalent sphere: $d_a = 10.7420$ mm

TABLE 3 : STEPWISE CALCULATION OF THE TERMINAL SETTLING VELOCITY FOR PUMPED PLATELETS USING THREE ALTERNATIVE VALUES OF Ke

PLATELET DIMENSIONS & OTHER PARAMETERS	4" PIPE TESTS			2" PIPE TESTS		
l (mm) b (mm) t (mm) d_a (mm) Ga_{da} Re_{da} V_{ts} (mm s^{-1})	12.466 9.615 1.919 11.258 2.269×10^7 8,250.06 <u>736.345</u>			11.5486 9.577 2.014 10.742 1.971×10^7 7,689.41 <u>719.272</u>		
ISOMETRIC SHAPE	CYLINDRICAL	CUBIC	ROUNDED	CYLINDRICAL	CUBIC	ROUNDED
Ke	0.785	0.696	0.560	0.785	0.696	0.560
$A_p = \dfrac{\pi (d_a)^2}{4}$ (mm^2)	99.543			90.629		
$K = \dfrac{Ke\ t}{(A_p)^{0.5}}$	0.1509	0.1338	0.1076	0.1661	0.1473	0.1185
K_A	0.3546	0.3290	0.2896	0.3762	0.3480	0.3047
$V_{tp} = V_{ts}\ K_A$ (mm s^{-1})	261.14	242.28	<u>213.25</u>	270.56	250.29	<u>219.16</u>

TABLE 4 : DIAGRAMATIC REPRESENTATION OF THE MODE OF DESCENT FOR ALUMINIUM PLATELETS

PLATELET TYPE (d_a)/mm	Re_{da} of DESCENT	TYPES OF SECONDARY MOTION				
		VERTICAL	SPIN	TILTING	SWINGING	SLIPPAGE
THE TRUE MOTION IS OBTAINED BY SUPERIMPOSING THE APPROPRIATE CONSTITUENT SECONDARY MOTIONS						
NEW (D) d_a = 10.444 mm	2,086	**	*	*	*	
NEW (C) d_a = 11.397 mm	2,287	**	*	*	**	*
NEW (B) d_a = 12.411 mm	2,464		*	**	***	**
USED (D) d_a = 10.355 mm	2,176	*	*	**	**	
USED (C) d_a = 10.657 mm	2,249	*	*	*	*	
USED (B) d_a = 10.947 mm	2,478	**	*	*	*	
c.f. GLASS SPHERE d_a = 11.827 mm	8,435	***				

(*): Number of (*) denote the relative intensity of each effect (approximate).

(H)* Denotes horizontal position.

TABLE 5 : COMPARISON BETWEEN EXPERIMENTAL AND PREDICTED TERMINAL
SETTLING VELOCITY (T.S.V.) FOR ALUMINIUM PLATELETS

	EXPERIMENTAL				PREDICTED	
GROUP	NEW PLATELETS V_t (mm s^{-1})	USED PLATELETS V_t (mm s^{-1})	CHANGE ON V_t %	MEAN (T.S.V.) $\overline{V_t}$ (mm s^{-1})	PLATELETS USED IN 4" PIPE TESTS	PLATELETS USED IN 2" PIPE TESTS
					Ke = 0.560	
					K_A ...	K_A ...
(D)	200.6 ± 7.7	211.5 ± 6.0	+5.4	206.0 ± 6.9		
(C)	201.6 ± 5.2	212.0 ± 6.2	+5.1	206.8 ± 5.7	(see Table 3)	
(B)	199.4 ± 5.9	227.4 ± 11.2	+14.0	213.4 ± 8.9		
OVERALL MEAN (T.S.V.)		220.2 ± 9.2		210.2 ± 7.8	213.3	219.2

1.4% OVERESTIMATED

0.5% UNDERESTIMATED
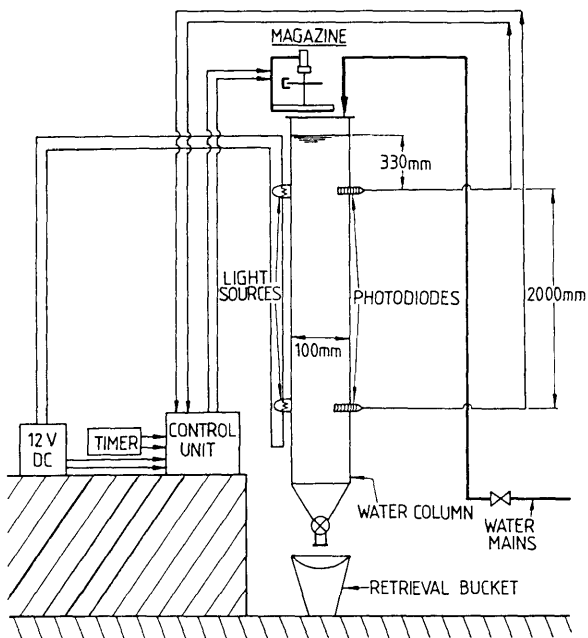
Fig. 1. A schematic presentation of the platelet characterisation apparatus.
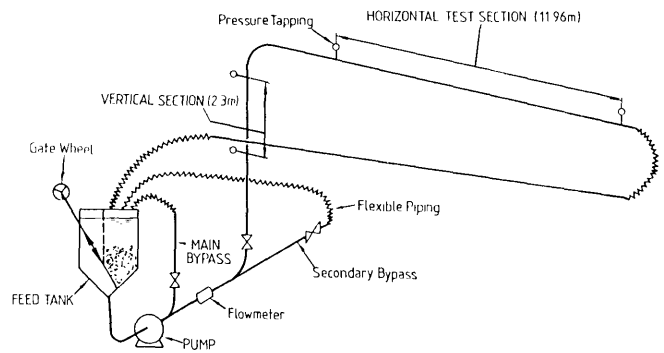
Fig. 2. Schematic presentation of 4" hydraulic conveying rig.
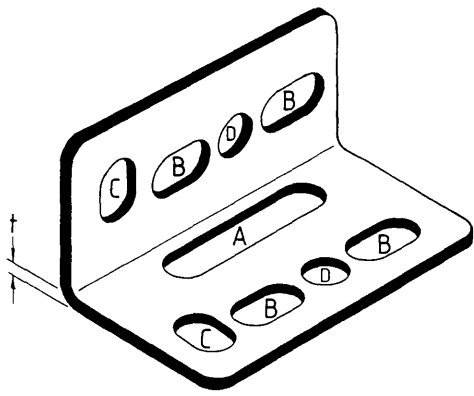
(a) Isometric view of Dexion Angle (one cycle).
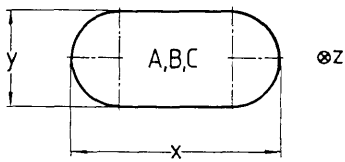
(b) Plan view of typical Dexion Stamping.

Fig. 3.
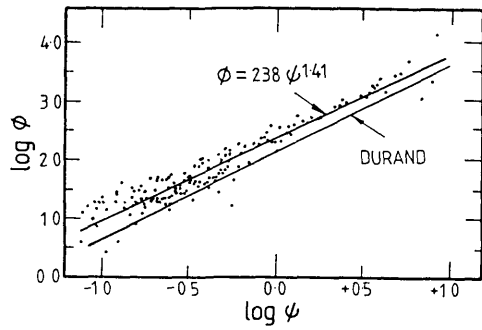
Fig. 5. Log ϕ vs log ψ data collected for 2" and 4" horizontal sections.
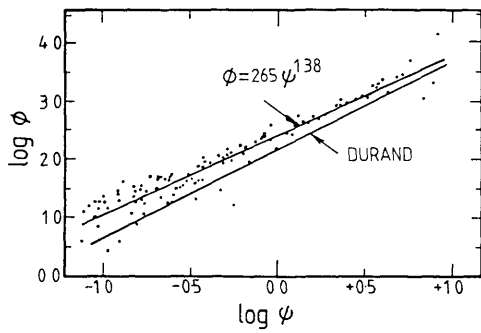
(a) 4" ID Test Section.
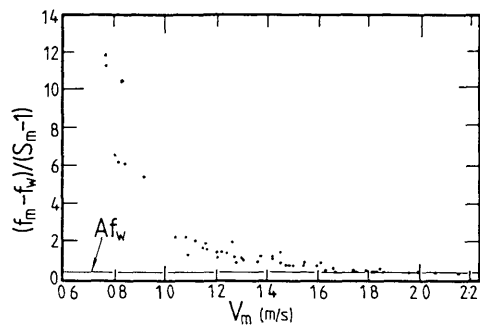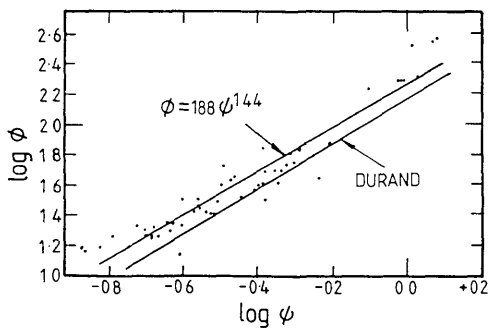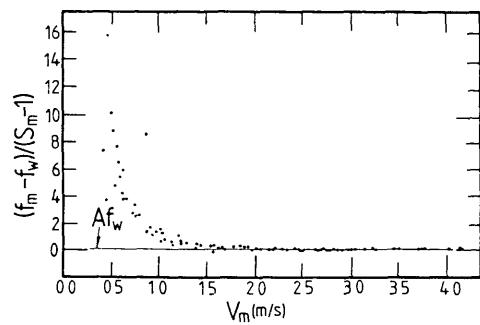
(b) 2" ID Test Section.

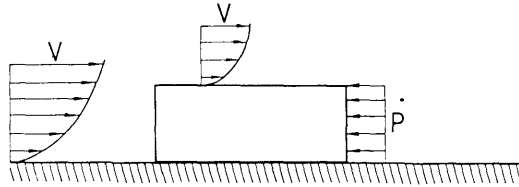Fig. 4. Log ϕ vs log ψ data for individual horizontal sections.

(a) 2" ID Test Section.

(b) 4" ID Test Section.

Fig. 6. $(f_m - f_w)/(S_m - 1)$ vs V_m data—horizontal.
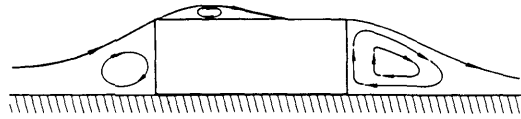
(a) Qualitative streamline pattern.

(b) Assumed velocity and pressure profiles.
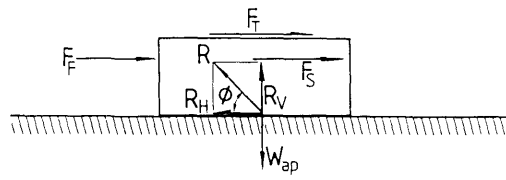
(c) Main forces acting on the platelet.

Fig. 7.

$$\Omega = \tan^{-1}\left|\frac{2h-t}{2x'}\right|$$

$$\left[\frac{2x'}{t\cos\theta}\right]^2 + \left[\frac{2h-t}{t}\right]^2 = 1$$
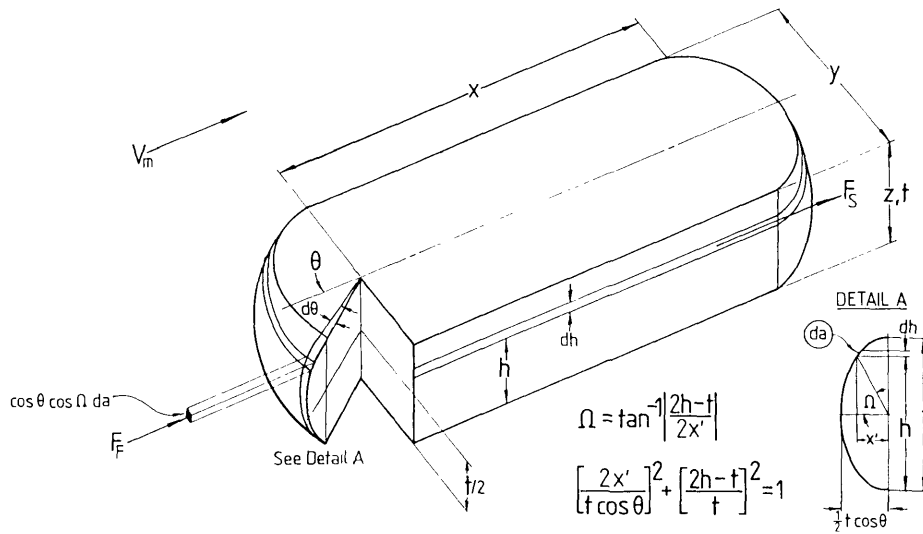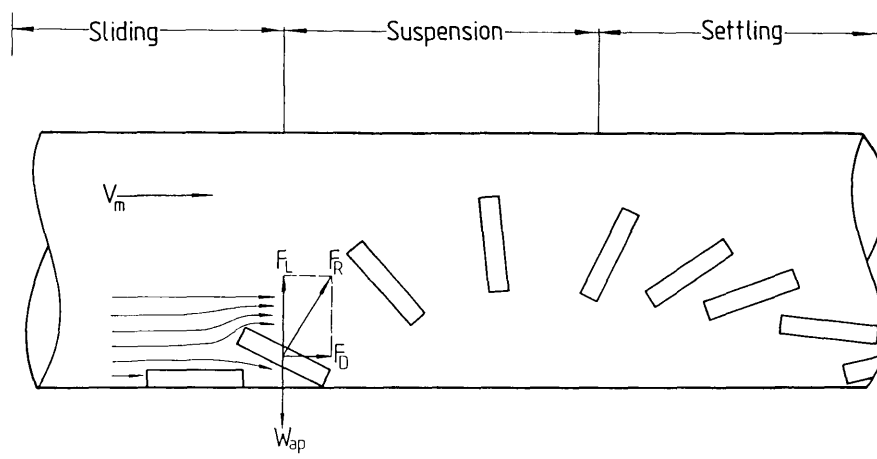
Fig. 8. Definition of a typical platelet profile.

Fig. 9. Likely trajectory of individual platelet in fully developed pipe flow.
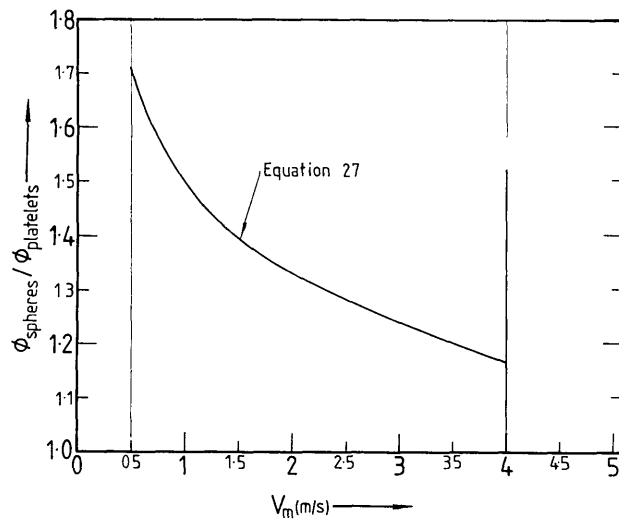

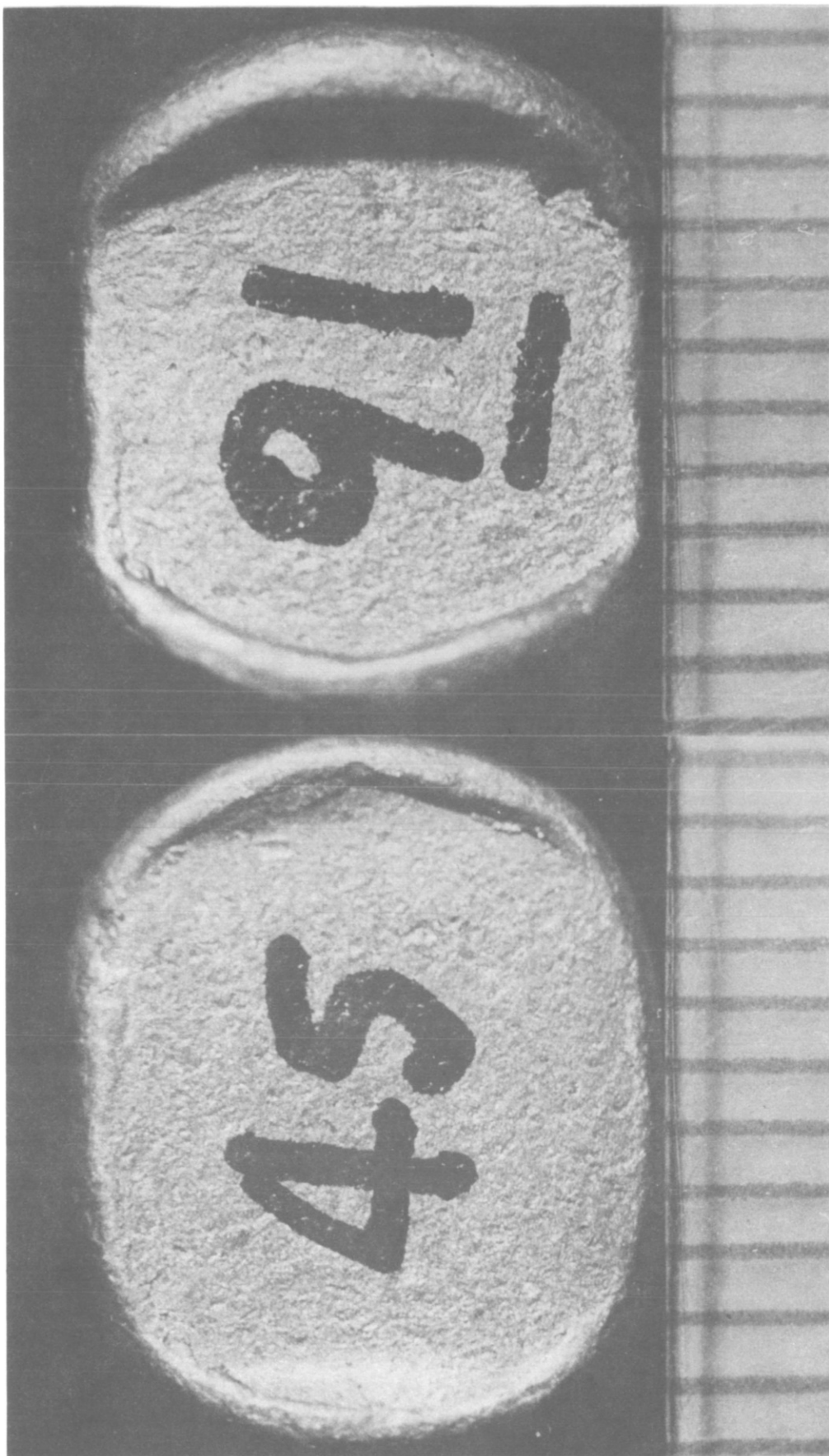*Fig. 10. The influence of particle shape on head loss.*

Plate 1. *A close-up view of two used platelets showing the curling at the edges. Group B, Scale: mm.*